Dynamic Characterisation of Soils and Seismic Analysis of Deep Foundations

A Thesis

Submitted in Partial Fulfilment of the Requirements

for the Degree of

DOCTOR OF PHILOSOPHY

by

Pradeep Kumar Dammala

(146104002)

Department of Civil Engineering

Indian Institute of Technology Guwahati

Guwahati – 781039

October 2019

DECLARATION

I hereby declare that except where specific reference is made to the work of others, the content of this dissertation are original and have not been submitted in whole or in part for consideration for any other degree or qualification at this or any other country. I do also declare that the matter embodied in this thesis is the result of investigations carried out by me in the Department of Civil Engineering, Indian Institute of Technology Guwahati, Guwahati, Assam, India and Surrey Advanced Geotechnical Engineering (SAGE) Laboratory, University of Surrey, United Kingdom.

In keeping with the general practice of reporting scientific observations, due acknowledgements have been made wherever the work described is based on findings of other investigators.

Place: IIT Guwahati

Date: **Pradeep Kumar Dammala**

CERTIFICATE

This is to certify that the thesis entitled "**Dynamic Characterisation of Soils and Seismic Analysis of Deep Foundations**", submitted by **Pradeep Kumar Dammala** (Roll No. 146104002), to the Indian Institute of Technology Guwahati, for the award of degree of Doctor of Philosophy in Civil Engineering, is a record of bonafide research work carried out by him under my supervision and guidance. The thesis work, in my opinion, has reached the requisite standard fulfilling the requirement for the degree of Doctor of Philosophy.

The results contained in this thesis have not been submitted in part or full to any other University or Institute for award of any degree or diploma.

Dr. A. Murali Krishna
Associate Professor
Department of Civil Engineering
Indian Institute of Technology Guwahati
Guwahati-781039, India

ACKNOWLEDGEMENTS

This research could not have been possible without the support of a number of individuals and I would like to extend my sincere thanks to them. First and foremost, my profound gratitude towards the Lord almighty, Jesus Christ through whom I have got eternal salvation. I take this opportunity to thank my supervisor **Dr. A. Murali Krishna** for his constant technical support, without which this research would not have been in its current shape. I am particularly indebted to him for his constant push irrespective of the situation, due to which I could able to rise my limits and realize my strengths and weaknesses. I am always indebted to him for his sponsorship of my first air-travel and consistent encouragement to apply for funding agencies.

I would also like to thank my collaborating supervisor **Prof. Subhamoy Bhattacharya** of University of Surrey, UK, from whom I have learnt the practical aspects of my research. His futuristic scientific thinking (research on offshore wind farms is one example) and writing skills are some characteristics that every researcher would love to possess. I would also like to thank my doctoral committee members, Dr. Arindam Dey, Dr. Abhishek Kumar and Dr. Ravi Shankar M, for their valuable suggestions and critical comments from time to time. Acknowledgements are due to Dr. Kaustubh Dasgupta for his help in SAP modelling. I would like to extend my sincere thanks to Prof. Sreedeep for instilling the basics of soil mechanics. The department of Civil Engineering, IIT Guwahati must be acknowledged for providing all the resources, as and when required.

My life at IIT Guwahati would not have been this smoother without my fellow researchers and to name a few: Dr. Shiv Shankar Kumar (my unofficial mentor), Dr. Bali Reddy Sodom (my first journal's first-author), Mr. Chiranjib (mature friend), and Dr. Doordarshi (coolest guy). Late nights in the lab and far away from home were not felt due to the help from many of the close friends, particularly, Dolla ji for his bro-like relation; Raji for being with me in my thick and thin; Jaswanth, Feba, Sneha for the coffee and barbeque times; Dr. Sudheer, Dr. Srikanth and Dr. Ashok for their helpful suggestions; Ravi anna and family for their love and strength; Kadam for his relaxing weekend phone calls. The Indian Institute of Technology Guwahati (IIT Guwahati) campus sprawled by the mighty Brahmaputra River, with lush green hills and lakes, provided enough energy for my concentration.

My sincere gratitude towards the Commonwealth scholarship commission for Split-Site Fellowship, tenable at the University of Surrey, UK. The stay at University of Surrey, UK was both fruitful and enjoying by the support of my colleagues: Dr. Georgios Nikitas (my pizza mate); Piyush (technical advisor); Dr. Mehdi, Dr. Emre, Dr. Saleh, Dr. Rajesh, Dr. Nitish and Abhijit for the technical and non-technical discussions. My home-like stay at Hazel Farm was only possible by the help of crazy friends: Prem, Ogo, Ayzan, William and Zobaer. My cricketing season with Uplands CC and Grafham CC was cherishable. The Europe trip with handsome bud, Dr. Hial will never be forgotten. I would also like to express my sincere thanks to: Mr. Thejesh for the technical suggestions in DEEPSOIL and Cambridge University trip; Dr. Ashuthosh Kumar for the technical suggestions; Dr. Anindya Pain for sending me the sand samples; Dr. SR Dash and Mr. Sunil for clearing my doubts in SAP and Dr. Sumanta Haldar for helping me with the Kobe motions.

Words are insufficient to describe my indebtedness to my family members whose tireless efforts, encouragement, love and guidance helped me to move forward in life: Mom (Surya Kala), Dad (Chandra Rao), Sister (Usha), Brother (Praveen), Brother-in-law (Ramesh), nephew (Leshawn). Thanks are also due to Karuna annayya and Deena vadina. I must say that their patience throughout the duration of PhD was the one that helped me move forward. I would not have taken the line of research had my brother (Praveen) not sacrificed his education. He has been a role model and constant source of encouragement throughout my life. The North Guwahati Christian Assembly had a significant role in my overall development, be it societal or spiritual. I will always cherish the moments spent with the fellow brothers and sisters in Christ.

Pradeep Kumar Dammala

ABSTRACT

Earthquakes are the most unexpected and unavoidable natural events which would often cause severe damage to both human and infrastructure. Infrastructure losses can be minimized by adopting effective earthquake resistant design. It is well recognised that the stability of a structure is governed by the integrity of super structure and foundation. Efficient assessment of behaviour of underlying soil to dynamic loading would yield effective seismic resistant design of a structure. Determination of dynamic soil behaviour involves the estimation of strain dependent dynamic soil properties along with the liquefaction potential assessment. Traditionally, dynamic soil properties are represented through maximum shear modulus (G_{max}), normalized shear modulus (G/G_{max}) and damping ratio (D) variation with shear strain (γ). Liquefaction potential is assessed in terms of generation of pore water pressures and its dependency with cyclic stress ratio (CSR) and number of cycles of seismic loading. Some of the regions may contain soils of similar characteristics based on origin and formation. Past studies highlighted the need of region-specific dynamic characteristics of soils, since the soils of different regions may differ in their dynamic behaviour. Therefore, the determination of region-specific dynamic properties of soils and associated dynamic response is essential.

Deep foundations (such as piles and caissons) are the preferred foundations for supporting heavy superstructure loads and in problematic surficial soils. Dynamic behaviour of deep foundations is still a subject of research for geotechnical engineers, due to the numerous failures observed during seismic events. As piles or caissons extend to deeper stratum, the dynamic characteristics of multi-layered soils (possible sandwiched soft layers) and the resulting soil-structure interactions are often detrimental which need to be analysed for site specific conditions using the appropriate dynamic soil properties. The present study focusses on the comprehensive characterisation of dynamic behaviour of soils; sampled from two active seismic regions of India and their application in seismic ground response studies and dynamic analysis of pile foundations.

Total of six soils are considered (four sand and two cohesive soil samples) for the study which represent the typical characteristics of river sediments in two seismically active regions of India (north and northeastern regions). Four independent testing techniques

(Bender Element (BE); Resonant Column (RC); Dynamic Simple Shear (DSS); and Cyclic Triaxial (CTX)) are adopted to comprehensively characterise the chosen soils over a wide range of shear strains (0.0001% to 5%). Tests were conducted with varying range of parameters, such as initial relative density (R_d), effective confining pressure (σ'_c), and cyclic shear strain (γ) to thoroughly understand their effect in dynamic behaviour of soils. In addition, cyclic triaxial (CTX) tests are performed in undrained conditions to assess the liquefaction behaviour of the soils.

Results obtained from each testing technique are analysed independently and discussions are presented for cohesionless and cohesive soils separately. The effect of R_d and σ'_c on G_{max} of soils is elaborately discussed based on BE tests. The RC and DSS tests results are analysed and discussed in terms of G and D variation with γ, with varying R_d and σ'_c conditions from low to high strain levels. Results of the individual tests in terms of G/G_{max} and D are combined to provide comprehensive dynamic soil properties over wide strain range. Empirical relationships and region-specific best-fit parameters have been proposed based on regression analysis of the experimental data. Further, the data of Indian soils from literature are collated and compared with the widely used empirical G/G_{max} and D curves. Design G/G_{max} and D curves have been established at practical range of σ'_c, so as to facilitate direct application of the test results in geotechnical earthquake applications. Cyclic triaxial test results are presented in terms of pore water pressure variation, stress path and stress-strain responses for chosen soils.

One dimensional ground response analyses (GRA) have been conducted using DEEPSOIL program, to demonstrate the applicability of established dynamic soil properties. Four sites have been chosen, out of which three are located in Assam (northeastern state in India) and the latter is from Rohtak region of Haryana state (northern state in India). The soils in the chosen sites closely represent the characteristics of investigated soils. Ground motions of varying peak bedrock intensity (0.05g to 0.36g) are chosen, which are consistent with the expected seismic intensity of the regions based on the seismic code of the country. Two set of analysis were performed. First set of analysis involves equivalent linear approach, to highlight the importance of region-specific dynamic soil properties in GRA studies. The second set of analysis is a comparative study on the results obtained from equivalent and nonlinear effective stress approaches. Nonlinear (NL) effective stress results are presented in terms of peak ground accelerations, pore pressure profiles and stress-strain response of soil deposits. The sites chosen in northeastern India showed high amplification to low

intensity motions (up to 0.138g input motion) and severe liquefaction proneness for high intensity motions.

The results of effective stress GRA are used for the seismic analysis of pile foundations. A multi-layered soil profile prone to liquefaction is chosen and two pile foundation configurations (single pile and 2×2 pile group) are used. Dynamic beams on nonlinear Winkler foundation (BNWF) approach is adopted for the analysis and the model is validated against the centrifuge test results reported in the literature. Nonlinear time history analysis is performed on the chosen pile configurations using SAP2000 and with soil displacement time histories obtained from NL GRA. The bilinear strain-hardening model has been used for modelling the soil pile interaction in liquefiable strata. Kinematic response of piles in terms of lateral displacements and bending moments are presented. An abrupt change of pile response is noted at the vicinity of liquefiable and non-liquefiable strata. The chosen 2×2 pile configuration showed lesser displacements and reduced bending moments as compared to the single pile in case of liquefiable soils.

The work presented in the thesis can aid as a comprehensive strategic plan for seismic analysis of deep foundation supported structures.

TABLE OF CONTENTS

ABSTRACT……..……..……..……..…..vii

TABLE OF CONTENTS…….……..…..…….……...xi

LIST OF FIGURES...…….……..…….……..xv

LIST OF TABLES..…….……..…….……..…..xxv

NOMENCLATURE..……..……..……...xxvii

CHAPTER I. INTRODUCTION **1**

1.0 PREAMBLE 1

1.1 DYNAMIC SOIL CHARACTERISATION 3

1.2 SEISMIC ANALYSIS OF DEEP FOUNDATIONS 5

1.3 BROAD OBJECTIVES OF THE STUDY 6

1.4 ORGANIZATION OF THESIS 6

CHAPTER II. LITERATURE REVIEW **9**

2.0 INTRODUCTION 9

2.1 DYNAMIC SOIL BEHAVIOUR 9

2.1.1 Laboratory Studies on Dynamic Soil Properties *11*

2.1.2 Studies on Comprehensive Dynamic Soil Properties *21*

2.1.3 Empirical Formulations *26*

2.1.4 Liquefaction Potential of Soils *31*

2.2 STUDIES ON SEISMIC GROUND RESPONSE 37

2.2.1 Studies on EQL and NL GRA Comparison *37*

2.2.2 GRA Studies in India *40*

2.3 SEISMIC ANALYSIS OF DEEP FOUNDATIONS 41

2.3.1 Kinematic Interaction of Pile Foundations in Layered Soils *43*

2.3.2 Modelling Seismic-Soil-Structure-Interaction *48*

2.4 SUMMARY OF LITERATURE REVIEW 51

2.5 OBJECTIVES AND SCOPE OF THE RESEARCH 52

CHAPTER III. MATERIALS AND EXPERIMENTAL PROGRAMME **53**

3. 0 INTRODUCTION 53

3.1 MATERIAL DESCRIPTIONS 53

3.1.1 Cohesionless Soils *55*

3.1.2 Cohesive Soils *57*

3.2 MONOTONIC STRENGTH TESTS 57

3.2.1 Testing Program *57*

3.2.2 Sample Preparation *58*
3.2.3 Saturation *60*
3.2.4 Monotonic Response of Cohesionless Soils *61*
3.2.5 Monotonic Response of Cohesive soils *68*
3.3 DYNAMIC TESTING PROGRAM 69
3.3.1 Bender Element Tests *69*
3.3.2 Resonant Column Tests *75*
3.3.3 Dynamic Simple Shear Tests *80*
3.3.4 Cyclic Triaxial Tests *85*
3.4 SUMMARY 89

CHAPTER IV. DYNAMIC CHARACTERISATION OF COHESIONLESS SOILS 91
4.0 INTRODUCTION 91
4.1 BENDER ELEMENT TEST RESULTS 91
4.2 RESONANT COLUMN TEST RESULTS 94
4.2.1 Maximum Shear Modulus (G_{max}) *97*
4.2.2 Comparison of RC and BE Test Results *98*
4.2.3 Secant Shear Modulus (G) *99*
4.2.4 Damping Ratio (D) *103*
4.3 DYNAMIC SIMPLE SHEAR TEST RESULTS 105
4.4 COMPREHENSIVE G/G_{max} AND DAMPING RATIO CURVES 112
4.5 EMPIRICAL FORMULATIONS 114
4.5.1 Maximum Shear Modulus (G_{max}) *115*
4.5.2 Normalized Shear Modulus (G/G_{max}) *117*
4.5.3 Damping Ratio (D) *121*
4.5.4 Design G/G_{max} and D Curves *123*
4.6 LIQUEFACTION ANALYSIS (CTX TEST RESULTS) 125
4.7 SUMMARY 133

CHAPTER V. DYNAMIC CHARACTERISATION OF COHESIVE SOILS 135
5.0 INTRODUCTION 135
5.1 BENDER ELEMENT TEST RESULTS 135
5.2 RESONANT COLUMN TEST RESULTS 136
5.3 DYNAMIC SIMPLE SHEAR TEST RESULTS 139
5.4 COMPREHENSIVE G/G_{max} AND DAMPING RATIO CURVES 142
5.4.1 Empirical Formulations (G_{max}) *144*
5.4.2 Empirical Formulations (G/G_{max}) *144*
5.4.3 Empirical Formulations (Damping Ratio) *145*
5.5 CYCLIC TRIAXIAL TESTS RESULTS 148
5.6 SUMMARY 151

CHAPTER VI. SEISMIC GROUND RESPONSE ANALYSIS 153

6.0 INTRODUCTION 153
6.1 METHOD OF ANALYSIS 153
6.1.1 Equivalent Linear (EQL) Approach *154*
6.1.2 Non Linear (NL) Approach *154*
6.2 SITES OF INTEREST 155
6.3 GROUND MOTIONS CONSIDERED 157
6.4 SUBSOIL PROPERTIES REQUIRED 160
6.4.1 G/G_{max} and Damping Ratio Curves for EQL Analysis *161*
6.4.2 NL Soil Parameters *167*
6.5 ANALYSES PERFORMED 169
6.6 RESULTS AND DISCUSSIONS 171
6.6.1 Significance of Site-Specific Properties in GRA *171*
6.6.2 Comparison of Soil Response from EQL and NL Analysis *174*
6.6.3 Nonlinear Analysis Results *179*
6.6.4 Comparison of Northeast Site Response *195*
6.7 SUMMARY 198

CHAPTER VII. SEISMIC ANALYSIS OF PILE FOUNDATIONS 199
7.0 INTRODUCTION 199
7.1 DYNAMIC BNWF MODEL 199
7.1.1 Components Involved in Dynamic BNWF Approach *200*
7.1.2 Numerical Program – SAP2000 ..... *201*
7.2 VALIDATION OF DYNAMIC BNWF MODEL 201
7.3 PROBLEM STATEMENT 205
7.4 NUMERICAL MODEL 207
7.4.1 P-Y Curves for Non-Liquefiable Soils *208*
7.4.2 P-Y Curves for Liquefiable Soils *209*
7.5 RESULTS AND DISCUSSIONS 214
7.5.1 Single Pile Response *214*
7.5.2 Group Pile Response *220*
7.6 SUMMARY 223

CHAPTER VIII. CONCLUDING REMARKS 225
8.0 SUMMARY OF THE THESIS 225
8.1 MAJOR CONCLUSIONS/CONTRIBUTIONS 225
8.2 LIMITATIONS OF THE STUDY 227
8.3 FUTURE RESEARCH SCOPE 228

REFERENCES 229
PUBLICATIONS 241

LIST OF FIGURES

Fig. 1.1 Example of foundation failure due to seismic soil liquefaction in Adapazari region of Turkey during 1999 Kocaeli earthquake (after Sezen 2000) ---------- 1
Fig. 1.3 Schematic representation of seismic body wave travel ---------- 3
Fig. 1.4 Flow chart of seismic analysis/requalification strategy for geotechnical structures (modified after Krishna et al. 2014)---------- 4
Fig. 1.5 (a) Crude slenderness ratio based classification of flexible pile and rigid caisson foundations (modified after Gerolymos and Gazetas 2006) (b) Collapsed Showa Bridge in Japan during 1964 Niigata earthquake (after Yoshida et al. 2007) (c) Pile failure observed during the excavation of NHK building after 1964 Niigata earthquake in Japan (after Kawamura et al. 1985) ---------- 5
Fig. 2.1 Typical representation of dynamic soil properties and the testing techniques....10
Fig. 2.2 (a) Effect of void ratio and effective confining pressure on G_{max} (b) Comparison of G_{max} of Berlin sand obtained from BE and RC tests (after Bai 2011).....16
Fig. 2.3 Effect of effective confining pressure on (a) G, (b) G/G_{max}, (c) D (after Darendeli 2001) and effect of void ratio on (d) G, (e) G/G_{max}, (f) D (after Kokusho 1980).....17
Fig. 2.4 Large strain dynamic behaviour of soils (a) after Kiku and Yoshida (2000) (b) and (c) after Kumar et al. (2017) and (d) after Pagliaroli et al. (2018) 18
Fig. 2.5 (a) G/G_{max} and (b) D of Indian sands 19
Fig. 2.6 Design (a) G/G_{max} and (b) D curves over wide strain range for sands (after Seed and Idriss 1970) 21
Fig. 2.7 (a) Dynamic soil properties from independent tests – RC and CTS (b) Combined G/G_{max} curves (after Iwasaki et al. 1978) 22
Fig. 2.8 Comprehensive (a) G/G_{max} and (b) D for clays (after Vucetic and Dobry 1991)23
Fig. 2.9 (a) G/G_{max} and (b) D of sands measured by Darendeli (2001).....23
Fig. 2.10 G/G_{max} and D curves for earthen dam core materials (after Yee et al. 2013) ...24
Fig. 2.11 G/G_{max} variation with shear strain for sand mixed with plastic fines (after El Mohtar et al. 2013) 25
Fig. 2.13 G/G_{max} variation with shear strain for Leda clay (after Torabi and Rayhani 2017) 26

Fig. 2.14 Hyperbolic stress-strain relationship of soils (after Hardin and Drenvich 1972) 27
Fig. 2.15 (a) Variation of cyclic strength with fines content at constant void ratio (after Troncoso 1990) (b) CSR variation at different relative densities for Ahmedabad sand (after Sitharam et al. 2004) 31
Fig. 2.16 (a) Liquefaction potential of Assam sand (after Kumar 2017) (b) Liquefaction phenomenon of Redsoil sampled from northeastern India (after Kumar 2017) 32
Fig. 2.17 Post liquefaction response of Redhill 110 sand (after Lombardi et al. 2014) ...33
Fig. 2.18 Comparison of experimental (centrifuge) data with the 1D EQL and NL GRA (a) 0.05g input motion (b) 0.15 input motion (after Garala and Madabhushi 2018) 39
Fig. 2.19 Comparison of EQL and NL GRA in Guwahati city (after Basu et al. 2019)...40
Fig. 2.20 Shear stress-strain response at 2.5 m depth of the modelled soil deposit (after Mercado et al. 2018) 40
Fig. 2.21 Typical bending moment profile of free-head pile in two layered soil medium (after Mylonakis 2001) 42
Fig. 2.22 Pile bending strain variation in different layered soils (A1) Homogeneous (A2) Surficial strength half of base layer (B3) Surficial soil strength is 25% of base layer (B4) Surficial soil strength is 10% of base layer (after Nikolaou et al. 2001) 43
Fig. 2.23 Different loads acting on a pile during seismic events in liquefiable soil conditions (after Sarkar et al. 2014).....45
Fig. 2.25 Application of Winkler beam approach to pile foundations in case of (a) Non-liquefied soils and (b) Liquefied soils (after Dash et al. 2009).....49
Fig. 2.26 (a) Dynamic *p-y* analysis model (after Boulanger at al. 1999) (b) Schematic of *p-y* procedure (after Mondal et al. 2012) 51
Fig. 3.1 (a) Seismic zonation map of India (redrawn after IS 1893-2016) marked with the considered soil locations and Soil samples location in (b) Haryana (c) Assam 54
Fig. 3.2 Grain size distribution of chosen soils.....55
Fig. 3.4 (a) Split mould for the preparation of sand specimen (b) Sand pouring into the mould for moist tamping specimen (c) Prepared sand specimen 59
Fig. 3.5 (a) Mould for the clay specimen preparation (b) Mould with one end closed and the other end ready to be filled with the soil-water mixture (c) Prepared clay specimen.60
Fig. 3.6 Response of BP sand in dry tests (a) Stress-strain response and (b) Stress path.62
Fig. 3.7 Response of BG sand in dry tests at different σ'_c values (a) Stress-strain response and (b) Stress path.....63

Fig. 3.8 Response of BP sand in saturated CU tests at different $\sigma'c$ values (a) Stress-strain response (b) Pore water pressure variation with strain (c) Stress path and (d) E_{sec} variation 64
Fig. 3. 10 Comparison of monotonic behaviour of BP and BG sands with that of sands collated from literature 66
Fig. 3.11 Comparison of dry and saturated (CU condition) response of BP sand (a) stress-strain behaviour at 50 kPa and 100 kPa σ'_c (b) Stress path in dry and saturated conditions and (c) E_{sec} variation 67
Fig. 3.13 Response of PC in saturated CU tests at different σ'_c (a) Stress-strain response (b) Pore water pressure variation with strain (c) stress path and (d) E_{sec} variation 69
Fig. 3.14 (a) Bender element apparatus (b) Schematic view of loading on the sample and (c) View of transmitting bender element at the base 71
Fig. 3.15 Bender element scope system and leads for generation of input signals and monitoring the output signals 71
Fig. 3.16 Schematic representation of (a) BE testing principle and (b) view of bender elements 72
Fig. 3.17 Typical input and output signals from CLISP STUDIO on BP sand 73
Fig. 3.18 Effect of input frequency on received signals for YF sand dense specimen 74
Fig. 3.20 RC apparatus available at the SAGE lab, Surrey and the schematic representation of loading conditions on the sample 76
Fig. 3.21 Schematic view of RC apparatus with various components 76
Fig. 3.22 (a) Schematic view of torsional excitation using magnetic coils and drive system and (b) pictorial view of electromagnetic drive system.....77
Fig. 3.23 Typical screenshot view of GDSRCA program for finding the fundamental mode of vibration.....78
Fig. 3.25 Variation of f_{nz} with input voltage, shear modulus and damping ratio with shear strain for BP sand at 100 kPa effective confining pressure 79
Fig. 3.26 Schematic representation of loading conditions in field and DSS testing (after Baxter et al. 2010).....80
Fig. 3.27 DSS apparatus available at the SAGE lab, Surrey with a schematic view of loading conditions on the specimen (after Nikitas et al. 2016) 81
Fig. 3.28 Steps for sample preparation and instrumentation setup for DSS testing 83
Fig. 3.29 Typical input and output results from DSS testing (BP sand at 100 kPa effective vertical stress for 1% strain controlled shearing at 1 Hz frequency) 85

Fig. 3.30 Typical stress-strain behaviour of BP sand for 1% strain controlled DSS test at 100 kPa effective confining stress for 10 cycles of loading 85
Fig. 3.31 Cyclic triaxial test system (Wykeham Farrance supplied) with the connections and components (after Kumar 2018) available at IIT Guwahati 86
Fig. 3.32 CTX system (GDSLab supplied) at SAGE laboratory 87
Fig. 3.33 Multi-stage testing in the CTX system 88
Fig. 3.34 Typical results obtained from CTX test 89
Fig. 4.1 G_{max} variation with σ'_c for BP sand (a) Normal axis and (b) Semi-log representation 92
Fig. 4.3 G_{max} variation with effective confining pressure for YF sand 93
Fig. 4.4 G_{max} variation for the three sands in loose conditions 94
Fig. 4.6 Typical results obtained from incremental strain approach in RC tests 96
Fig. 4.7 Shear wave velocity & resonant frequency variation with cell pressure for BP sand at shear strains < 0.001% 97
Fig. 4.8 Variation of G_{max} with confining pressure at different relative densities for BP sand 98
Fig. 4.9 G_{max} comparison from BE and RC testing for (a) BP (b) BG and (c) YF sands .99
Fig. 4.10 Variation of G with γ for BP and BG sands at different effective confining pressures.....100
Fig. 4.11 Variation of G/G_{max} with γ for BP and BG sands 101
Fig. 4.12 Variation of G with γ for BP and BG sands at different relative densities.....102
Fig. 4.13 Variation of G/G_{max} with γ for BP and BG sands at different R_d states.....103
Fig. 4.14 Variation of D with γ for BP and BG sands at different effective confining pressures.....104
Fig. 4.15 Variation of D with γ for BP and BG sands at different R_d states 105
Fig. 4.16 Stress-strain response of BG sand at 150 kPa effective vertical stress condition for the first loading cycle 107
Fig. 4.17 Stress-strain response of BG sand at 150 kPa effective vertical stress condition for the 100th loading cycle 107
Fig. 4.18 Stress-strain response of BG sand at 0.1% shear strain for different loading cycles 108
Fig. 4.19 Stress-strain response of BG sand at 0.5% shear strain for different loading cycles 108

Fig. 4.20 Stress-strain response of BG sand at 1% shear strain for different loading cycles 109
Fig. 4.21 Effect of loading cycles on normal settlement of BG sand at different strain amplitudes 109
Fig. 4.22 Stress-strain response of BG sand at 0.5% shear strain for different effective vertical stress conditions 110
Fig. 4.23 Stress-strain response of BG sand at 1% shear strain for different effective vertical stress conditions 110
Fig. 4.24 Methodology adopted for determination of G and D (modified after Kumar et al. 2017) 111
Fig. 4.25 Variation of (a) G (b) G/G_{max} and (c) D with γ for BP sand at high shear strains 112
Fig. 4.26 (a) G/G_{max} and (b) damping ratio of BP sand 113
Fig. 4.27 (a) G/G_{max} and (b) damping ratio of BG sand 113
Fig. 4.28 (a) G/G_{max} and (b) damping ratio of YC sand 114
Fig. 4.29 (a) G/G_{max} and (b) damping ratio of YF sand 114
Fig. 4.30 Regression results of BP sand using Eqn. 4.1 independently for RC and BE data 116
Fig. 4.31 Regression results of BP sand using Eqn. 4.1 combined for RC and BE data 117
Fig. 4.33 Comparison of Matasovic and Vucetic (1994) and Darendeli (2001) in modelling G/G_{max} of sands 118
Fig. 4.34 Normalized reference shear strain for the tested sands 119
Fig. 4.35 Regression analysis for G/G_{max} of sands 120
Fig. 4.36 Efficiency check of the proposed best-fit parameters of G/G_{max} 121
Fig. 4.37 The b value determination for BP sand at 50% R_d and 300 kPa effective confining pressure 123
Fig. 4.38 Regression analysis for damping ratio of all the sands 124
Fig. 4.39 Design stiffness curves for all the sands 125
Fig. 4.40 (a) Plot of PWP ratio and (b) stress-path for loose (30% R_d) BP sand specimens 127
Fig. 4.41 (a) Plot of PWP ratio and (b) stress-path for medium dense (60% R_d) BP sand specimens 127
Fig. 4.43 Stress-strain response of BP sand in (a) loose and (b) medium dense conditions 129

Fig. 4.44 Effect of R_d on the PWP generation in BP sand 129
Fig. 4.46 CSR versus number of cycles for liquefaction for BP sand 131
Fig. 5.1 G_{max} variation with effective confining pressure for clays 136
Fig. 5.2 Variation of shear modulus with shear strain for (a) PC and (b) RS 137
Fig. 5.3 Variation of G/G_{max} with shear strain for (a) PC and (b) RS 138
Fig. 5.4 Variation of damping ratio with shear strain for (a) PC and (b) RS 139
Fig. 5.5 Stress-strain response of RS at different loading cycles (a) N=1 (b) N=10 (c) N=100 and (d) N=1000 140
Fig. 5.6 Stress-strain loops of RS at shear strains of (a) 0.1% (b) 0.25% (c) 0.5% (d) 1% (e) 2.5% (f) 5% 141
Fig. 5.7 Variation of normal settlement for RS specimen in DSS test conditions at 100 kPa effective vertical stress 142
Fig. 5.8 (a) Modulus reduction and (b) damping ratio of PC soil 143
Fig. 5.10 Regression analysis of G_{max} of both cohesive soils 144
Fig. 5.11 Regression analysis for G/G_{max} of clays 145
Fig. 5.12 Regression analysis for damping ratio of clays 146
Fig. 5.13 Design G/G_{max} and D curves of both the cohesive soils 147
Fig. 5.14 Comparison of developed G/G_{max} curves of PC and RS with literature curves at PI=20 147
Fig. 5.15 Comparison of developed D curves of PC and RS with literature curves at PI=20 148
Fig. 5.16 (a) Plot of excess PWP and (b) stress-path for PC specimen at 0.2 CSR 149
Fig. 5.17 (a) Plot of excess PWP and (b) stress-path for PC specimen at 0.4 CSR 149
Fig. 5.18 PWP ratio and axial strain variation of PC for (a) CSR 0.20 and (b) CSR 0.40 150
Fig. 5.19 Stress-strain response of PC at (a) CSR 0.20 and (b) CSR 0.40 151
Fig. 6.1 Location of chosen soil profiles in northeastern India 156
Fig. 6.3 (a) Indian seismic zone map (IS 1893-2002) (b) Seismotectonic map of northeastern India (redrawn after Raghu Kanth et al. 2008) 158
Fig. 6.4 Artificial ground motions for Guwahati city (redrawn after Raghu Kanth et al. 2008) 159
Fig. 6.5 Recorded Chamoli (1999) motion (Source:COSMOS) 159
Fig. 6.6 Comparison of acceleration spectrum of chosen motions to the global spectrum 160

Fig. 6.7 G/G_{max} and damping curves for Site-1 162
Fig. 6.8 G/G_{max} and D curves adopted for Site-2 163
Fig. 6.9 G/G_{max} and damping curves for Site-3 163
Fig. 6.10 G/G_{max} and damping curves for Site-4 164
Fig. 6.11 Various curves used at 25 k′a overburden depth for first series of analysis ... 170
Fig. 6.12 PGA profiles from EQL study for Site-1 172
Fig. 6.13 Effective shear strain profile for Site-1 based on EQL GRA 173
Fig. 6.14 PSA response obtained for Site-1 based on EQL GRA 174
Fig. 6.15 PGA profiles for 0.05g and 0.138g ground motions 176
Fig. 6.16 PGA profiles for 0.24g and 0.36g ground motions 176
Fig. 6.17 Peak strain profiles for 0.05g and 0.138g ground motions 177
Fig. 6.18 Peak strain profiles for 0.24g and 0.36g ground motions 177
Fig. 6.20 Shear strain histories of (a) 0.24g and (b) 0.36g motions at 10 m depth for Site-1 178
Fig. 6.21 Shear stress-shear strain response obtained from EQL and NL approaches at 10 m depth for Site-1 for (a) 0.05g (b) 0.138g (c) 0.24g and (d) 0.36g motions 179
Fig. 6.22 Acceleration histories along the depth for four motions at Site-1 181
Fig. 6.23 Acceleration histories along the depth for four motions at Site-2 182
Fig. 6.24 Acceleration histories along the depth for four motions at Site-3 183
Fig. 6.25 Profiles of (a) PGA (b) Amplification/attenuation (c) r_u for Site-1 184
Fig. 6.26 Profiles of (a) PGA (b) Amplification/attenuation (c) r_u for Site-2 185
Fig. 6.27 Profiles of (a) PGA (b) Amplification/attenuation (c) r_u for Site-3 186
Fig. 6.29 PSA response for Site-1 187
Fig. 6.30 The r_u histories for four chosen motions at Site-1 188
Fig. 6.31 The r_u histories for four chosen motions at Site-2 189
Fig. 6.32 The r_u histories for four chosen motions at Site-3 190
Fig. 6.33 r_u histories for different motions at Site-1 at (a) 10 m and (b) 3 m depth 191
Fig. 6.34 r_u histories for different motions at Site-3 at (a) 5 m and (b) 0.5 m depth from surface 192
Fig. 6.35 Shear strain variation and stress-strain response at different depths (a) 15m (b) 10m (c) 5m and (d) surface, for 0.05g motion at Site-3 193
Fig. 6.36 Shear strain variation and stress-strain response at different depths (a) 15m (b) 10m (c) 5m and (d) surface, for 0.138g motion at Site-3 193

Fig. 6.37 Shear strain variation and stress-strain response at different depths (a) 15m (b) 10m (c) 5m and (d) surface, for 0.24g motion at Site-3 194
Fig. 6.38 Shear strain variation and stress-strain response at different depths (a) 15m (b) 10m (c) 5m and (d) surface, for 0.36g motion at Site-3 195
Fig. 6.39 Comparison of (a) PGA (b) Amplification/attenuation and (c) r_u profiles for northeastern India region for 0.05g motion 196
Fig. 6.40 Comparison of (a) PGA (b) Amplification/attenuation and (c) r_u profiles for northeastern India region for 0.138g motion 197
Fig. 6.41 Comparison of (a) PGA (b) Amplification/attenuation and (c) r_u profiles for northeastern India region for 0.24g motion 197
Fig. 6.42 Comparison of (a) PGA (b) Amplification/attenuation and (c) r_u profiles for northeastern India region for 0.36g motion 198
Fig. 7.1 Overview of dynamic BNWF approach for seismic analysis of pile foundations in liquefiable soils 200
Fig. 7.2 (a) Schematic view of centrifuge setup for the dynamic testing of pile foundations (Boulanger et al. 1999) (b) SAP2000 model adopted for validation 202
Fig. 7.3 Peak displacements of pile for Kobe (1995) motions (a) 0.055g (b) 0.20g and (c) 0.58g.....204
Fig. 7.4 Peak bending moments of pile for Kobe (1995) motions (a) 0.055g (b) 0.20g and (c) 0.58g 205
Fig. 7.5 (a) Schematic view and (b) numerical model of single pile and 2×2 pile group 206
Fig. 7.6 *p-y* curves for non-liquefiable soils based on API (2014) recommendations....209
Fig. 7.7 Schematic representation of obtaining liquefied *p-y* curve (redrawn after Dash et al. 2017) 210
Fig. 7.8 (a) Comparison of liquefied and standard *p-y* curve at 3m depth (b) developed p-y curves for liquefied soil for the Site-3 212
Fig. 7.9 Free field soil displacements along the depth for 0.05g PBRA motion 213
Fig. 7.10 Free field soil displacements along the depth for 0.24g PBRA motion 213
Fig. 7.11 Pile foundation displacement response along the depth for 0.05g PBRA motion 215
Fig. 7.12 Pile foundation displacement response along the depth for 0.24g PBRA motion 216

Fig. 7.13 Comparison of free field and single pile displacements for (a) 0.05g (b) 0.138g events 217
Fig. 7.14 Comparison of free field and single pile displacements for (a) 0.24g (b) 0.36g events 217
Fig. 7.15 Peak displacements in the single pile for different seismic events 218
Fig. 7.16 Peak shear forces in the single pile for different seismic events.....219
Fig. 7.17 Peak bending moments in the single pile for different seismic events 219
Fig. 7.18 Single pile and 2×2 pile group performance comparison in terms of (a) peak displacement (b) peak bending moment 220
Fig. 7.19 Peak pile displacements comparison for single and 2×2 pile group 221
Fig. 7.20 Peak pile bending moments comparison for single and 2×2 pile group 222

LIST OF TABLES

Table 2.1 Abridged list of laboratory investigations on dynamic properties of soils -----12
Table 2.2 Parameters affecting shear modulus and damping ratio of soils (modified after Hardin and Drnevich 1972; Bai 2011)----------15
Table 2.3 Studies on dynamic characterisation of Indian soils through laboratory tests -20
Table 2.4 Studies on empirical formulations for strain dependent dynamic soil properties ----------29
Table 2.5 Various researchers' contribution to evaluate liquefaction potential of soils --34
Table 2.6 Widely used pore water pressure models ----------36
Table 2.7 Major seismic ground response studies in India ----------41
Table 2.8 Abridged summary of studies on behaviour of pile foundations in liquefiable soils ----------46
Table 3.1 Materials and their location 53
Table 3.2 Index properties of chosen soils 56
Table 3.3 Monotonic triaxial testing program 58
Table 3.4 Dynamic testing programme and the parameters of investigation 70
Table 4.1 BE tests and their loading conditions 91
Table 4.2 Output and G_{max} determination from a typical BE test.....92
Table 4.3 RC testing program and loading conditions 95
Table 4.4 DSS testing programme and loading conditions 106
Table 4.5 List of fitting parameters for various sands using Hardin's formulation 116
Table 4.6 Fitted parameters for Eqn. 4.1 116
Table 4.7 Regression results for G/G_{max} and D 120
Table 4.8 Summary of the CTX tests performed on BP sand specimens.....126
Table 5.2 Output and G_{max} determination from a typical BE test on PC specimen.....136
Table 5.3 RC testing programme and loading conditions 137
Table 5.4 DSS testing programme and loading conditions 139
Table 5.5 Best fit parameters for G/G_{max} and D of tested clays 145
Table 5.6 Summary of the CTX tests performed on PC.....148
Table 6.1 Sites chosen for the study 155
Table 6.2 Design soil profile of Saraighat Bridge site (Site-1) 165

Table 6.3 PWP model parameters for sand layers of four chosen sites 168
Table 6.4 List of analysis performed and parameters of investigation 171
Table 6.5 Comparison of percentage difference in surface PGA using different soil curves 173
Table 7.1 Design soil profile of Site-3 (Tezpur).....206
Table 7.2 Pile geometry and material properties 207
Table 7.3 Nonlinear analysis programme in SAP2000.....208

NOTATIONS AND ABBREVIATIONS

Δu	Excess pore water pressure
$\Delta\sigma'_c$	Change in effective confining pressure
α, β	Hyperbolic curve fitting coefficients
$A_1 \ldots A_{n+1}$	Amplitude of free-vibration curve
B-value	Skempton's B-parameter
CSR	Cyclic stress ratio
C	Cohesion
C_c	Coefficient of curvature
C_u	Coefficient of uniformity
C_L *and* C_R	Foundation flexibility coefficients
C_1, C_2, C_3	Functions of curvature coefficient
D	Damping ratio
D_{10}	10% of particles are finer than this size
D_{30}	30% of particles are finer than this size
D_{50}	50% of particles are finer than this size
D_{60}	60% of particles are finer than this size
D_{min}	Minimum damping ratio
D_{mas}	Masing damping
DU_{liq}	Duration of liquefaction
e	Void ratio
E_{sec}	Elastic modulus
f	Loading frequency
ϕ	Friction angle
F	High strain damping cap
f_{nz}	Fundamental frequency
f_{fb}	Fixed base fundamental frequency
$F(e)$	Function of void ratio
G_s	Specific gravity
G_1	Initial shear modulus for bilinear model
G_2	Critical state shear modulus for bilinear model
G	Secant shear modulus
G/G_{max}	Normalized shear modulus
G_{max}	Maximum shear modulus
H	Lateral load
K	Stiffness of foundation
K_e	Elastic stiffness
K_L	Lateral stiffness
K_R	Rocking stiffness
K_{LR}	Coupled stiffness
K_V	Vertical stiffness
L	Length
M	Moment
m	Pressure dependent coefficient
M_w	Moment magnitude of earthquake
N_s	Stress-scaling factor

M_s	Strain-scaling factor
N	Number of cycles
N_L	Number of cycle to liquefaction
L_{eff}	Effective length of the specimen
λ	Wavelength
η_L, η_R, η_{LR}	Foundation stiffness parameters
r_u	Excess PWP ratio
R_d	Relative density
w	Water content, used to prepare cohesive soil specimen
γ	Cyclic shear strain amplitude
γ_h	Hyperbolic shear strain
γ_{ref}	Reference shear strain
γ_{max}	Maximum shear strain
γ_{tl}	Elastic threshold shear strain
$\gamma_{take\text{-}off}$	Take off shear strain
σ'_c	Effective confining pressure
$\sigma'_{m\text{-}i}$	Effective confining stress of each minor layer
q_{cyc}	Single amplitude cyclic deviatoric stress
$q_{d,\,max}$	Maximum or peak deviatoric stress
τ	Shear stress
p	Soil resistance
p'	Mean effective confining pressure
P_{atm}	Atmospheric pressure (≈101 kPa)
ρ	Density
τ_{max}	Maximum shear stress
T_s	Arrival time of the shear wave
y	Pile displacement
ϕ	Internal frictional angle of soil
V_s	Shear wave velocity
$V_{s\text{-}30}$	Average shear wave velocity of surficial 30 m of soil deposit
API	American Petroleum Institute
BE	Bender element
BP	Back pressure
BNWF	Beams on nonlinear Winkler Foundation
BP	Back pressure
BP sand	Brahmaputra sand
BG sand	Bongaigaon sand
CP	Cell pressure
CDC	Compact dynamic controller
CPT	Cone penetration test
CSR	Cyclic stress ratio
CTS	Cyclic torsional shear
CTX	Cyclic triaxial
CU	Consolidated undrained
DA	Double amplitude
DSS	Dynamic simple shear
EI	Flexural stiffness
EA	Axial stiffness
EQL	Equivalent linear

FAR	Fourier amplitude acceleration
FDM	Finite difference model
FEM	Finite element model
FESEM	Field emission scanning electron microscope
GRA	Ground response analysis
GSD	Grain size distribution
I, II, III, IV, V	Seismic zoning identification of India
KS	Kasai
OCR	Over consolidation ratio
OWT	Offshore wind turbine
OMC	Optimum moisture content
LVDT	Linear variable differential transducer
LL	Liquid limit
MASW or SASW	Multi or single channel analysis of surface waves
MDD	Maximum dry density
MKZ	Modified Kondner Zelasko
NL	Nonlinear
PBRA	Peak bedrock acceleration
PC	Pachoria Cohesive
PGA	Peak ground acceleration
PSA	Peak spectral acceleration
PL	Plastic limit
PI	Plasticity index
PWP	Pore-water pressure
RC	Resonant column
RS	Red soil
S	Soil stiffness coefficient
SAGE	Surrey advanced geotechnical engineering
SHA	Seismic hazard assessment
SL	Saloni
SSSI	Seismic soil structure interaction
SP	Poorly graded sand
SPT N	Standard penetration resistance value
SPSI	Soil pile structure interaction
USCS	Unified soil classification system
UU	Unconsolidated undrained
YC sand	Yamuna coarse sand
YF sand	Yamuna fine sand

CHAPTER I. INTRODUCTION

1.0 PREAMBLE

Despite the advent of scientific technology and improved understanding of the effect of earthquakes on structures, numerous failures during seismic events, have been witnessed in the recent past. As there is no effectively established scientific approach in estimating the source and magnitude of an earthquake till date, it is of engineering body's concern to design the structures as seismic resistant as possible, based on the knowledge accumulated over the past decades. It is mostly the failure of structures such as buildings, bridges, etc. that leads to widespread destruction during earthquakes. Fig. 1.1 depicts the tilted building due to the dynamic failure of underlying soil during 1999 Kocaeli earthquake in Turkey. Similarly, Fig. 1.2 shows the unseated concrete decks from the piers of Tubul Bridge during 2010 Chile earthquake. Many such collapses were reported in literature, despite being structurally intact, the failure was witnessed in the foundation, for example, famous Showa Bridge failure in Japan during the 1964 Niigata earthquake (Yoshida et al. 2007; Bhattacharya et al. 2014) and collapsed Nishinomia-Ko Arch Bridge in Japan during 1995 Kobe earthquake (Anastasopoulos et al. 2008).

Fig. 1.1 Example of foundation failure due to seismic soil liquefaction in Adapazari region of Turkey during 1999 Kocaeli earthquake (after Sezen 2000)

Fig. 1.2 (a) Elevation and **(b)** Sectional views of collapsed Tubul Bridge during Chile earthquake (after Yashinsky et al. 2010)

All such failures invoke a primary question to the scientific community: whether the adopted seismic resistant design underperformed or the fundamental behaviour of foundation soil less understood in seismic conditions?

Any effective earthquake resistant design should comprehensively consider the structural phenomenon as well as the underlying soil behaviour as it is not only the structure that proves to be volatile during seismic event, but also the underlying soil which dictates the seismic stability of overlying structure. During any seismic event, induced waves travel through the earth's crust before reaching ground surface and during the travel, waves interact with many layers of soil/rock and often get modified (amplify or attenuate). Such wave modification depends on the soil characteristics along with the ground motion parameters. Fig. 1.3 schematically presents the path of seismic waves from a source to the ground surface. At a site of interest, the wave path along the depth depends on the local soil conditions, and hence understanding the dynamic behaviour of underlying soil stratum is essential for effective seismic resistant design of new structures or requalification studies of existing structures. Fig. 1.4 present the various stages for a strategic seismic analysis as

proposed by Krishna et al. (2014). It can be understood from Fig. 1.4 that the investigation of local soil conditions against dynamic loads is critical for ground response studies, liquefaction assessment and also foundation stability analysis in the framework of seismic analysis of a structure.

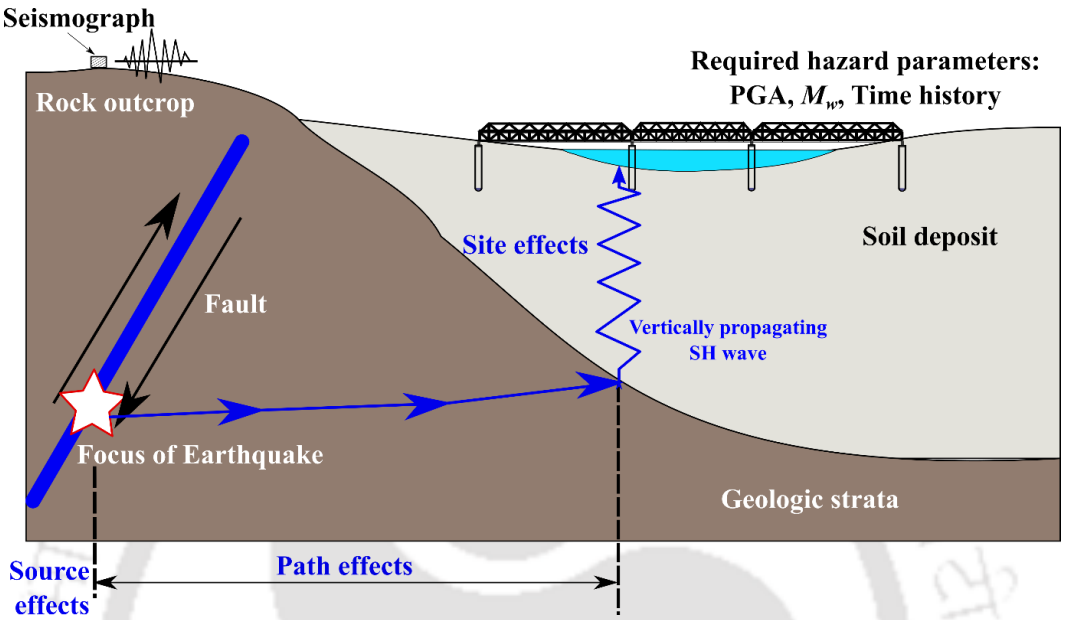

Fig. 1.3 Schematic representation of seismic body wave travel

1.1 DYNAMIC SOIL CHARACTERISATION

Dynamic behaviour of soils is a complex phenomenon, due to its dependence on many influencing parameters (Seed and Idriss 1970; Kumar et al. 2014) and is represented by dynamic soil properties and liquefaction parameters. Dynamic soil properties include the shear modulus and damping ratio, while liquefaction parameters are quantified by the induced pore water pressures and resulting accumulated strains. The dynamic soil behaviour is evaluated through field or laboratory tests. Field tests involve the measurement of wave velocities propagating through the soil or the response of soil structure systems to dynamic excitation (Saran 1999). Some of the widely used field tests include: analysis of surface waves (MASW, SASW), seismic cross/up/down borehole surveys, etc. Laboratory tests are classified based on the range of strain levels they deal with: low strain stiffness of soils (bender element test, resonant column test) and high strain behaviour (dynamic simple shear test, cyclic triaxial test, and cyclic torsional shear test). Each of these tests has their own inherent advantages and limitations, which makes the selection of proper testing more vital.

Unlike concrete or steel or any artificial materials which are homogeneous and uniform in general, soil is heterogeneous due to its composition and its dynamic behaviour is also

soil-specific. Many regions often contain soils of typical characteristics due to their origin and formational properties and in this view, several researchers pointed the need of having region-specific dynamic characteristics of soils for efficient seismic resistant design (Hanumantharao and Ramana 2008; Chattaraj and Sengupta 2016; Kirar and Maheswari 2017).

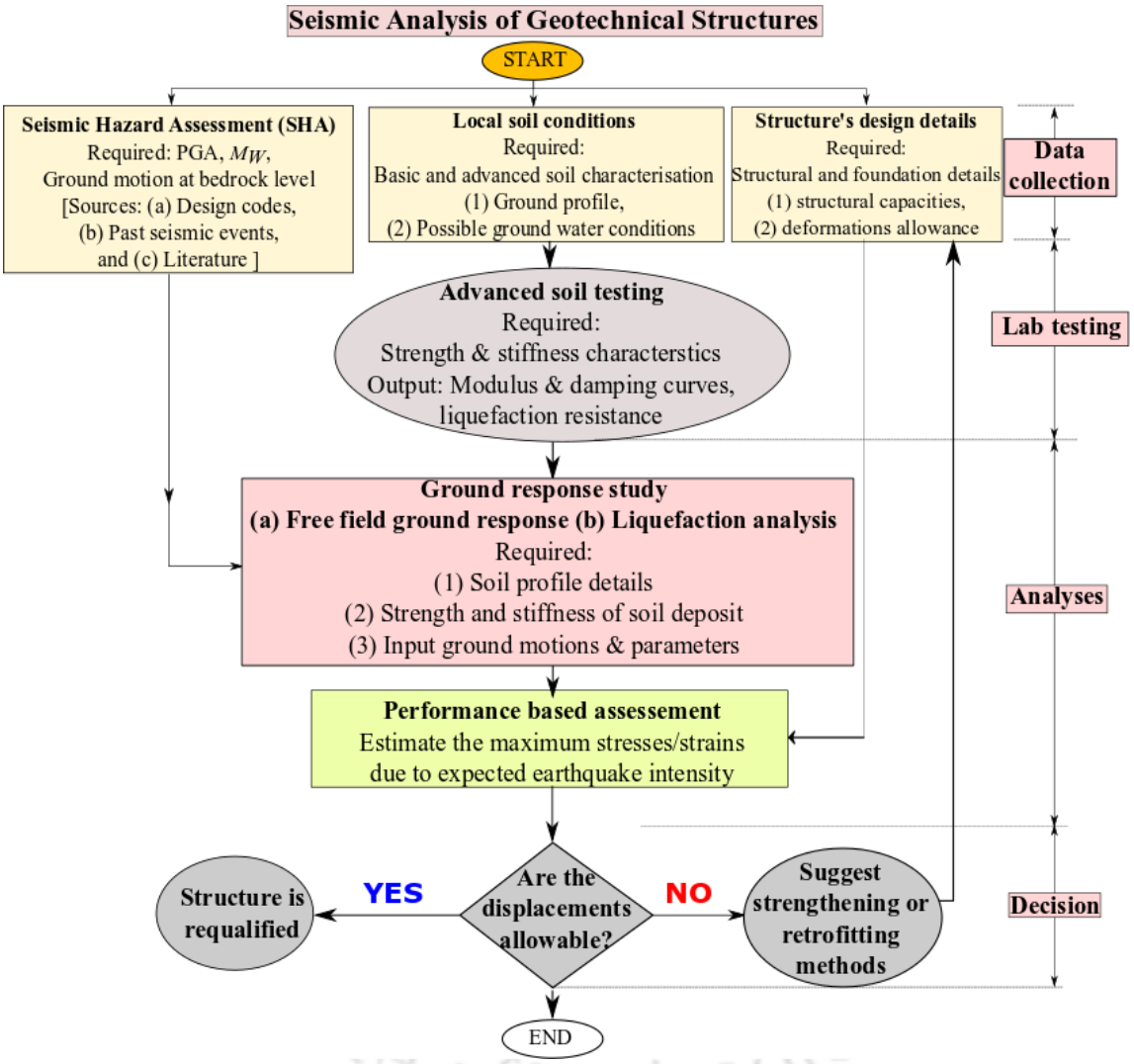

Fig. 1.4 Flow chart of seismic analysis/requalification strategy for geotechnical structures (modified after Krishna et al. 2014)

Based on these observations, the dynamic behaviour of six different soils sampled from two active seismic regions of India (north and northeastern India) are focused in the present study. North and northeastern India witnessed significant earthquakes in the recent past with moment magnitude (M_w) ranging up to 8.8, causing severe destruction to human and built environment. The proximity to Himalayan seismic belt and the continuous deformation of Indian plate and Eurasian plate towards north, makes these regions highly seismic prone (Kayal et al. 2012). In addition, researchers warn of a potential earthquake

in the region owing to the seismic gap (Khattri 1999). With such intense seismic proximity and increasing infrastructure development, investigation of dynamic behaviour of soils of these regions is essential, both for design of new structures and for requalification studies of existing important structures.

1.2 SEISMIC ANALYSIS OF DEEP FOUNDATIONS

Deep foundations are the preferred foundations for supporting heavy superstructure loads and in case of problematic surficial soils. Piles and caissons are the widely used deep foundations and many important structures such as high rise buildings, bridges, offshore wind turbines, etc. are supported by such foundations. Fig. 1.5 (a) depicts crude classification of deep foundations based on slenderness ratio. The stability analysis of deep foundations has been well established in static loading conditions. However, the dynamic behaviour of deep foundations is still a subject of debate for geotechnical engineers, due to the numerous failures observed during natural calamities (earthquakes, floods and tsunamis). Fig. 1.5b and Fig. 1.5c are few examples manifesting the devastating effects of seismic loads on deep foundation supported structures. Most of such failures are attributed to the problematic soils (liquefiable soils in case of earthquakes) or incompetent foundation design (Hamada and O'Rourke 1992; Mylonakis et al. 2006). As piles or caissons extend to deeper stratum, the dynamic characteristics of multi-layered soils (possible sandwiched soft layers) and resulting soil-structure interactions are often detrimental (Mylonakis and Gazetas 2000).

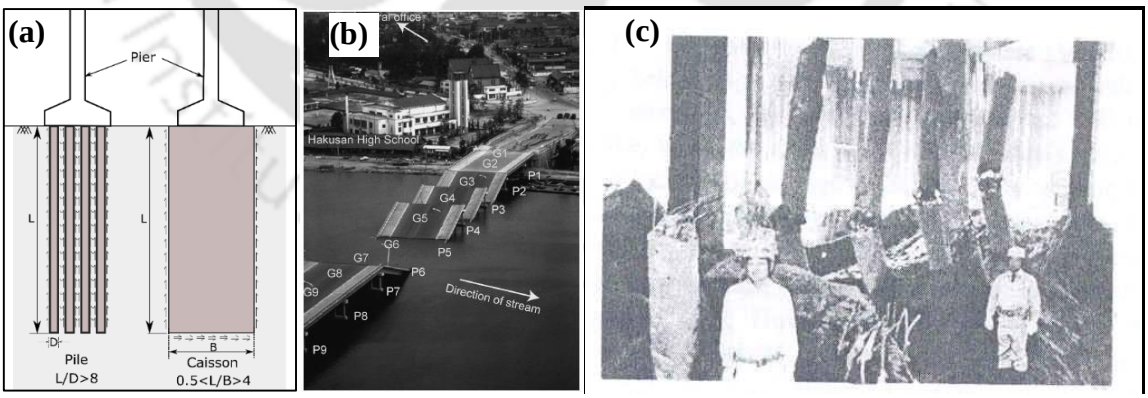

Fig. 1.5 (a) Crude slenderness ratio based classification of flexible pile and rigid caisson foundations (modified after Gerolymos and Gazetas 2006) **(b)** Collapsed Showa Bridge in Japan during 1964 Niigata earthquake (after Yoshida et al. 2007) **(c)** Pile failure observed during the excavation of NHK building after 1964 Niigata earthquake in Japan (after Kawamura et al. 1985)

Seismic analysis approaches for deep foundations vary from simple elastic to complex nonlinear methods and their selection is guided by the importance of the project. Despite the fact that advanced nonlinear approaches (such as continuum finite element, finite difference, and boundary element models) provide accurate results, they involve high computational effort and budgetary constraints due to which their adoptability is often limited to theoretical understanding rather than practical application. Simplified Winkler spring approach (Winkler 1867; Hetenyi 1946) is a widely used and globally accepted method for performing seismic analysis of structures considering the soil structure interaction (SSI) phenomenon. A nonlinear seismic analysis of any structure can be reliably assessed using the Winkler approach (Nogami et al. 1992; Wang et al. 1998). In this approach, surrounding soil is modelled as independent discrete springs and the foundation and structure are simulated as linear or nonlinear elements. This is a decoupled analysis whereby the nonlinear soil displacements for a given input motion are evaluated first based on the free field ground response, and the results will be applied to a Winkler model to obtain the seismic response of the structure (Boulanger et al. 1999; Tombari et al. 2017). With efficient dynamic soil characterisation and simplified Winkler modelling, seismic safety of deep foundations can be assessed following the strategy shown in Fig. 1.4.

1.3 BROAD OBJECTIVES OF THE STUDY

Main objective of the study is to investigate the dynamic properties of soils collected from two active seismic regions of India and establish region-specific soil parameters for application in seismic site response studies and seismic analysis of pile foundations. Total of six soils are sampled from two active seismic regions of India: four sands (two from Guwahati city of northeastern India, a highly active seismic zone and the rest from Haryana region, a moderate seismic zone from northern India) and two cohesive soils (from Guwahati city). Independent laboratory element testing techniques are employed to comprehensively characterise the chosen soils for their dynamic soil properties and liquefaction potential. Empirical formulations are developed based on the experimental results. Demonstration of experimentally obtained soil properties in seismic ground response studies and seismic analysis of pile foundations is performed.

1.4 ORGANIZATION OF THESIS

The present thesis is divided in to 8 chapters. After the introduction to the subject in the first chapter, further chapters are divided as follows:

Chapter 2 provides a detailed review of studies pertinent to the dynamic behaviour of soils, seismic ground response analysis and seismic analysis of deep foundations. The chapter concludes with a critical appraisal of literature and a detailed scope of the work.

Chapter 3 describes in detail the soil materials chosen, their basic characterisation and the monotonic response evaluated from triaxial tests. The adopted experimental approaches along with the details of equipment, principles of testing, testing program and basic outcome from each apparatus is clearly presented.

Chapter 4 presents the dynamic behaviour of cohesionless soils and the results are presented in terms of strain dependent dynamic properties and liquefaction parameters.

Chapter 5 presents the results obtained pertaining to the dynamic behaviour of cohesive soils and relevant analysis and discussions are presented.

Chapter 6 presents the seismic ground response studies performed for four different sites based on the established dynamic soil properties and liquefaction parameters.

Chapter 7 investigates the seismic behaviour of two pile foundation configurations (single and 2×2 pile group) using dynamic BNWF approach.

Chapter 8 summarizes the critical findings obtained from the study, limitations of the work and identifies the areas for future research.

CHAPTER II – LITERATURE REVIEW

2.0 INTRODUCTION

This chapter presents a consolidated view of the literature review based on broad objectives of the study. The chapter is categorized in to three main sections. The first section discusses the studies on dynamic behaviour of soils evaluated using various laboratory techniques. Second section describes the application aspects of dynamic soil behaviour in seismic ground response studies. Studies pertaining to the dynamic behaviour of soils of India are reviewed along with the major seismic site response studies of some Indian cities. The third section reviews the studies on dynamic behaviour of pile foundations and the simplified modelling techniques available for soil structure interaction. The chapter concludes with a summary of the literature along with the objectives and scope of the present research work.

2.1 DYNAMIC SOIL BEHAVIOUR

As the stability of structures during earthquakes is dictated by the strength of underlying soil, investigation of the response of soils to seismic loading is essential. Understanding the dynamic response of soils is complex due to the significant number of parameters involved (Seed and Idriss 1970; Kumar et al. 2014). Traditionally, response of soils to dynamic loads is represented using strain dependent dynamic soil properties and liquefaction potential. The strain dependent dynamic soil properties include maximum shear modulus (G_{max}), secant shear modulus (G) and hysteretic damping (D) of soil. As globally known, soil behaves linearly elastic in the low strain range (strains≈0.001%), and possesses the maximum shear strength, often represented using G_{max}. However, with increase in the induced shear strains (γ), inelasticity is exhibited and dynamic shear strength (hereafter referred as secant shear modulus, G) decreases due to the loss of interparticle contact (Drnevich et al. 1967). At large strains, nonlinearity of the soil is exhibited, resulting in significant reduction in G. The rate of reduction of shear modulus with respect to G_{max} is called the normalized shear modulus reduction curve (G/G_{max}). In contrast, damping of the soil (measure of energy dissipated to stored) is minimum at low strains and increases with strains based on the stress-strain response (Kramer 1996). The variation of damping ratio with shear strain is termed as damping curve. The G_{max} combined with the variation of G/G_{max} and D over wide range of γ (from very low strains,

0.001% to strains beyond 5%) are traditionally termed as the strain dependent dynamic soil properties. Any seismic analysis study desirous of incorporating the realistic nonlinearity of the soil must consider these strain dependent dynamic soil properties. Fig. 2.1 schematically presents the typical variation of strain dependent dynamic soil properties (G/G_{max} and D with γ). Similarly, liquefaction potential of soil must also be assessed in case of soils in seismically active regions. Liquefaction of soils is a phenomenon mostly witnessed in saturated sandy soils whereby the shear strength of soils is lost due to the sudden rise of pore pressures expected in dynamic undrained loading conditions such as earthquakes or blast loads (Seed and Lee 1966).

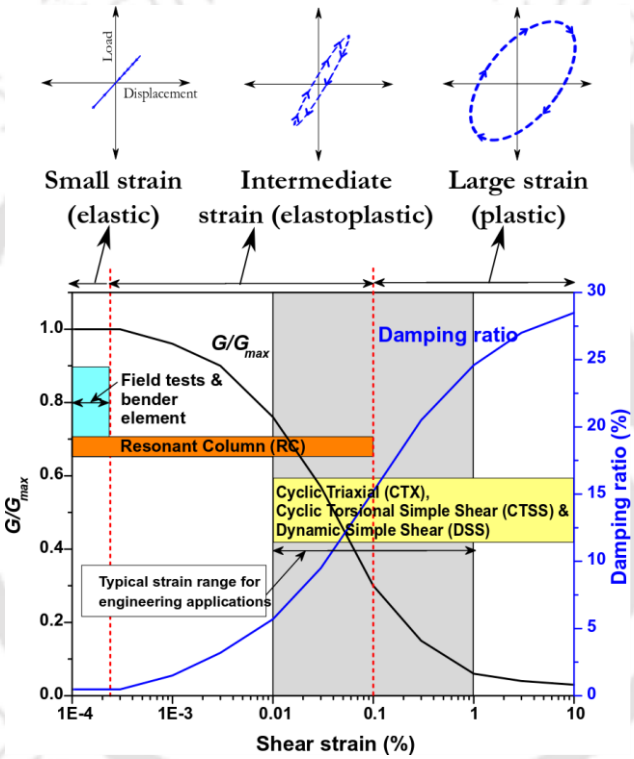

Fig. 2.1 Typical representation of dynamic soil properties and the testing techniques

Numerous laboratory and field testing techniques are available for evaluating the dynamic response of soils. Field tests generally involve the measurement of wave velocities propagating through the soil or the response of soil structure systems to dynamic excitation (Saran 1999). Some of the widely used field tests are: spectral or multichannel analysis of surface waves (SASW/MASW) (Park et al. 1999), seismic cross/up/down borehole surveys (Stokoe and Woods 1972), cyclic plate load test and block vibration tests (Saran 1999). Despite the fact that the field tests provide reliable in-situ properties, their application is relatively limited in soil dynamics due to the large scale of testing involved and high skillset required. In addition, field tests can only provide the dynamic stiffness at

very low strains (through wave velocities interpretation) and damping characteristics cannot be estimated. Laboratory element tests are considered as the potential superseders due to their ease of handling and ability to simulate different types of loading conditions (such as different void ratios, effective confining pressures and strain amplitudes). Some widely used laboratory element tests include: piezoelectric bender element (BE) test (Shirley 1978), resonant column (RC) test (Iida 1938; Hardin 1970), cyclic triaxial (CTX) test (Seed and Lee 1966), dynamic simple shear (DSS) test (Peacock and Seed 1968), and cyclic torsional shear (CTS) test (Ishihara and Li 1972). All the mentioned element test techniques are strain-specific and can only assess the dynamic soil behaviour at particular range of strains (Fig. 2.1). Each of these testing techniques has their inherent advantages and limitations, and their applicability is dependent on the required output parameters (Kramer 1996). Further sections review the available studies pertaining to the dynamic soil properties and liquefaction behaviour through various laboratory testing techniques.

2.1.1 Laboratory Studies on Dynamic Soil Properties

Laboratory studies pertaining to the dynamic properties of soils have been initiated during 1960's (Hardin and Richart 1963) and with the advancement of technology and instrumentation since then, the techniques have been constantly evolving. Most of the laboratory tests meant to determine dynamic soil properties can be grouped in to two main categories:

1. Tests dealing with free or forced vibrations (axial, torsional, shear) such as BE and RC tests. The main principle of this type of tests is to induce a shear or compressional wave of relatively smaller magnitude and correlate it to the dynamic soil properties.

2. Tests involving direct determination of stress-strain response such as CTX, DSS and CTS. This type of tests deals with intermediate to large strains (from 0.01% to as high as 5%) and therefore, the dynamic soil properties can be estimated directly from the obtained stress-strain response.

Several researchers investigated the dynamic properties of various soils and determined the factors affecting them, employing different laboratory tests. Table 2.1 presents the laboratory investigations carried out by various researchers for determining the dynamic soil properties and the significant contributions drawn from each study.

Table 2.1 Abridged list of laboratory investigations on dynamic properties of soils

Investigators	Soil type	Test	Strain range	Major contribution
Drnevich et al. (1967)	Ottawa sand	RC	Strains <0.01%	Evaluated G_{max} and effects of number of cycles at low strain amplitudes; Increased G_{max} with increased loading cycles
Seed and Idriss (1970)	Cohesionless soils	Data collated till 1970	Strains < 1%	Proposed boundaries for modulus reduction and damping ratios for cohesionless soils; factors affecting dynamic soil properties highlighted
Kuriyabashi et al. (1975)	Dry and saturated sands	RC	Strains <0.02%	Insignificant effect of gradation, water content, particle shape on G_{max} of tested sands; High G/G_{max} and low D for increased effective confining pressures
Iwasaki and Tatsuoka (1977)	Sands with different grain size and fines content	RC	G_{max} various low strains	Effect of fines content and gradation properties on G_{max} in clean and artificial sands; G_{max} decreased with uniformity coefficient and fines content and increased with relative density and effective confining pressure
Iwasaki et al. (1978)	Japanese sands	RC and torsional shear (TS)	0.0001 to 0.01%	Proposed relationships for G_{max}, G/G_{max} and D with shear strain increase; G/G_{max} increased with loading cycles and effective confining pressure; insignificant effect of void ratio on G/G_{max}
Tatsuoka et al. (1978)	Clean and natural sands	RC and static TS	0.0001 to 0.01%	Effects of various parameters on D of sands are investigated; insignificant effect of void ratio, testing type on D for sands; decreased D for effective confining pressure and loading cycles
Kokusho (1980)	Sands	CTX	0.0001 to 0.1%	Evaluated dynamic soil properties of sands at small to high strains and reported the effect of fines on modulus reduction rate; insignificant effect of loading cycles on shear modulus, high G for low void ratio and high effective confining pressure
Chung et al. (1984)	Monterey sand No. 0	RC	0.0001 to 0.05%	Effects of specimen type (hollow or solid) and type of testing (single/multi stage) on G_{max}, G/G_{max} and D; G_{max} of hollow specimens higher and D_{min} is higher relative to solid specimens
Seed et al. (1986)	Sands and gravels	CTX	Strains <0.1%	Related initial shear moduli to shear wave velocity through standard penetration test (SPT) N value and proposed

Investigators	Soil type	Test	Strain range	Major contribution
				boundaries for modulus reduction and damping ratio of gravels
Ishibashi and Zhang (1993)	Data collected	----	----	Proposed G_{max}, G/G_{max} and D relationships. Developed a relationship between G/G_{max} and Damping ratio
Souto et al. (1994)	Sands and crushed gravel	RC and BE	Strains <0.0001%	Pointed out the limitation of both the testing; the effect of fines content on G_{max} and D_{min} is highlighted; BE tests and RC tests yield similar results up to effective confining pressures of 100 kPa
Matasovic and Vucetic (1994)	Saturated sands	Monotonic and CTX	Strains <1%	Proposed modified Kondner and Zelasko model for nonlinear response of saturated sands in liquefiable conditions; Masing criteria has been adopted for damping formulations
Lin et al. (1996)	Dry sands	CTX	0.004 to 0.01%	Determined the effect of frequency on the dynamic soil properties of sands; increased G_{max} and D; insignificant effect on G/G_{max}
Lanzo et al. (1997)	Sands and clays	DSS	0.001 to 0.04%	Estimate the effect of PI, OCR, effective overburden pressure, frequency of loading, silt content, and strain amplitude; increase in G for increased PI, OCR and effective confining pressure
Kiku and Yoshida (2000)	Toyoura sand	Cyclic torsional shear (CTS)	0.008 to 6%	High strain dynamic soil properties investigated; untraditional damping noted at high strains
Xenaki and Athanasopoulos (2003)	Sand with fines content	CTX	0.001 to 0.04%	Decreases the cyclic strength up to 30% of fines content by weight and then increases
Menq (2003)	Sands and gravels	RC	0.0001 to 0.02%	Effect of gradation properties, effective confining pressure, void ratio, fines content was investigated
Sitharam et al. (2004)	Saturated sands	CTX	0.05 to 5%	Effect of shearing strain and relative density nonlinear properties of sands
Govindaraju (2005)	Indian sands	CTX	0.15 to 1%	Influence of various parameters on dynamic soil properties and liquefaction resistance of Indian sands
Hanumantharao and Ramana (2008)	Silty sand	CTX	0.1 to 1%	Effect of fines content on the dynamic properties of sands; decreased G and D with increase in fines content of sands

Investigators	Soil type	Test	Strain range	Major contribution
Bai (2011)	Germany sands	RC and BE	0.0001 to 0.05%	Preloading increases the G_{max} of sands; G/G_{max} and D are not influenced by void ratio but highly affected by effective confining pressure
Kirar and Maheswari (2013)	Fibre reinforced sand	CTX	0.04 to 1.5%	Increase in fibre content decreased the G and increases D of sands
El Mohtar et al. (2013)	Sands mixed with Bentonite	CTX and RC	0.0001 to 1%	Bentonite in sands reduced the rate of reduction of shear modulus and increased the elastic behaviour of sands; Combined the results from RC and CTX and provided wide strain range dynamic soil properties
Kumar et al. (2014)	Saturated Assam sand	CTX	0.015 to 4.5%	Evaluated the influence of frequency, strain level, density and effective confining pressure on saturated sand specimens
El Mohtar et al. (2014)	Sands mixed with Bentonite	RC, static and CTX	0.0001 to 0.01%	Effect of Bentonite, aging on threshold shear strains and cyclic shear strength of soils; Increased G/G_{max} with increase in Bentonite content of soils; increased threshold for pore pressure generation with Bentonite content
Kumar (2018)	Northeast Indian sand and clay	CTX	0.015% to 5%	Focused on the parameters affecting high strain dynamic soil properties; Proposed a modified approach for considering high strain asymmetric behaviour of hysteretic loops in determining G and D
Torabi and Rayhani (2017)	Leda clay (Canada)	RC and DSS	0.001% to 7%	Established the comprehensive G/G_{max} and D properties of Leda clay and used the data in seismic ground response analysis
Chehat et al. (2018)	Champlain clay (Canada)	CTS	0.001 to 1%	Highlighted the dilative behaviour of clays at high strains; Proposed a modified Masing formulation for high strain G/G_{max} and D of clays
Park and Kishida (2018)	Earthen dam core materials	RC	0.0001 to 0.1%	Developed G/G_{max} and D data for core materials of earthen dams; undisturbed clay samples yielded higher G/G_{max} and lower D than Vucetic and Dobry (1991) ranges at similar plasticity levels

Factors influencing the dynamic properties of sands and clays ($G_{max,}$ G/G_{max} and D) deduced from experimental studies (as listed in Table 2.1) are summarized in Table 2.2. It can be understood that some of the listed factors are significantly affecting the dynamic properties of soils. Major factors affecting $G_{max,}$ G/G_{max} and D of soils is briefly reviewed below.

Table 2.2 Parameters affecting shear modulus and damping ratio of soils (modified after Hardin and Drnevich 1972; Bai 2011)

Increasing parameter	**Significance**					
	Clean sands			**Cohesive soils**		
	G_{max}	G/G_{max}	D	G_{max}	G/G_{max}	D
Strain amplitude	--	D	I&D	--	D	I&D
Effective confining pressure	I	I	D	I	I	D
Void ratio	D	NA	NA	D	NA	NA
Loading cycles	NA	NA	NA	NA	NA	NA
Degree of saturation	NA	NA	NA	SA	SA	SA
Over consolidation ratio	I	SI	SD	I	NA	NA
Plasticity	--	--	--	I	I	D
Frequency of loading	NA	NA	NA	NA	NA	NA
Gradation properties	SA	NA	NA	NA	NA	NA
Method of testing	NA	NA	NA	NA	NA	NA
Geologic age	NA	NA	NA	SA	I	D

Notes: I denotes increase; D denotes decrease; NA denotes not affected significantly; SA denotes slightly affected; SD denotes slightly decrease

Relative density (or void ratio), effective confining pressure (σ'_c), overconsolidation ratio (OCR) and plasticity index (PI) are the prime factors influencing the G_{max} of soils. Fig. 2.2 (a) depicts the effect of void ratio and σ'_c on G_{max} of sands as reported by Bai (2011). Void ratio decreases G_{max} linearly while σ'_c increases the G_{max} with a power-law (Hardin and Richart 1963; Iwasaki and Tatsuoka 1977). Bai (2011) based on RC and BE tests concluded that increase in relative density of the specimens (decrease in the void ratio) increases the particle-to-particle contact and thereby the quick propagation of shear waves, ultimately resulting in higher G_{max}. Bai (2011) also concluded that G_{max} values obtained by RC tests often yield higher results than BE tests, due to the assumed fixity conditions

and relatively large loading cycles in RC testing (Souto et al. 1994), see Fig. 2.2b for typical G_{max} results obtained from both the tests.

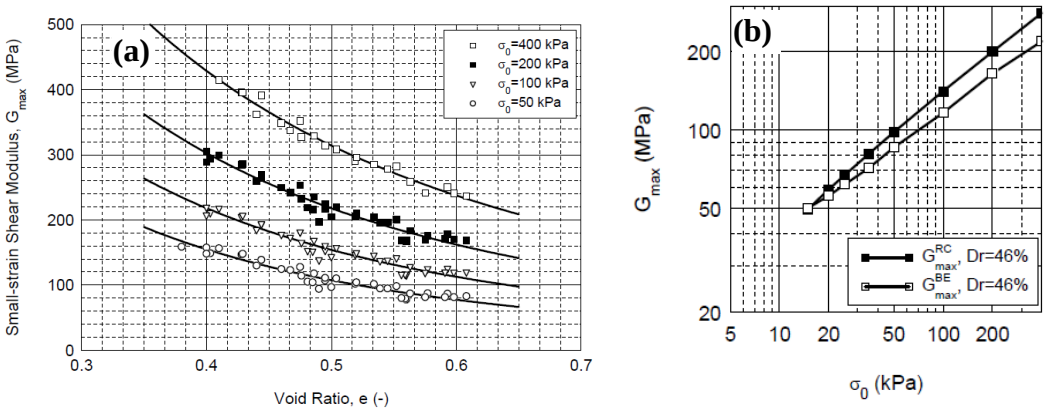

Fig. 2.2 (a) Effect of void ratio and effective confining pressure on G_{max} **(b)** Comparison of G_{max} of Berlin sand obtained from BE and RC tests (after Bai 2011)

Seed and Idriss (1970), Kokusho (1980) and Menq (2003) concluded that σ'_c increases the G/G_{max} and reduces D at a given shear strain while void ratio would slightly or negligibly affect the same, keeping all other conditions same.Fig. 2.3 depicts the effect of σ'_c and void ratio on G, G/G_{max} and D of sandy soils as reported by Kokusho (1980) and Darendeli (2001). This means that the deeper granular soils tend to have relatively high elasticity than the surficial sands, with all other conditions constant.

Few researchers focussed on the high strain (as high as 5%) dynamic behaviour of soils (Matasovic and Vucetic 1994; Kiku and Yoshida 2000; Kumar et al. 2017; Chehat et al. 2018). Fig. 2.4 presents the large strain dynamic behaviour of soils evaluated through laboratory tests by various researchers (Kiku and Yoshida 2000; Pagliaroli et al. 2018). An asymmetric stress-strain response has been observed for sands at large strains (Fig. 2.4c). In addition, untraditional damping ratio variation (increase and decreasing trend with shear strain) has also been reported (see Fig. 2.4c for sands and Fig. 2.4d for clays). Matasovic and Vucetic (1994) attributed such response to the dilative behaviour of soils in saturated undrained conditions.

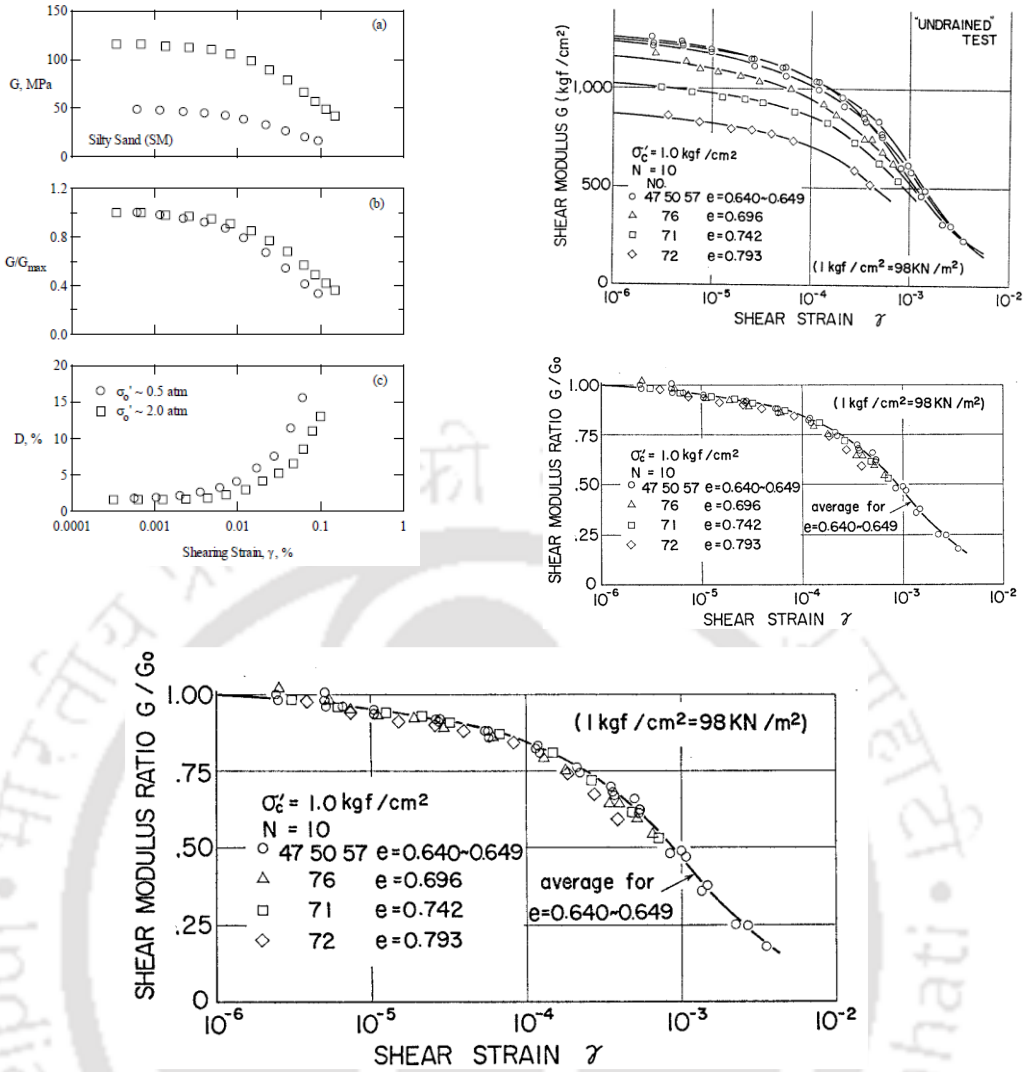

Fig. 2.3 Effect of σ'_c on **(a)** G, **(b)** G/G_{max}, **(c)** D (after Darendeli 2001) and effect of void ratio on **(d)** G, **(e)** G/G_{max}, **(f)** D (after Kokusho 1980)

After carefully reviewing the available literature on dynamic characterisation of soils worldwide, studies on dynamic behaviour of soils of India have been focused. Table 2.3 lists the prime studies conducted for dynamic characterisation of soils sampled from various regions of India. It can be seen that most of the studies focused on understanding the behaviour of soils from active seismic regions (zones IV and V as per IS:1893-2016). The reason being that most of these regions are often affected by mild to moderate (rarely large to great) seismic events and hence, understanding the dynamic behaviour of soils would help in effective seismic resistant design of structures. It must be noted that most studies only could provide the dynamic soil properties either in low strain range or in high strain range except the study of Chattaraj and Sengupta (2016). This was primarily due to the lack of proper experimental facilities. Fig. 2.5 shows the data of Indian sands collated

together and comparison of the data with Seed and Idriss (1970) and Darendeli (2001) ranges for sands. It must be noted that G/G_{max} data of some sands plot above the Seed and Idriss (1970) proposed range for sands and lower than the proposed range in case of D. However, many studies dealing with nonlinear response of soils in these regions adopt Seed and Idriss (1970) data, due to the lack of comprehensive dynamic soil properties (Govindaraju and Bhattacharya 2012; Choudhury et al. 2015; Kumar 2017).

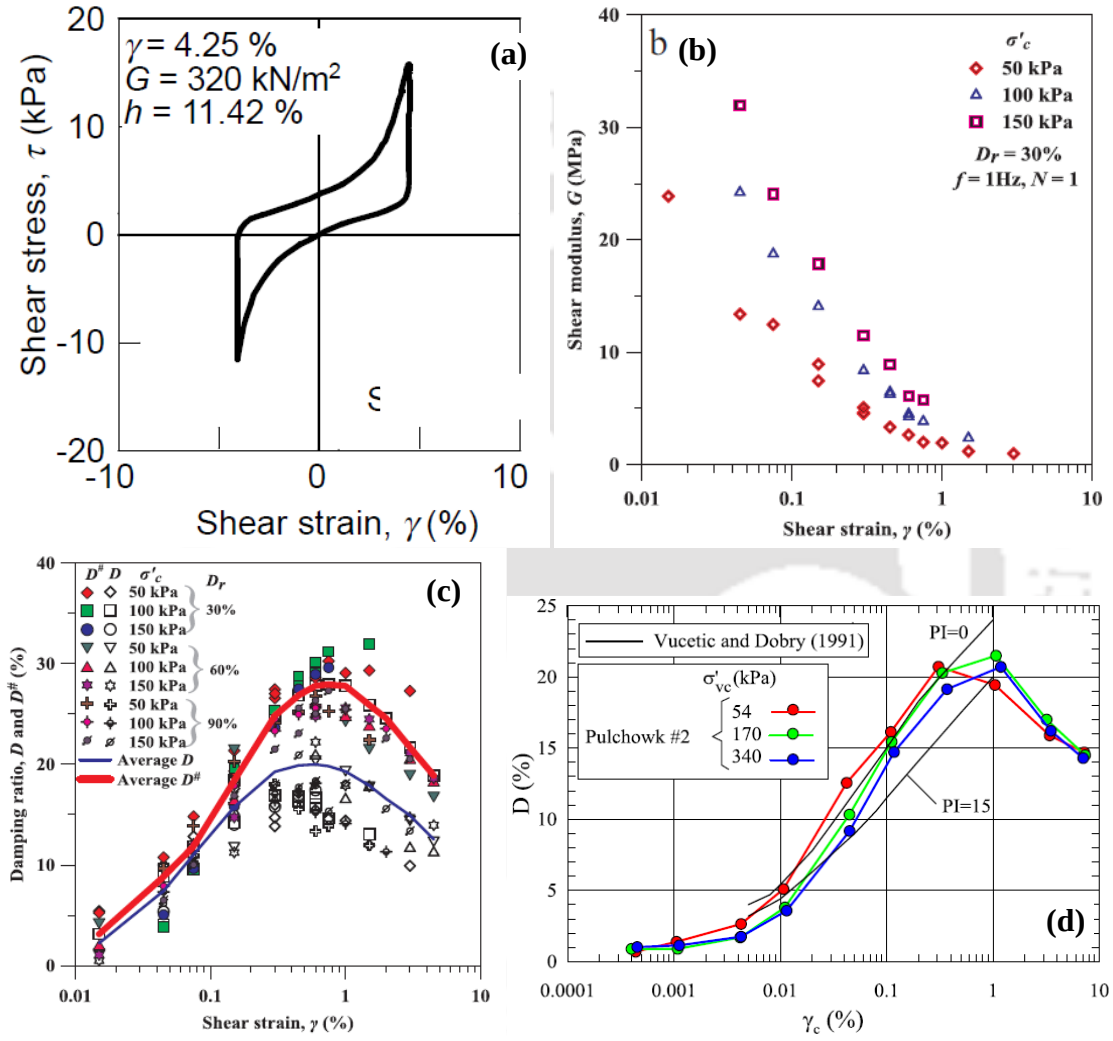

Fig. 2.4 Large strain dynamic behaviour of soils **(a)** after Kiku and Yoshida (2000) **(b)** and **(c)** after Kumar et al. (2017) and **(d)** after Pagliaroli et al. (2018)

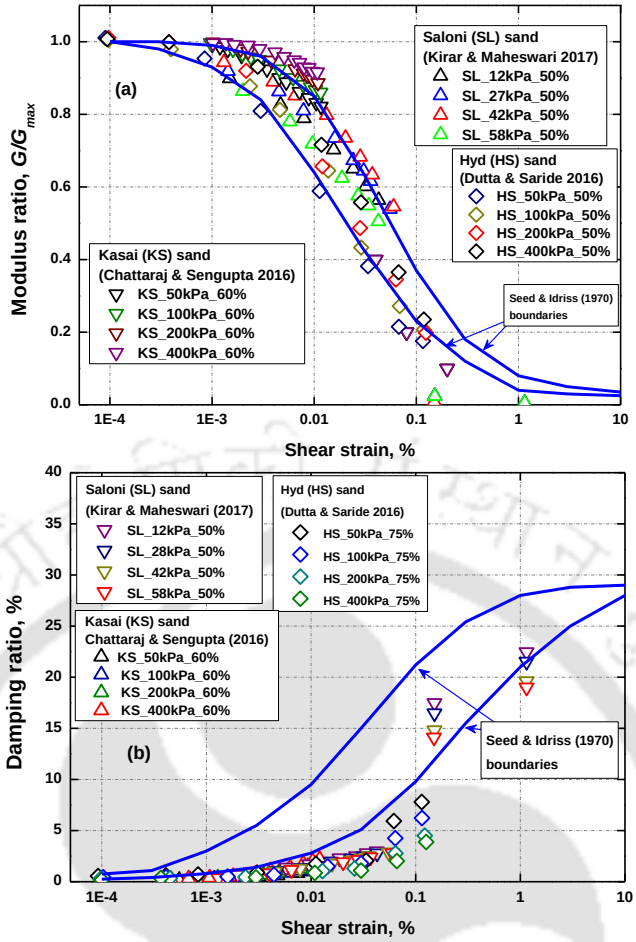

Fig. 2.5 (a) G/G_{max} and **(b)** D of Indian sands

Table 2.3 Studies on dynamic characterisation of Indian soils through laboratory tests

Author/s	Soil type	Location	Seismicity level	Apparatus utilised	Remarks
Sitharam et al. (2004)	Silty sand	Bhuj (Gujarat)	V	CTX	*G* and *D* (0.03% to 2%); liquefaction potential determined in terms of CSR and N
Govindaraju (2005)	Sands	Bhuj, Ahmedabad, Assam	IV, V	CTX	Dynamic soil properties and liquefaction potential determined in terms of CSR and N at different R_d and σ'_c
Hanumantharao and Ramana (2008)	Sand silt mixtures	Delhi	V	CTX	*G* and *D* (0.1% to 1%); Pore water pressure variation with loading cycles
Chattaraj and Sengupta (2016)	Clean river sand	West Bengal	IV	RC and CTX	*G* and *D* over wide strain range (0.01% to 0.2%) and liquefaction potential under different loading conditions; plot higher than Seed and Idriss (1970) G/G_{max} and lower than *D*
Kirar and Maheshwari (2017)	Mixed soils	Uttarakhand	IV	BE and CTX	*G* and *D* (0.03% to 1.5%) and liquefaction properties
Maheshwari and Kirar (2017)	Mixed soils	Uttarakhand	IV	RC	*G* and *D* (0.001% to 0.05%); fall higher than Seed and Idriss (1970) G/G_{max} and lower than *D*
Dutta and Saride (2016)	Clean sands	Hyderabad	III	RC	*G* and *D* (0.0001% to 0.1%); effect of various parameters on the Poisson ratio of sands was investigated
Kumar (2018)	Clean sand and clay	Assam	V	CTX	Established high strain properties and liquefaction potential

2.1.2 Studies on Comprehensive Dynamic Soil Properties

Geotechnical problems involving transient loads (or seismic) require the strain dependent dynamic soil properties over wide strain range (typically from 0.001% to about 5%), as the level of strains induced in the soil is unpredictable. Hinged on this, several researchers combined the data of dynamic soil properties obtained using either a modified equipment which can provide the data over wide strain range or by using two or more apparatus to achieve the desired properties over wide range of shear strains (Iwasaki et al. 1978; Kokusho 1980; El Mohtar et al. 2013; Chattaraj and Sengupta 2016; Subramaniam and Banerjee 2016; Torabi and Rayhani 2017). Some of the studies pertaining to the comprehensive dynamic characterisation of soils is briefly presented in this section.

Studies on comprehensive dynamic characterisation of soils were initiated by Seed and Idriss (1970). Data of dynamic soil properties available till 1970 were collated and design curves in terms of range of effective confining pressures (lower, mean and upper boundaries) have been proposed (Fig. 2.6). These curves are the first well defined data and have become the most sought-after data for many soil dynamics applications.

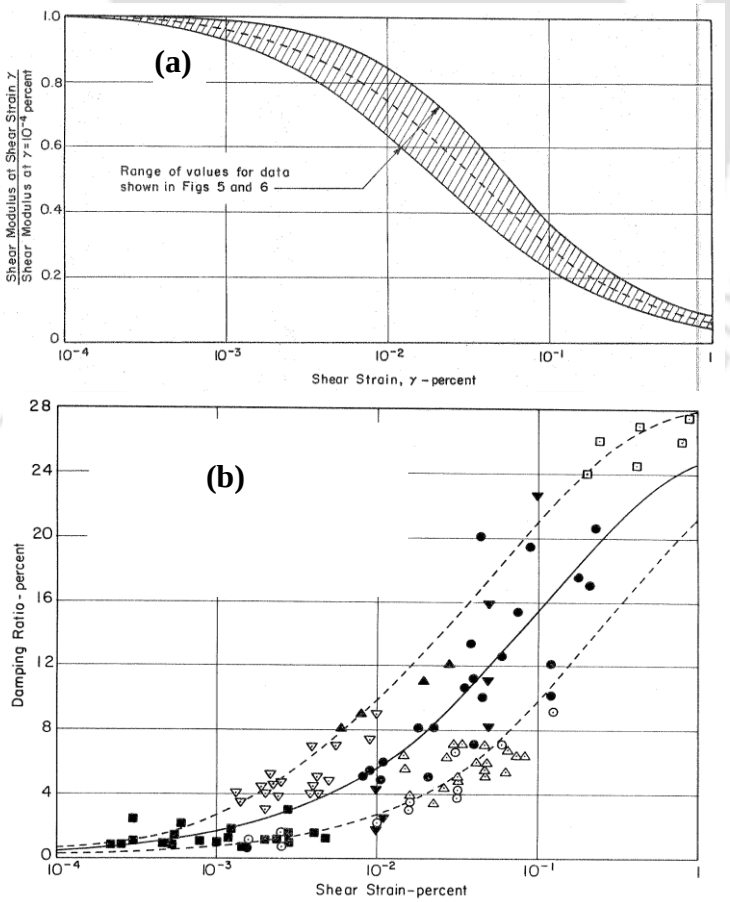

Fig. 2.6 Design **(a)** G/G_{max} and **(b)** D curves over wide strain range for sands (after Seed and Idriss 1970)

Iwasaki et al. (1978) adopted two apparatus: RC for strain range of 0.0001% to 0.01% and CTS for strains>0.01% for comprehensive characterisation of Japanese sands. The data obtained from independent tests were combined together to provide the range of dynamic soil properties over wide strain range at different effective confining pressures (Fig. 2.7). Kokusho (1980) modified the CTX apparatus by introducing additional sensors and transducers to facilitate the measurement of low strain dynamic soil properties (G_{max}) using CTX apparatus. This yielded reliable properties from a shear strain of 0.0005% to 0.2% (Fig. 2.3 d, e and f). Vucetic and Dobry (1991) collated the data on cohesive soils till 1991 and developed design charts which are a function of plasticity index and over consolidation ratio of clays (Fig. 2.8). These curves have become benchmark for cohesive soils since then for many earthquake geotechnical applications.

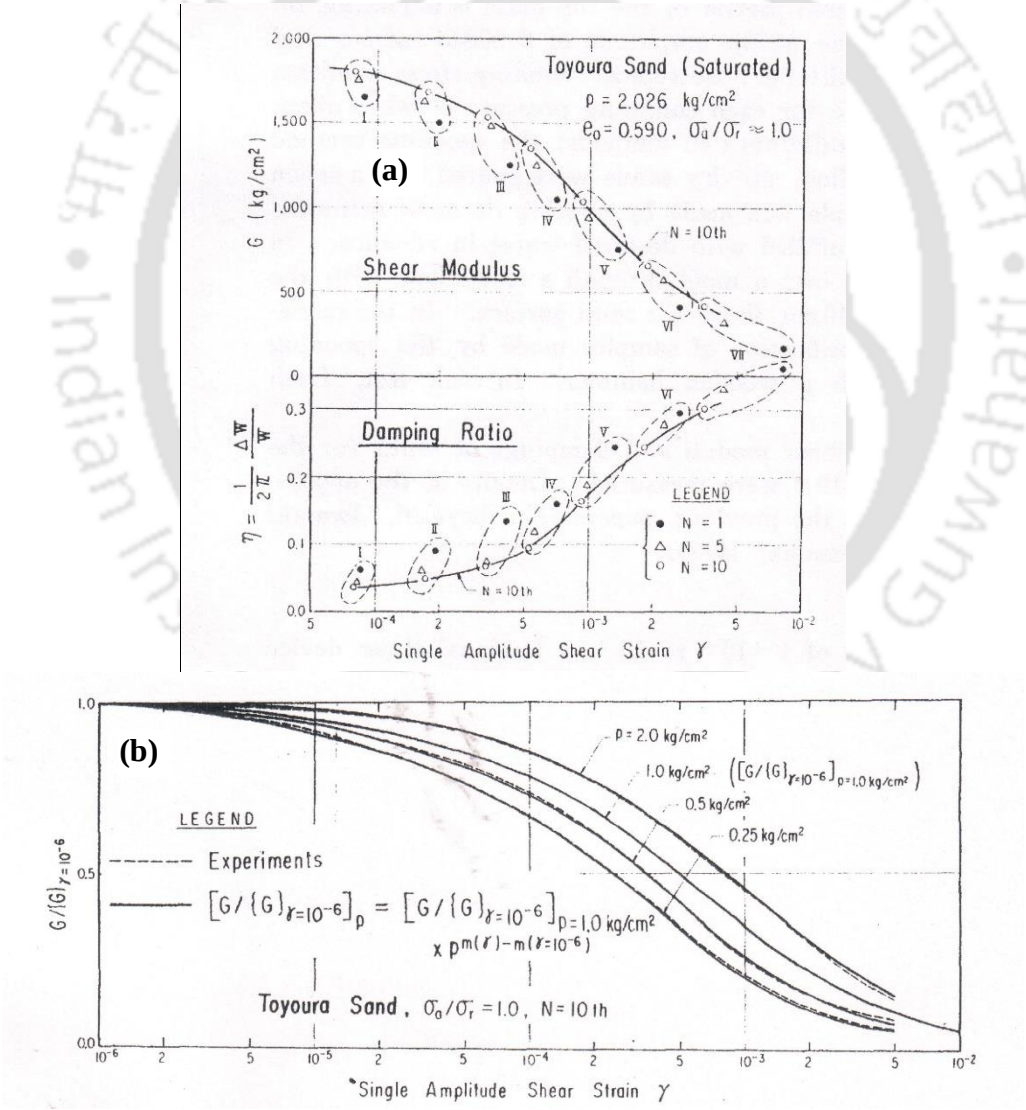

Fig. 2.7 (a) Dynamic soil properties from independent tests – RC and CTS **(b)** Combined G/G_{max} curves (after Iwasaki et al. 1978)

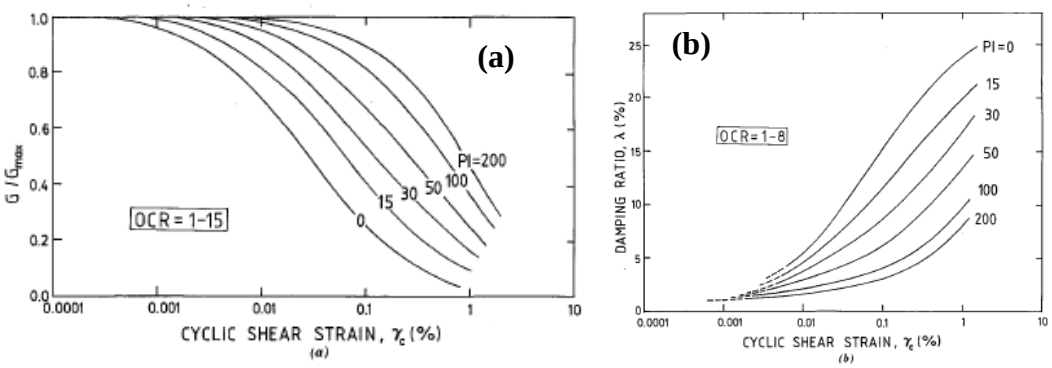

Fig. 2.8 Comprehensive **(a)** G/G_{max} and **(b)** D for clays (after Vucetic and Dobry 1991)

Darendeli (2001) performed extensive laboratory tests on undisturbed specimens of sands and clays, sampled from different regions of US. RC and CTS apparatus have been utilised to comprehensively characterise the dynamic soil properties over wide strain range (0.0001% to 0.8%), see for Fig. 2.9. A family of design curves both for sands and clays have been developed which are considered relatively stiffer than that of Seed and Idriss (1970) ranges. Interesting part from this study was that the curves were defined for very high effective confining pressures (1600 kPa) and simplified hyperbolic formulations also were proposed.

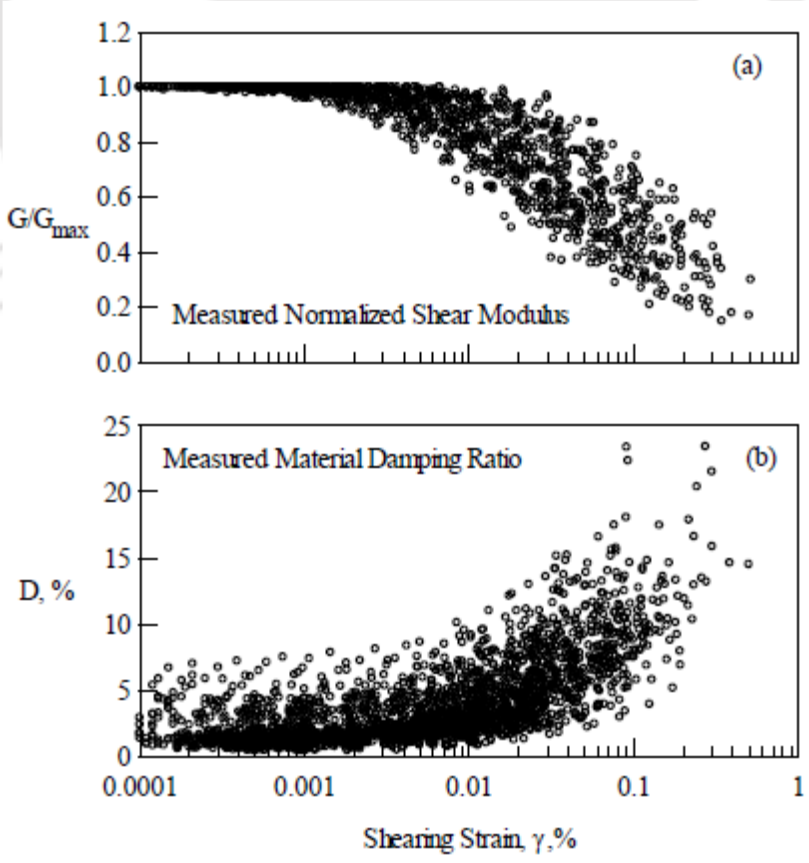

Fig. 2.9 (a) G/G_{max} and **(b)** D of sands measured by Darendeli (2001)

Bai (2011) utilised RC and CTS apparatus to understand the dynamic behaviour of sands and clays sampled from Germany and studied the effect of various influencing parameters. The results were finally combined together to provide design engineers the required data over wide strain ranges. Bai (2011) also pointed out that the ranges proposed by Seed and Idriss (1970) were relatively lower for G/G_{max} and higher for damping ratio. Yee et al. (2013) performed RC and CTS tests on samples collected from earthen dam core sections and investigated their dynamic behaviour in terms of G/G_{max} and D variation with shear strain. The sampled soils are mostly cohesive in nature and yielded higher G/G_{max} and lower D compared to the Vucetic and Dobry (1991) ranges for clays at comparable plasticity conditions. Fig. 2.10 presents the G/G_{max} and D variation for the investigated clays.

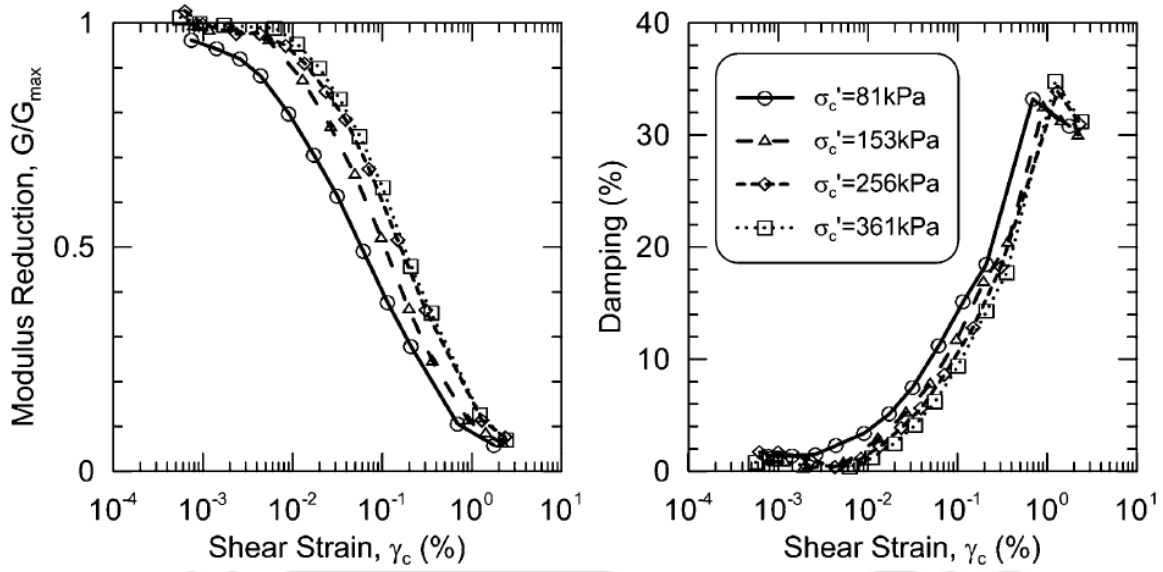

Fig. 2.10 G/G_{max} and D curves for earthen dam core materials (after Yee et al. 2013)

El Mohtar et al. (2013) performed RC (up to 0.02%) and CTX tests (beyond 0.02%) on saturated specimens of sand mixed with plastic fines and the results obtained were combined together for a comprehensive data (Fig. 2.11). It was pointed out that the results of G/G_{max} were in close range proposed by Seed and Idriss (1970) for sands. Chattaraj and Sengupta (2016) adopted two independent apparatus (RC for strains<0.01% and CTX tests beyond 0.01%) to evaluate the strain dependent dynamic soil properties and liquefaction parameters of Kasai river sand (India). The RC tests (low strain tests) were conducted on dry samples as the saturation is not a predominant factor for low strain dynamic soil properties (Saxena and Reddy 1989). The achieved results are then combined to provide the data over wide strain range (Fig. 2.12).

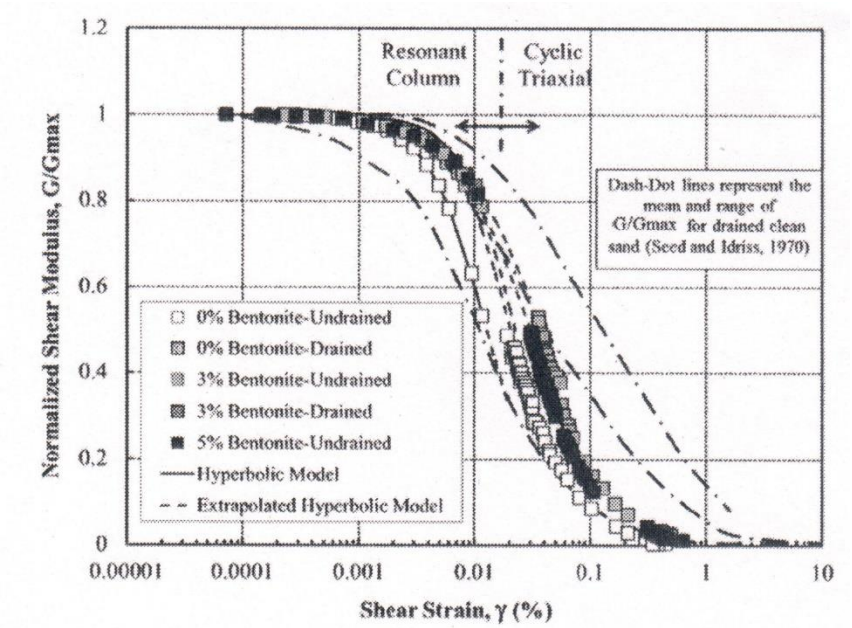

Fig. 2.11 G/G_{max} variation with shear strain for sand mixed with plastic fines (after El Mohtar et al. 2013)

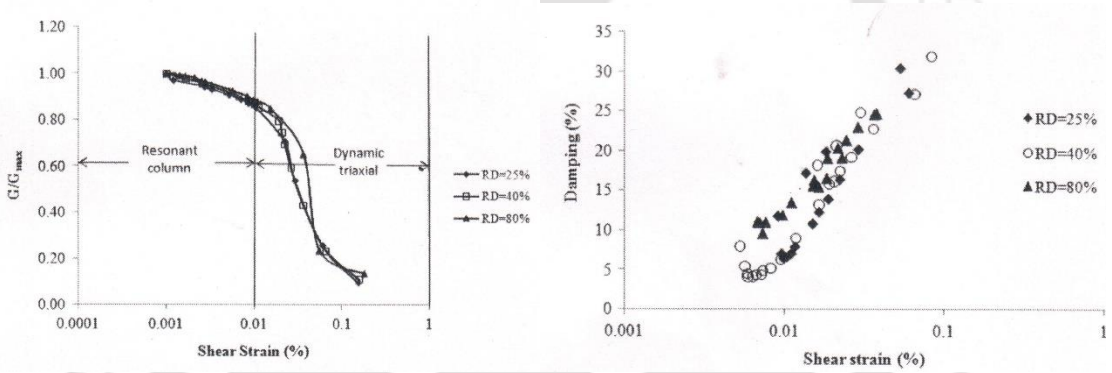

Fig. 2.12 Wide strain range dynamic soil properties of Kasai River sand (after Chattaraj and Sengupta 2016)

Kirar and Maheswari (2017) performed BE (for G_{max}) and CTX (from 0.03% to 1%) tests on sand samples collected from Uttarakhand region of India. Similarly, Torabi and Rayhani (2017) performed independent RC and cyclic simple shear (CSS) tests on clay samples collected from Leda region of Canada and the results are finally combined (Fig. 2.13). Chehat et al. (2018) adopted a modified cyclic torsional simple shear (CTSS) device which could provide the desired properties over wide range of shear strains (0.001% to 5%). Clay samples collected from Quebec (Canada) were tested and modified hyperbolic formulations to incorporate the high strain untraditional damping was proposed.

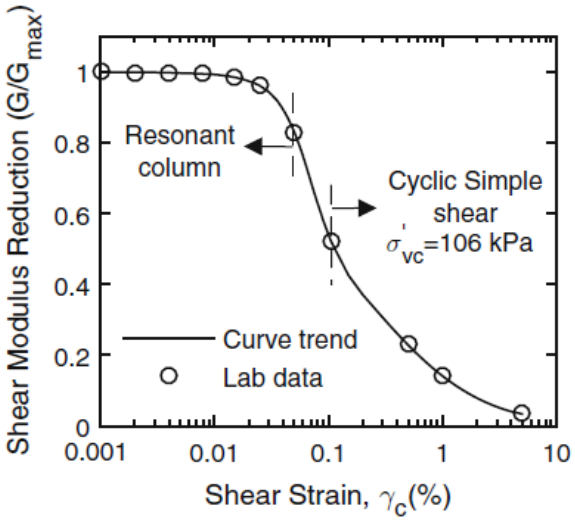

Fig. 2.13 G/G_{max} variation with shear strain for Leda clay (after Torabi and Rayhani 2017)

2.1.3 Empirical Formulations

Empirical formulations will be handy in the absence of experimental data. Various forms of empirical functions have been developed by many researchers worldwide to estimate both G_{max} and strain dependent dynamic soil properties, and are summarized in Table 2.4. Bai (2011) collated the available empirical forms and discussed their applicability. Some widely used forms of G_{max}, G/G_{max} and D are briefly reviewed below.

Maximum shear modulus (G_{max})

The G_{max} variation with effective confining pressure can be conveniently modelled using the power law (Drnevich et al. 1978; Chung et al. 1984). However to include other parameters in the formulation (as listed in Table 2.2), three basic forms of equations (Eqns. 2.1-2.3) have been developed by various researchers (Seed and Idriss 1970; Iwasaki and Tatsuoka 1977; Drnevich et al. 1978; Chung et al. 1984).

$$G_{max} = S \cdot F(e)\sigma_c'^{m} \quad \text{(Hardin and Richart 1963)} \quad (2.1)$$

$$G_{max} = S \cdot F(e) \cdot P_a^{1-m} \cdot \sigma_c'^{m} \quad \text{(Hardin and Drenvich 1972)} \quad (2.2)$$

$$G_{max} = 1000 \cdot F(e) \cdot K_{2-max} \cdot \sigma_c'^{m} \quad \text{(Seed and Idriss 1970)} \quad (2.3)$$

where S is a soil stiffness coefficient (depends on type of soil); $F(e)$ is void ratio function (defined differently by different researchers); m is the pressure dependent factor; P_a is the atmospheric pressure (can be considered as 101 kPa); σ'_c is the effective confining pressure; and $K_{2\text{-}max}$ is the maximum soil modulus coefficient, for sands it ranges from 30 to 75 and for gravels, it ranges from 80 to 180 (Seed et al. 1986). The empirical equations

along with the parameters (*S*, *m* and *F(e)*) are briefly summarized in Table 2.4 for various soils.

G/G*$_{max}$ *and Damping Ratio

Hardin and Drenvich (1970 and 1972) study is considered to be the first comprehensive study discussing the parameters controlling the nonlinear behaviour of soils through empirical formulations. Hyperbolic relationship (Eqn. 2.4) was employed to model the shear stress (τ) and shearing strain (γ).

$$\tau = \frac{\gamma}{\left(\frac{1}{G_{max}} + \frac{\gamma}{\tau_{max}}\right)} \tag{2.4}$$

where τ_{max} is the maximum shear strength of soil. Fig. 2.14a depicts a hyperbolic stress-strain relationship and the parameters defining the shape. Fig. 2.14b presents the typical stress-strain trends for sands and clays as presented by Hardin and Drenvich (1972).

Following the hyperbolic stress-strain relationship, *G/G*$_{max}$ can be modelled as per Eqn. 2.5.

$$\frac{G}{G_{max}} = \frac{1}{\left(1 + \frac{\gamma}{\gamma_{ref}}\right)} \tag{2.5}$$

where γ_{ref} represents the reference shear strain ($\frac{\tau_{max}}{G_{max}}$).

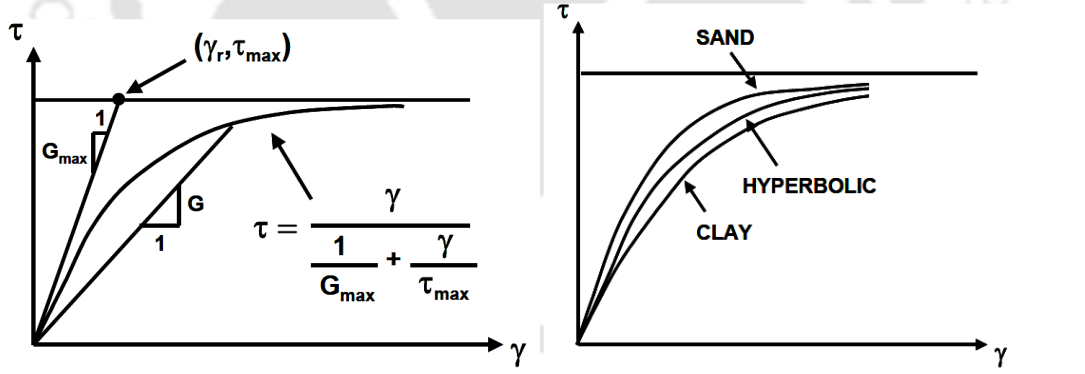

a. Hyperbolic stress-strain relationship

b. Effect of soil type on stress-strain relationship

Fig. 2.14 Hyperbolic stress-strain relationship of soils (after Hardin and Drenvich 1972)

Similarly, damping ratio was related to the *G/G*$_{max}$ (Eqn. 2.6) as essentially, damping is a quantifiable manifestation of stress-strain response of soil.

$$\frac{D}{D_{max}} = \frac{\left(\frac{\gamma}{\gamma_{ref}}\right)}{\left(1 + \frac{\gamma}{\gamma_{ref}}\right)} \tag{2.6}$$

where *D*$_{max}$ is the maximum damping ratio depending upon the soil type, effective confining pressure, loading cycles and loading frequency.

Having Hardin and Drenvich (1972) study as a benchmark, many other forms of G/G_{max} and damping ratio have been established by various researchers with slight or remarkable improvements (Table 2.4). The prime modification is the definition of reference shear strain (γ_{ref}). Stokoe et al. (1995) and Darendeli (2001) proposed that γ_{ref} can be conveniently considered at half the initial shear modulus (G/G_{max}=0.5) so as to reduce the number of unknowns in the equation. Similar modification was also adopted for clays by Zhang et al. (2005) and Vardanega et al. (2013).

Table 2.4 Studies on empirical formulations for strain dependent dynamic soil properties

Researchers	G_{max}	G/G_{max}	**Damping ratio**
Hardin and Black (1968) (For sands and clays)	$\frac{1230 \cdot (2.973 - e)^2}{(1+e)} \cdot (OCR)^K \cdot (\sigma_c')^{0.5}$	----	----
Hardin and Drenvich (1970) (Both clays and sands)	$\frac{3230 \cdot (2.97 - e)^2}{(1+e)} \cdot (OCR)^k \cdot (\sigma_c')^{0.5}$	$\frac{1}{1+\frac{\gamma}{\gamma_{ref}}}$	$\frac{D_{min} \cdot \left(\frac{\gamma}{\gamma_{ref}}\right)}{1+\left(\frac{\gamma}{\gamma_{ref}}\right)}$
Seed and Idriss (1970) (For sands)	$1000 \cdot K \cdot (\sigma_c')^{0.5}$	Proposed boundaries (lower, middle, upper)	
Hardin and Drenvich (1972) (Both clays and sands)	-----	$\frac{1}{1+\left(\frac{\gamma}{\gamma_{ref}}\right) \cdot \gamma_h}$	$\frac{\gamma_h}{1+\left(\frac{\gamma}{\gamma_{ref}}\right) \cdot \gamma_h}$
Hardin (1978) (cohesive soils)	$\frac{625 \cdot (OCR)^k}{0.3 + (0.7)^2} \cdot \left(\frac{\sigma_c'}{Pa}\right)^{0.5}$	----	----
Kuriyabashi et al. (1975) (for sands)	$\frac{900 \cdot (2.17-e)^2}{(1+e)} \cdot (\sigma_c')^{0.38}$ (G_{max} & and σ'_c are in kg/cm^2)	---	$(0.1 \cdot \gamma^{0.2} \cdot (\sigma_c')^{0.5}) + D_{min}$
Shibata and Soelarno (1975)	----	$\frac{1}{\left\{1+1000 \cdot \left(\frac{\gamma}{\sigma_c'^{0.5}}\right)\right\}}$	----
Iwasaki and Tatsuoka (1977) (Sands)	$\frac{A(\gamma) \cdot B \cdot (2.17-e)^2}{(1+e)} \cdot (\sigma_c')^{m(\gamma)}$ (G_{max} and σ'_c are in kg/cm^2)	---	---
Iwasaki et al. (1978) (Sands)	$\frac{A(\gamma) \cdot B \cdot (2.17-e)^2}{(1+e)} \cdot (\sigma_c')^{m(\gamma)}$ (G_{max} and σ'_c are in kg/cm^2)	$\left[\frac{G}{G_{\max}}\right]_{1kPa} \cdot \left[(\sigma_c')^{m(r)-m}\right]$	----
Imai and Tonouchi (1982)(Sands)	$G_{max} = 325 \cdot N_{60}^{0.68}$ (G_{max} is in ksf)	----	----
Chung et al. (1984) – Sands and Clays	$\frac{523 \cdot OCR^k}{(0.3 + 0.7^2)} \cdot (\sigma_c')^{0.52} \cdot P_a^{0.48}$	----	----
Seed et al. (1986) - Sands	$1000 \cdot 20 \cdot (N_1)_{60} \cdot (\sigma_c')^{0.5}$	----	----

	(G_{max} and σ'_c are in psf)		
Ishibashi and Zhang (1993) (Sands and clays)	$K_o \cdot f(e) \cdot (\sigma'_c)^m$	$log\left(\frac{G}{G_{\max}}\right) = \log K(\gamma) + (m(\gamma) - m) \cdot \log\sigma'_c$	$0.1818\left(\frac{G}{G_{\max}}\right)^2 - 0.515\left(\frac{G}{G_{max}}\right) + 0.333$
Matasovic and Vucetic (1994)	----	$\frac{1}{1+\beta \cdot \left[\frac{\gamma}{\gamma_{ref}}\right]^{\alpha}}$	$\frac{D - D_{min}}{} = 1 - \frac{1}{1+\beta \cdot \left[\frac{\gamma}{\gamma_{ref}}\right]^{\alpha}}$
Kyle et al. (1998) (Gravels)	$1000 \cdot K \cdot (\sigma'_c)^{0.5}$	$\frac{1}{1.2+16\cdot\gamma(1+10^{-20\gamma})}$	$D = 0.8 + 18 \cdot (1 + 0.15 \cdot \gamma^{-0.9})^{-0.75}$
Stokoe et al. (1995)	----	$\frac{1}{1+\left[\frac{\gamma}{\gamma_r}\right]^{\alpha}}$	----
Darendeli (2001) (Sands and clays)	----	$\frac{1}{1+\left[\frac{\gamma}{\gamma_{ref}}\right]^{\alpha}}$	$\frac{2}{\pi} \cdot \left[\frac{2 \cdot \int_0^{\gamma_o} \tau \cdot d\gamma}{\tau \cdot d\gamma} - 1\right]$
Vardanega and Bolton (2013) (Clays)	----	$\frac{1}{1+\left[\frac{\gamma}{\gamma_{ref}}\right]^{\alpha}}$	----
Chehat et al. (2018) Sig4 Model (Clays)	----	$y_o + \frac{\alpha}{1+exp\left(-\left(\frac{l_y - x_o}{\beta}\right)\right) \cdot \gamma}$	$\frac{2}{\pi} \cdot \left[\frac{2\int_0^{\gamma_o} \tau \cdot d\gamma}{\tau \cdot d\gamma} - 1\right]$
Note: OCR=over consolidation ratio; σ'_c= effective confining pressure; e=void ratio; γ=shear strain; γ_{ref}=reference shear strain; γ_h=hyperbolic shear strain; D_{min}=minimum damping ratio; P_a=atmospheric pressure; A(γ), $m(\gamma)$ $K(\gamma)$ are functions of shear strain; F(e)=function of void ratio; α, β = curve fitting parameters; τ=shear strength; y_o, l_y, x_o, γ_o=curve fitting parameters; $(N_1)_{60}$=corrected SPT N value; K=soil modulus coefficient			

2.1.4 Liquefaction Potential of Soils

Liquefaction of soils is a frequently witnessed phenomenon during dynamic loading conditions, (such as earthquakes, blast loads, etc.) typically observed in saturated sandy soils. Liquefaction potential of soil deposits can either be measured indirectly using field tests like standard penetration tests (SPT) or cone penetration tests (CPT) (by correlating to cyclic strength of soils) (Seed and Idriss 1971; Idriss and Boulanger 2006), shear wave velocity tests (Andrus and Stokoe 2000), by performing element tests on samples collected from the field (Seed and Lee 1966). Some of the widely used laboratory element tests include cyclic triaxial (CTX) test, cyclic simple shear (CSS) test and torsional shear (CTS) test. Ishihara (1996) and Kramer (1996) in their textbooks elaborately explained the various aspects of liquefaction and the factors influencing the liquefaction susceptibility of soils.

Laboratory Studies on Liquefaction Behaviour of Soils

Significant number of laboratory studies are available on the subject of liquefaction and due to the complex mechanism involved, the subject is still evolving (Seed and Lee 1966; Sitharam et al. 2004; Jakka et al. 2010; Kumar 2018). Table 2.5 presents the summary on laboratory studies of liquefaction characteristics of soils. Liquefaction resistance of soil depends on many parameters, which are listed in Table 2.5. Traditionally, liquefaction potential is represented using the cyclic stress ratio (CSR) curves, which is the variation of number of loading cycles (N_L) causing excess pore pressure to reach the initial σ'_c. Fig. 2.15a presents the typical CSR curve for a silty sand as reported by Troncoso (1990). The liquefaction resistance of soils increases with relative density, σ'_c, past loading history and stress condition, silt content and decreases with loading intensity and void ratio (Fig. 2.15b).

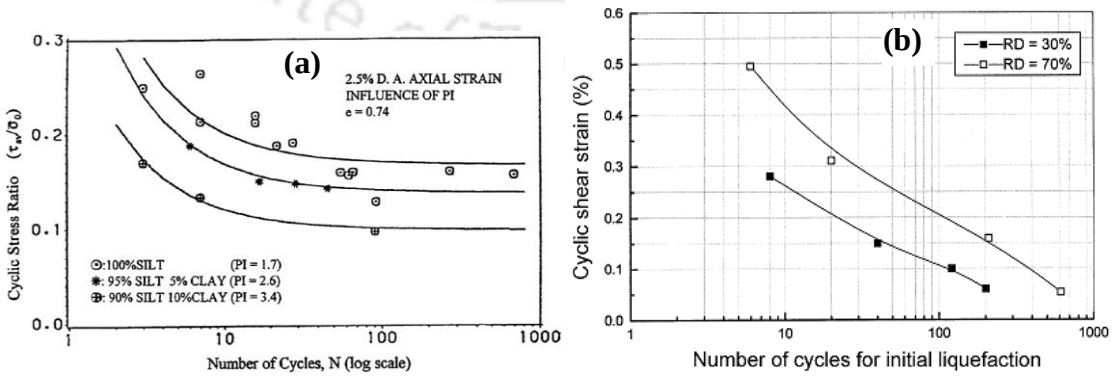

Fig. 2.15 (a) Variation of cyclic strength with fines content at constant void ratio (after Troncoso 1990) **(b)** CSR variation at different relative densities for Ahmedabad sand (after Sitharam et al. 2004)

Concerning the liquefaction studies on Indian soils, researchers (Sitharam et al. 2004; Govindaraj 2005; Hanumantharao and Ramana 2008; Kumar 2018) investigated the liquefaction characteristics of soils obtained from various parts of the country.

Govindaraju (2005) collected sand samples from the earthquake hit regions of Bhuj, Ahmedabad and Assam from India. Stress and strain controlled CTX tests have been conducted at testing conditions. The liquefaction resistance of the soils has been established using the CSR plot and concluded that most of the chosen soils are prone to liquefaction for mild to moderate seismic events. The dynamic properties of the soils have been determined at high strains and compared with the traditional literature data. Recently, Kumar (2018) performed stress and strain controlled tests on soils (sandy as well as cohesive samples) sampled from northeastern region of India. The tests were aimed to understand the liquefaction characteristics. It was concluded that the sands in the region are highly susceptible to liquefaction even for low amplitude vibrations (Fig. 2.16a). However, the clayey samples did not yield liquefaction for low cyclic loads (up to 0.1 CSR) beyond which the samples showed significant pore water pressures and axial strains (Fig. 2.16b).

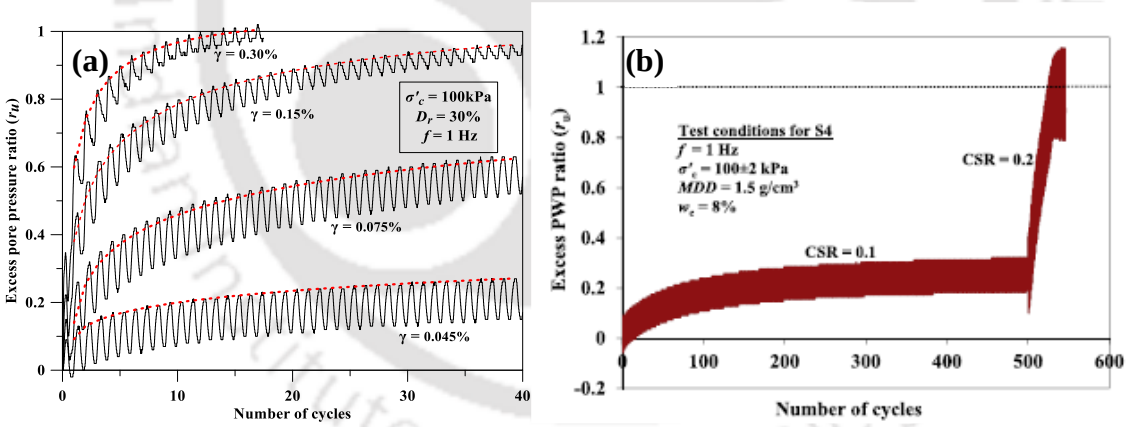

Fig. 2.16 (a) Liquefaction potential of Assam sand (after Kumar 2017) **(b)** Liquefaction phenomenon of Redsoil sampled from northeastern India (after Kumar 2017)

Recently, researchers (Lombardi et al. 2014; Rouholamin et al. 2017) focused on the practical implications of liquefaction on pile foundations by performing multi-stage CTX tests whereby the sample undergoes loads in three different stages (Fig. 2.17a). The post-liquefaction behaviour of soils is assessed through such tests and utilise the response in practical applications such as developing stress-strain curves for pile foundation analysis (Rouholamin et al. 2017), etc. Lombardi et al. (2014) and Rouholamin et al. (2017) concluded that the post liquefaction response of granular soils is a function of effective

confining pressure and void ratio (Fig. 2.17 c and d). For liquefied samples, no initial stiffness was noticed and a strain-hardening behaviour with strain was observed (Fig. 2.17c). With increase in relative density of the specimens (increase in inter-particle contact), lower strains were required to initiate the strength regain post-liquefaction while the loose specimens require relatively large strains. This strain was named as take-off shear strain ($\gamma_{take\text{-}off}$). The effect of effective confining pressure on $\gamma_{take\text{-}off}$ was minimal (Fig. 2.17d).

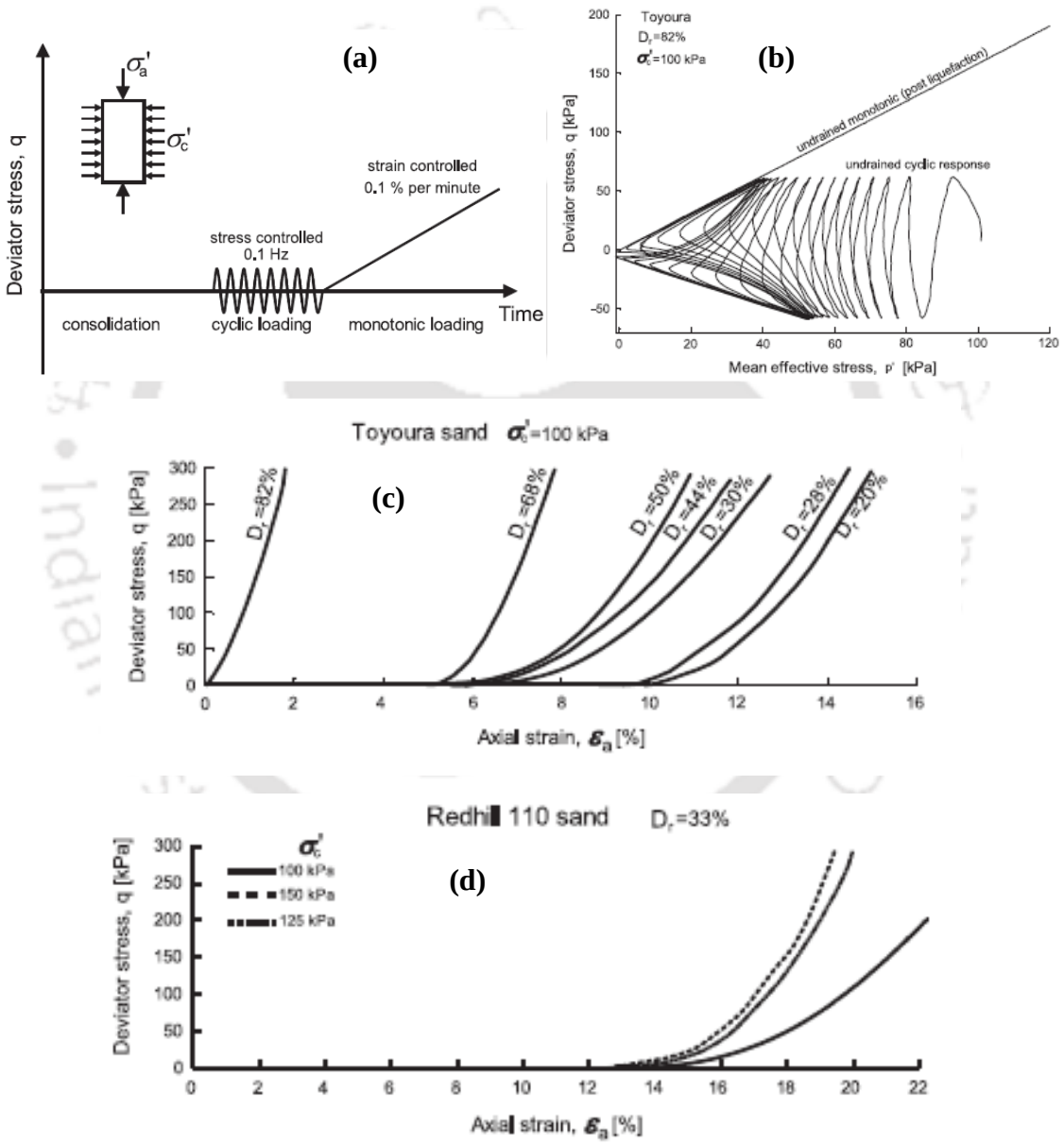

Fig. 2.17 Post liquefaction response of Redhill 110 sand (after Lombardi et al. 2014)

Table 2.5 Various researchers' contribution to evaluate liquefaction potential of soils

Investigators	Soil type	Test	Contribution
Seed and Lee (1966)	Sands	CTX	Effect of density and effective confining pressure on liquefaction resistance of sands; Increased liquefaction resistance with relative density and effective confining pressure noted
Seed and Idriss (1971)	Sands	Data collected	Proposed the simplified procedure for liquefaction evaluation initially
Finn et al. (1971)	Sands	CTX & DSS	Found that the liquefaction resistance evaluated by CTX is almost 50% more than that of field
Seed and Peacock (1971)	Sands	CTX and DSS	Proposed a relationship between field CSR and CTS CSR value
Silver et al. (1980)	Sands	CTX and DSS	Effect of sample preparation type and testing type on CSR was investigated
Tokimatsu and Yoshimi (1983)	Silty sands	Data collected	Proposed the zones of potential liquefiable and non-liquefiable based on silt content in sands
Troncoso (1990)	Sand tailings	CTX	Effect of fines content on the liquefaction potential of sands; increased; Increased liquefaction resistance with fines content observed
Prakash and Sandoval (1992)	Silty soils with low PI	CTX	Effect of PI and clay percent in soils; Increase in PI and clay content increased the resistance of soils to liquefaction
Erten and Maher (1994)	Sand and silt	CTX	Effect of silt content and loading cycles along with the strain level
Andrus and Stokoe (2000)	Sands	Shear wave velocity tests	Procedure for liquefaction evaluation using shear wave velocity (V_s) measurements (V_s with cyclic resistance ratio, CRR)
Youd and Idriss (2001)	Sands and clays	Data collected	Modified the liquefaction evaluation procedure
Sitharam et al. (2004)	Sands	CTX	Effect of relative density and effective confining pressure on liquefaction resistance of sands investigated
Boulanger and Idriss (2004)	Fine gained soils	Data collected	Proposed methodologies for liquefaction evaluation of clay like soils

Investigators	Soil type	Test	Contribution
Govindaraju (2005)	Fine grained soils	CTX	Effect of various parameters on liquefaction resistance of Bhuj, Ahmedabad and Assam sands
Idriss and Boulanger (2006)	Saturated sands	Data collected	Revised CRR with SPT N value and CPT resistance (*q*) are proposed
Jakka (2007)	Pond ash	CTX	Liquefaction potential of pond ash collected from thermal plant
Hanumantharao and Ramana (2009)	Sand with plastic fines	CTX	Increased CRR up to 20% of plastic fines and then decreased CSR observed
Dabiri et al. (2011)	Sand-silt mixtures	CTX and RC	Reported that the field based CRR measurements are over estimating the laboratory measured CRR with 60% fines
Askari et al. (2011)	Sand silt mixtures	CTX and RC	Effect of silt content on liquefaction resistance of sands
Maheswari et al. (2012)	Fibre reinforced sands	CTX	Inclusion of fibres to sand increased the LR of mixtures
Lombardi et al. (2014)	Saturated sands	CTX	Liquefaction and Post liquefaction behaviour of sands; Increased post-liquefaction strength of high relative density samples observed
Kumar et al. (2014)	Sands	CTX	Effect of shear strain and loading frequency on LR of sands
Rouholamin et al. (2017)	Saturated sands	CTX	Evaluated post liquefaction behaviour of sands and proposed a bilinear strain-hardening model
Kumar (2018)	Saturated sands and clays	CTX	Northeastern Indian sand and clay are tested at different loading conditions; Liquefaction curves proposed at different void ratios, CSR, and effective confining pressures

Pore Water Pressure Models

Various researchers worked on developing empirical formulations to predict the build-up of pore water pressure (PWP) in soils based on undrained triaxial or simple shear tests. Such formulations help in understanding the liquefaction behaviour of soils more qualitatively even at the absence of experimental data. Seed et al. (1975) initiated such studies through undrained CTX tests on granular specimens. The achieved results (pore water pressure) were then used to propose simplified liquefaction models. Several modifications and improvements have been made by various researchers since then. Table 2.6 presents the widely used pore water pressure models in earthquake geotechnical applications. Such PWP models have been employed by many finite element (such as PLAXIS 2D&3D) and finite difference (such as FLAC 2D&3D) software handling geotechnical problems, to incorporate the liquefaction characteristics of soils (Table 2.6).

Table 2.6 Widely used pore water pressure models

Researchers	**PWP model**	**Basis**	**Adopted in**
Seed et al. (1975)	$r_u = \frac{1}{2} + \frac{1}{\pi} \cdot arcsin\left[2 \cdot \left(\frac{N_L}{N}\right)^{1/\beta} - 1\right]$	Undrained CTX tests on sands	----
Booker et al. (1976)	$r_u = \frac{2}{\pi} \cdot arcsin\left(\frac{N_L}{N}\right)^{1/\beta}$	Literature data	GADFLEA
Martin et al. (1975)	$\Delta\varepsilon_{vd} = C_1^c \cdot (\gamma - C_2^c \cdot \varepsilon_{vd}) + \left\{\frac{C_3^c \cdot {\varepsilon_{vd}}^2}{\gamma + C_4^c \cdot \varepsilon_{vd}}\right\}$	Strain controlled CTX tests	FLAC 2D & 3D
Dobry et al. (1985)	$r_{u,N} = \frac{P \cdot N \cdot F \cdot (\gamma - \gamma_t)^S}{1 + N \cdot F \cdot (\gamma - \gamma_t)^S}$	Sands (CTX)	*DEEPSOIL*
Byrne (1991)	$\left(\frac{\Delta\varepsilon_{vd}}{\gamma}\right) = C_1^c \cdot exp\left(-C_2^c \cdot \frac{\varepsilon_{vd}}{\gamma}\right)$	Literature data	FLAC 2D & 3D
Matasovic and Vucetic (1994)	$r_u = A \cdot N_L^{-3x} + B \cdot N_L^{-2x} + C \cdot N_L^{-x} + D$ $x = s \cdot (\gamma - \gamma_{tvp})^{\gamma}$	DSS tests on clays	*DEEPSOIL*
Park et al. (2015)	$r_u = \frac{2}{\pi} \cdot arcsin\left(\frac{K}{K_{ru=1.0}}\right)^{1/2\beta}$	Literature data	----
Chiaradonna et al. (2018)	$r_u = a \cdot \left(\frac{N}{N_L}\right)^b + c \cdot \left(\frac{N}{N_L}\right)^d$	CSS tests on silty sands	SCOSSA

Note: N_L=number of cycles for liquefaction; N=number of loading cycles; γ=shear strain; γ_{tvp}=threshold shear strain for PWP generation; ε_{vd}=accumulated volumetric strain; $\Delta\varepsilon_{vd}$=incremental volumetric strain; β, C_1, C_2, C_3, C_4, A, B, C, D, F, P, s, b, d = curve fitting parameters; K= damage parameter

2.2 STUDIES ON SEISMIC GROUND RESPONSE

Seismic ground response studies are helpful in understanding the response of soil deposits to dynamic loads in terms of stresses and strains and form an integral part of dynamic analysis of structures. Tremendous developments in seismic ground response studies have emerged following the 1985 Mexico earthquake as it provided scientific body with sufficient evidences of ground motion amplification and liquefaction triggers (Esteva 1988). Some of the widely used ground response analysis (GRA) programs include SHAKE (Idriss and Sun 1992), EERA DEEPSOIL (Hashash et al. 2016), Cyclic1D (Wang et al. 2006) etc. The applications include micro zonation, liquefaction mapping, seismic hazard maps, etc. All such programs require the user to define the strain dependent dynamic soil properties (some of them seek pore water pressure parameters) and it is a common trend to adopt empirical data (such as Seed and Idriss (1970) and Darendeli (2001)) from literature. This is mainly due to the lack of experimental based site-specific or region-specific soil properties and acquiring such properties involve both budgetary and skillset constraints. Recent studies highlight that the utilisation of empirical data in GRA studies often leads to unreliable results and suggested to adopt the site or region specific data in the analysis (Chiaradonna et al. 2018; Kumar et al. 2018b).

Ground response studies can be classified based on the dimensionality of the problem (1D, 2D or 3D) as well as the level of strains involved (linear elastic, equivalent linear and nonlinear analyses). Although 1D GRA studies are simplified in nature, they were effectively validated against field and laboratory tests and therefore, many researchers have been practicing such studies (Hashash and Park 2001; Torabi and Rayhani 2017). Linear elastic analysis utilises only the low strain stiffness characteristics of soil and can only be adopted for analysis dealing with very small strains, such as low intensity seismic motions, etc. Equivalent linear (EQL) analysis is an approximation to full nonlinear analysis and cannot simulate the generation of pore water pressures and resulting plastic yielding of soils. Nonlinear analysis (NL) is a time domain analysis whereby all the possible (mostly) dynamic characteristics of soil can be considered such as liquefaction, plastic yielding, etc. Kramer (1996) and Yoshida (2015) thoroughly describes the methodologies and associated background and corresponding literature.

2.2.1 Studies on EQL and NL GRA Comparison

Both the EQL and NL studies are in wide use since the inception of 1D GRA programs. Few literature highlighting the comparable aspects of EQL and NL studies is reviewed

here. Garala and Madabhushi (2018) performed scaled centrifuge tests on soft clay bed with increasing intensity of input motions (harmonic 0.05g to 0.15g). A comparative 1D GRA has been performed using DEEPSOIL program, adopting both the EQL and NL approaches. Both the approaches yield comparable seismic soil response for low intensity motions (Fig. 2.18a), however, for high intensity motions, EQL analysis yielded severe amplifications (Fig. 2.18b) than that of experimental and NL analysis. As EQL analysis cannot consider the soil yielding or high strain nonlinearity, shear strength of the soil was still in contact and showed severe amplifications. In contrast, NL analysis considers both the soil yielding and pore pressure generation, appreciable results were achieved (Garala and Madabhushi, 2018). It was finally suggested to use EQL approach for low intensity motions where soil yielding is not expected, and in cases of high intensity motions with significant soil yielding, the NL analysis was recommended (Garala and Madabhushi 2018).

Similar recommendations were proposed by Yee et al. (2013), Yoshida (2014), Kumar et al. (2018a), Mercado et al. (2018) and Basu et al. (2019). Basu et al. (2019) performed comparative studies on EQL and NL in Guwahati region of India with increased intensity of input motions and observed severe amplification for low intensity motions and attenuation for high intensity motions. This was attributed to the high damping at high strains, caused by the intense motions. Also, plastic soil deformations for NL analysis were observed which were absent in EQL analysis (Fig. 2.19). Plastic soil deformations in NL analysis can be understood by the stress-strain response adopted in the 1D program. For low amplitude motions (0.005g), the stress-strain response evaluated from both EQL and NL approaches yielded similar magnitudes (Fig. 2.20a), while the high amplitude motions (0.25g) produced differential response for both the approaches (Fig. 2.20b). This is again attributed to the soil yielding characteristics considered in NL analysis (Mercado et al. 2018).

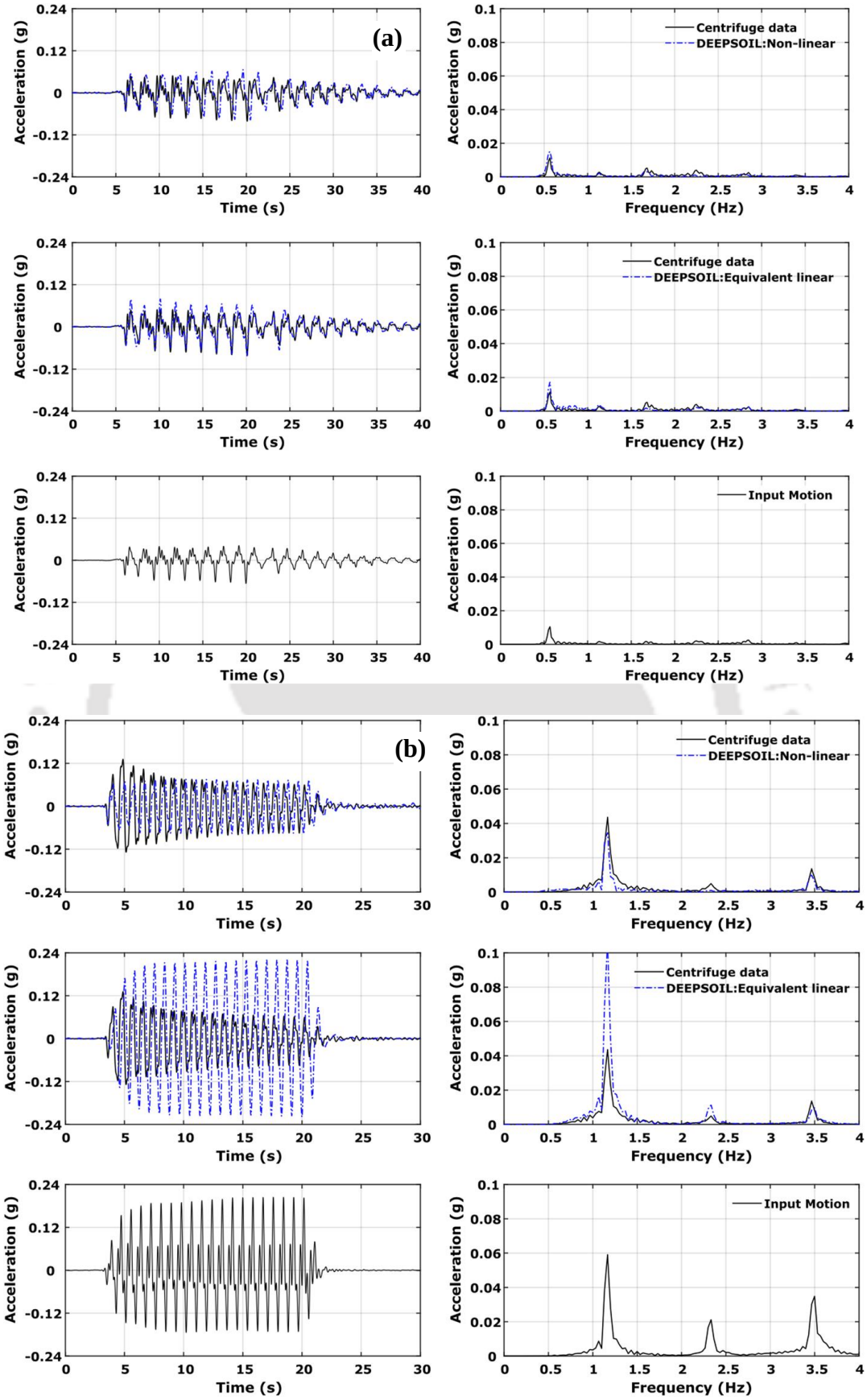

Fig. 2.18 Comparison of experimental (centrifuge) data with the 1D EQL and NL GRA **(a)** 0.05g input motion **(b)** 0.15 input motion (after Garala and Madabhushi 2018)

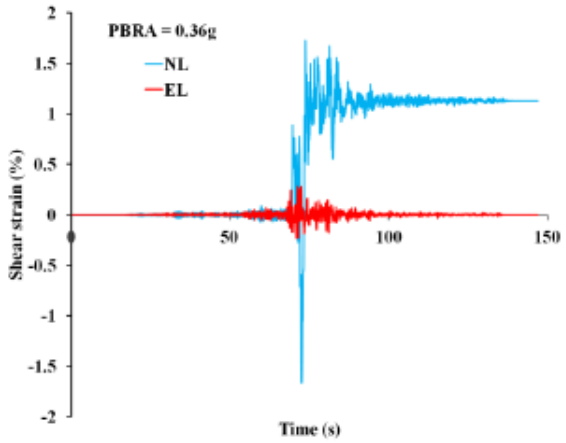

Fig. 2.19 Comparison of EQL and NL GRA in Guwahati city (after Basu et al. 2019)

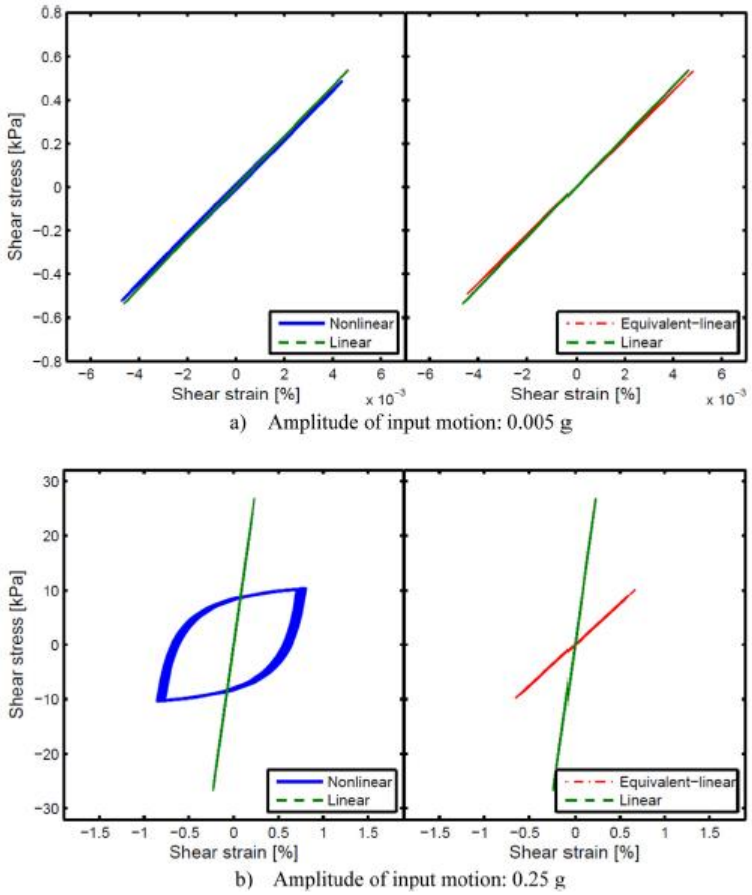

Fig. 2.20 Shear stress-strain response at 2.5 m depth of the modelled soil deposit for **(a)** 0.005 g and **(b)** 0.25 g input motions (after Mercado et al. 2018)

2.2.2 GRA Studies in India

Some of the available literature pertaining to the major GRA studies in India are collated and summarized in Table 2.7. It is worth noting here that almost all the studies (except Hanumantharao and Ramana 2009; Kumar et al. 2018b) adopted literature based empirical strain dependent dynamic soil properties in the analysis. The GRA studies that considered

experimentally obtained G/G_{max} and D data highlighted the necessity of use of site-specific data in GRA studies (Kumar et al. 2018b). It must also be noted from the Table 2.7 that NL analysis is almost rarely adopted (except Basu et al. 2019 study) and EQL is mostly used. This is essentially due to the lack of sufficient information on the large number of parameters required for the NL analysis and also the lack of efficient technical expertise.

Table 2.7 Major seismic ground response studies in India

Researchers	Approach	Program	Contribution
Ranjan (2005)	EQL	SHAKE2000	Developed PGA and PSA maps for Dehradun city
Boominathan et al. (2008)	EQL	SHAKE91	Performed MASW tests and established spectral acceleration and site period maps for Chennai city
Raghu Kanth et al. (2008)	EQL	SHAKE91	Surface acceleration and liquefaction maps for Guwahati city were developed
Nath et al. (2009)	EQL	SHAKE91	Developed PGA, amplification and spectral maps for Guwahati city
Hanumantharao and Ramana (2009)	EQL	SHAKE91	MASW and CTX tests performed; site specific ground motions adopted; PGA values reported for Delhi city
Anbazhagan et al. (2010)	EQL	SHAKE2000	Amplification, liquefaction and PGA maps were developed for Bangalore city
Govindaraju and Bhattacharya (2012)	EQL	SHAKE2000	Spectral acceleration and amplification ratios were developed for Kolkata city
Phanikanth et al. (2011)	EQL	DEEPSOIL	PGA and amplification maps for typical sites in Mumbai city were developed
Shukla and Choudhury (2012)	EQL	SHAKE2000	Spectral accelerations and PGA amplification magnitudes were developed for ports in Gujarat
Kumar and Krishna (2013)	EQL	DEEPSOIL	PGA, amplification, FAR factors were developed for Guwahati city
Desai and Choudhury (2015)	EQL	DEEPSOIL	Developed site-specific ground motions and seismic hazard maps in terms of pseudo-acceleration for port sites in Mumbai city
Basu et al. (2019)	NL	DEEPSOIL	Developed PGA, spectral acceleration maps for Guwahati; highlighted the need of NL effective stress analysis
Kumar et al. (2018a)	EQL	DEEPSOIL	High strain dynamic properties have been adopted in developing seismic response maps for Guwahati city

2.3 SEISMIC ANALYSIS OF DEEP FOUNDATIONS

Realistic soil deposits are mostly multi-layered with different layer properties sandwiched in-between. Deep foundations are the most affected due to the layering affects in case of

seismic events. Two basic types of deep foundations exist, based on the slenderness ratio and working principle: pile and caisson foundations. Fig. 1.5a shows a typical sectional view of pile and caisson foundation based on the slenderness ratio (length compared to the smallest cross sectional dimension). During seismic loadings, mutual interaction of soil-foundation-structure (also called seismic soil-structure interaction, SSSI) leads to two types of failure interactions: kinematic and inertial. Researchers observed numerous pile foundation damages during the post-earthquake investigations around the world and most of the failures were attributed to the inconsideration of SSSI effects in the seismic design (Hamada and O'Rourke 1992; Mylonakis and Gazetas 2000). Kinematic interaction arises due to the seismic wave induced lateral soil stresses on the pile while the inertial loads are caused by the superstructure loads at the pile head. As inertial interaction governs the surficial seismic behaviour of piles (Mylonakis 2001), kinematic interactions and resulting bending moments are pronounced at deeper locations along the pile. In addition, kinematic interaction is detrimental in case of multi-layered soils, as described by Mylonakis (2001) and Nikolaou et al. (2001). Fig. 2.21 shows a typical kinematic bending response of a free-headed single pile embedded in two-layered soil profile. At the interface of the layers, difference in dynamic stiffness exists leading to strain discontinuities. This will induce higher soil curvature on piles (derivative of strains) at the juncture of layers which would ultimately yield in additional bending moments.

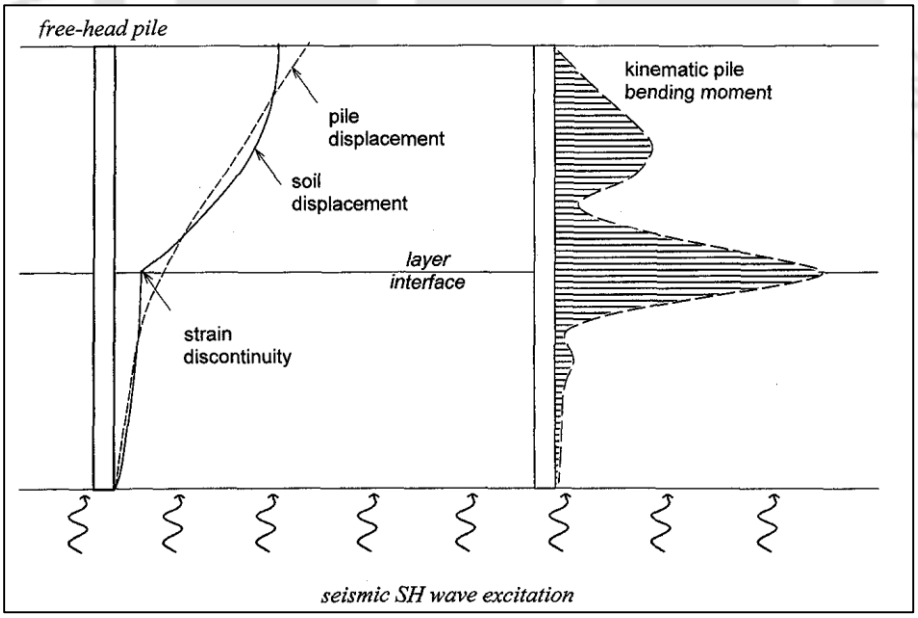

Fig. 2.21 Typical bending moment profile of free-head pile in two layered soil medium (after Mylonakis 2001)

2.3.1 Kinematic Interaction of Pile Foundations in Layered Soils

A rigorous and comprehensive study on kinematic interaction of pile foundations in layered soil deposits was performed by Nikolaou et al. (2001). Investigations were carried on the kinematic response of free-head and fixed-head single piles. Fig. 2.22 shows the kinematic bending strain induced in the pile for free and fixed head conditions in different soil profiles. It can be seen that the behaviour is quite complex in case of layered soils (Fig. 2.22 A2, B3 and B4) and especially pronounced at the interface of two layers, especially if there is sharp stiffness contrast.

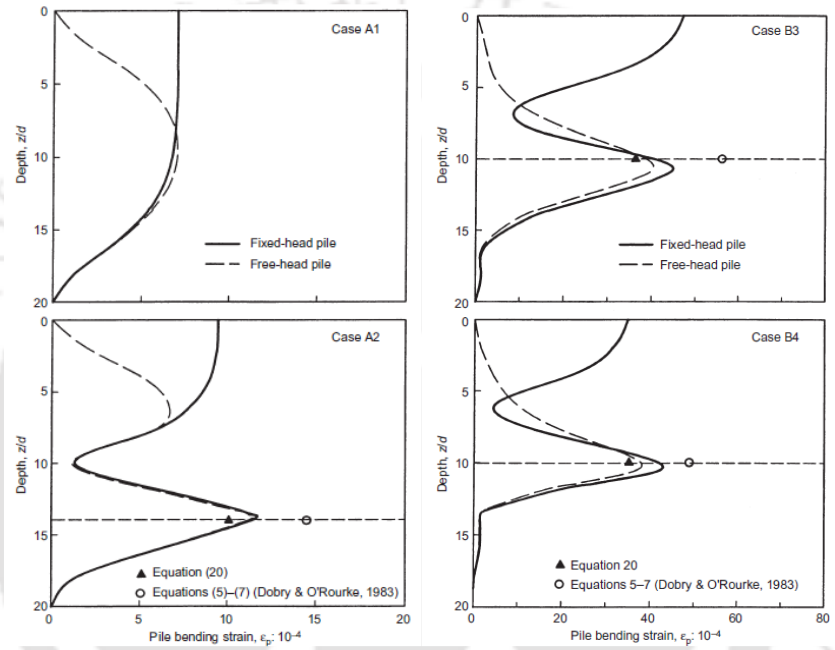

Fig. 2.22 Pile bending strain variation in different layered soils (A1) Homogeneous (A2) Surficial strength half of base layer (B3) Surficial soil strength is 25% of base layer (B4) Surficial soil strength is 10% of base layer (after Nikolaou et al. 2001)

Significant research has been published concerning the kinematic pile interactions (Novak 1991; Kavvadas 1993; Nikolaou et al. 2001; Haldar and Babu 2010; Simonelli et al. 2014). Many global seismic codes acknowledge this phenomenon and recommend to incorporate it in the seismic design of pile foundations (NEHRP 1997; JRA 2002; Eurocode 8 2004; IS:2911 2010).

Kinematic interactions of pile foundations in liquefiable soils is another important concern which was brought in to scientific attention after the Niigata (Japan) and Alaska (US) earthquakes and their effects. Such liquefaction induced stresses on piles are termed as lateral spreading loads and this aspect has been experimentally as well as numerically investigated by numerous researchers (Hamada and O'Rourke 1992; Wilson et al. 2000; Abdoun et al. 2003; Bhattacharya 2003; Brandenberg 2005; Dash et al. 2009; Madabhushi

et al. 2010; Haldar and Babu 2010; Lombardi and Bhattacharya 2014; Sarkar et al. 2014; Rouholamin 2016). Fig. 2.23 schematically depicts the seismic loads acting on end bearing pile foundation in liquefiable soil conditions. Table 2.8 briefly summarizes the numerical and experimental studies on seismic behaviour of pile foundations in liquefiable soils. All the studies highlight the consideration of additional lateral stresses induced by the liquefied ground on the pile foundations. Bhattacharya et al. (2004) and Mohanty et al. (2017) critically reviewed the failure mechanisms of pile foundations in liquefiable soils which are listed below.

1. ***Bending failure*** due to the additional lateral deformations caused by liquefied soils (stage II in Fig. 2.23) (Hamada and O'Rourke 1992; JRA 2002)
2. ***Buckling failure*** due to the excessive inertial effects (stage III in Fig. 2.23) (Bhattacharya 2003; Shanker et al. 2007)
3. ***Combined bending-buckling*** interaction (stage IV in Fig. 2.23) (Dash et al. 2010)
4. ***Change of dynamics*** of the soil-pile-structure, i.e., elongation of pile flexibility due to the increase in time period in liquefied soils (Bhattacharya et al. 2014; Lombardi and Bhattacharya 2014, 2016)

For an effective seismic resistant design of pile foundation, all these mechanisms must be verified. Incorporating all the mechanisms, case studies of seismically damaged pile supported bridges have been reported elsewhere (Mohanty et al. 2017).

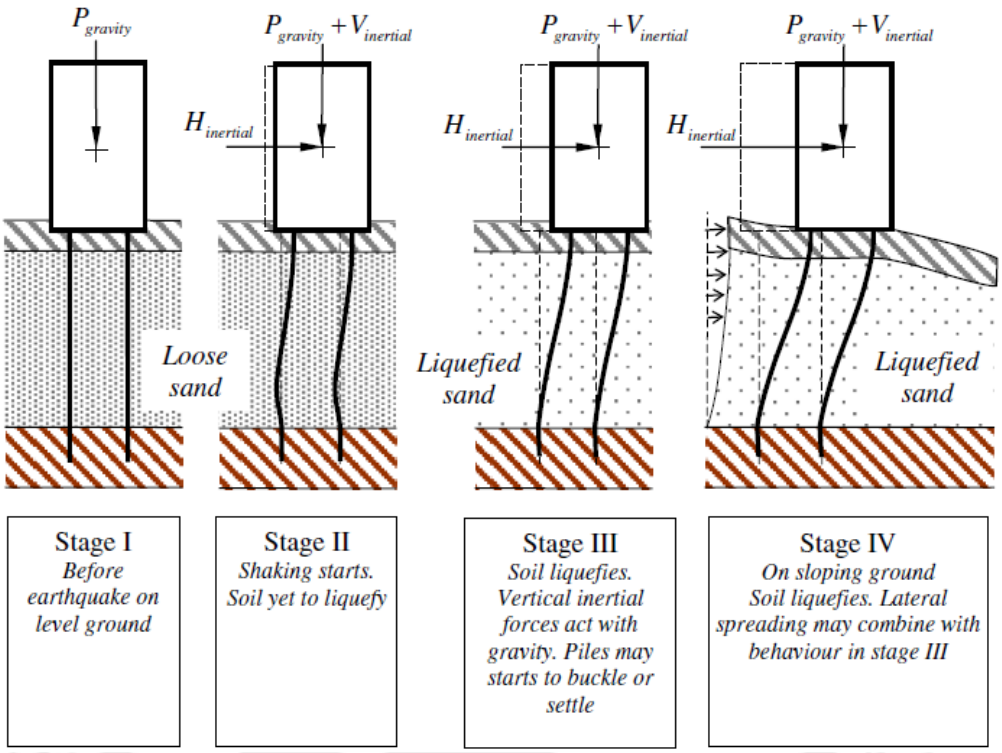

Fig. 2.23 Different loads acting on a pile during seismic events in liquefiable soil conditions (after Sarkar et al. 2014)

Table 2.8 Abridged summary of studies on behaviour of pile foundations in liquefiable soils

Reference	Configuration	Methodology	Program	Soil model	Major findings
Abdoun and Dobry (2002)	Single pile	Centrifuge	---	---	Lateral spreading effect introduced with scientific justification
Bhattacharya (2003)	Single pile	Centrifuge testing	---	---	Buckling of pile invented, due to the p-Δ effect in liquefiable soils
Ashour and Norris (2003)	Single pile	Analytical	---	Strain wedge model	Lateral loading behaviour of pile in developing (partial) and fully liquefied conditions
Klar et al. (2004)	Single pile	FDA	FLAC 2D	Byrne	Seismic SSI studies both using free field liquefiable soil displacements and coupled analysis
Weaver et al. (2005)	Single pile	Field testing	---	---	Blast induced liquefaction and modified *p-y* curves incorporating the strain hardening behaviour of liquefied soils
Brandenberg (2005)	Single piles and pile groups	Centrifuge	---	---	Lateral spreading and liquefaction forces on pile foundations
Dash et al. (2009)	Piled mat foundation-Kandla Port tower	FEA	SAP2000	BNWF (*p-y*)	Investigated the possible reasons for the tilted Kandla port tower and convinced that Mat pile foundation served better in liquefaction scenario
Knappett and Madabhushi (2008)	Pile group	FEA	ABAQUS	Modified *p-y* approach	Effect of axial load on the lateral response of pile foundations
Dash et al. (2010)	Single pile	FEA	SAP2000	BNWF (*p-y*)	Bending buckling interaction mechanism for pile foundations in liquefiable soils; Pseudo-static analysis based on force and displacement based approaches
Haldar and Babu (2010)	Single pile	FDM	FLAC 2D	Byrne model	Proposed the pile failure mechanisms in liquefiable soils; parametric studies performed
Brandenberg et al. (2013)	Single and pile group	Centrifuge and FE analysis	Opensees	PyLiq1 model	A residual pore pressure (effective stress based) liquefaction *p-y* model is validated against centrifuge results
Bhattacharya et al. (2014)	Pile supported Showa Bridge	FEA	SAP2000	BNWF (*p-y*)	Elongation of the natural period of the pile supported pier due to liquefaction induced fixity length, leading to excessive spectral displacement by resonance
Ashour and Ardalan (2012)	Single pile	Analytical	---	Strain wedge model (*p-y*)	Proposed a technique for estimating the lateral response of piles in liquefiable/partial liquefiable soils using scaled element test results

Reference	Configuration	Methodology	Program	Soil model	Major findings
Sarkar et al. (2014); Sarkar and Maheswari (2012)	Single pile	3D FE	Matlab	Ducker Prager with Byrne model	Developed seismic requalification strategy for analysing pile foundations in seismic liquefiable soils
Lombardi (2014)	Single and pile group	Shaking table and Numerical	SAP	Bilinear model	Established a unique strain-hardening bilinear model for bending moment calculations in liquefiable soils
Ghasemi-fare and Pak (2016)	Single pile	FDA	FLAC 2D	Byrne model	Gapping elements were modelled
Choobbasti and Zahmatkesh (2016)	Single pile	FEA	OpenSees	Two surface plasticity model	Pseudo static method with decoupled free field with subsequent BNWF analysis
Lombardi and Bhattacharya (2016)	Single pile and pile group	Shaking table	---	---	Elongated natural period of the pile foundations in liquefied soils; Increased damping ratio (even up to 40%) in liquefied soils
Rouholamin (2016)	Single and pile groups	Shake table and analytical	SAP	BNWF (*p-y*)	Studied the transient behaviour of pile foundations during liquefaction
Shrimal and Maheswari (2016)	Single pile	FDM	FLAC 3D	Byrne	Validation of site response and final model is a single pile in liquefied soil
Ashour and Helal (2017)	Single pile	FEA	PLAXIS 3D	HS model	Investigated the axial behaviour of pile foundation before (PLAXIS 3D) and after liquefaction; Effect of partial (limited) liquefaction in medium dense sands on axial response also explored.
Dash et al. (2017); Lombardi et al. (2017)	Pile group	Centrifuge testing	COMSOL	BNWF (Bilinear *p-y*)	Proposed a bilinear *p-y* approach for performing pseudo static analysis of pile foundations in liquefiable soils
Chatterjee et al. (2019)	Single pile	FDM	FLAC 3D	Byrne model	Inclusion of P-Delta effect in the numerical model of single pile with liquefiable stratum; parametric studies on depth of liquefaction

2.3.2 Modelling Seismic-Soil-Structure-Interaction

Structural engineers often tend to neglect the underlying soil behaviour by assuming a rigid fixity of the foundation/structure at the bed level which was proved to be detrimental due to the adverse effects of foundation flexibility or SSI (Mylonakis and Gazetas 2000). Any effective structural analysis would require the stiffness of foundation to consider the underlying soil's flexibility in contrast to a rigid fixity. Such stiffness or interaction can be modelled using simple to complex approaches. Simple methods involve the adoption of Winkler spring theories (Hetenyi 1946) whereby the soil reaction to the loading are modelled using load-displacement behaviour. These approaches are also termed as discrete spring approaches. Despite the fact that advanced two-dimensional (2D) or three-dimensional (3D) continuum non-linear approaches provide satisfactory results, they involve considerable time and computational effort due to which their adoptability in engineering practice is restricted in comparison to the simplified spring approaches. In addition, the Winkler spring approaches were successfully validated against experimental results by various researchers and found to provide reasonable results (Boulanger et al. 1999; Gerolymos and Gazetas 2006; Mondal et al. 2012; Shadlou and Bhattacharya 2014). Two types of Winkler approaches exist: lumped spring approach (Randolph 1981) and distributed spring approach (Novak 1991).

Distributed Winkler Spring Approach

This is the widely used method for modelling the laterally loaded deep foundations in both static and dynamic loading conditions. The method was initially developed by Hetenyi (1946) based on Winkler idealization of soil (Winkler 1867). The main hypothesis is that the reaction exerted by the soil at a given depth on the pile shaft is proportional to the relative pile-soil lateral deflection. In this approach, a pile is modelled by a series of consecutive beam-column elements, whereas the lateral pile-soil interaction is analysed using linear/nonlinear springs attached to nodal points between two consecutive pile elements. Fig. 2.24 presents a view of the Winkler approach. Each spring is independent in nature and only be responsible for the deflection of pile element connected to that particular spring. Each of the springs are defined by means of linear/nonlinear relationship between the soil reaction (per unit length of pile) p and the corresponding relative soil pile lateral movement, y. The ratio of p to y is termed as the modulus of subgrade reaction, k with dimensions of pressure divided by length (Prakash and Sharma 1990). These are termed as p-y curves in general practice. Fig. 2.25 schematically shows the application of

p-y curves for laterally loaded piles in liquefiable (Fig. 2.25b) and nonliquefiable soils (Fig. 2.25a). Both the linear and nonlinear systems can be analysed using this approach. It can be seen that the small amplitude of vibrations can be analysed by the initial elastic behaviour of *p-y* springs while the large amplitude systems are needed to be analysed using the nonlinear behaviour of the soil.

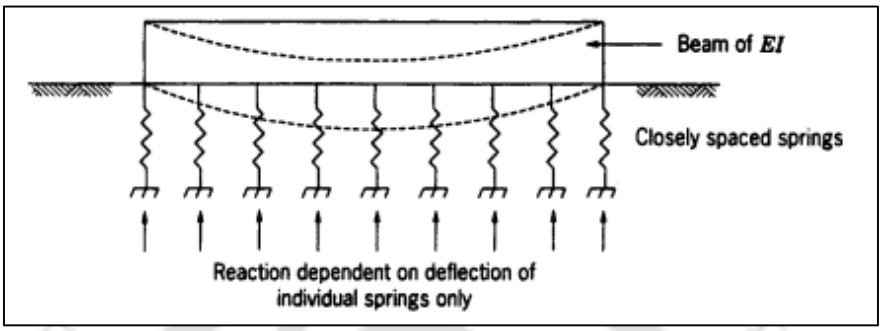

Fig. 2.24 Representation of Winkler approach for vertically loaded horizontal beams (after Prakash and Sharma 1990)

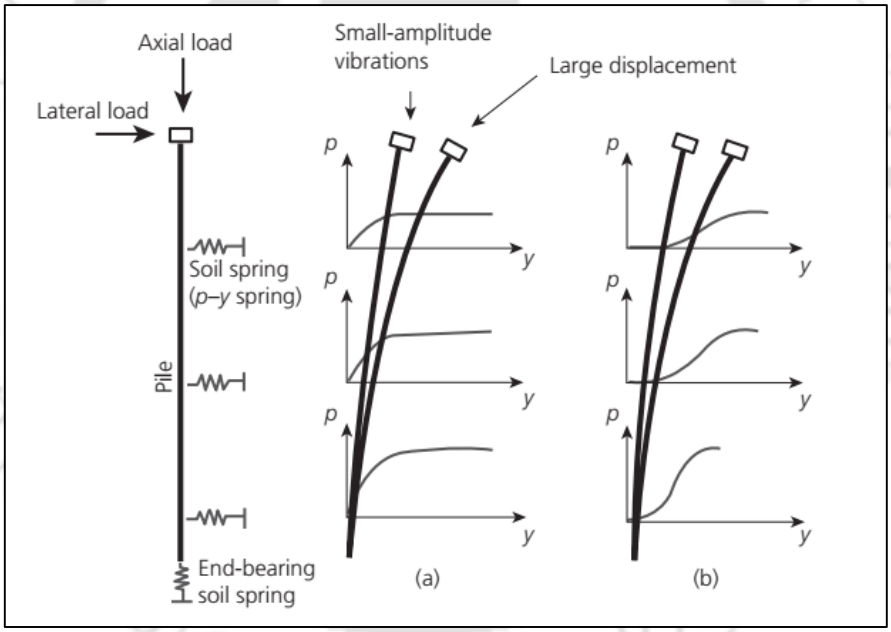

Fig. 2.25 Application of Winkler beam approach to pile foundations in case of **(a)** Non-liquefied soils and **(b)** Liquefied soils (after Dash et al. 2009)

The *p-y* curves (both for sands and clays) for static and cyclic loading were developed by the empirical relationships established during the 1970s-1980s. Based on a relatively limited number of full-scale tests carried out on small diameter piles subjected to slow-cyclic loading (Matlock and Reese 1961; Blaney and O'Neill 1986). The major limitation of this approach is the discrete (discontinuous) nature of the springs. However, due to the mathematical simplicity and ability to incorporate the nonlinearity of the soil and ground stratification, their application has become widely acceptable in engineering practice.

In case of linear elastic *p-y* curves, Novak (1974) proposed dynamic impedance functions assuming plane-strain conditions, for rigid foundations. The work has been widely used to analyse deep foundation problems with linear elastic system application and was subsequently improved and validated successfully for caissons (Mondal et al. 2012). Concerning the nonlinearity of the soil, some organizations such as American Petroleum Institute (API 2014) and DNV (2013) provide guidance in developing nonlinear *p-y* curves for sands and clays for both static and cyclic loading conditions. Applicability of nonlinear *p-y* curves has been successfully validated by various researchers against the experimental results (shaking table tests and centrifuge tests) in simulating the dynamic response of pile foundations (Wang et al. 1998; Boulanger et al. 1999, Finn and Fujita 2002, Dash et al. 2010, Lombardi et al. 2017).

In general, *p-y* curves can be used both for static and dynamic analysis. In case of static loading, a simple push-over analysis is considered sufficient to simulate a lateral load or a pseudo-static load. However, in case of dynamic analysis, two types of analysis are possible, one with the linear elastic modal analysis to find the fundamental mode of vibration of a structure whereas the latter is a fully dynamic analysis incorporating the nonlinearity of the soil pile interaction. Boulanger et al. (1999) validated the *p-y* springs for fully nonlinear dynamic analysis against the centrifuge results of single pile and group pile supported structures. A dynamic *p-y* analysis is a decoupled analysis whereby the free field soil displacements are evaluated individually (without the structure) by any ground response programs (such as DEEPSOIL or SHAKE) in the first phase. The second phase involves the application of free field soil displacements/accelerations (obtained in the first phase) at the end of each corresponding spring along the depth (Fig. 2.26b). This is considered as the component of kinematic interaction for deep foundations and the inertial interaction is modelled by the axial loads on the model. Then, a fully nonlinear dynamic time history analysis is performed using any standard FE programs such as GeoFEAP or SAP2000 (CSI Inc. 2011). Fig. 2.26 (a and b) schematically presents the procedure of dynamic *p-y* analysis for pile foundations. In the nonlinear time history analysis (SAP2000), the dynamic equilibrium equations (Eqn. 2.10) are solved using either modal (linear elastic case) or direct-integration (nonlinear system) methods (CSI Inc. 2000).

$$K \cdot u(t) + C \cdot \frac{du(t)}{dt} + M \cdot \frac{d^2u(t)}{dt^2} = F(t) \qquad (2.10)$$

where *K*, *C* and *M* are the stiffness, damping and mass matrices while *u* and F are the deformation and external forces, respectively.

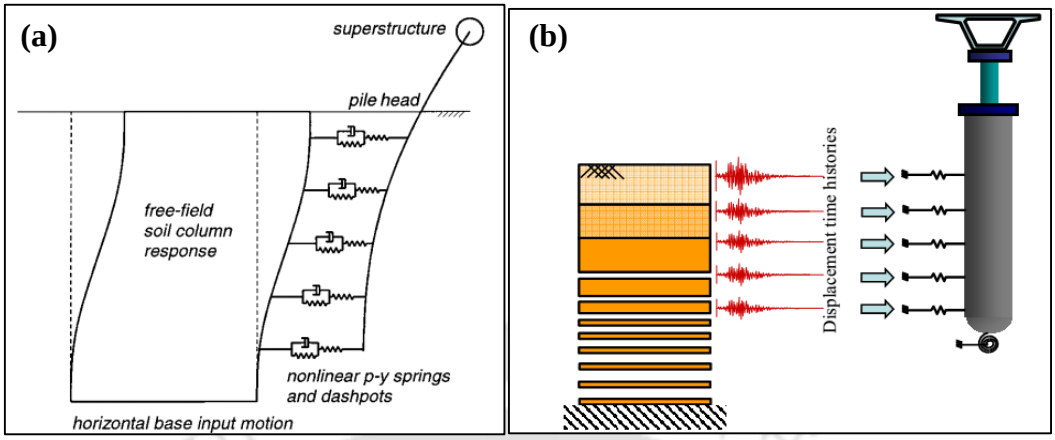

Fig. 2.26 (a) Dynamic *p-y* analysis model (after Boulanger at al. 1999) **(b)** Schematic of *p-y* procedure (after Mondal et al. 2012)

2.4 SUMMARY OF LITERATURE REVIEW

- Behaviour of soils to dynamic loading is complex and governs the seismic stability of overlying structures. Thorough investigation of underlying soil behaviour is required either through field or laboratory testing techniques or sometimes using both, in pursuit of efficient seismic analysis.
- A distinct difference exists in the dynamic behaviour of cohesionless and cohesive soils due to the dependency on many factors such as geologic, formational, and index properties, it is therefore, highly recommended to perform soil specific or regional specific soil investigations.
- Either a single hybrid apparatus with local strain measurements or two or more independent apparatus are required to comprehensively characterise the dynamic behaviour of soils over wide range of strains
- The empirical formulations available in the literature may not be generalized for all the soils and hence require soil/regional specific formulations.
- Seismic GRA studies evaluated using the literature suggested empirical dynamic soil properties often yield unreliable results.
- Only limited comprehensive studies on dynamic properties of soils of active seismic regions of India over wide strain range are available. The need for developing such properties for seismically active regions should not be ignored.

- Equivalent linear GRA cannot fully incorporate the nonlinear effects of soil such as pore pressure generation and soil yielding and hence, nonlinear effective stress studies must be performed in active seismic regions. No major nonlinear effective stress studies exist till date, for active seismic regions of India.
- Winkler spring based approaches for deep foundation analysis should consider the effects of liquefaction induced stresses.

2.5 OBJECTIVES AND SCOPE OF THE RESEARCH

Hinged on the extensive literature survey carried out, it is concluded that the dynamic soil behaviour is soil specific and hence, for any efficient seismic resistant design of structures, reliable estimation of dynamic soil behaviour is crucial. Therefore, the main objective of the study is to establish the strain dependant comprehensive dynamic properties for the sampled soils and provide the region-specific stiffness curves (G/G_{max} and D variation with γ). The study is also aimed to understand the significance of utilizing experimentally obtained soil properties in seismic ground response studies and seismic analysis of pile foundations. Based on the formulated objectives, scope of the work is planned in a systematic way as briefed below.

1. Collection of soil samples from highly active seismic regions of India (north and northeastern regions of India) and their basic characterisation for determining index properties.
2. Dynamic characterisation tests are conducted in order to comprehensively characterise the chosen soils over wide strain range. Liquefaction analysis are performed on the chosen soils in consolidated undrained conditions using multistage cyclic triaxial tests.
3. The achieved results are combined to obtain the properties over wide strain range and development of simplified region-specific empirical formulations.
4. Demonstration of established soil properties in equivalent and nonlinear ground response studies incorporating liquefaction phenomenon for typical borehole profiles, representative of the tested soils.
5. Seismic analysis of pile foundations is performed using Winkler beam approach, considering the effects of liquefaction, deduced from element test program and seismic ground response studies.

CHAPTER III –MATERIALS AND EXPERIMENTAL PROGRAMME

3. 0 INTRODUCTION

As per the objectives and scope defined, soils (four sandy soils and two clayey type) from two active seismic regions of India were considered for their detailed and comprehensive dynamic soil characterisation. The study utilised four independent and highly advanced laboratory element testing techniques. The chapter is divided into three sections in which the first one presents the introduction of chosen soils, their basic geotechnical characterisation while the second section describes the monotonic strength response of soils, evaluated through laboratory tests. The third section discusses the details of experimental program intended for dynamic soil characterisation, with the description of testing apparatus, methodology and typical output from each test.

3.1 MATERIAL DESCRIPTIONS

Total of six representative soils (four sandy soils and two clayey soils) were chosen from two states of active seismic regions in India. Table 3.1 briefs the location of soils and their abbreviated names. Fig. 3.1a presents the marked locations of soil sampling in seismic zonation map of India. Four soils (two cohesionless and two cohesive samples) were collected from Assam state in northeastern India (a high seismic zone (V), as per IS:1893-2016) and two sand samples have been collected from northern India (state of Haryana, classified as a mild to intense seismic zone-III-V). Fig. 3.1 (b and c) depicts the locations of soil sampling in Haryana and Assam, respectively.

Table 3.1 Materials and their location

Material	Location	River	Abbreviation
Brahmaputra sand	Northeastern India	Brahmaputra	BP
Bongaigaon sand			BG
Pachoria Cohesive			PC
Red soil			RS
Yamuna fine sand	Northern India	Yamuna	YF
Yamuna coarse sand			YC

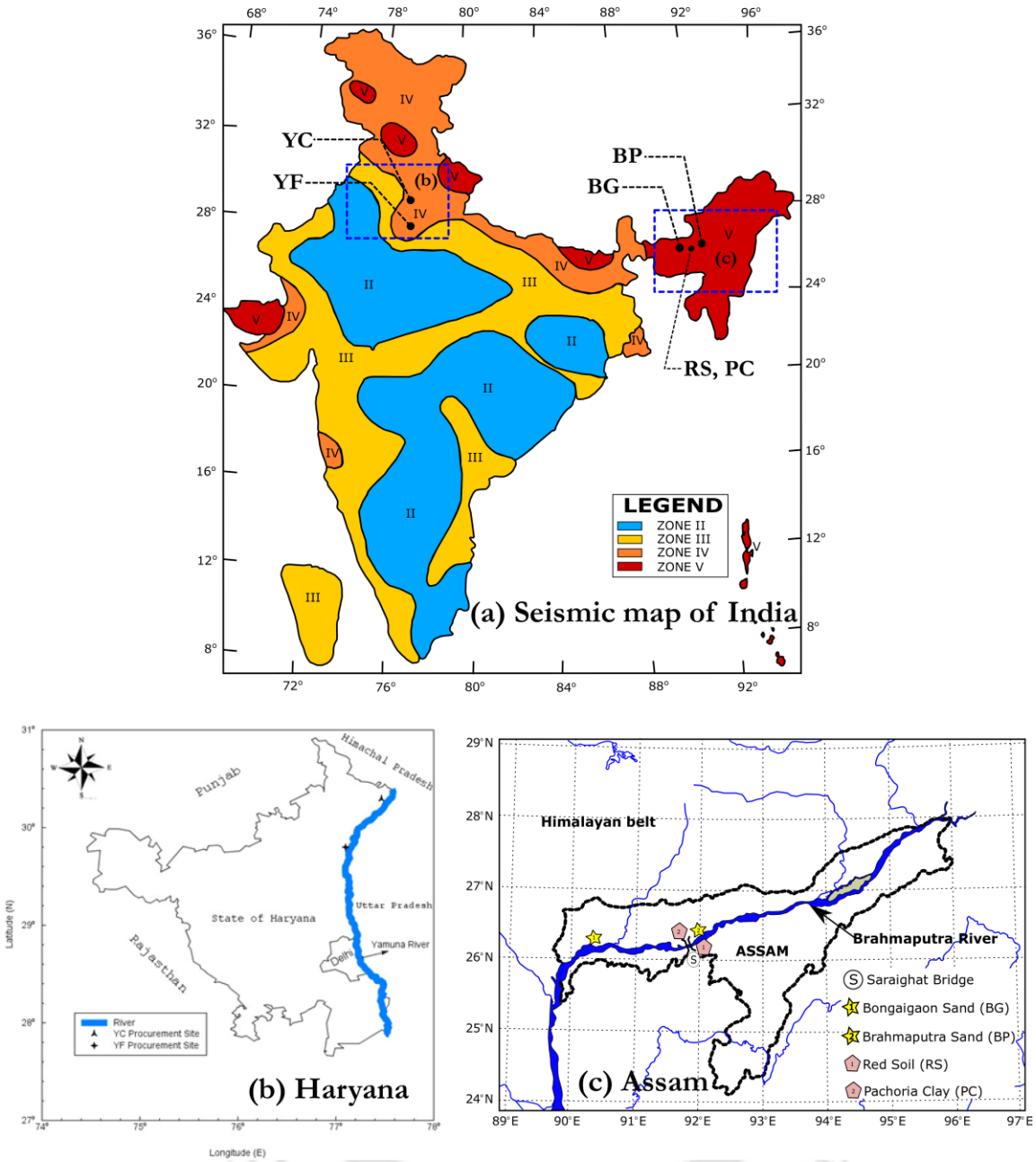

Fig. 3.1 (a) Seismic zonation map of India (redrawn after IS 1893-2016) marked with the considered soil locations and Soil samples location in **(b)** Haryana (**c)** Assam

The sandy soils sampled from northeastern India are from the shore of Brahmaputra River, one at Guwahati city named as Brahmaputra (BP) sand and the latter at Bongaigaon city abbreviated as BG (Bongaigaon) sand (Fig. 3.1c). The cohesive soils (Red Soil-RS and Pachoria Cohesive –PC soil) were sampled from Guwahati city of Assam (Fig. 3.1c). Both the cohesive soils are sampled at a depth of 2 m from the surface. It can be seen that the collected soil samples in Guwahati city are close to a bridge site (Saraighat Bridge). The remaining sandy soils were collected from the shore of another major river (Yamuna River) in Haryana (as shown in Fig. 3.1b), flowing through the northern India. The soils

are named as Yamuna Fine (YF) and Yamuna Coarse (YC) based on their visual grain size classification. All the sands were sampled on the shores of the two mentioned rivers and it is expected that most soils in the regions are river sediments. Selection of these particular soils is justified as no previous attempts were found to the author's knowledge in comprehensive dynamic characterisation of these soils.

3.1.1 Cohesionless Soils

The chosen sandy soils (BP, BG, YF and YC) were initially characterised based on their index properties. The grain size distribution (GSD) curves of the sands were developed using the dry sieve analysis as per the codal provisions (IS 2720: Part IV; ASTM D6913 2017). Fig. 3.2 presents the GSD curves of the sands superimposed with the zones of probable and highly liquefiable soils (PHRI 1997). It can be depicted from the GSD analysis that BP, BG and YF sands are highly susceptible to liquefaction while YC sand falls in the zone of probable liquefaction.

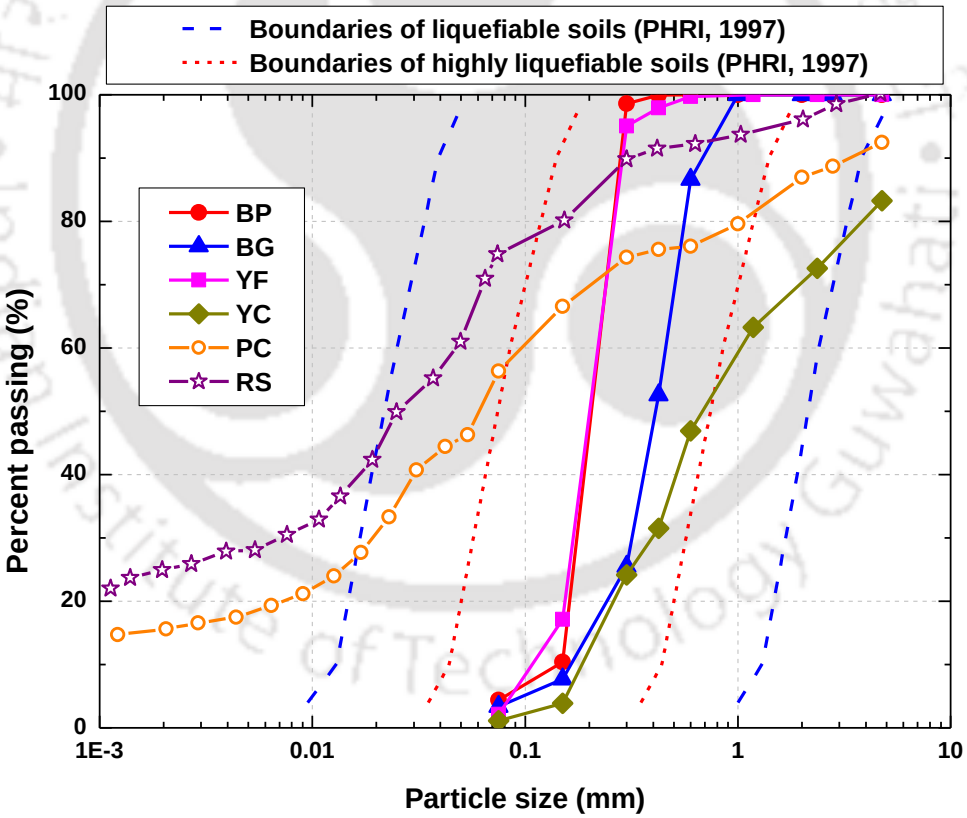

Fig. 3.2 Grain size distribution of chosen soils

Index properties of the sands such as specific gravity, minimum and maximum void ratios were determined following the relevant standards (IS 2720: Part III; ASTM D422-63 2007). All the index and GSD properties of the sands are summarized in Table 3.2. Based on the index properties and GSD analysis, all the sands are classified as poorly graded (SP)

as per the Unified Soil Classification System (USCS) (ASTM D2487 2014). To understand the shape of the chosen sands, Field Emission Scanning Electron Microscope (FESEM) pictures were obtained and presented in Fig. 3.3 (a-d). A sub-angular shape can be noted for all the sand samples.

Table 3.2 Index properties of chosen soils

Index properties	**BP**	**BG**	**YF**	**YC**	**PC**	**RS**
Gravel content, %	0	0	0	16.8	2.5	0
Sand content, %	95.6	96.6	97.8	82.1	8.6	30.3
Silt content, %	4.4	3.4	2.2	1.1	56.4	48.5
Clay content, %	---	---	---	---	32.5	21.2
D_{10}, mm	0.15	0.18	0.13	0.19	---	---
D_{30}, mm	0.19	0.32	0.18	0.40	0.02	0.007
D_{50}, mm	0.21	0.40	0.21	0.66	0.06	0.02
D_{60}, mm	0.22	0.46	0.23	1.00	0.09	0.05
C_u	1.46	2.55	1.78	5.24	---	---
C_c	1.09	1.23	1.04	0.84	---	---
Specific gravity (G_s)	2.72	2.70	2.72	2.70	2.70	2.65
e_{min}	0.622	0.580	0.65	0.38	---	---
e_{max}	0.962	0.910	1.02	0.59	---	---
Liquid limit, %	---	---	---	---	45	41.5
Plastic limit, %	---	---	---	---	23	22.6
Plasticity Index (PI)	---	---	---	---	22	18.9
USCS Classification	SP	SP	SP	SP	ML	ML

3.1.2 Cohesive Soils

Two cohesive soils were collected from two locations in Guwahati city and were named as Red Soil (RS) according to its visual identification and Pachoria Cohesive (PC) soil based on the location of sampling. Wet sieve, hydrometer and dry sieve analyses were performed to obtain the GSD of both the soils following the standards (ASTMD6913 2017). Fig. 3.2 and present the GSD curve and index properties of both the soils, respectively. The maximum dry density and optimum moisture content (OMC) of RS were found to be 1.78 g/cc and 19.3%, respectively. The field density and moisture content of PC was 1.6 g/cc and 23.86%, respectively. Both the cohesive soils are classified as low plastic silts (ML) based on the USCS classification system.

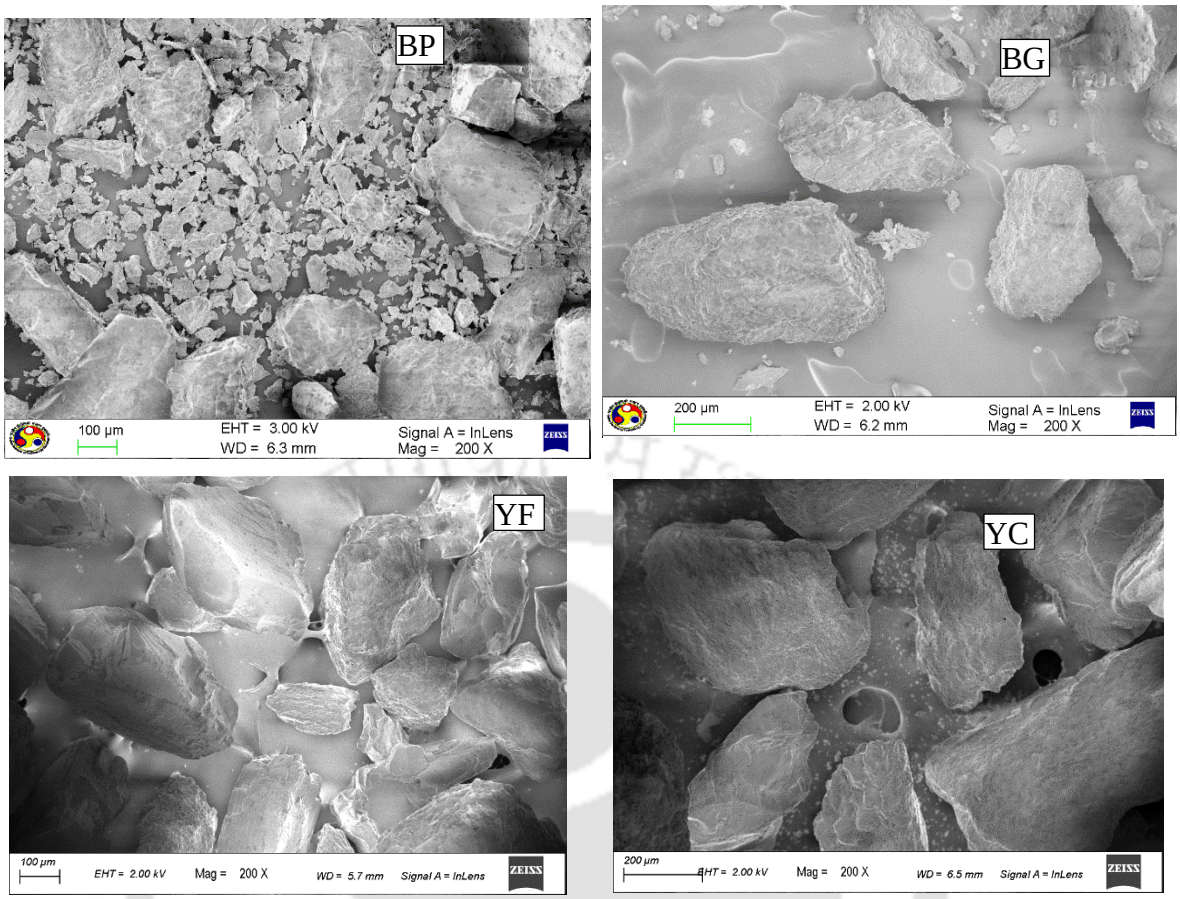

Fig. 3.3 FESEM pictures of chosen sands

3.2 MONOTONIC STRENGTH TESTS

The static response (referred as monotonic hereafter) is useful to understand the strength and stiffness characteristics of the soil. Elastic modulus (or secant modulus) of the soil is the most sought-after parameter which is useful in predicting the foundation response. This section describes the monotonic response of chosen soils, evaluated through triaxial compression tests.

3.2.1 Testing Program

Monotonic strength tests have been conducted on two sandy soils (BP and BG) and one clay (PC) while the static strength characteristics of YC, YF and RS were already reported elsewhere (Puri and Jain 2014; Kumar et al. 2018b). Table 3.3 briefs the monotonic testing programme adopted. In case of sandy soils (BP and BG), tests were conducted at both dry and saturated conditions while the tests on PC were conducted in only saturated conditions. Three effective confining pressures (σ'_c) of 50 kPa, 100 kPa and 300 kPa were chosen for the sandy soils at one initial relative density (R_d=30%) condition. In case of PC, tests were conducted at the field density, with a range of σ'_c (30-150kPa) (Table 3.3) with an aim to

utilize the results in analysis of pile foundations at the site. Only the initial relative density of the specimens is used for the calculations and possible void ratio changes during consolidation are not considered. Since, the tests on saturated conditions were conducted in undrained state, pore water pressures (PWP) were monitored for predicting effective stress response.

Table 3.3 Monotonic triaxial testing program

Soil	Condition	Type of triaxial test	R_d (%)	σ'_c (kPa)
BP	Dry	UU	30	50, 100 & 300
	Saturated	CU	30	50, 100 & 300
BG	Dry	UU	30	50, 100 & 300
	Saturated	CU	30	50, 100 & 300
PC	Saturated	CU	Field density	30-150

3.2.2 Sample Preparation

Cohesionless soils

Cylindrical soil specimens were prepared in reconstituted condition with the sample geometry of 70 mm in diameter and 140 mm length. Different sample preparation techniques such as moist tamping, water sedimentation, dry pluviation have been tried by Kumar (2018) for the sandy specimens and it was found that the dry pluviation technique linked with CO_2 flushing has yielded an expedited saturation process compared to the other sample preparation techniques. Tokimatsu and Hosaka (1986) reported that the dry pluviation technique with CO_2 saturation yields dynamic strength of soils similar to that of field samples collected through tube samplers. In addition, Tatsuoka et al. (1979) concluded that the dynamic shear modulus and damping properties may not significantly be affected by the method of reconstitution for clean sands. Based on these observations, the dry pluviation technique with CO_2 flushing has been adopted for the sample preparation. Using the targeted initial relative density (30%) and the dry unit weight of samples (1.46 g/cc), the quantity of soil required is determined. The calculated volume of soil is slowly poured in to the split mould fitted with a membrane (Fig. 3.4a) using a cone shaped funnel, adopting dry pluviation technique (Fig. 3.4b). Low magnitude of vacuum pressure (15 to 20 kPa) is then applied to the sample to keep the specimen intact after the removal of the mould (Fig. 3.4c). Then the split mould is removed, triaxial cell is slowly mounted and filled with the de-aired water. Once the cell is filled with de-aired water, vacuum pressure applied is slowly removed by applying the same amount of cell pressure. In case of unconsolidated undrained (UU) tests in dry condition, effective confining pressure on the specimen was increased by inputting the required pressure value in the

system connected to the pressure controller. However, in case of consolidated undrained (CU) tests, the samples were completely saturated. The method of saturation is elaborated in further sections.

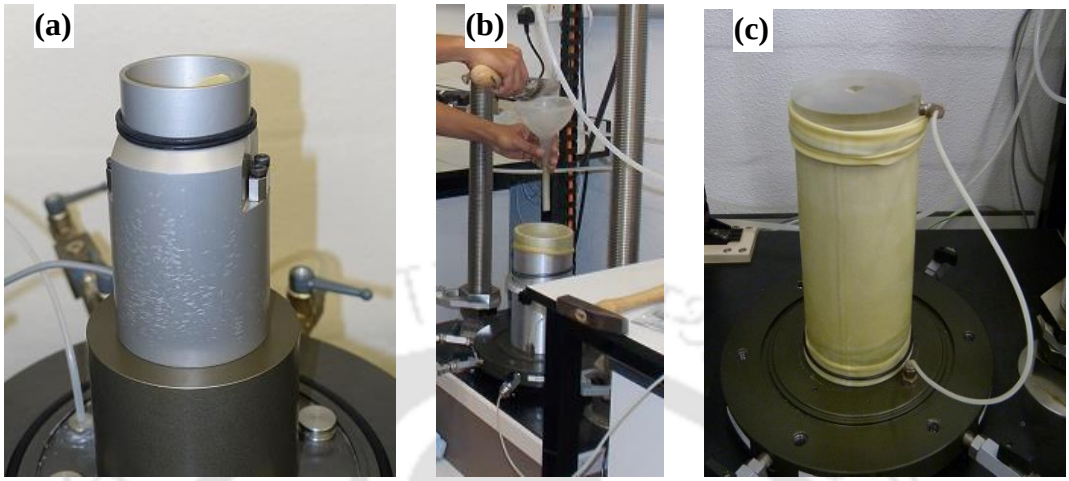

Fig. 3.4 (a) Split mould for the preparation of sand specimen (**b**) Sand pouring into the mould for moist tamping specimen (**c**) Prepared sand specimen

Cohesive soils

The remoulded clayey specimens (PC) were prepared at the saturated field density. The mould used for clayey specimen preparation is shown in Fig. 3.5 (a). Initially, dry volume of soil required based on the targeted density (1.6 g/cc) and water content (23%), is calculated and mixed thoroughly with the amount of water to form a uniform mixture. Then the mixture is slowly transferred in to the mould from one end, with the other end of the mould kept closed (Fig. 3.5b). Once filled, compaction was done from both the ends by rotating both the collars simultaneously, to maintain the uniform density of the specimen. Then the prepared sample is extruded using a sample extruder (Fig. 3.5 c). The sample is then kept on the base pedestal of triaxial system. A membrane is stretched over the extruded sample and triaxial cell is mounted and filled with de-aired water followed by cell pressure application. Next stage in specimen preparation is the saturation process.

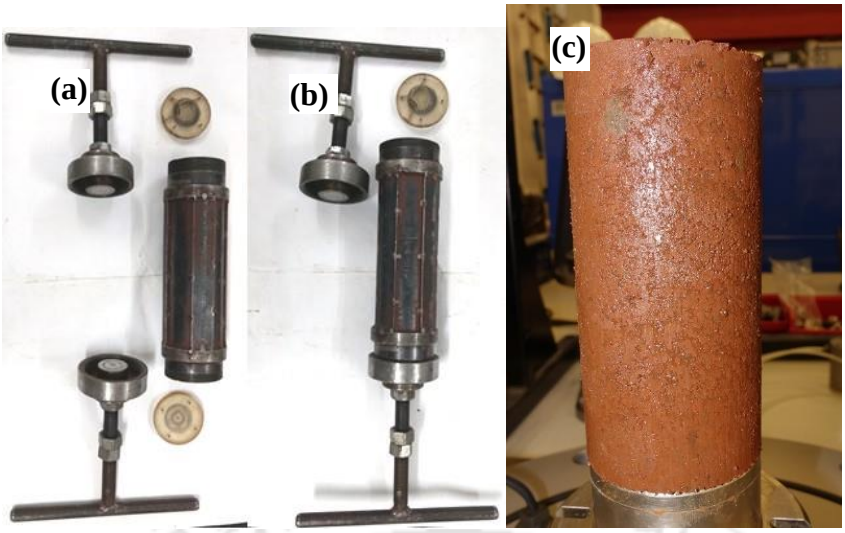

Fig. 3.5 (a) Mould for the clay specimen preparation (**b)** Mould with one end closed and the other end ready to be filled with the soil-water mixture (**c**) Prepared clay specimen

3.2.3 Saturation

Saturation process is similar for both the sandy and clayey specimens. Saturation is performed to create the specimens of fully saturated conditions for undrained tests. This phase involves the forced replacement of air voids in the sample with the de-aired water at high pressures. Initially, de-aired water is flushed through the sample so that the air voids can be replaced with that of the water molecules at prevailing normal head conditions. However, complete dissolution of air voids using de-aired water require huge amount of time. Therefore, the specimens were flushed with CO_2 for some duration (10-15 minutes) at pressure lower than the applied initial cell pressure. The CO_2 gas is made to flow through the sample from the bottom inlet of the triaxial cell base plate, and the voids are removed from the outlet attached at the top of the specimen. The complete dissolution of CO_2 (or the complete replacement of CO_2 with the air voids) can be ensured by checking no more release of air bubbles from the outlet. De-aired water is then allowed to flow through the CO_2 flushed specimen under normal gravity conditions. The complete dissolution of CO_2 in water is ensured by checking the escape of water from the outlet. In order to expedite the saturation process, both the cell pressure (CP) and the back pressure (BP) were gradually increased in multiple stages with constant maintenance of differential pressure of 10 kPa (Head 1992).

The degree of saturation of the specimen at each increment of cell pressure, is checked by monitoring the Skempton's pore pressure parameter (*B*-value). The *B*-value is defined as the ratio of excess pore water pressure (Δu) to the change in cell pressure ($\Delta\sigma'_c$). In order to determine the *B*-value, cell pressure is increased and the drainage valves are closed (to

maintain undrained conditions) and the corresponding Δu is measured. The complete saturation of the specimen is ensured upon a *B*-value of 0.95 or beyond. Typically, BP and BG sand specimens at loose condition (30% R_d) require 4-5 hours for complete saturation while PC sample needed more than 24 hours. Once the saturation of the sample is ensured, the samples were brought to the required σ'_c by isotropic consolidation. This is achieved by increasing the CP while maintaining a constant BP and opening the drainage value (drained conditions allowed in consolidation). As the water drains, volume changes and effective stress increases, and the difference of CP and residual pore pressure of the specimen is represented as the effective stress.

The desired σ'_c was assumed to be achieved when the difference between CP and pore pressure becomes equal to the targeted σ'_c value. In case of sandy specimens, consolidation stage was assumed to be completed when the excess Δu reaches the applied BP. However, in case of cohesive samples, as the time required for complete consolidation is significantly long, the consolidation stage was assumed to be finished when the volume changes become almost constant or when 95% of excess PWP is dissipated.

3.2.4 Monotonic Response of Cohesionless Soils

Monotonic shear tests (under constant axial compression) were conducted on the prepared cylindrical specimens at different σ'_c conditions for cohesionless (50 kPa, 100 kPa and 300 kPa) and cohesive soils (30 kPa to 150 kPa). It must be mentioned that the initial relative density of the specimen was only considered for all the tests and not the consolidated density. Kumar (2018) conducted strain-controlled monotonic triaxial tests with a wide range of strain rate (0.05 mm/min to 5 mm/min) and reported that strain rate beyond 1.2 mm/min was not significantly affecting the strength properties of soils as well as equilibrate the pore water pressures for sandy specimens. Therefore, a strain rate of 1.2 mm/min is adopted for the current tests. As sandy specimens were tested in both dry and saturated conditions, the description is also made independently first and then followed by a comparison of the response in both the cases at different effective confining pressures. Since, the saturated tests involve pore pressure monitoring, the undrained response is also presented for all the CU tests.

Fig. 3.6 (a and b) presents the monotonic response of BP sand in terms of stress-strain behaviour and stress path at different σ'_c values. It can be inferred that the increase in the σ'_c increases the deviatoric stress at any axial strain. This means that the increase in the

depth of over burden increases the resistance to deformation at all other conditions keeping same. To confirm the reliability of the experimental results, test at 100 kPa σ'_c for BP sand was repeated and results were found to be consistent (Fig. 3.6a). It can also be noted that the increased σ'_c resulted in less dilative tendency and a gradual contractive response at 300 kPa σ'_c. This manifests that the increased depth of overburden results in overlocking of particles in loose and medium dense granular soils. Similar reduced dilative response for high σ'_c conditions has been reported for Fraser River sand by Vaid and Thomas (1995) in loose conditions, and for Ahmedabad sand (India) by Dash and Sitharam (2011). The stress-path which is represented by the variation of deviatoric stress (q) (Eqn. 3.1) to the mean effective confining pressure (p') (Eqn. 3.2) is shown in Fig. 3.6b for BP sand at 30% R_d for three σ'_c conditions.

$$q = \sigma_1' - \sigma_3' \quad (3.1)$$

$$p' = \left(\frac{\sigma_1' + 2\sigma_3'}{3}\right) \quad (3.2)$$

where σ_1' and σ_3' are the major and minor principal stresses, respectively.

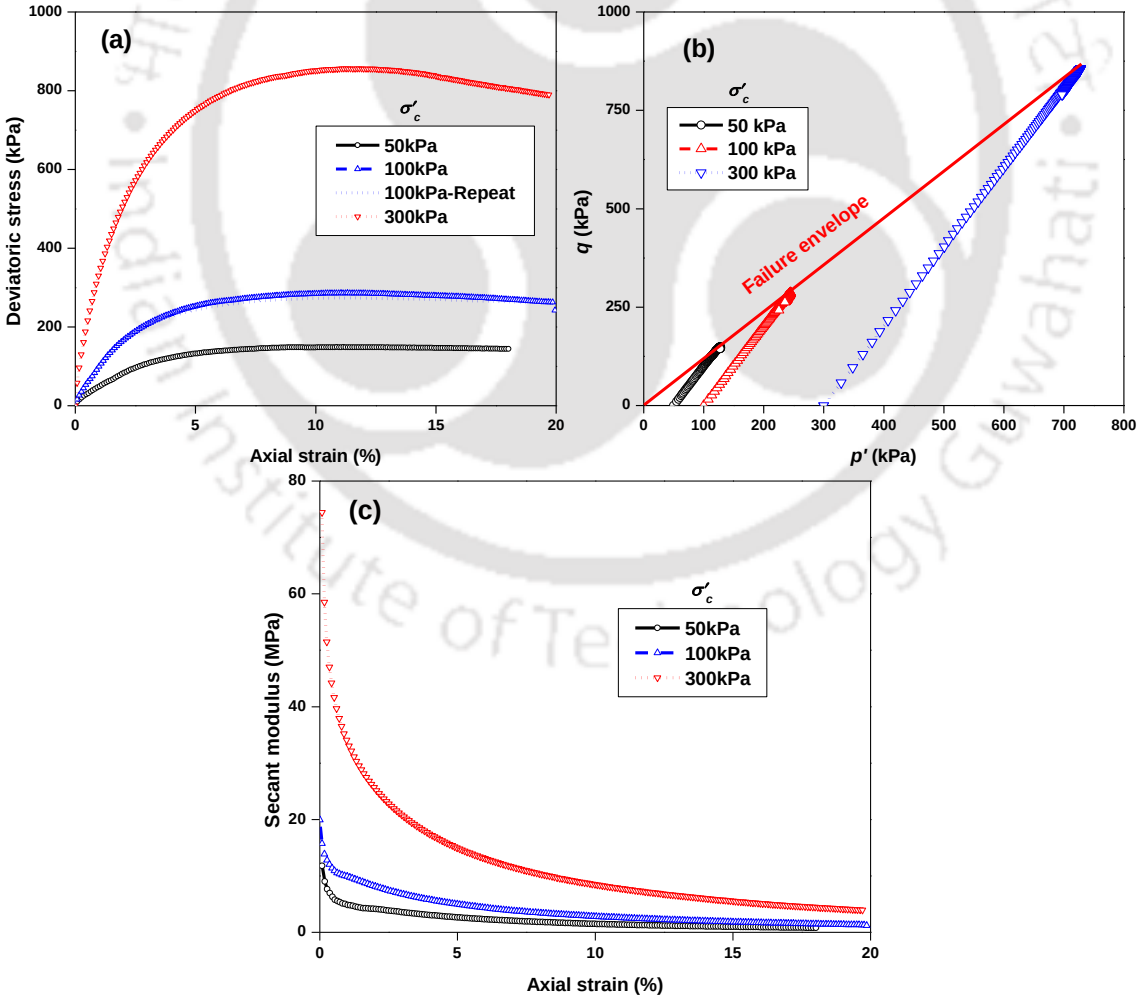

Fig. 3.6 Response of BP sand in dry tests **(a)** Stress-strain response and (**b**) Stress path

With no pore pressures existing in the dry conditions, a linear stress path trend is visible. Fig. 3.6 (c) presents the variation of secant modulus (E_{sec}) with strain for BP sand at different σ'_c conditions. Secant modulus is evaluated as the ratio of deviatoric stress to axial strain. With increase in the axial strain, E_{sec} reduces and with increase in the σ'_c, E_{sec} is increased showing the effect of depth of overburden on the static strength of granular soils. However, with strains approaching very high values (beyond 5%), E_{sec} values are stabilized owing to the stabilized stress-strain response (Fig. 3.6a). It can also be noted that the difference of E_{sec} at high strains for different σ'_c is narrowed down. The values of E_{sec} are essential for many geotechnical applications. Similar response in dry conditions was also observed for BG sand as shown in Fig. 3.7 (a-c).

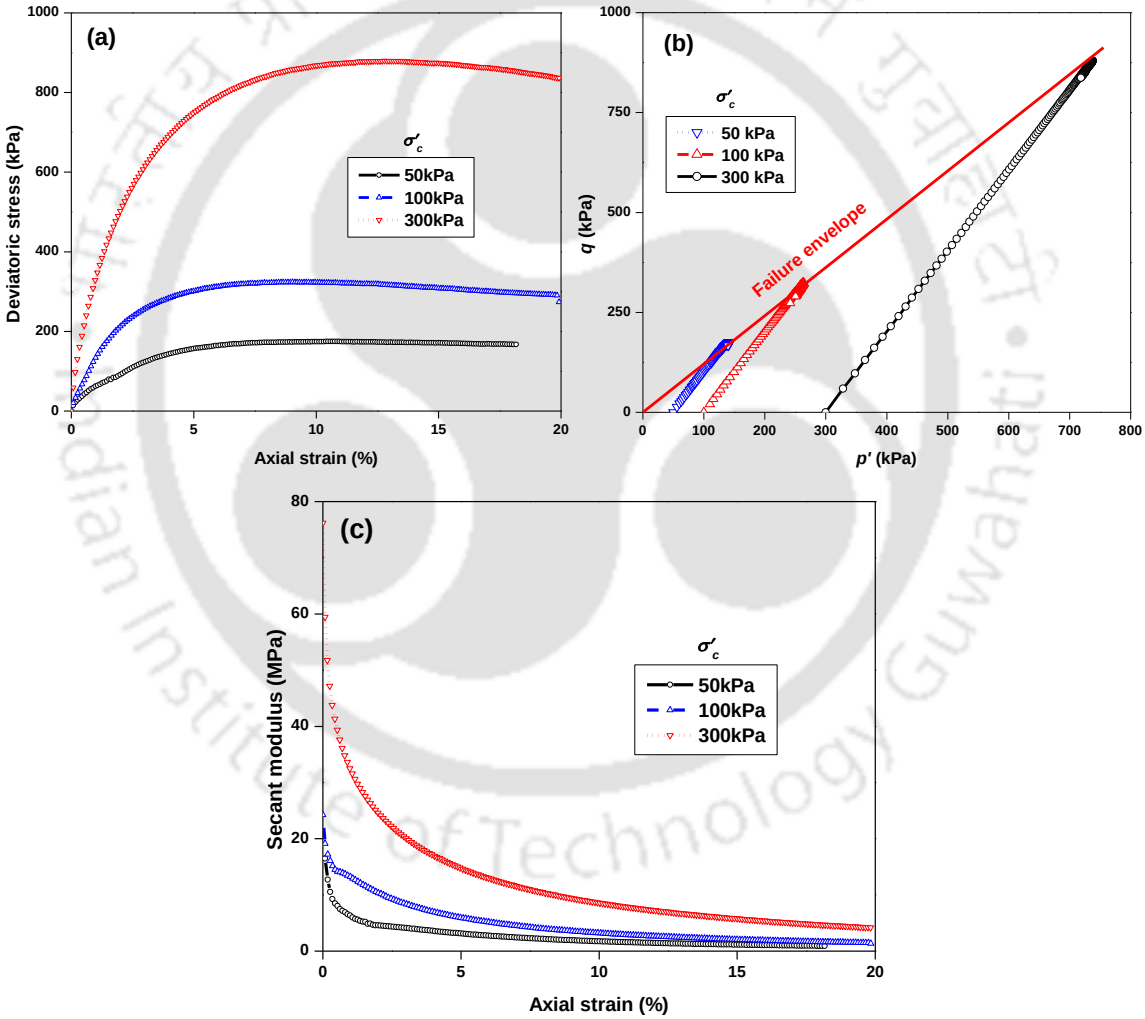

Fig. 3.7 Response of BG sand in dry tests at different σ'_c values **(a)** Stress-strain response and (**b**) Stress path

The response of BP and BG sand specimens under saturated CU conditions is presented in Fig. 3.8 and Fig. 3.9, respectively. Fig. 3.8 (a) presents the variation of deviatoric stress with the axial strain for BP sand at different effective confining stress conditions. Increase

in the strength of the granular soil with increase in σ'_c is obvious. Fig. 3.8 b and c present the variation of pore water pressure and stress path for BP sand respectively. At the initial straining of the specimen (<1%), the pore pressures increased (Fig. 3.8b) leading to reduced effective stress (Fig. 3.8c), due to the contractive behaviour of the loose granular soils and this behaviour is prominent at high σ'_c. However, with increase in the axial strains, dilative behaviour of the sandy specimens (due to redistribution of pore pressures within the specimen) is witnessed owing to the reduced pore pressure (Fig. 3.8b) and increased effective stress (Fig. 3.8c). The variation of secant modulus for BP sand at different effective confining pressures is also presented (Fig. 3.8d). Similar undrained response was also observed for BG sand (Fig. 3.9). The peak friction angle obtained from the CU tests is 30.17° for BP sand and 28.4° for BG sand at 30% relative density condition.

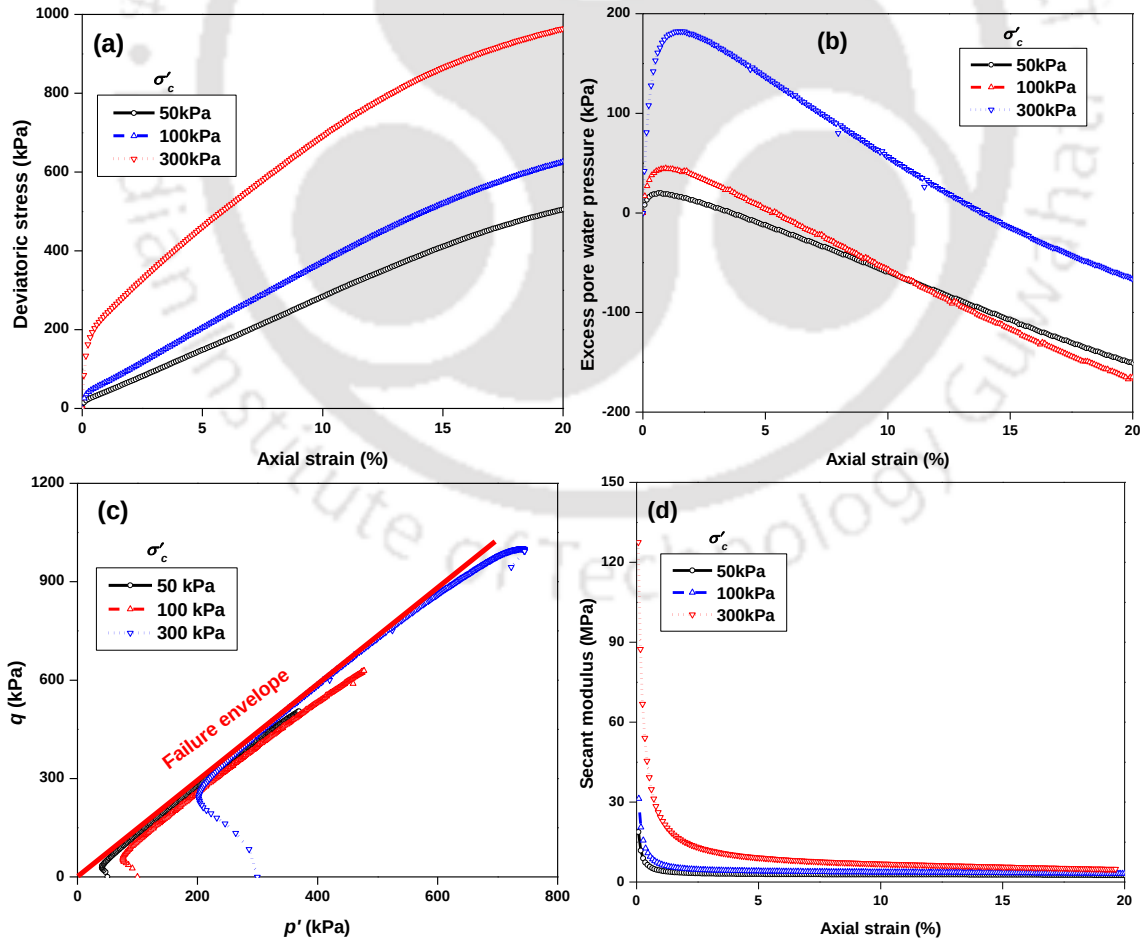

Fig. 3.8 Response of BP sand in saturated CU tests at different $\sigma'c$ values **(a)** Stress-strain response (**b**) Pore water pressure variation with strain (**c**) Stress path and (**d**) E_{sec} variation

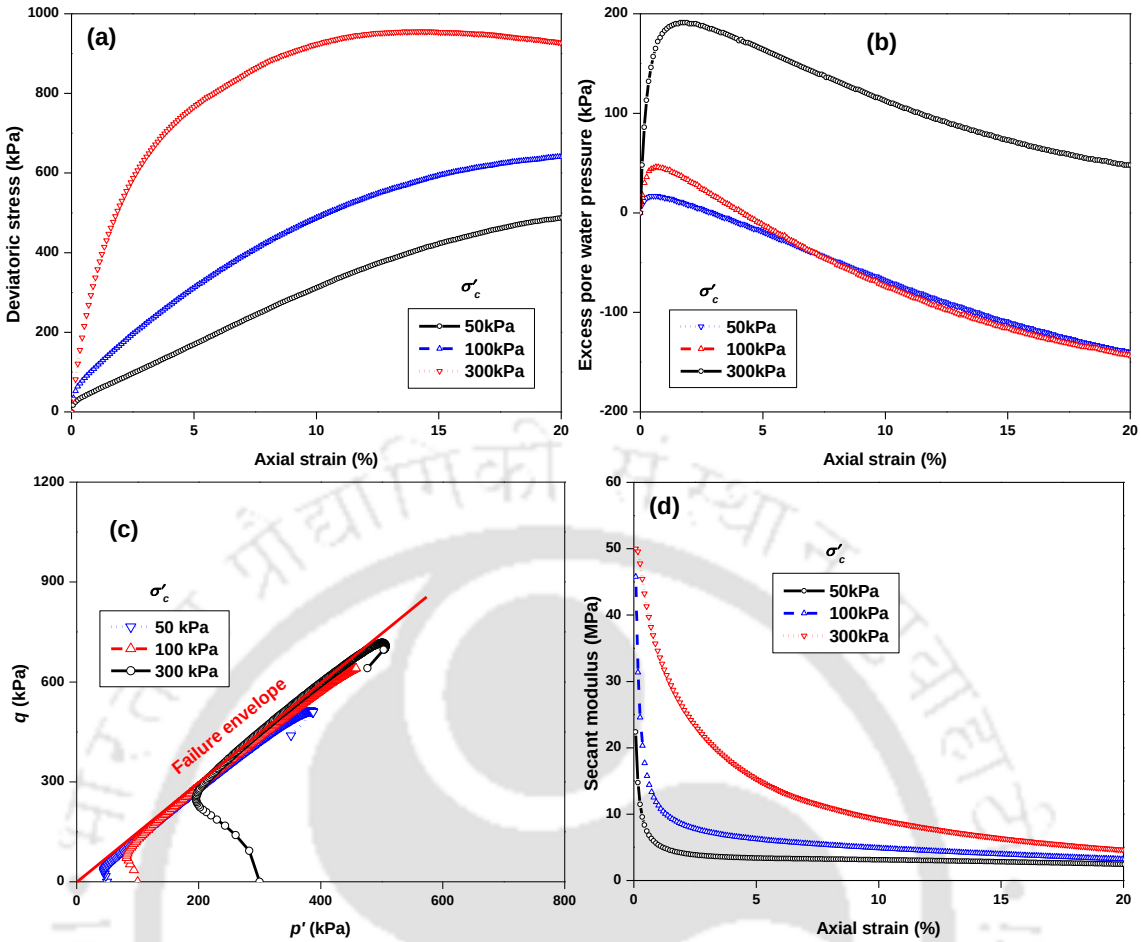

Fig. 3.9 Response of BG sand in saturated CU tests at different σ'_c values **(a)** Stress-strain response (**b**) Pore water pressure variation with strain (**c**) Stress path and (**d**) E_{sec} variation

A comparison is made for the response of tested sand specimens in CU conditions and few sandy soils from literature: Fraser River sand (Vaid and Thomas 1995), Toyoura sand (Ishihara, 1993), and Ahmedabad sand (Dash and Sitharam 2011). Fig. 3. 10 presents the comparison of monotonic response for the sandy soils at comparable R_d conditions. It must be mentioned that Fraser River sand specimens (R_d=40%) and Toyoura sand specimens (R_d=38%) were prepared through water pluviation technique. Ahmedabad sand (Gujarat, India) specimens were prepared by dry pluviation technique. It should also be noted that all the sands are poorly graded and the specimens were consolidated and tested under CU conditions at σ'_c of 100 kPa. Fraser River sand was tested up to 7% of axial strains while Toyoura sand specimens were tested up to 25% axial strain. It can be seen that Fraser River sand yielded similar response of BP sand while Toyoura sand showed significantly higher strength at 38% R_d conditions. Ahmedabad sand (36% R_d) showed similar response of BP sand in the strain range up to 5% and the differences are prominent with increased axial strains. Such differences in strength (and resulting shear strength parameters) can be

attributed to various characteristics such as index, geological and formational properties and therefore, it is necessary to evaluate the monotonic strength of soils of interest.

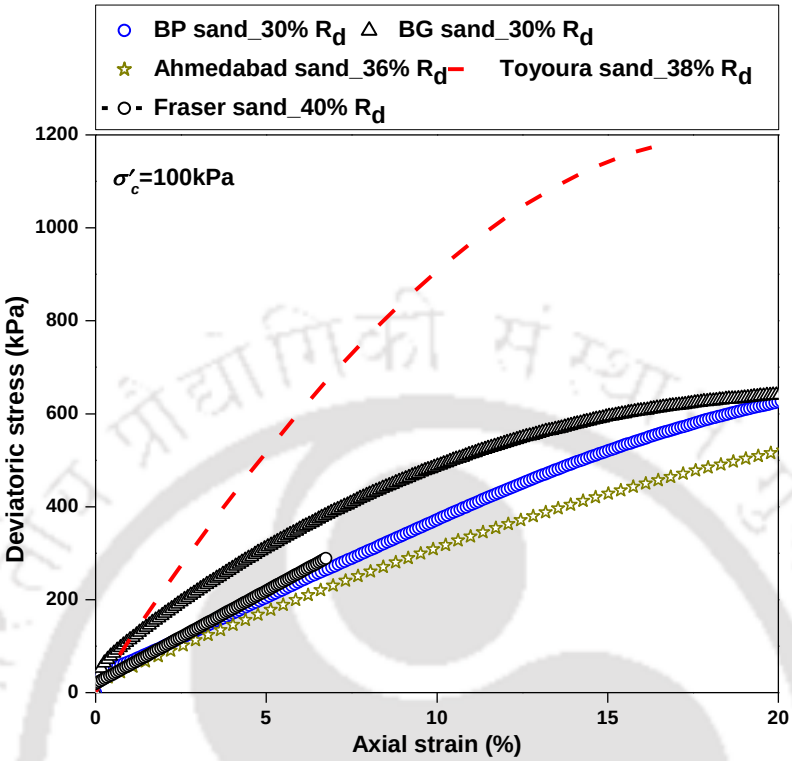

Fig. 3. 10 Comparison of monotonic behaviour of BP and BG sands with that of sands collated from literature

A comparison is made between the response obtained from dry and saturated tests for sandy specimens. Fig. 3.11 and Fig. 3.12 presents the comparison in terms of stress-strain, stress path and E_{sec} for both the soils, respectively. It can be observed that the specimens in saturated conditions showed lower strength at strains<6% while higher strength was observed at high strains than the dry specimens. This behaviour can be explained by the stress path shown in Fig. 3.11b. It can be seen that during the initial straining, pore pressures increase in the saturated specimen leading to reduced effective stresses causing lower stress-strain response compared to the dry specimen (with no pore pressure generation). However, with further straining, due to the dilative behaviour of sands in saturated conditions, pore pressures redistribute within the particles (reduction of pore pressures) and effective stress increases leading to higher stress-strain response. The point at which the soil behaviour changes from contractive to dilative behaviour (deviatoric stress changes its sign from minimum to increasing trend) is known as the state of phase transformation (Ishihara 1993). Fig. 3.11d presents the variation of E_{sec} with axial strain for BP sand. It is clear that the initial E_{sec} (also called tangent modulus-E_{tan}) is relatively

higher for saturated specimens (32 MPa for saturated specimen and 20.6 for dry specimen at 100 kPa σ'_c). The discussed decreased and increased response of saturated specimen is also clear from the E_{sec} plot. Similar observations were noticed for BG sand at similar effective confining pressures (Fig. 3.12).

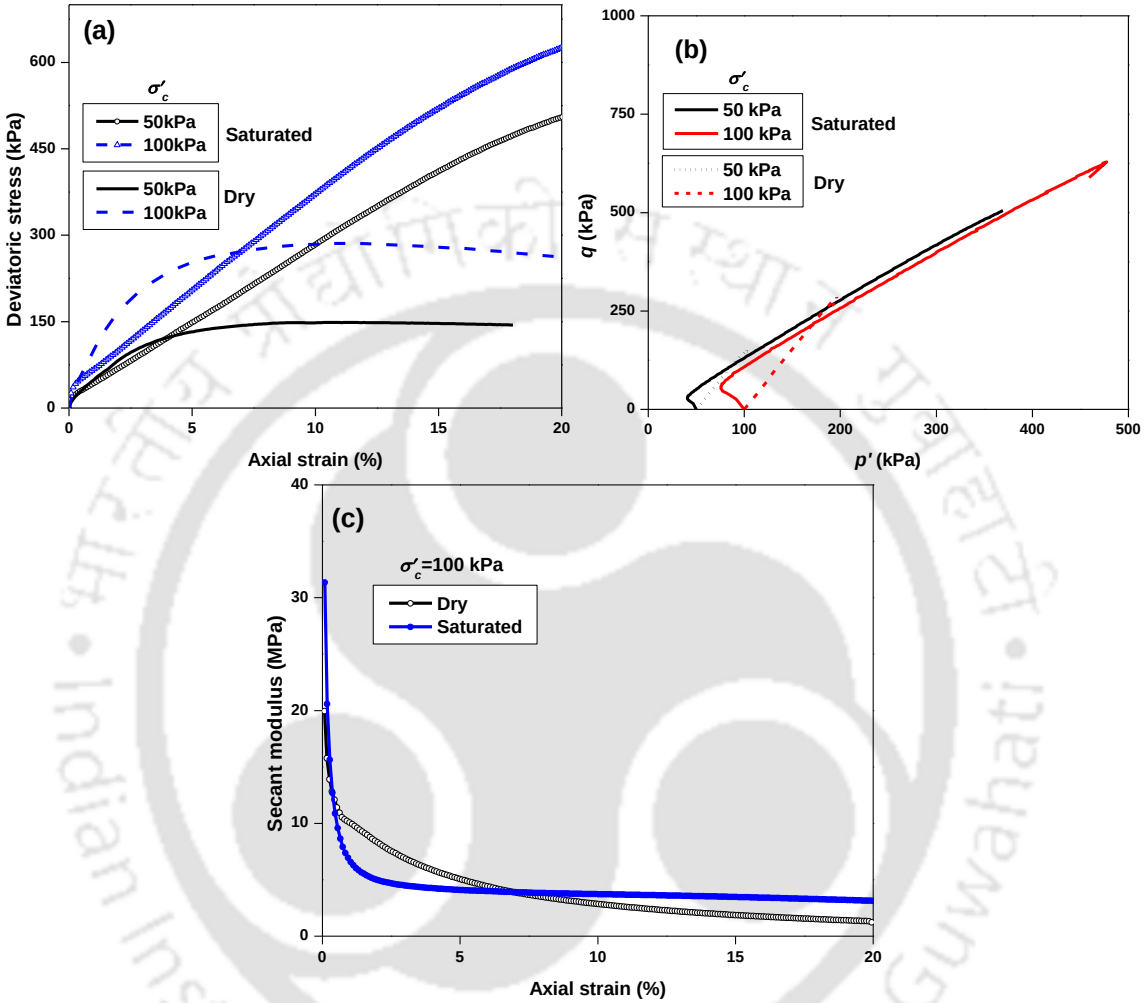

Fig. 3.11 Comparison of dry and saturated (CU condition) response of BP sand (**a**) stress-strain behaviour at 50 kPa and 100 kPa σ'_c (**b**) Stress path in dry and saturated conditions and (**c**) E_{sec} variation

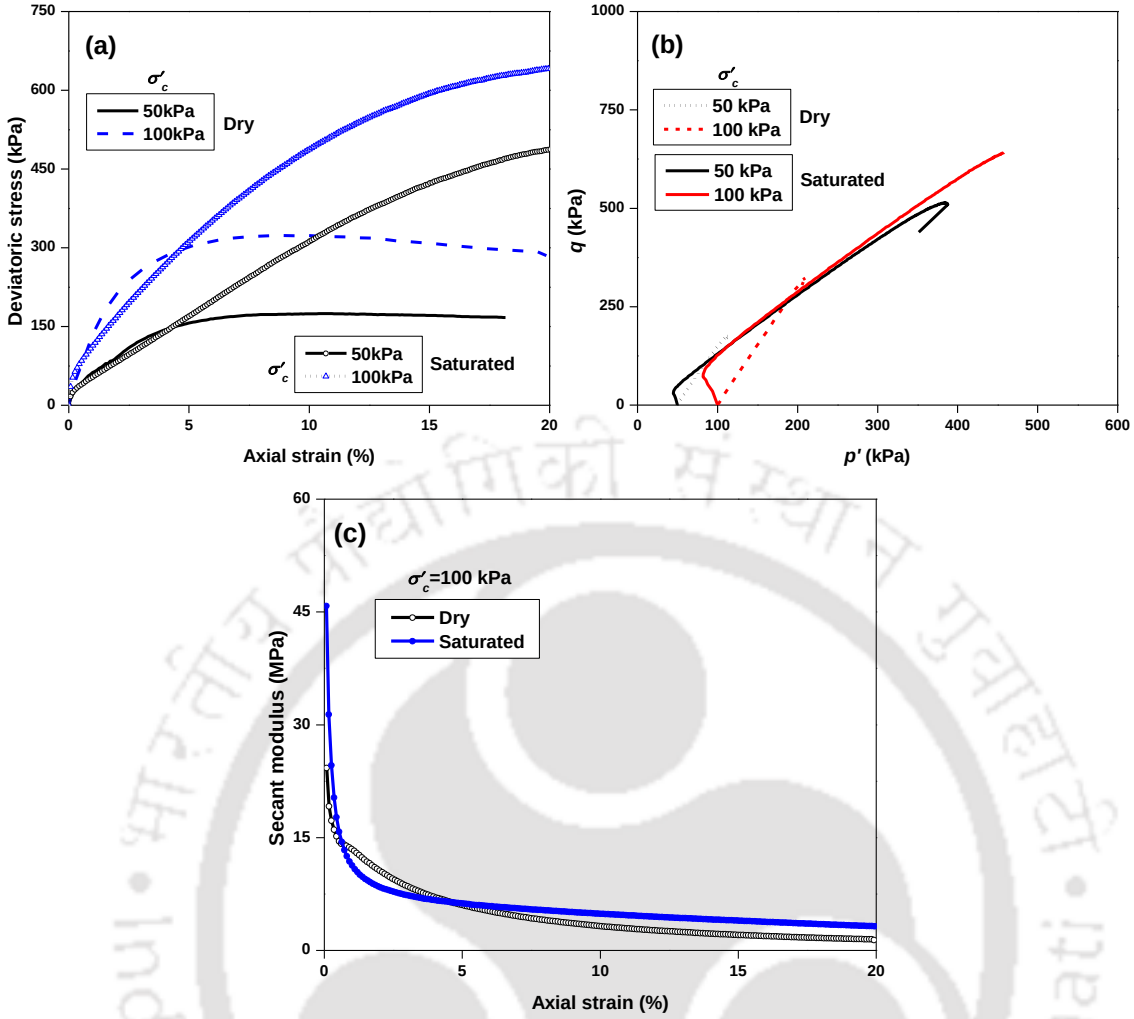

Fig. 3.12 Comparison of dry and saturated response of BG sand (**a**) stress-strain behaviour at 50 kPa and 100 kPa σ'_c (**b**) Stress path in dry and saturated conditions and (**c**) E_{sec} variation for 100 kPa σ'_c

3.2.5 Monotonic Response of Cohesive soils

Monotonic triaxial compression tests were conducted on Pachoria cohesive specimens (PC) at different σ'_c conditions. The testing procedure is similar as explained in the cohesionless soil section. Fig. 3.13 (a-d) presents the monotonic response of PC in terms of stress-strain, pore pressure generation, stress path and E_{sec} variation along the axial strain. With increase in σ'_c, the deviatoric stress increased at all the effective confining pressures, similar to the response of sandy specimens. The deviatoric stress reached peak values in the initial straining, followed by stabilized response, which can be described by the pore pressure generation shown in Fig. 3.13b. It can be seen that the pore pressures increased in the initial strain levels followed by constant values. Since, the samples are prepared at field density, dissipation of pore pressures was not seen during the testing. The stress path and E_{sec} of PC is presented in Fig. 3.13c and d respectively. The peak cohesion and friction angle of PC are 12 kPa and 10°, respectively.

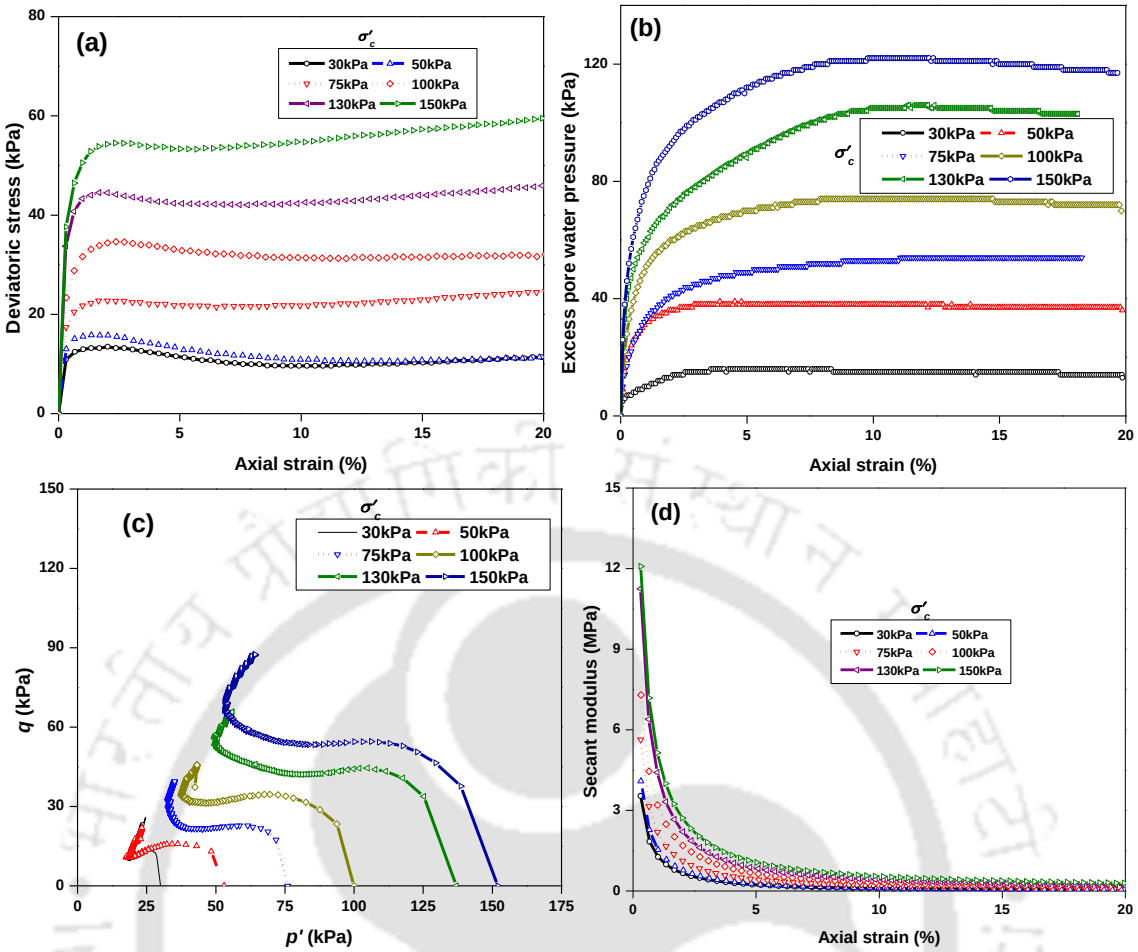

Fig. 3.13 Response of PC in saturated CU tests at different σ'_c **(a)** Stress-strain response (**b**) Pore water pressure variation with strain (**c**) stress path and (**d**) E_{sec} variation

3.3 DYNAMIC TESTING PROGRAM

In the present study, four widely used advanced element testing techniques were adopted to strategically investigate the dynamic behaviour of the chosen soils. Bender Element (BE) tests were conducted to understand the low strain (strains≤0.0001%) elastic behaviour (essentially the low strain shear modulus, G_{max}). Resonant Column (RC) apparatus was adopted for low to intermediate strain behaviour (0.0001% to 1%) assessment while Dynamic Simple Shear (DSS) apparatus was utilised for high strain testing (strains>1%). In addition, Cyclic Triaxial (CTX) apparatus was adopted for liquefaction assessment of soils. Table 3.4 presents the dynamic testing programme and associated parameters of investigation.

3.3.1 Bender Element Tests

Bender Element (BE) test is a low strain test as it provides the dynamic shear modulus (G_{max}) upon relation to the shear wave velocity (V_s) of the soil at shear strains $<10^{-6}$. The BE test by name consists of piezoelectric bender elements which are essentially electro-

mechanical transducers that can generate voltage as they bend (Viggiani and Atkinson 1995). Lawrence (1963) initially developed shear plate apparatus for measuring small strain shear modulus through application of shear waves which was further refined by researchers (Shirley et al. 1978) by using bender elements. Both the shear (V_s) and compressional (V_p) wave stiffness can be measured using the bender elements. Basic principle involved is the *wave propagation through a prismatic rod*. The bender elements are normally installed at top and bottom of a soil sample in a triaxial cell and measurements are done.

Table 3.4 Dynamic testing programme and the parameters of investigation

Test	Soil	Range of R_d (%)	Range of σ'_c (kPa)	Range of γ (%)	f (Hz)	Range of CSR	No of tests	Results targeted
BE	BP	30-70	50-1000	<0.0001 %	----	----	2*	G_{max} with varying σ'_c
	BG				----	----	2	
	YF				----	----	2	
	PC	Field density	50-600		----	----	2*	
	RS	MDD			----	----	2	
RC	BP	30-70	50, 100, 300	0.001%-0.1%	5-250	----	12*	G and D variation with γ for strains≤0.1%
	BG					----	12	
	YF	45-85	50, 100, 200, 300			----	12	
	YC	30-60				----	12	
	PC	Field density	50, 100, 200			----	3	
	RS	MDD				----	3*	
DSS	BP	50	50, 100, 300	0.05% to 5%	0.5-1	---	22	G and D variation with γ for strains≤5%
	BG					---	16	
	YF					---	16	
	YC					---	16	
	PC	Field density	100	0.1% to 5%	1	---	6	
	RS	MDD			1	---	6	
CTX	BP	30-90	100	---	1**	0.15, 0.225*, 030	9	CSR with loading cycles and r_u
	PC	MDD	100	---	1	0.20, 0.40	2	

Note: Tests with * symbol are repeated to check the repeatability of the apparatus; ** denotes tests up to liquefaction

BE Apparatus and Components

The BE apparatus shown in Fig. 3.14a supplied by VJ Tech Ltd, available at the Surrey Advanced Geotechnical Engineering (SAGE) laboratory, University of Surrey, UK has been utilised for the testing. The test basically comprises of sending a wave from a transmitting element (also called transmitter), through a soil sample to a receiving bender

element (receiver) and measuring the arrival time of the input signal at the receiver. Effective sample height, L_{eff} (tip-to-tip distance between transmitter and receiver bender elements) divided by the time of wave travel yields the velocity of wave propagation. The effective sample height is calculated as the difference of initial specimen height to the twice of bender element penetration (each bender element protrudes 2 mm in to the specimen).

BE apparatus composes of a triaxial system for consolidating the sample, bender element scope system with a pair of leads (Fig. 3.15) for generating the required input signals, pair of bender elements to record the input and output signals, and a computer equipped with CLISP STUDIO programme for inputting the instructions to the bender element scope arrangement. A schematic view of the isotropic test conditions prevail in the BE test are shown in Fig. 3.14b.

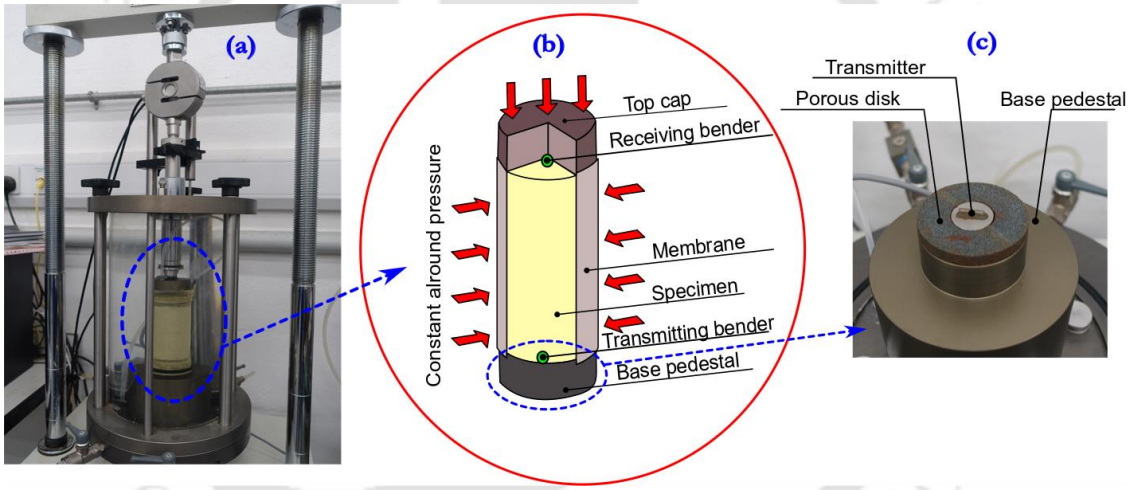

Fig. 3.14 (a) Bender element apparatus (**b**) Schematic view of loading on the sample and (**c**) View of transmitting bender element at the base

Fig. 3.15 Bender element scope system and leads for generation of input signals and monitoring the output signals

Testing Procedure

Sample preparation is similar to a standard triaxial test specimen. The sand samples were tested in dry conditions as the saturation is not expected to alter the low strain dynamic properties (Saxena and Reddy 1989; Chattaraj and Sengupta 2016). Sample geometry is 50 mm in diameter to 100 mm in height with an aspect ratio of 2. Before the sample preparation, a bender element is installed on the pedestal (Fig. 3.14c) around which a porous plate is placed. Once the specimen is prepared, the top cap fitted with the receiver bender element amidst the top porous stone, is installed over the specimen. Fig. 3.16 (a and b) presents the schematic view of specimen condition in BE tests and the view of bender elements used for the testing. The top cap should be aligned in such a way that both the bender elements (top and bottom) are parallel. Required isotropic consolidation is provided to bring the sample to the targeted effective confining pressure (σ'_c).

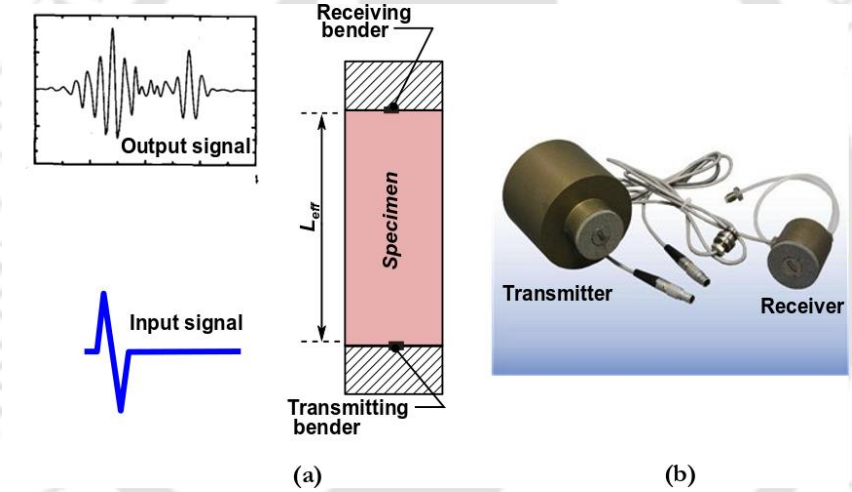

Fig. 3.16 Schematic representation of **(a)** BE testing principle and **(b)** view of bender elements

Once the specimen is prepared and the required σ'_c is applied (let us say 50 kPa), source signals in the form of shear waves with a range of frequencies (typically from 1 kHz to 30 kHz) is passed through the transmitter and the response (wave form) is recorded at the top bender element (receiver). Computer program CLISP STUDIO is connected to the system which records the travelling time using the top bender element. Once the velocity at one effective confining pressure is obtained, cell pressure (σ'_c) is then increased (100 kPa) to establish velocity at the corresponding effective confining pressure. The procedure of determining V_s at incremental effective confining pressures is continued up to the maximum considered σ'_c.

Typical Results

A typical wave form of input frequency (f) 1 kHz is shown in Fig. 3.17, for a dense BP sand sample. The difference of time from the peak of the transmitted wave to the first noticeable peak of the receiver wave is considered to be the arrival time of the wave (T_s). For a clear identification of arrival signals at the receiver and elimination of near-field effects, high frequencies (f) of input signals are recommended as they ensure efficient separation of the near-field coupled compression and shear. For this purpose, researchers adopted varying range of frequencies (5 Hz to 25 kHz) with wavelength ratio (L_{eff}/λ, λ is the wavelength) range of 1 to 15 to quantify the near-field effects (Arulnathan et al. 1998; Ec et al. 2005). Hinged on this, in the present study, input pulse frequencies are varied from 1 kHz to 30 kHz at each effective confining pressure to identify the optimum frequency at which characteristic peak of the output signal is identified. Fig. 3.18 presents the input and output signals for dense YF sand specimen at 50 kPa effective confining pressure. It can be seen that a wavelength ratio of 5 can provide an observable output signal with reduced noise effects. It must be noted that such optimum wavelength ratio depends on type of soil, compactness of soil and the effective confining pressure, therefore, the optimum ratio should be determined for every scenario.

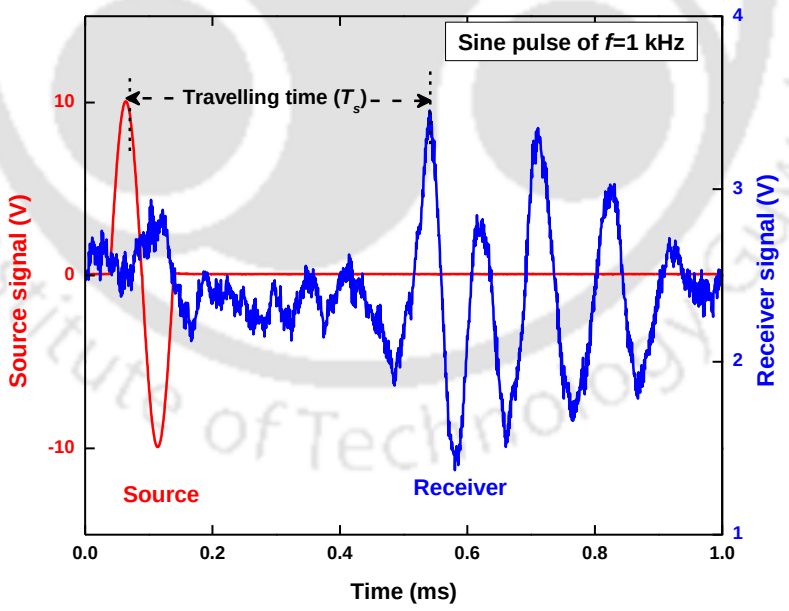

Fig. 3.17 Typical input and output signals from CLISP STUDIO on BP sand

Once the optimum wavelength ratio is determined for a soil specimen, automatic stacking technique (with two or more input signals of same frequency and amplitude) was used which provides the average arrival time (T_s). Using the physics of time and distance (height

of sample), one can simply estimate V_s and the required shear modulus (G_{max}) can be obtained using the wave propagation principle (Eqn. 3.3).

$$G_{max} = \rho \cdot V_s^2 = \rho \cdot (\frac{L_{eff}}{T_s})^2 \quad (3.3)$$

where ρ is the density of the sample; L_{eff} is the effective length of the specimen; and T_s is the arrival time of the shear wave. Fig. 3.19 presents the variation of V_s over the range of forcing frequencies for 50 kPa, 100 kPa and 600 kPa effective confining pressures. It can be observed that the measurements of V_s are sensitive to the input frequency and a stable equilibrium is achieved beyond an input frequency of 5 kHz.

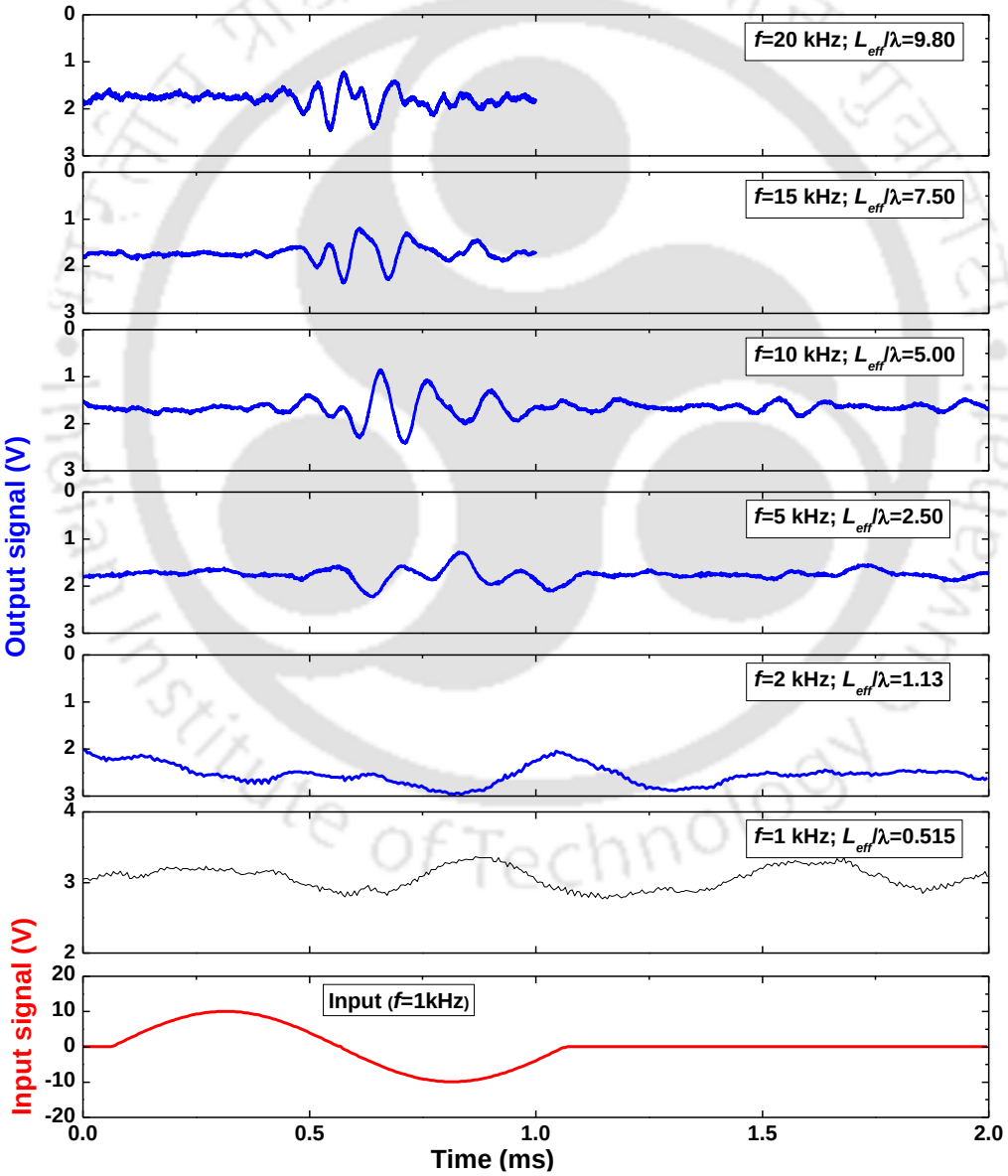

Fig. 3.18 Effect of input frequency on received signals for YF sand dense specimen

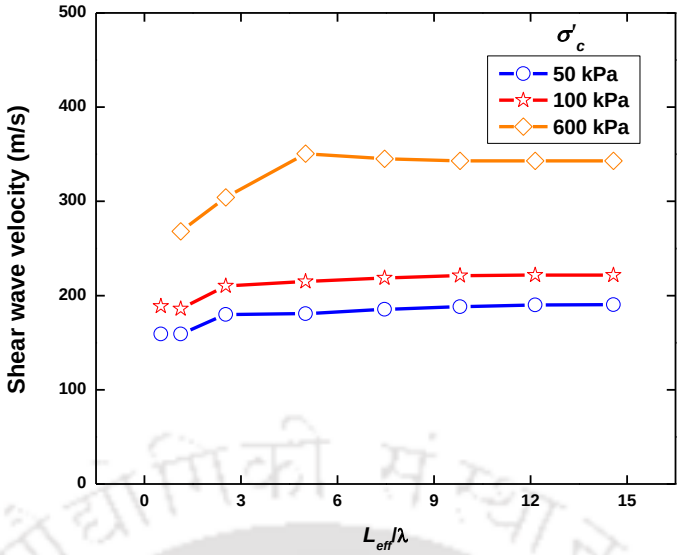

Fig. 3.19 V_s variation over forcing frequency for BP sand

3.3.2 Resonant Column Tests

Resonant Column (RC) test is used to measure the shear modulus and damping characteristics of soils from low to intermediate strain levels ($0.001\% \leq \gamma \leq 0.1\%$). The RC technique was initially used for soils by Iida (1938), following which the method was modified by many researchers (Hardin and Music 1965; Hardin 1970; Clayton et al. 2009) and was also standardized in (ASTM D4015 2014). Basic principle involved in RC test is to vibrate a cylindrical soil specimen in a fundamental mode of vibration, either in torsion or in flexure. Once the fundamental mode is established, measurements of resonant frequency (f_{nz}) and amplitude of vibration in terms of γ, are made.

RC Apparatus and Components

A fixed-free configuration of the Stokoe type RC apparatus, supplied by GDS Instruments UK, available at the SAGE Laboratory, University of Surrey, UK has been utilised for the testing. Fig. 3.20 shows the view of RC apparatus along with the schematic view of loading conditions prevailing during testing.

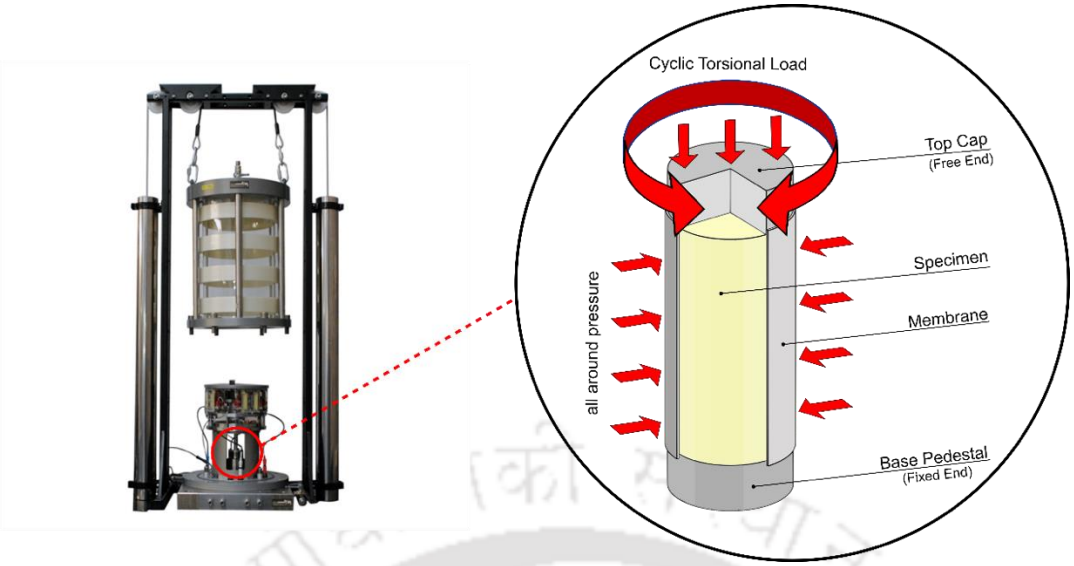

Fig. 3.20 RC apparatus available at the SAGE lab, Surrey and the schematic representation of loading conditions on the sample

The RC apparatus mainly consist of: a standard Triaxial cell of 1MPa cell pressure for effective confining the sample to the required effective confining pressure (σ'_c); electromagnetic drive system with composite Sintered Neodymium Iron Boron (NdReB) "rare-earth" magnets for applying required magnitude of harmonic torque; four pairs of energisation mode drive coils; an LVDT for monitoring axial displacements; an accelerometer to measure the response at the top of the specimen; a drive amplifier for the generation of input signal, a high speed 16-bit data acquisition; computer controlled proportional gas valve; pressure controller for back pressure application; GDS-RCA and GDS-LAB programs for control and data acquisition and cell pressure application (GDS Inc. 2008). Fig. 3.21 schematically details various components involved in RC apparatus.

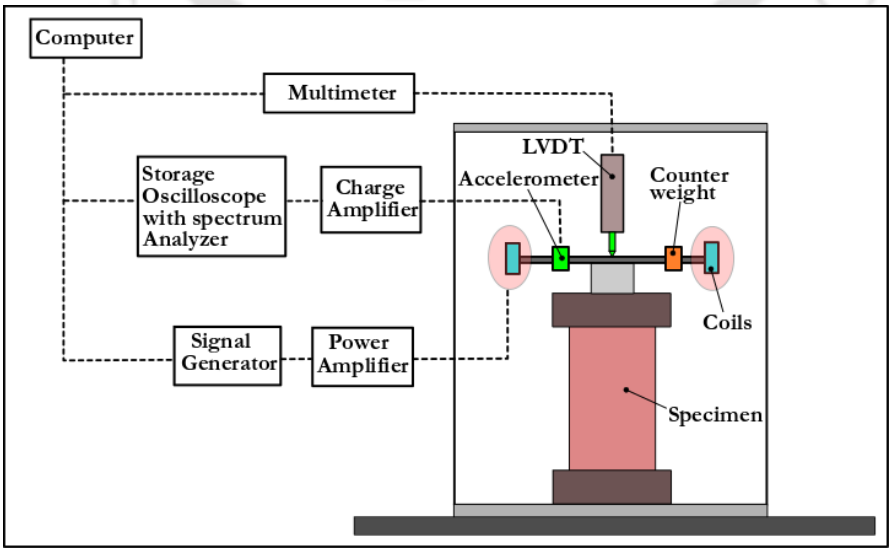

Fig. 3.21 Schematic view of RC apparatus with various components

Testing Procedure

Specimen preparation was carried out according to the standards (ASTM D 4015) and is similar to the one described for triaxial tests. After the sample preparation, electromagnetic driving system (Fig. 3.22) is carefully placed over the top cap on the specimen, levelled and fixed. The driving system should be arranged in such a way that the coils should not be too close to the boundaries.

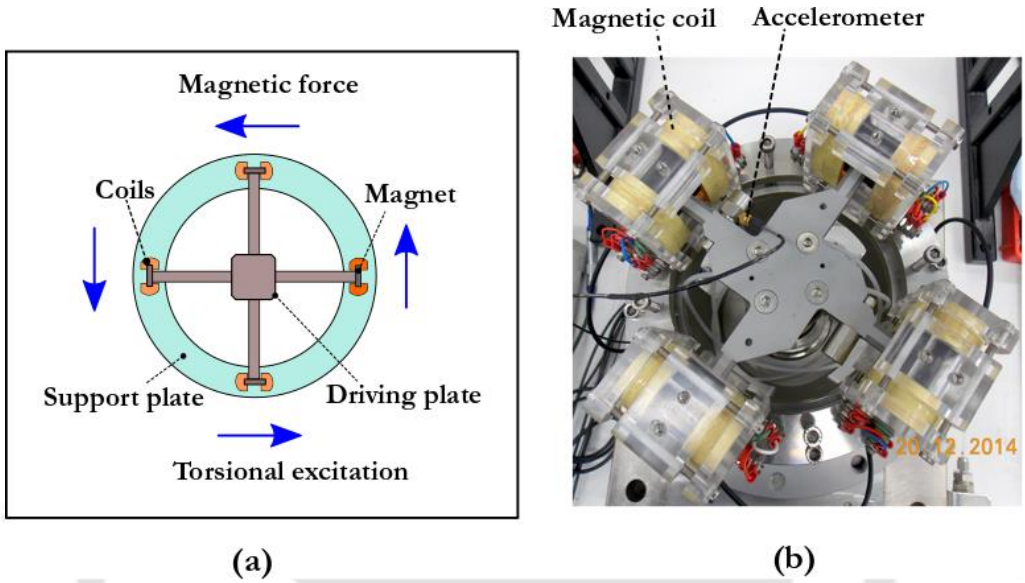

Fig. 3.22 (a) Schematic view of torsional excitation using magnetic coils and drive system and **(b)** pictorial view of electromagnetic drive system

Instrumentation like LVDT and accelerometer were installed after confirming the system alignment, and then the triaxial cell is slowly lowered on to the resonant apparatus to allow it for confining the sample to the required initial state of the stress. The targeted effective confining pressure is then applied using the pressure controller in GDSLAB program and axial deformations (if any) are monitored using the vertical LVDT. The measurement has been used to calculate exact density of the sample achieved.

To find the fundamental mode of the specimen, a harmonically varying input voltage with a broad range of frequency is passed through the sample using the electromagnetic drive system and the power amplifier. The application of sinusoidal voltage results in the magnetic field generation and induces an oscillatory motion at the top of the sample in torsional mode. The system software allows such gradual loading application via broad and fine sweep operations. Broad sweep run is performed from 1 Hz to 250 Hz with an increment of 5 Hz. The frequency corresponding to the maximum amplitude of vibration is considered as the resonant frequency of the sample. Once the rough estimation of fundamental frequency at 5 Hz interval is completed, then a fine sweep is performed with

±5 Hz on either side of the fundamental mode with a frequency increment of 0.1 Hz in order to find the exact resonant frequency of the system and the corresponding strains induced in the soil sample. Fig. 3.23 shows the typical screenshot view of broad sweep run from 30 Hz to 150 Hz.

Using this resonant frequency (f_{nz}), sample geometry and instrument constants, shear wave velocity (V_s) can be estimated using Eqn. 3.4.

$$V_s = \frac{2 \cdot \pi \cdot f_{nz} \cdot H}{\beta} \tag{3.4}$$

where H is the sample height and β is the instrument constant, obtained as 0.15689, through calibration following the standards (ASTM D 4015).

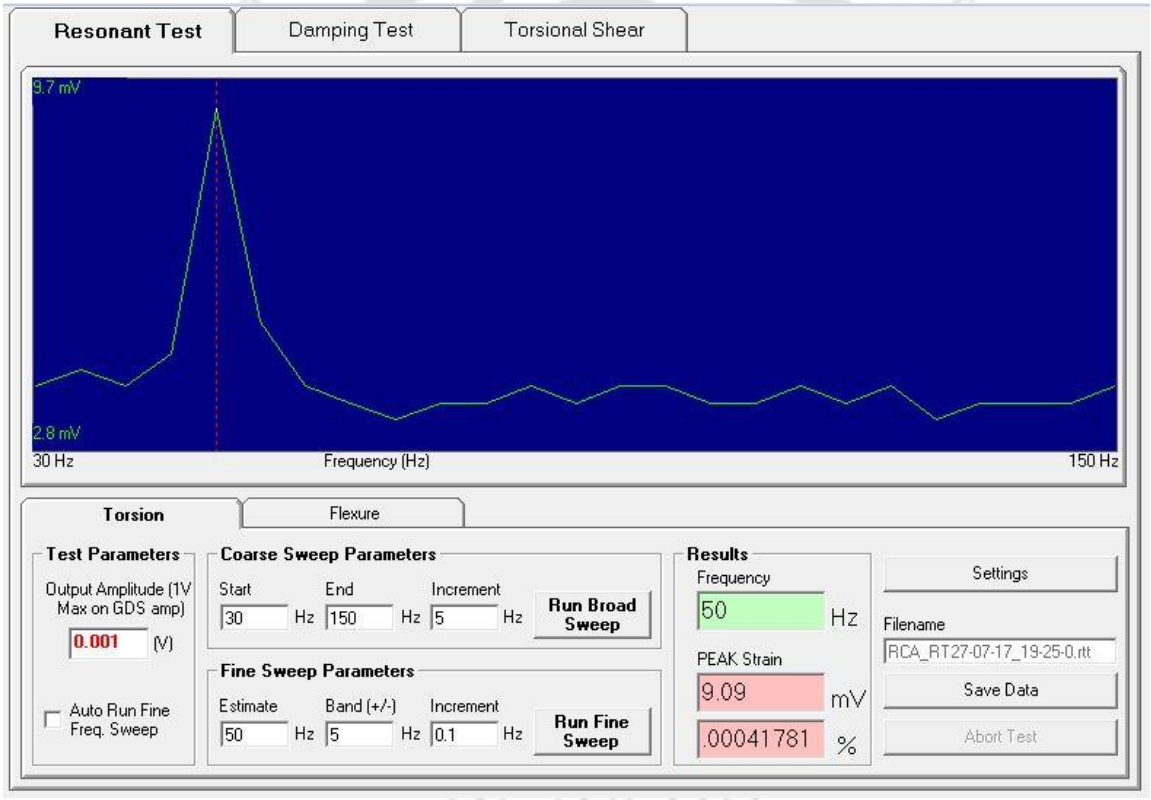

Fig. 3.23 Typical screenshot view of GDSRCA program for finding the fundamental mode of vibration

Once the resonant frequency is attained at a particular input voltage, input current to the coils is switched off to obtain a free-vibration response. Fig. 3.24 depicts a typical free-vibration response. The response of the accelerometer (in terms of voltage) with time is recorded from which the amplitude decay curve is obtained from which the corresponding damping ratio (D) is evaluated (Eqn. 3.5) as suggested in ASTM D 4015.

$$D = \left(\frac{1}{n}\right)\ln\left(\frac{A_1}{A_{n+1}}\right) \tag{3.5}$$

where n is the number of free vibration cycles; $A_{1....n+1}$ are the amplitudes of voltage at corresponding loading cycle.

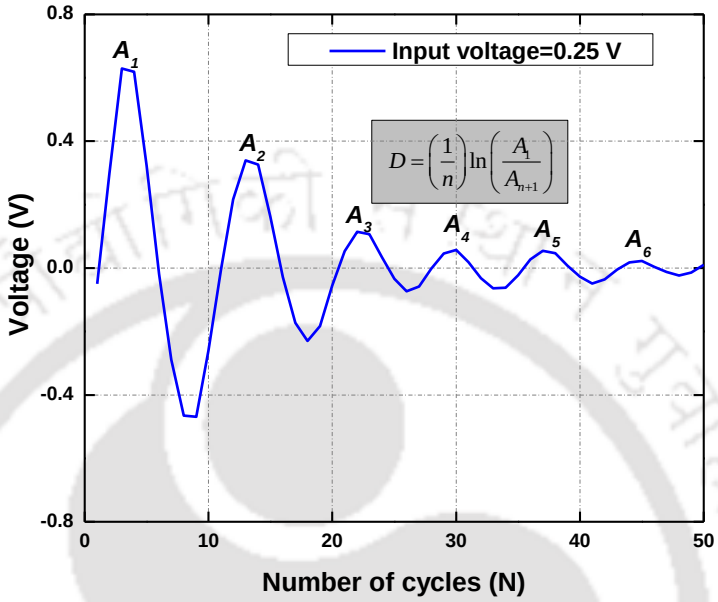

Fig. 3.24 Typical free-vibration response obtained from RC test

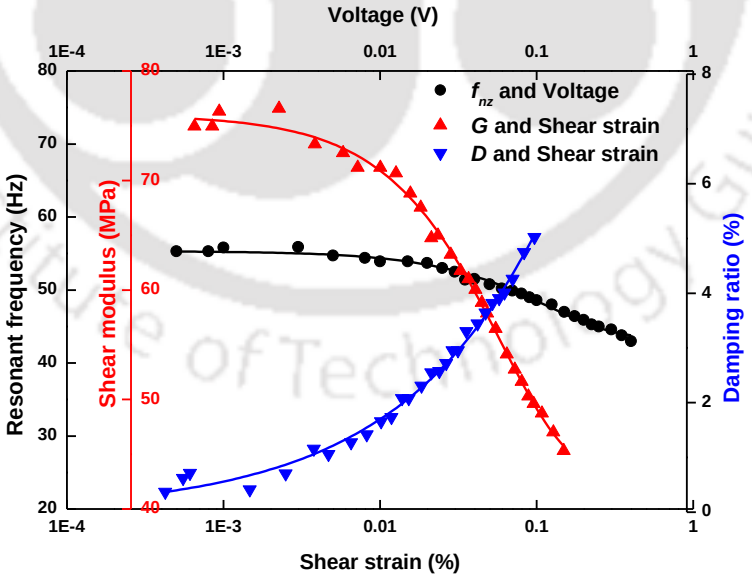

Fig. 3.25 Variation of f_{nz} with input voltage, shear modulus and damping ratio with shear strain for BP sand at 100 kPa effective confining pressure

Once the shear modulus and damping ratio at a particular strain (particular voltage) are obtained, then the input voltage to the system is further increased which in turn increases the strain in the soil specimen and the corresponding shear modulus and damping ratio are

determined as described above. Repeating the test till the strains of 0.1% will yield in the variation of shear modulus with shearing strains. Fig. 3.25 presents the typical result obtained from a torsional RC test. It can be observed that the resonant frequency (f_{nz}) at small shear strains (strains<0.001%) is almost constant and the resulting shear modulus is termed as initial shear modulus or maximum shear modulus (G_{max}). With increase in the input voltage, corresponding strains are increased in the specimen leading to reduction of f_{nz}. The resulting secant shear modulus (G) and damping ratio (D) are also shown in Fig. 3.25.

3.3.3 Dynamic Simple Shear Tests

Dynamic Simple Shear (DSS) apparatus can be used to investigate the dynamic behaviour of soils from intermediate (0.01%) to high strains (about 5%). The advantages of DSS apparatus are: (a) better simulation of horizontal shear wave loading conditions, (b) continuous rotation of principal stress planes, (c) anisotropic consolidation (representing at-rest condition in the field), (d) specimen preparation is easier, (e) less degree of disturbance due to smaller size of specimens compared to CTX test (Monkul et al. 2015) and (f) simple to run and does not require saturation or pore pressure measurement which would reduce the sample preparation time significantly. In addition, Poisson ratio assumption effects can be minimized in DSS testing as the direct shear loading can be applied on the specimen unlike traditional CTX apparatus whereby the shear strain would be calculated by axial strain and Poisson ratio assumption. Fig. 3.26 describes schematically the loading conditions prevailing in field and DSS testing during shearing.

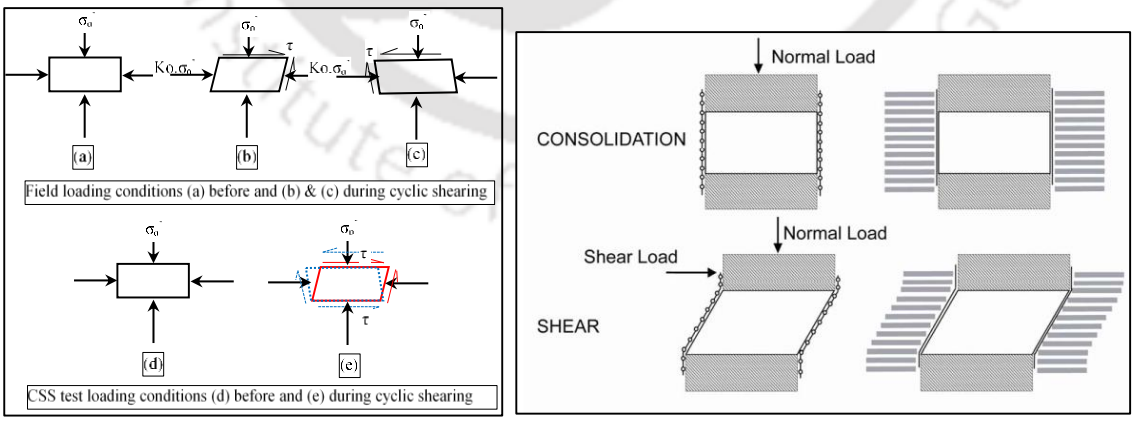

Fig. 3.26 Schematic representation of loading conditions in field and DSS testing (after Baxter et al. 2010)

DSS Apparatus

The DSS apparatus supplied by VJ Tech Ltd, UK (shown in Fig. 3.27a) available at the SAGE Laboratory, University of Surrey, UK has been utilised for the testing. The main components of DSS apparatus are: servo-controlled vertical actuator for effective vertical stress application (±5 kN axial load or 25 mm settlement); servo-controlled horizontal actuator with 0-5Hz frequency range for shear load/displacement application (±5 kN or ±15 mm horizontal displacement); a pair of LVDTs with (5 mm capacity) to measure axial and lateral displacements; a pair of load cells for axial and lateral loads measurements; stacked steel shearing rings of 2 mm thickness; data acquisition system and CLISP STUDIO program in the computer. Two kinds of testing conditions exist in the DSS apparatus, undrained testing and drained constant volume/effective vertical stress testing. Present tests are performed in *drained constant effective vertical stress condition* in which the axial strain adjusts automatically to keep the volume changes to minimum with no change in the effective vertical stress acting on the specimen. Both the stress (and load) and strain (or displacement) controlled shearing are possible with the instrument. As the main objective of present study is to determine the dynamic behaviour of soils at various strain ranges, strain controlled testing was adopted. Fig. 3.27b shows a schematic view of cycling shearing conditions prevail on the sample. The sample geometry can be 75 mm or 50 mm in diameter and 25 mm in depth. Different forms of wave forms can be applied: sinusoidal, square, triangular, haversine, saw-tooth, or user defined waveform.

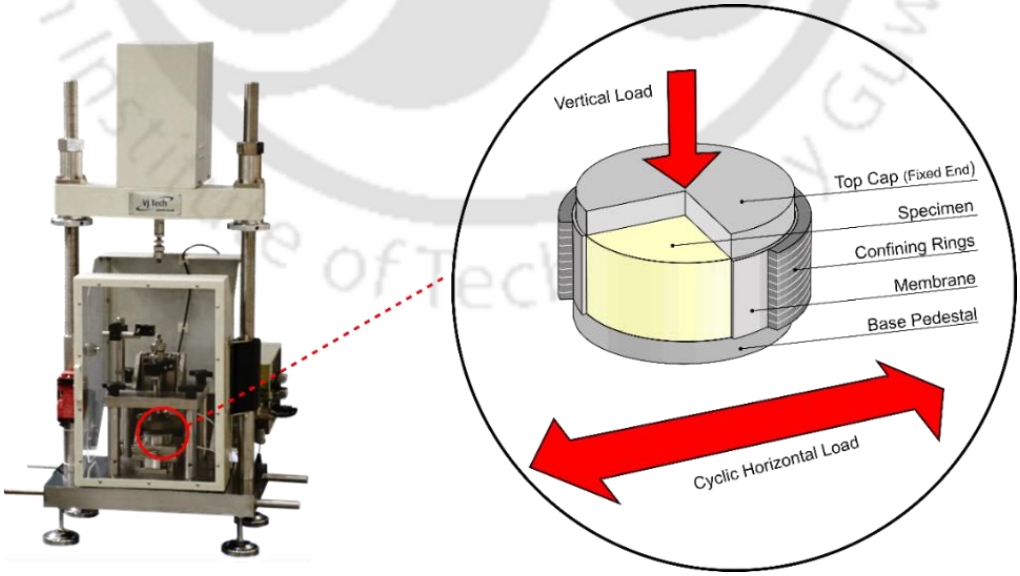

Fig. 3.27 DSS apparatus available at the SAGE lab, Surrey with a schematic view of loading conditions on the specimen (after Nikitas et al. 2016)

Testing Procedure

All the DSS tests on sand samples were conducted in dry condition as saturation was not possible in the current DSS system. The tests were carried out in strain controlled mode with constant effective vertical stress condition during shearing. Required amount of granular soil (for 50 mm diameter and 25 mm length sample) is collected based on the chosen initial relative density and the geometry of the specimen. The prepared base pedestal is shown in Fig. 3.28 a. A rubber membrane is stretched over the base pedestal and a rubber O-ring is fixed for alignment. A two-split O-ring is placed around the membrane on the pedestal surrounded by a detachable mould (Fig. 3.28b). The stacked shearing O-rings (Fig. 3.28c) are placed around the membrane and the membrane is stretched over it (Fig. 3.28d). The calculated amount of soil sample is poured in to the space formed in the membrane with four layers of approximately equal thickness for homogeneous density (Fig. 3.28e). After each layer is filled with the sand, small tamping was given at the sides of the mould to accommodate the required amount of sand within the desired height as per the targeted R_d. Top cap is placed over the soil specimen without significant disturbance and a bracket for O-rings alignment is fixed (Fig. 3.28f). The mould arrangement is removed. Load cells and LVDTs are installed for monitoring the load displacement response in axial and lateral directions (Fig. 3.28g and h), respectively. Once the sample preparation is successful and the instrumentation is setup, the computer program-CLISP STUDIO should be used to check the apparatus as per the testing conditions.

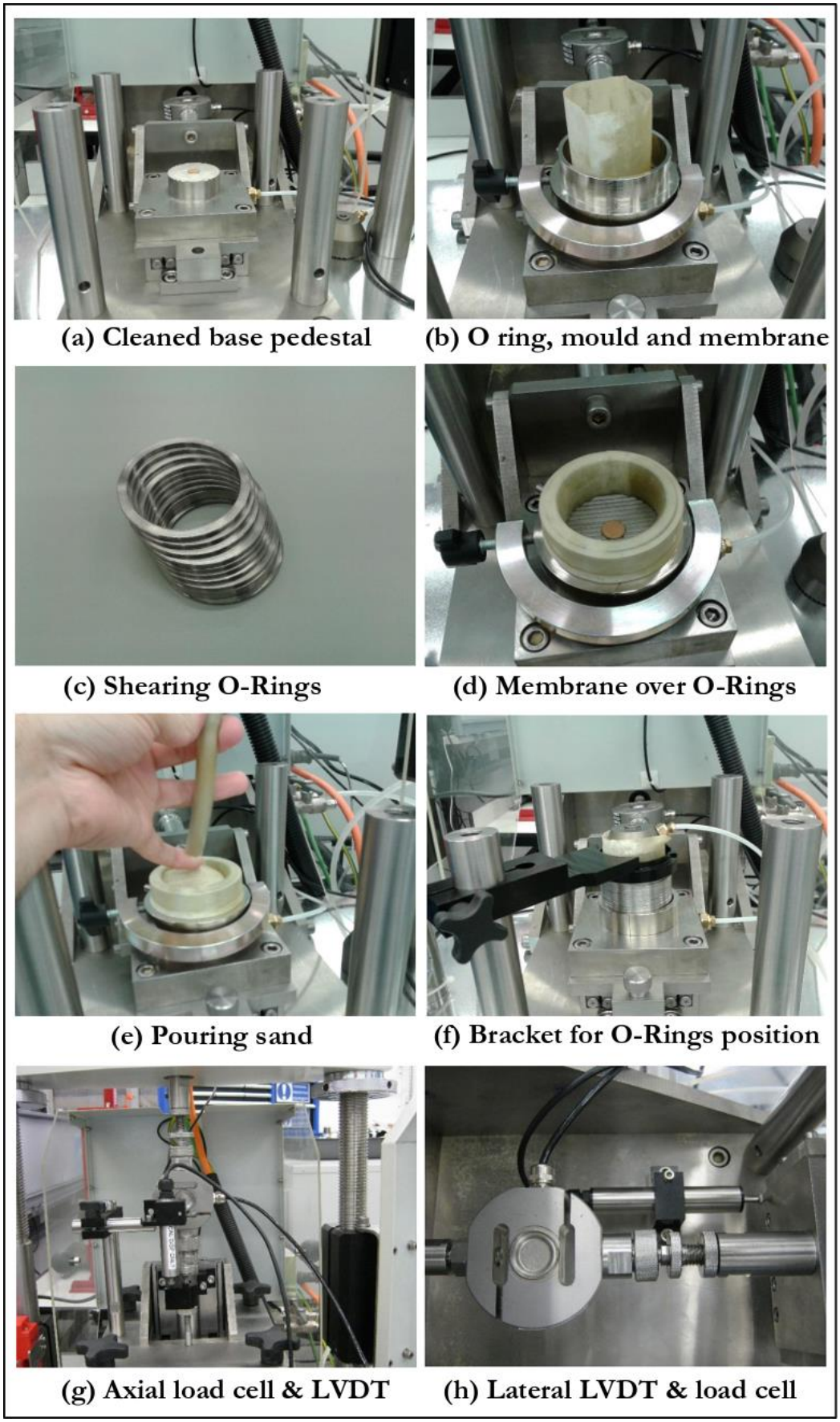

Fig. 3.28 Steps for sample preparation and instrumentation setup for DSS testing

After making sure of all the above mentioned procedure, the specimen can be brought under the targeted effective vertical stress (σ'_n) using the axial servo controlled actuator. This can be done through DSC option available in the CLISP STUDIO program. The LVDTs and load cells monitor the displacements and loads during the consolidation stage. A typical sand specimen takes around 30 min for consolidation. After successful consolidation, cyclic shearing can be performed by inputting the required parameters such as shear displacement, frequency of loading, number of cycles and the test ending conditions. Tests were conducted with varying parameters (Table 3.4) such as: shear strain amplitude, effective vertical stress magnitude and frequency of loading. Since, no measurements of lateral stress are available in the employed DSS apparatus, a K_o condition of 0.5 was assumed based on angle of internal friction of sandy specimens at 50% R_d (ranging from 30 to 33 deg). The chosen effective vertical stress magnitudes for the assumed K_o condition of 0.5 (75, 150 and 300 kPa) represent the σ'_c of 50, 75 and 200 kPa. All the tests were performed for 1000 number of loading cycles or a maximum normal settlement of 1mm.

Typical Results

Fig. 3.29a shows the typical input to the DSS system (shear strain variation with loading cycles) and resulting output (shear stress variation in Fig. 3.29b) from the system. An increasing trend of shear stress with increasing loading cycles can be observed, depicting the increase in compactness (or strength) with the loading cycles. The shear stress-shear strain response thus obtained is used to determine the shear modulus and damping ratio. Fig. 3.30 depicts a typical shear stress shear strain response, which is traditionally termed as hysteretic loop in soil dynamics applications.

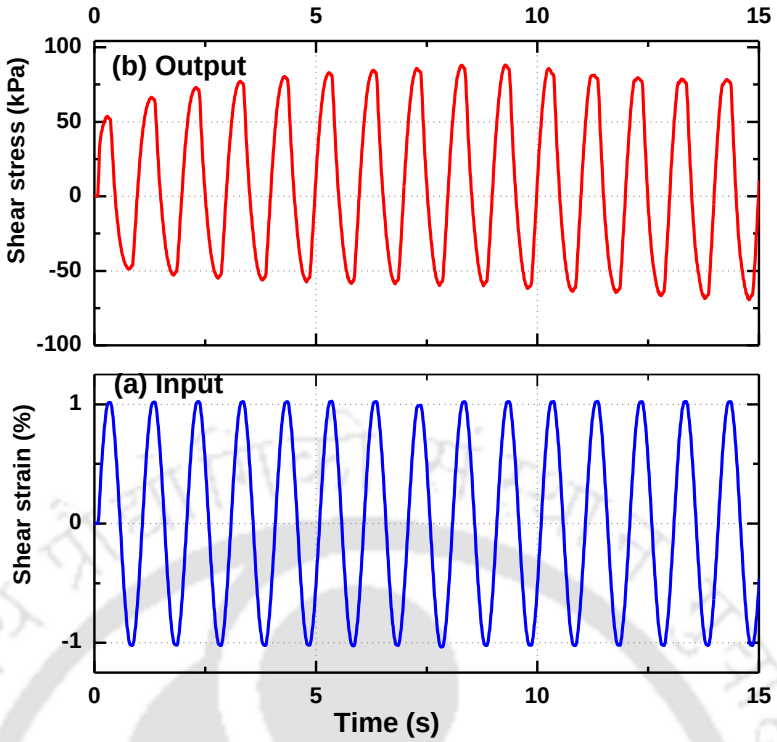

Fig. 3.29 Typical input and output results from DSS testing (BP sand at 100 kPa effective vertical stress for 1% strain controlled shearing at 1 Hz frequency)

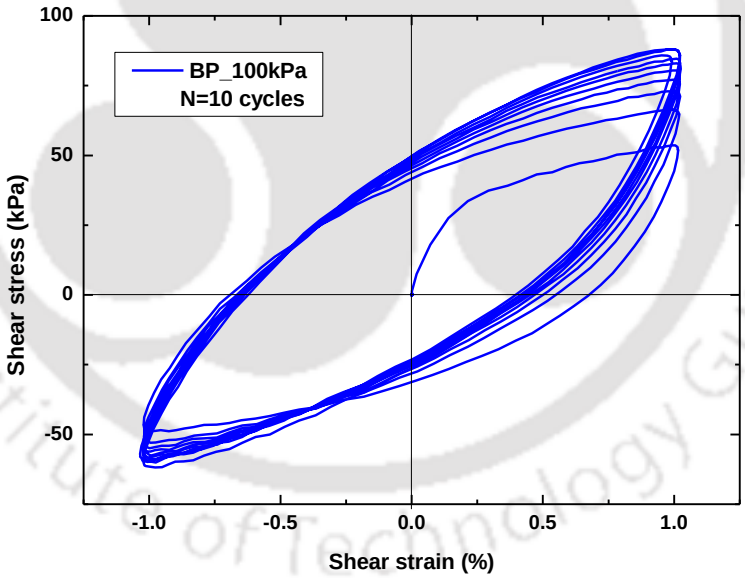

Fig. 3.30 Typical stress-strain behaviour of BP sand for 1% strain controlled DSS test at 100 kPa effective confining stress for 10 cycles of loading

3.3.4 Cyclic Triaxial Tests

Cyclic triaxial (CTX) system has been in use for soil dynamics problems since 1960s and is best known for liquefaction assessment of soils (Seed and Lee 1966) and determination of high strain dynamic soil properties (Kokusho 1980; Sitharam et al. 2004). In the present research, two automated pneumatic controlled CTX systems have been utilised for the liquefaction assessment of chosen soils. One CTX system is available at Geotechnical

Engineering Laboratory of IIT Guwahati and was supplied by Wykeham Farrance Inc (Fig. 3.31) while the second system was supplied by GDSLab Instruments, available at the SAGE laboratory of University of Surrey, UK (Fig. 3.32). The main components involved in the CTX system are: triaxial cell, pneumatic controlled loading frame, pressure transducers, cell pressure controllers, automatic volume change device, dry air receiver units, data logger and software installed in the computer. In case of GDSLab system, samples were of 100 mm diameter and 200 mm length while the Wykeham Farrance system used samples of 38 mm diameter and 76 mm length. The detailed descriptions and working procedure of different components of Wykeham Farrance system were reported in Kumar (2018). The detailed description of GDSLab system and the instrumentation details can be found in Nikitas et al. (2016), Lombardi et al. (2016) and Rouholamin et al. (2017).

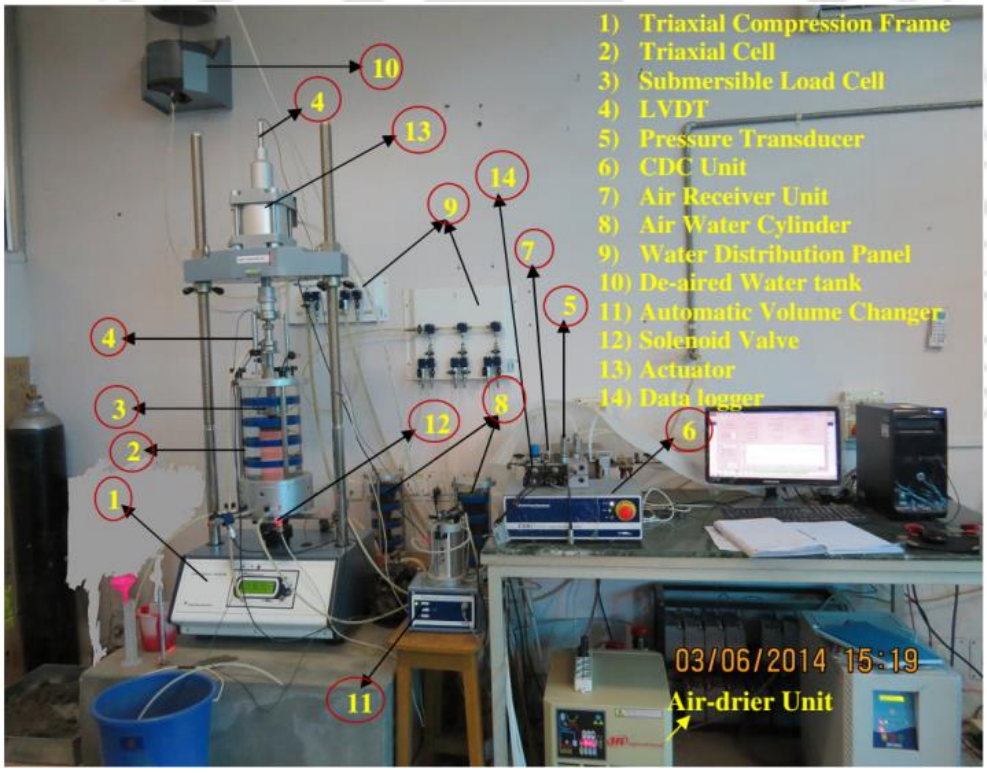

Fig. 3.31 Cyclic triaxial test system (Wykeham Farrance supplied) with the connections and components (after Kumar 2018) available at IIT Guwahati

Fig. 3.32 CTX system (GDSLab supplied) at SAGE laboratory

Multi-stage triaxial testing has been implemented whereby the isotropic consolidation stage is followed by cyclic and monotonic shearing stages. It is to be mentioned that the sand samples were prepared using the dry pluviation technique while the cohesive specimens are prepared using the sample preparation mould (as described in Sec. 3.2.2). Fig. 3.33 schematically illustrates the loading path employed in the multi-stage triaxial tests. Once the sample is brought to full saturation condition as explained in the monotonic tests sample preparation, isotropic consolidation is initiated to bring the sample to the required effective confining pressure level. This stage is followed by the cyclic load in terms of sinusoidal varying deviatoric stress, application. The application of cyclic loading was ceased with the initiation of the liquefaction (when the effective confining stress reaches zero). The stress invariants (q and p') were used for representing cyclic deviatoric stress and mean effective confining stress.

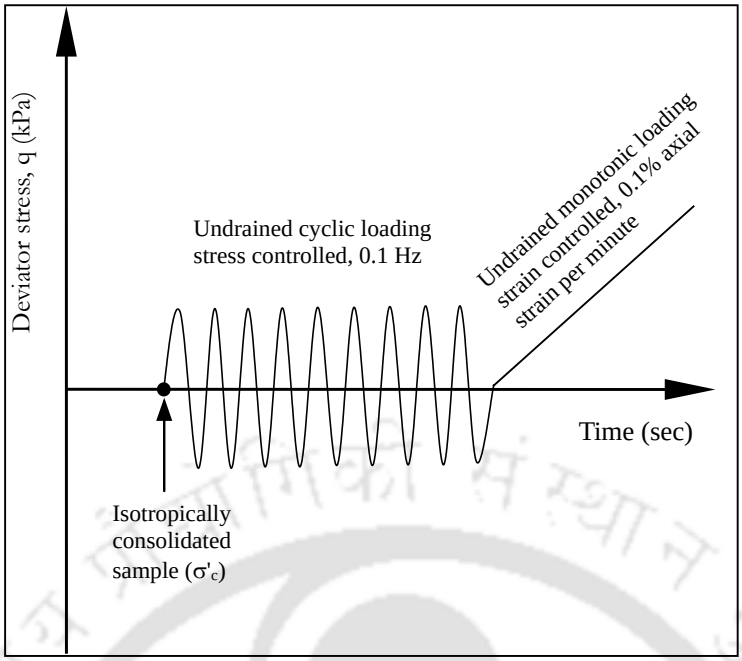

Fig. 3.33 Multi-stage testing in the CTX system

Typical input and output in CTX tests, from the stress-controlled tests on BP sand are shown in Fig. 3.34. Fig. 3.34 a depicts a typical input (in the form of deviatoric stress with loading cycles) in a stress-controlled test. The output in a stress-controlled CTX test for liquefaction assessment is traditionally presented in terms of strain accumulation, stress-strain response and pore water pressure accumulation which are presented for saturated BP sand specimen in Fig. 3.34 b, c, and d, respectively. It can be observed from Fig. 3.34 b that the sample experienced low level of strains (in the initial loading cycles) with narrow hysteresis loops. With increase in loading cycles, significant strains were accumulated in the extension side (as high as 3% as seen in Fig. 3.34 c) resulting in broader loops. Such high axial strains can be attributed to the significant rise of pore water pressures (Fig. 3.34 d) leading to liquefaction phenomenon (loss of strength of soil) by the increased loading cycles. Further analysis of the CTX test results is presented in the subsequent chapters.

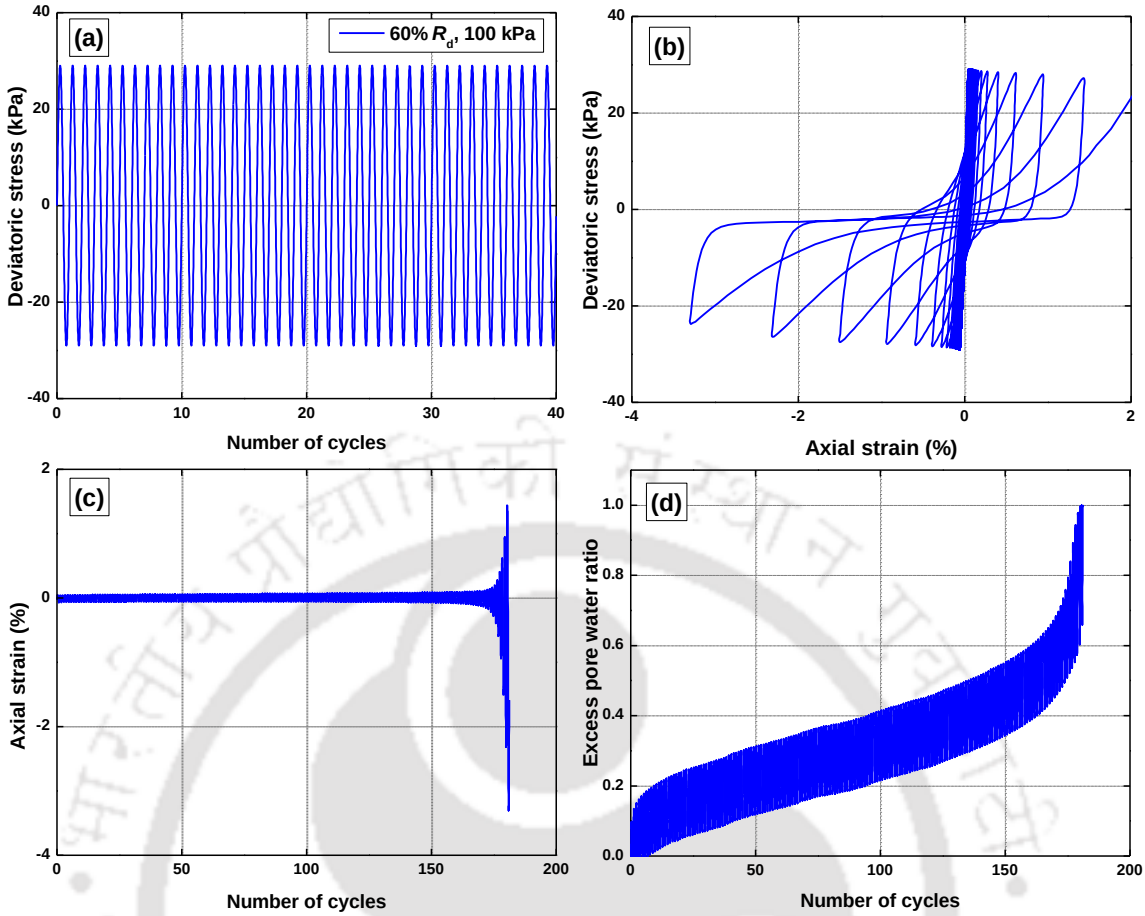

Fig. 3.34 Typical results obtained from CTX test

3.4 SUMMARY

To understand the dynamic behaviour of soils of seismic origin in India, six soils from active seismic regions were sampled, of which four are sandy soils collected from major river shores and the rest are clays collected from northeastern region of India. The chapter has been divided in to three main sections: material description, monotonic strength tests followed by the description of dynamic testing program. All of the chosen soils were classified based on their index properties. Monotonic strength tests have been conducted both in dry and saturated conditions. The obtained results have been presented in terms of stress-strain response, stress path and secant modulus variation with axial strain. Four advanced testing techniques have been adopted for the dynamic characterisation of the chosen soils. Details of each apparatus have been described in detail with the working principle, testing methodology and the typical output from each test.

CHAPTER IV. DYNAMIC CHARACTERISATION OF COHESIONLESS SOILS

4.0 INTRODUCTION

Results and analysis pertaining to the dynamic behaviour of cohesionless soils, determined using the four testing techniques are presented in this chapter. Test results from each testing technique are presented in separate sections followed by combination of the results to provide the comprehensive data of dynamic soil properties over wide strain range. Empirical formulations are proposed for the region-specific soils based on the regression analysis of the experimental data. In addition, G/G_{max} and D data (from literature) of cohesionless soils of seismic origin in India have been collated from the literature and design stiffness curves (in terms of G/G_{max} and D) are established. Liquefaction behaviour of the BP sand is evaluated and empirical function for a pore water pressure model is implemented.

4.1 BENDER ELEMENT TEST RESULTS

Bender element (BE) tests provide the low strain (strains≤ 0.0001%) dynamic stiffness of soils and hence, BE tests were conducted on the chosen sands at different R_d and σ'_c conditions. It must be noted that all the BE tests on cohesionless soils were conducted in dry condition, as saturation is not expected to alter the low strain dynamic characteristics of granular soils (Saxena and Reddy 1980; Chattaraj and Sengupta 2016). Table 4.1 enlists the BE test programme on cohesionless soils and the associated loading conditions. It is to mention that the considered density conditions are the initial bulk densities. This section presents the results obtained from BE tests and the relevant analysis.

Table 4.1 BE tests and their loading conditions

Soil	R_d (%)	σ'_c (kPa)	Targeted output
BP	30	50-1000	G_{max} variation with σ'_c
	70	50-1000	
BG	30	50-1000	
	70	50-1000	
YF	30	50-1000	
	70	50-1000	

The expected output from a BE test is the shear wave velocity (V_s) correlated using the arrival time (T_s) and effective sample height (L_{eff}). Maximum shear modulus (G_{max}) can then be determined using the sample density (ρ). In order to demonstrate briefly the typical output and G_{max} determination from a BE test, experimental data of BP sand specimen at 30% R_d and at different effective confining pressures are presented in Table 4.2.

Table 4.2 Output and G_{max} determination from a typical BE test

Input				Output	Correlation	
R_d (%)	σ'_c (kPa)	L_{eff} (mm)	ρ (g/cc)	T_s (ms)	V_s (m/s)	G_{max} (MPa)
30	50	96	1.46	0.486	187.09	51.10
	100			0.422	215.66	67.90
	200			0.356	255.34	95.19
	300			0.321	283.00	116.92
	400			0.299	304.43	135.31
	500			0.284	320.43	149.90
	600			0.269	337.61	166.41
	800			0.249	365.23	194.76
	1000			0.236	385.03	216.44

Fig. 4.1 a and b present the variation of G_{max} of BP sand with σ'_c in normal linear axis (both x and y axes) and semi-log (confining pressure axis-x) representation, respectively. The power law was known to represent the relationship of G_{max} with σ'_c (as seen from Table 2.4) adequately and therefore, similar representation is presented. Fig. 4.2, and Fig. 4.3 present the variation of G_{max} with σ'_c for BG and YF sands, respectively in a semi-logarithmic representation. Two observations can be made from the trends: increase of G_{max} with R_d at any given effective confining pressure and also non-linear increase of G_{max} with σ'_c. The increase of G_{max} is due to the increase in compactness as both the R_d and σ'_c decrease e.

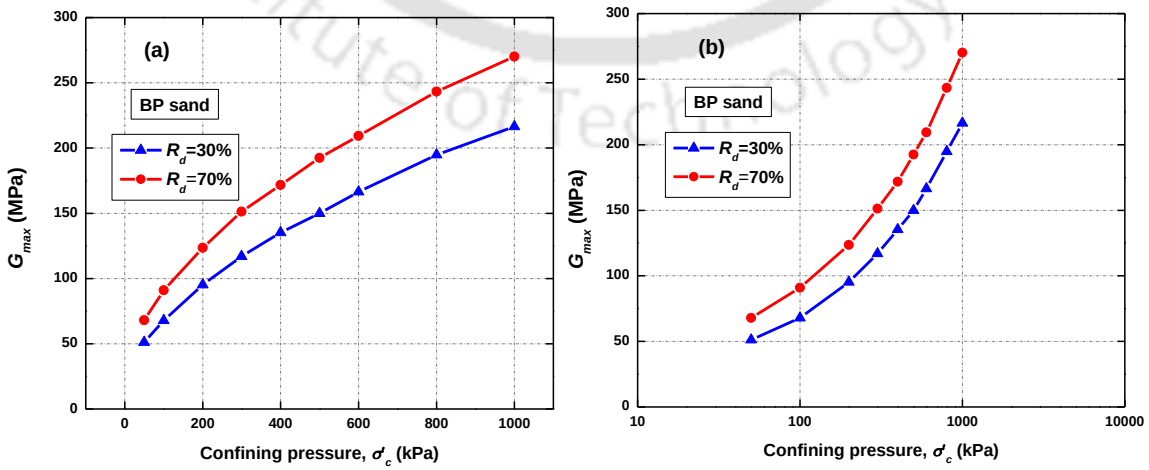

Fig. 4.1 G_{max} variation with σ'_c for BP sand **(a)** Normal axis and **(b)** Semi-log representation

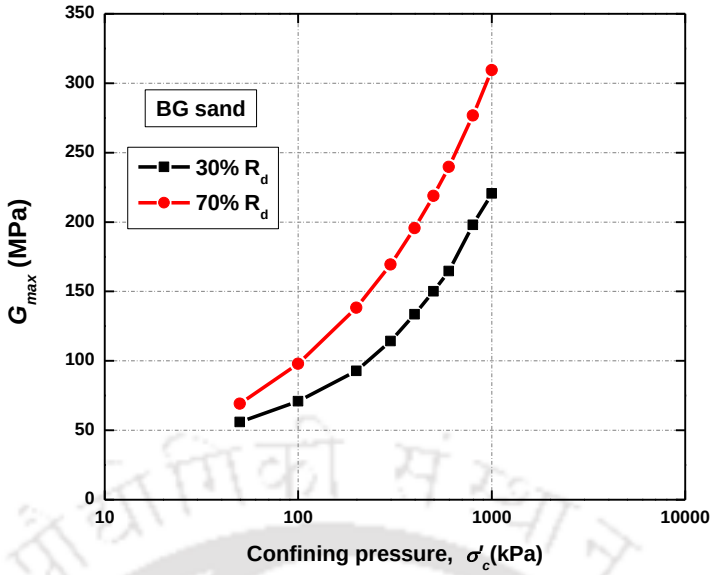

Fig. 4.2 G_{max} variation with effective confining pressure for BG sand

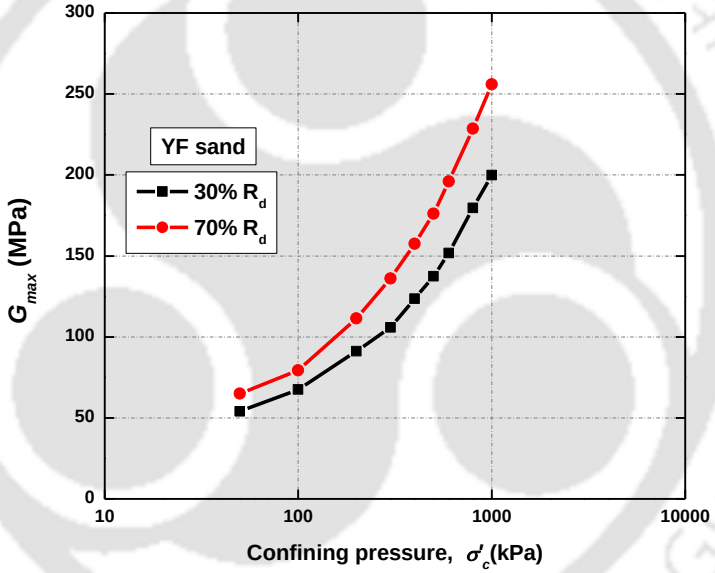

Fig. 4.3 G_{max} variation with effective confining pressure for YF sand

In order to understand the effect of sand type (of chosen sands) on the G_{max} values, a comparison is made for all the three sands in both loose and dense conditions (Fig. 4.4 and Fig. 4.5). As can be observed, G_{max} values of all the three sands fall in the narrow range with YF sand yielding slightly lower values compared to BP and BG sands at loose (30% R_d) and dense (70% R_d) conditions. At 600 kPa effective confining pressure, at 30% R_d, BP and BG sands yielded 161 MPa while YF sand showed 150.5 MPa. Similarly, at dense condition (70% R_d), a G_{max} value of 196 MPa was observed for YF sand, while BP and BG sands showed 209 MPa and 210 MPa, respectively.

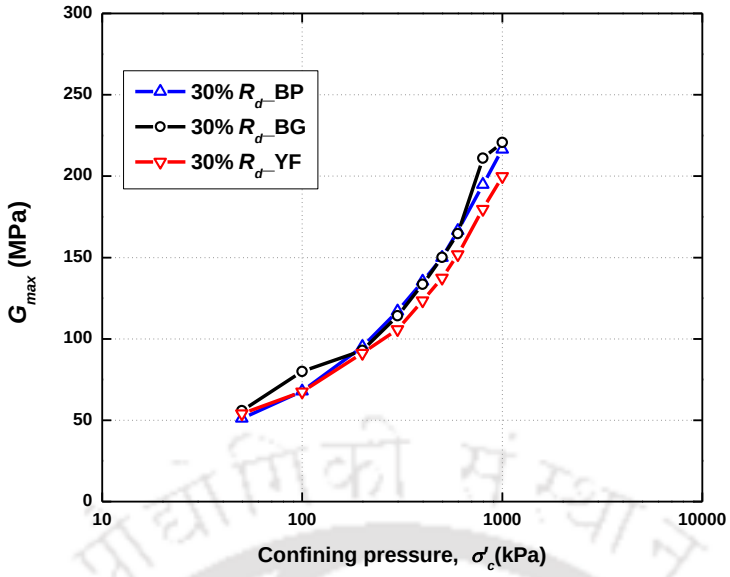

Fig. 4.4 G_{max} variation for the three sands in loose conditions

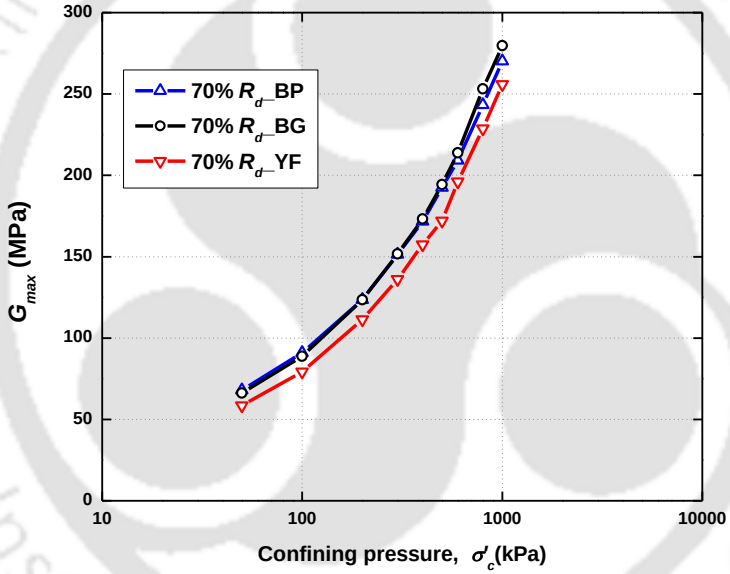

Fig. 4.5 G_{max} variation for the three sands in dense conditions

4.2 RESONANT COLUMN TEST RESULTS

RC tests were performed on the sand samples in dry condition at different σ'_c and R_d conditions. Two types of RC testing approaches were adopted to achieve the desired dynamic properties (G_{max}, G/G_{max} and damping) at different effective confining pressures (σ'_c) and relative densities (R_d). Table 4.3 presents the RC testing program and the associated loading conditions. The first method involves the application of incremental shear strains (starting from strains<0.001%) up to a shear strain of 0.1% at a fixed effective confining pressure to establish the shear modulus and damping variation. The second approach involves the application of incremental effective confining pressures on the sample (keeping the input strain as low as possible, typically <0.001%) to establish G_{max}

over wide range of effective confining pressures (test IDs BP10-BP12 and BG10-BG12 in Table 4.3).

Table 4.3 RC testing program and loading conditions

Test ID	Soil	R_d (%)	σ'_c (kPa)	Output
BP1	BP sand	30	50*	*G-γ, D-γ*
BP2			100	
BP3			300	
BP4		50	50	
BP5			100*	
BP6			300	
BP7		70	50	
BP8			100	
BP9			300	
BP10		30	50 to 600	G_{max} vs σ'_c
BP11		50	50 to 600*	
BP12		70	50 to 600	
BG1	BG sand	30	50	*G-γ, D-γ*
BG2			100	
BG3			300*****	
BG4		50	50	
BG5			100	
BG6			300*****	
BG7		70	50	
BG8			100	
BG9			300	
BG10		30	50 to 600	G_{max} vs σ'_c
BG11		50	50 to 600	
BG12		70	50 to 600	
YF1	YF	45	50	*G-γ, D-γ*
YF2			100	
YF3			200	
YF4			300	
YF5		65	50	
YF6			100	
YF7			200	
YF8			300	
YF9		85	50	
YF10			100	
YF11			200	
YF12			300	
YC1	YC	30	50	
YC2			100	
YC3			200	
YC4			300	
YC5		45	50	
YC6			100	
YC7			200	
YC8			300	
YC9		60	50	
YC10			100	
YC11			200	
YC12			300	

Note: Tests with symbol ***** are repeated to confirm the repeatability.

The second approach (incremental pressures) was started with an effective confining pressure of 50 kPa and repeated for intermediate pressures up to a maximum effective confining pressure of 600 kPa. Total of 48 number of tests have been conducted on chosen sandy samples. In addition to the planned tests, additional tests at similar testing conditions (Test IDS: BP5, BP11, BG3 and BG6) have been performed to confirm the repeatability.

Typical results obtained from incremental approach for the chosen sands are shown in Fig. 4.6. It is evident that the value of f_{nz} and corresponding G is constant up to a certain strain level (≈0.003%), beyond which the induced strains lead to non-linear behaviour of the soil. The shear modulus at such linear range is considered as the G_{max} of the soil (from incremental strain approach). With increase in shear strains, the granular packing becomes loosened and the path length of the shear wave increases, ultimately resulting in reduced stiffness (f_{nz} and G). In contrast, damping ratio increases with shear strains. As damping ratio is a measure of internal damping within the soil, and the internal damping can be represented by the inside area of the hysteresis loop (Saran 1999), with increase in strains, the area of the loop increases leading to an increase in the damping of the soil.

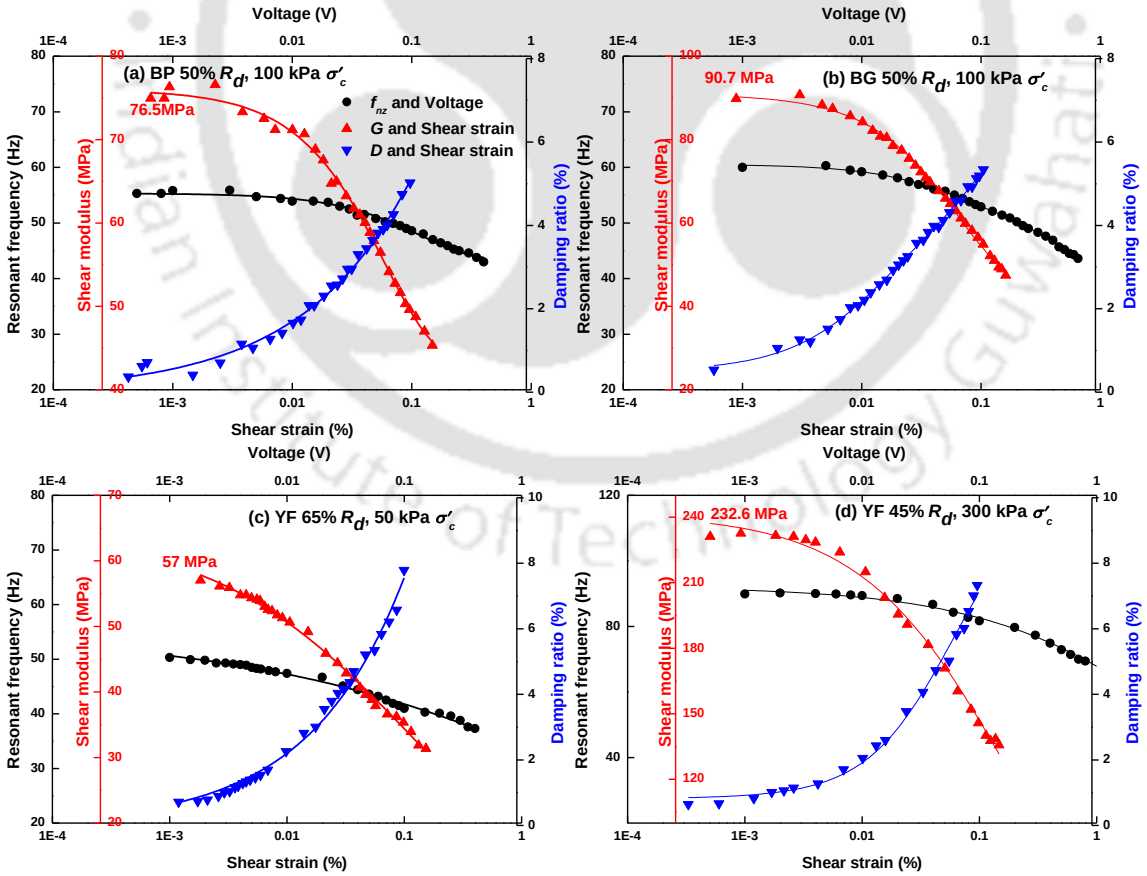

Fig. 4.6 Typical results obtained from incremental strain approach in RC tests

4.2.1 Maximum Shear Modulus (G_{max})

The G_{max} values have been determined from RC testing using both the aforementioned approaches (incremental pressure and incremental strain). Fig. 4.7 presents the results obtained from incremental pressure approach (in terms of f_{nz} and the corresponding V_s) for BP sand at different R_d conditions. Similar to the BE test results, exponential increase of G_{max} with effective confining pressure can be noted, at any given R_d condition. In case of incremental strain approach, G_{max} is considered from the lowest strain possible (Fig. 4.6). In contrast, incremental pressure approach yields directly the G_{max} values (after correlation with V_s), as the corresponding strains are always less (≈0.001%).

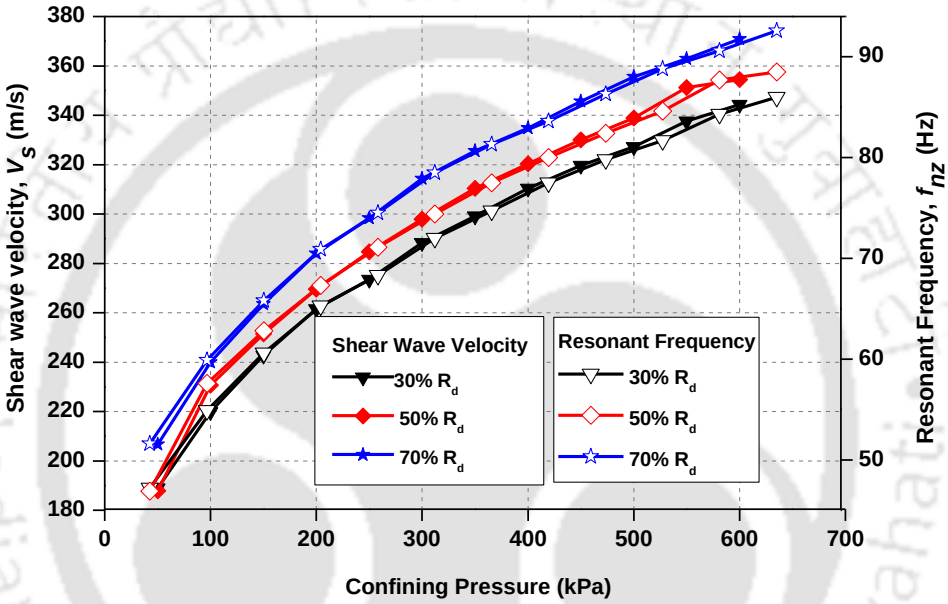

Fig. 4.7 Shear wave velocity & resonant frequency variation with cell pressure for BP sand at shear strains < 0.001%

A comparison is made for the G_{max} values obtained using both the approaches. Fig. 4.8 presents the variation of G_{max} with an effective confining pressure using both the approaches. It must be mentioned that as the samples were tested in only three to four σ'_c conditions in incremental strain approach, only three to four G_{max} values exist. It can be seen that both the approaches yield similar G_{max} values with minor differences (±5%), which shows that the effect of pre-confinement (in case of incremental pressure approach) on low strain stiffness characteristics may not be significant. Similar negligible effect (±5%) of pre-confinement on G_{max} was observed for Monterey No 0 sand by Chung et al. (1984).

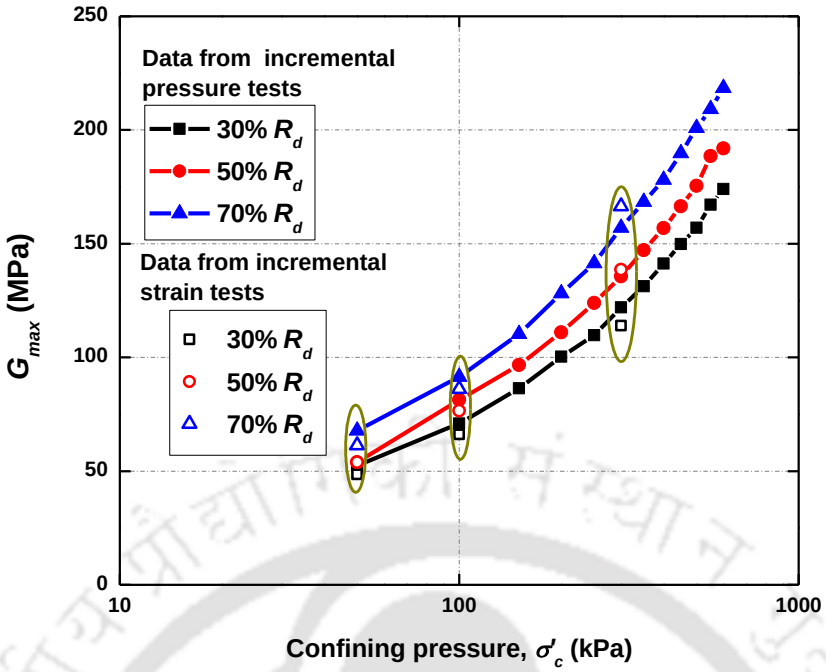

Fig. 4.8 Variation of G_{max} with confining pressure at different relative densities for BP sand

4.2.2 Comparison of RC and BE Test Results

A comparison is made for the G_{max} values obtained using both the BE and RC tests. Fig. 4.9 a, b and c present the variation of G_{max} for BP, BG and YF sands, respectively, determined using both the techniques. An obvious increase of G_{max} with an effective confining pressure can be noted owing to the fact that the depth of over burden increases the stiffness. The G_{max} values obtained by RC test seem to be relatively higher than that of BE tests. At 300 kPa effective confining pressure for BG sand, G_{max} of 149 MPa was obtained by RC test at 30% R_d, while at the same R_d condition, BE test yielded 121 MPa, which shows a difference of 18%. Similarly, at 100 kPa σ'_c in dense condition (70% R_d), BG sand yielded 99 MPa in RC test while at the same testing conditions in BE test, a G_{max} of 88 MPa was observed, resulting in 11% reduction. This shows that there exists a difference of 10 to 20% for the G_{max} results obtained from both the tests. Such relative increase of G_{max} in RC tests is due to the differences in testing conditions in both the tests, such as different strain mechanisms in RC and BE; boundary conditions (fixed-free) in RC; use of calibration constants in RC while direct measurements of V_s in BE; and possible high relative strains for G_{max} (>0.0001%). Yang and Guo (2013) observed increased G_{max} values in RC test in comparison with BE tests. Since, BE test conditions provide the lowest strain conditions possible compared to the RC tests and with relatively fewer assumptions

in BE testing conditions, it is recommended to adopt the results of BE tests in the design/analysis.

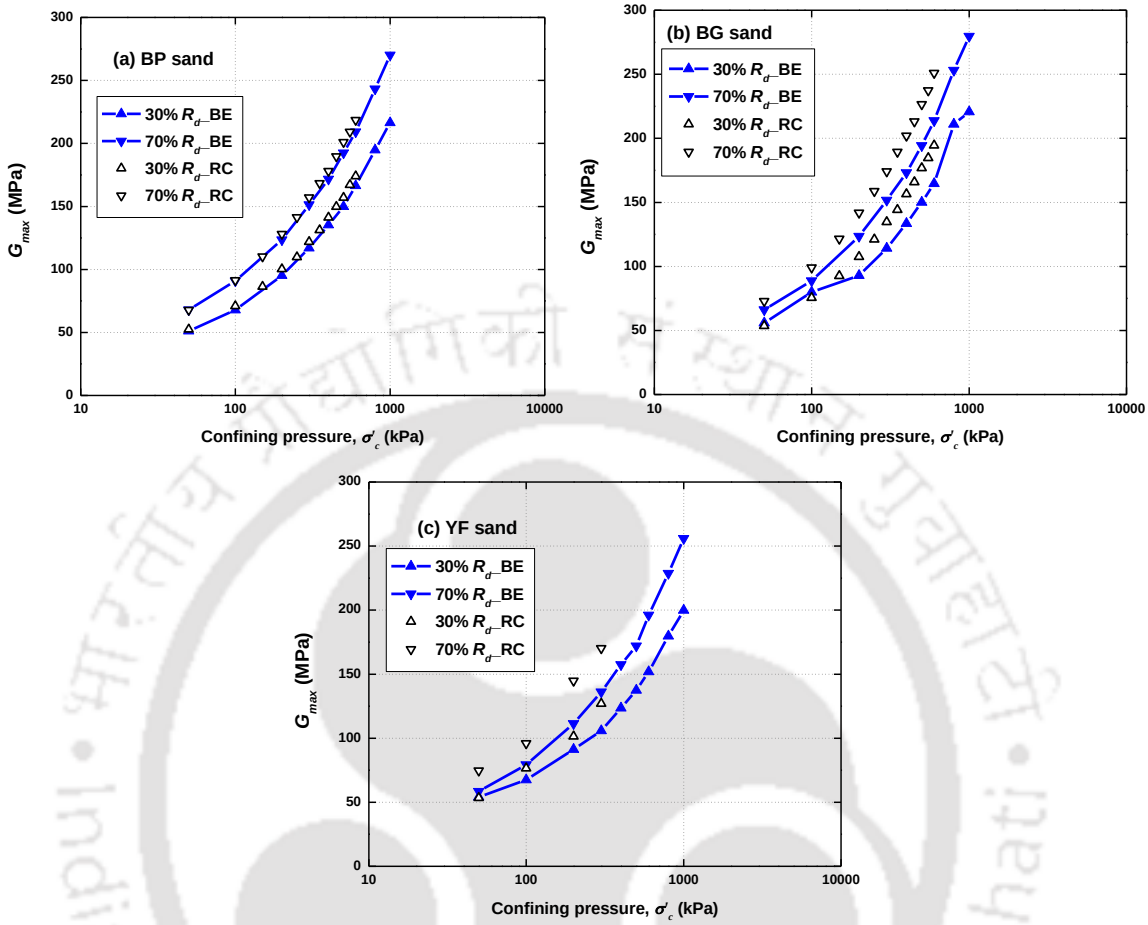

Fig. 4.9 G_{max} comparison from BE and RC testing for **(a)** BP **(b)** BG and **(c)** YF sands

4.2.3 Secant Shear Modulus (*G*)

The section discusses the nonlinear behaviour of cohesionless soils in intermediate strain range and the factors influencing it. Shear modulus was evaluated at three effective confining pressures (50, 100 and 300 kPa) for BP and BG sands while an effective confining pressure of 200 kPa was also considered for YC and YF sands, to check the effect of effective confining pressure on G at various strain levels. Fig. 4.10 presents the variation of G with γ for BP and BG sands at different σ'_c and R_d conditions. As it is a known fact that the increase in shear strains decrease the slope of the secant line of the hysteresis loop resulting in the reduced G, the same is reflected in Fig. 4.10. It can also be observed that the increase in the σ'_c increases G. This testifies the fact that the increase in the depth of overburden increases the shear resistance for granular soils with all other factors being same. Similar results were also observed for YC and YF sands, which are not presented here to avoid repetition of similar trends presentation.

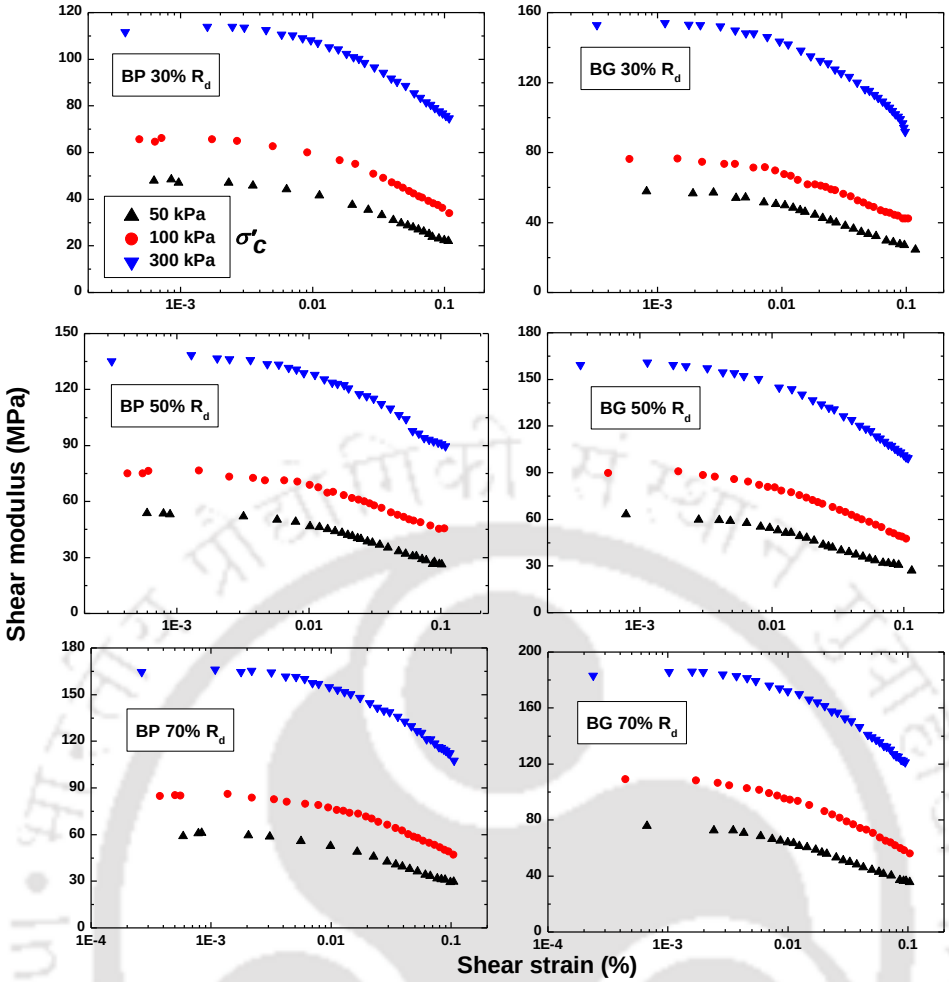

Fig. 4.10 Variation of G with γ for BP and BG sands at different effective confining pressures

Traditionally, secant shear modulus is normalized over G_{max} in order to understand the rate of reduction of shear stiffness and such variation is termed as normalized shear modulus reduction curves (G/G_{max}). Such curves are pivotal in most of the soil dynamics applications. Fig. 4.11 presents the variation of G/G_{max} with γ for BP and BG sands at different effective confining pressures. It can be seen that a constant G/G_{max} exists until a certain strain level (≈0.002 to 0.003%), which is typically the boundary of elastic limit of sands (also termed as elastic threshold strain, γ_{tl}). Beyond the elastic strain range, the inelastic or non-linear trend of G/G_{max} can be noted. Vucetic (1995) suggested the range of γ_{tl} for sands to be in 0.0001% to 0.001%. It can also be noted that as the effective confining pressure increases, G/G_{max} (and also γ_{tl}) of sands increases. For BP sand at 30% R_d, G/G_{max} of 0.90 was observed at 0.01% shear strain for 50 kPa effective confining pressure, while G/G_{max} of 0.95 was noted for 300 kPa. This means that the depth of overburden increases the elastic range of sands, keeping other conditions same.

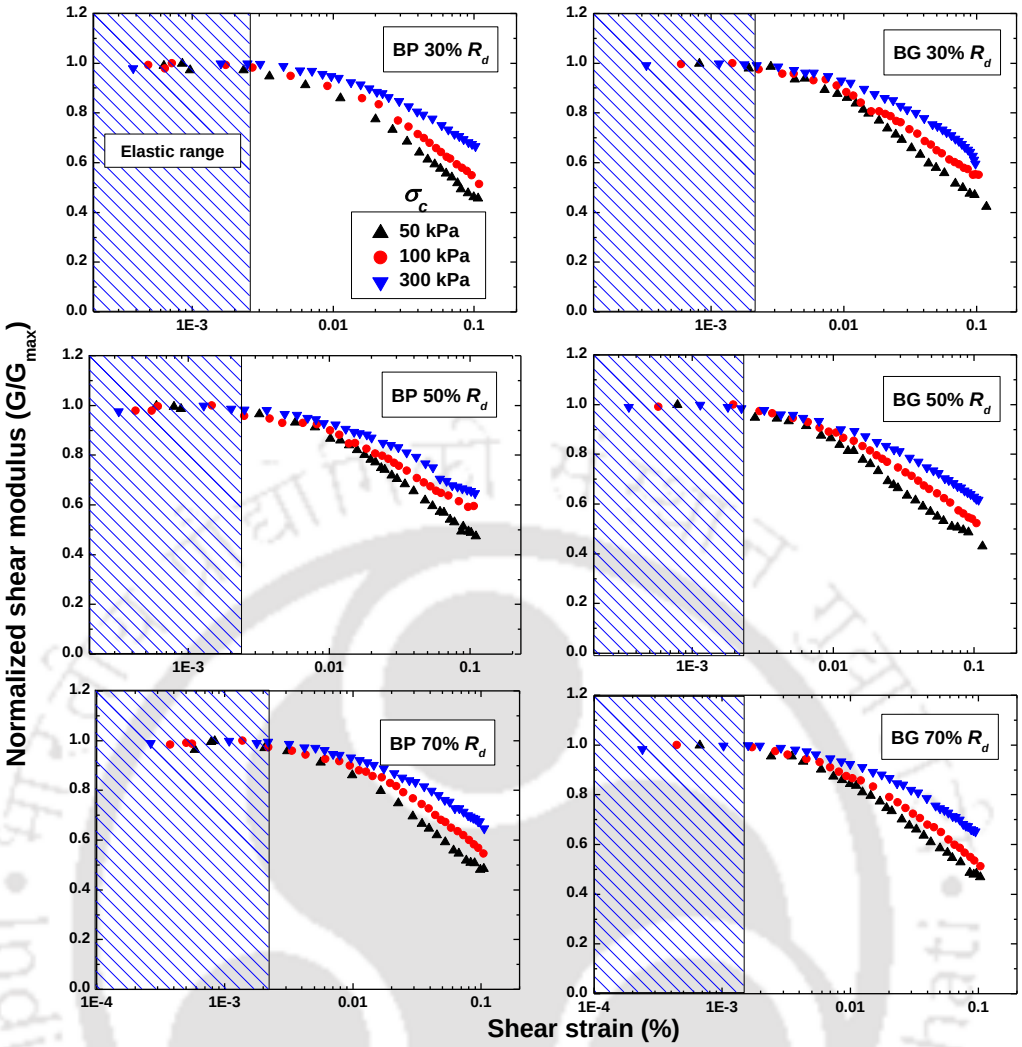

Fig. 4.11 Variation of G/G_{max} with γ for BP and BG sands

The effect of initial relative density on G and G/G_{max} is shown in Fig. 4.12 and Fig. 4.13, respectively, for BP and BG sands. It can be depicted that the relative density increases the G at any given shear strain with other parameters kept constant. Seed et al. (1986) made similar observations for gravels and Kumar et al. (2017) for sands. This is due to the increase of inter-particle contact with increased R_d, resulting in increased shear stiffness. A closer look on the variation of G of BG sand at 50 kPa and 300 kPa σ'_c yields an interesting observation. The difference in G of BG sand for 30% and 50% initial relative densities is nominal compared to 50% and 70% initial relative density conditions. Similar nominal difference of G was also observed at 30% and 45% R_d conditions for YC sand compared to 45% and 60% R_d conditions. Such phenomenon could possibly be due to the presence of relatively wide range of size particles than that of other tested sands: BP sand and YF sand (as seen from Fig. 3.2). Since sands with wide range of particle sizes contain relatively less void ratio and more compacted state than poorly graded sands (as seen from

Table 3.2), with all other conditions keeping same, the effect of increasing R_d (reducing void ratio much further) may not be highly influential on *G* at loose and medium dense conditions but could be instrumental at high R_d conditions. The results reported by Seed et al. (1986) on well-graded sands support this observation.

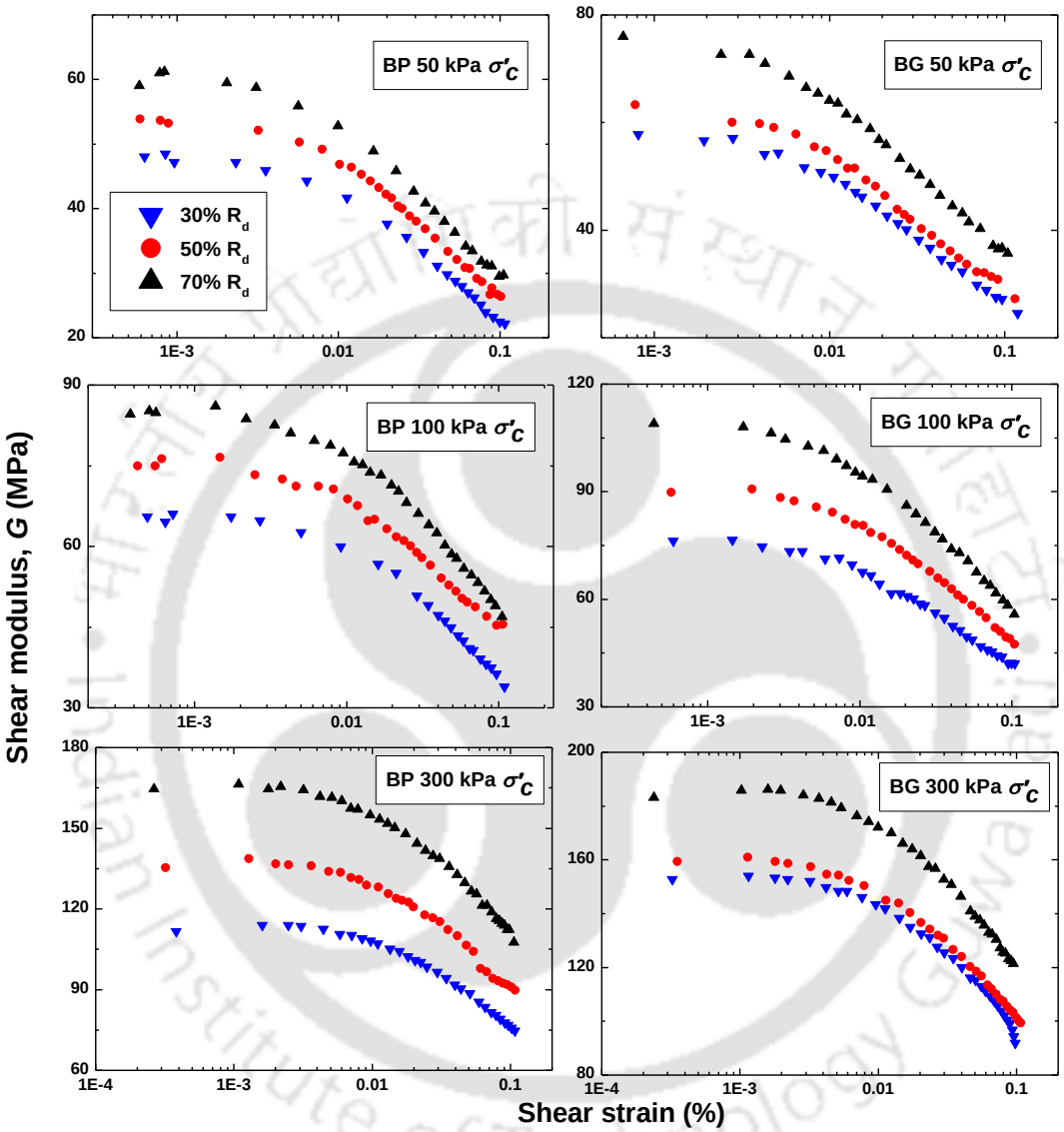

Fig. 4.12 Variation of *G* with γ for BP and BG sands at different relative densities

The effect of R_d is minor in case of G/G_{max} (Fig. 4.13). This is because the change in compactness due to increased R_d is resulting in consistent rate of change of G_{max} and *G*, thereby yielding similar ratio of G/G_{max}. It may be inferred from this observation that the effect of increase of σ'_c (in the tested range of 50 to 300 kPa) is higher in the particle rearrangement and consequent increased elasticity. The similar negligible effect of R_d (or void ratio) on G/G_{max} has been observed by various researchers (Kokusho 1980; Saxena and Reddy 1989; and Bai 2011). This confirms the fact that the change in compactness

due to change in R_d of sands would not alter the modulus degradation behaviour (G/G_{max}) at any given depth.

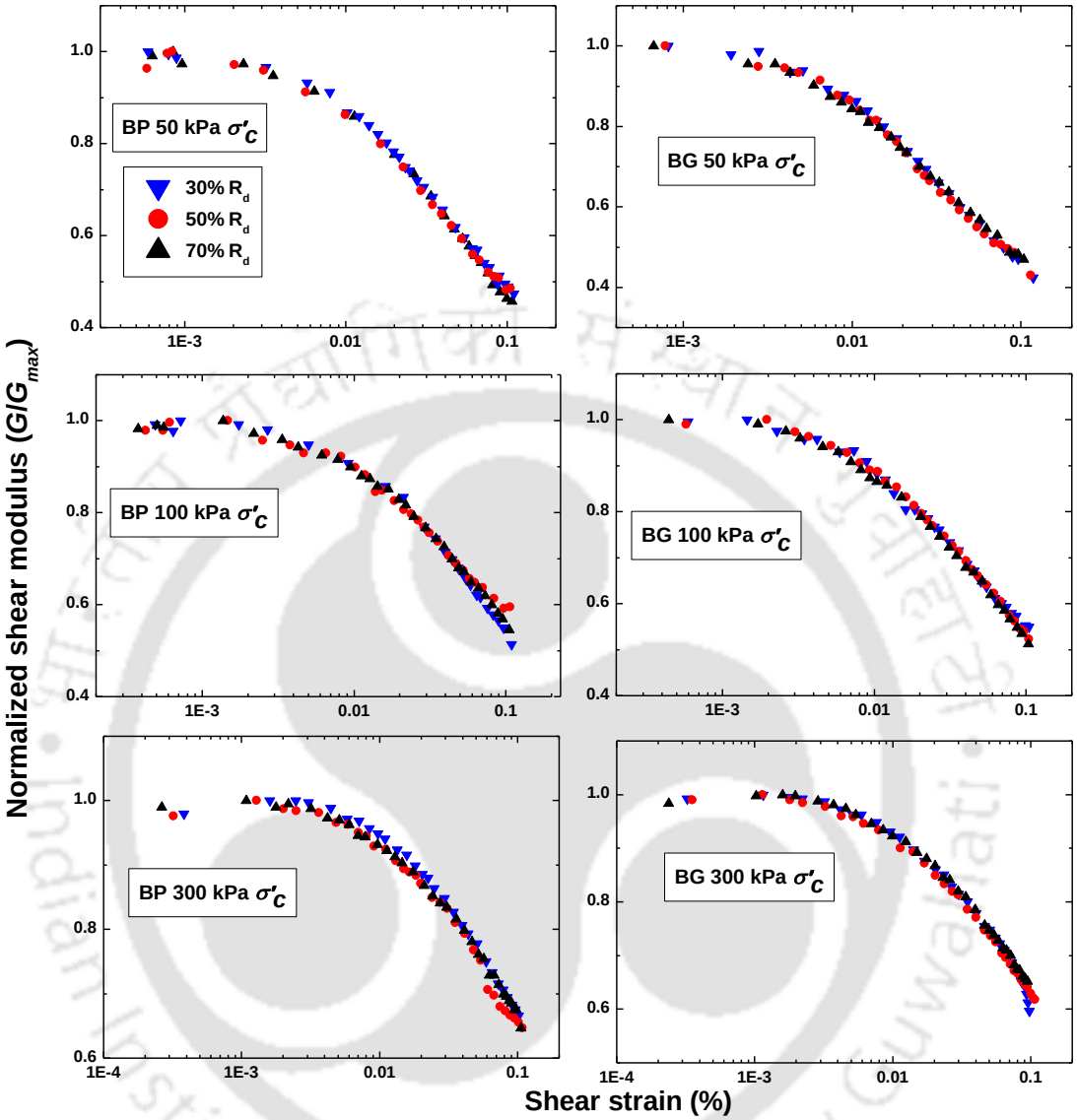

Fig. 4.13 Variation of G/G_{max} with γ for BP and BG sands at different R_d states

4.2.4 Damping Ratio (*D*)

Damping ratio is the measure of stored to dissipated energy, in the soil grains upon shearing. Similar to the *G*, damping ratio (*D*) also shows behavioural changes under dynamic loading conditions. The variation of *D* with shear strain is called damping ratio curve (*D* vs γ) and such variation combined with G/G_{max} are the crucial inputs for any soil dynamics problems involving the nonlinearity of soils. Further sections discuss the effects of effective confining pressure and initial relative density on damping ratio behaviour of sands.

The effect of effective confining pressure on damping ratio at various R_d conditions is depicted in Fig. 4.14. Noticeable variations of D in the initial straining conditions ($\gamma \leq 0.002\%$) can be observed, which are attributed to the high sensitivity of free vibration decay curve at the low strain tests (Bai, 2011). Decreased D with increased effective confining pressure can be noted at any given shear strain. This observation can be justified by the hysteresis loop theory. As the effective confining pressure increases, the stiffness of the loop increases with reduced strain and less loop area, ultimately resulting in low damping of the soil. Similar observations were noted for YC and YF sands.

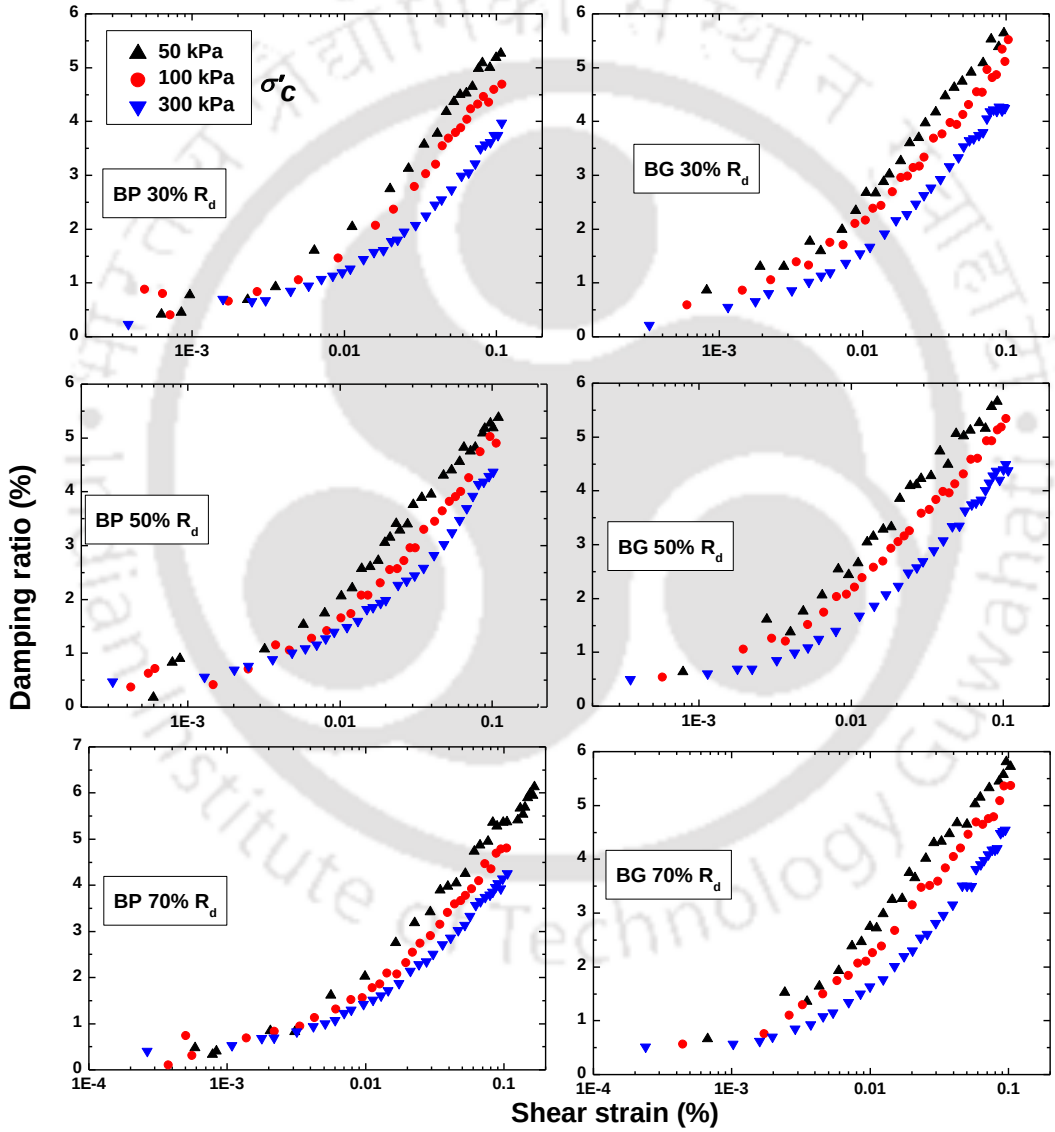

Fig. 4.14 Variation of D with γ for BP and BG sands at different effective confining pressures

The effect of R_d on damping ratio is shown in Fig. 4.15, for BP and BG sands. In most cases (except in case of BP sand in 300 kPa σ'_c condition), no remarkable change in

damping ratio with R_d was observed. Damping ratio being the ratio of stored to dissipated energy, with change in R_d, consistent change in the ratio was observed which means that both the energy contents (both stored and dissipated) are equally being effected with compactness change due to R_d. Similar insignificant effect of R_d on damping ratio has been observed for sands by Kokusho (1980), Saxena and Reddy (1989) and Bai (2011). It may be concluded based on these observations that the state of the granular material (due to change in R_d) would not significantly alter the damping ratio with shear strain, at other conditions being same.

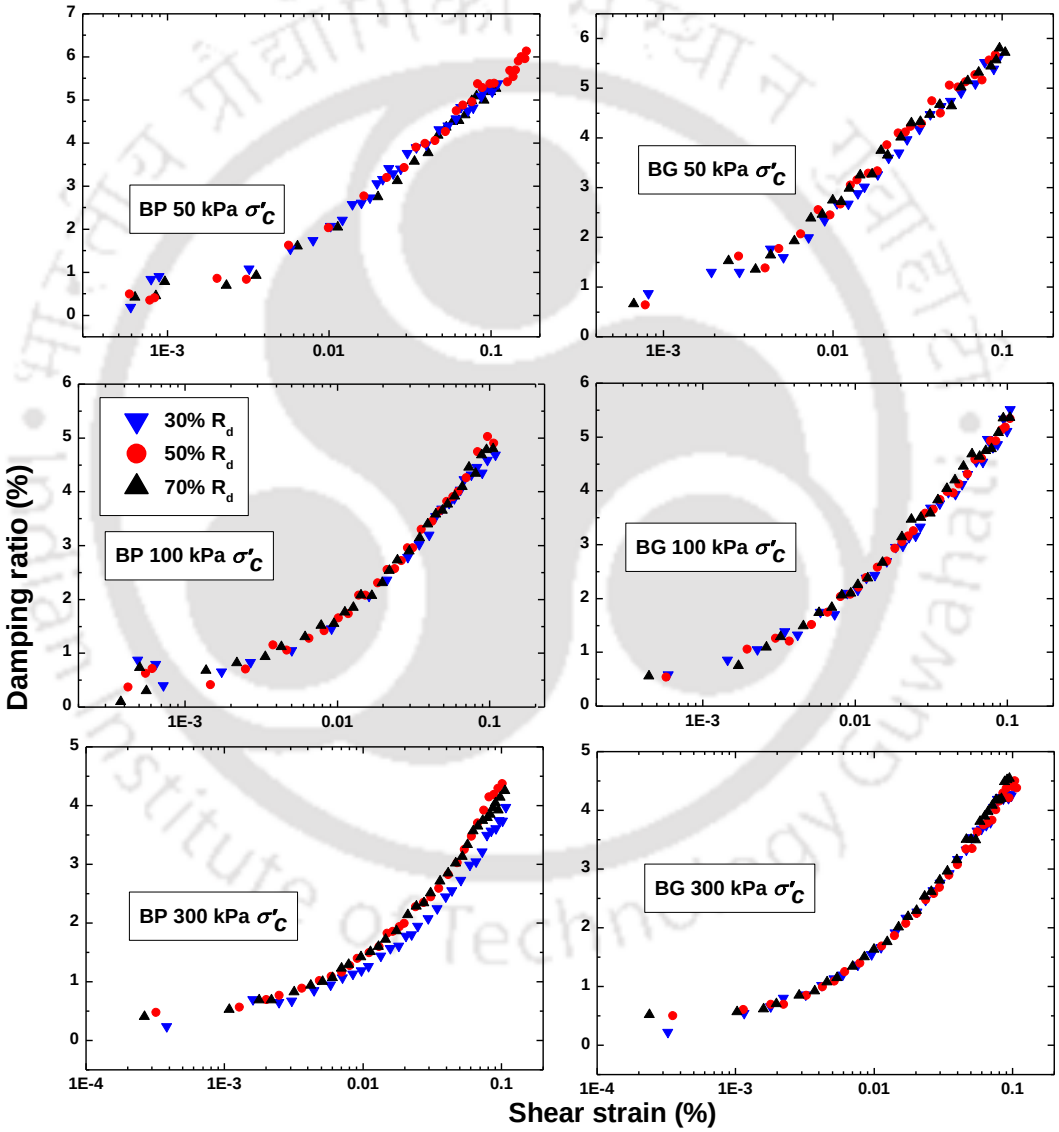

Fig. 4.15 Variation of D with γ for BP and BG sands at different R_d states

4.3 DYNAMIC SIMPLE SHEAR TEST RESULTS

DSS apparatus was utilised to understand the dynamic behaviour of chosen soils under high strain range (>0.05%). Table 4.4 briefs the DSS testing programme on cohesionless

soils with the investigated parameters. Three effective vertical stress conditions have been employed (75 kPa, 150 kPa and 300 kPa) which would represent the mean effective confining pressures of 50 kPa, 100 kPa and 200 kPa with an at-rest coefficient (K_o) of 0.5. All the sandy specimens were tested in dry condition. Since, most earthquake motions have their predominant frequencies in the range of 0.5 to 5 Hz, frequencies of 0.5 Hz and 1 Hz were chosen for the study. Only one R_d (50%) was chosen for all the sands, as the effect of R_d was found to be insignificant at high strain ranges for granular soils (Kumar et al. 2017). The shear loading was continued until 1000 cycles to check the effect of high number of loading cycles on dynamic characteristics of sands at high strains. Total of 64 DSS tests have been conducted.

Table 4.4 DSS testing programme and loading conditions

Soil	R_d (±5%)	Shear strain (%)	Effective vertical stress (kPa)	Frequency (Hz)	Number of cycles
BP sand	50	0.05, 0.1, 0.25, 0.5, 1	75	1	1000
			150		
			300		
		2.5, 5, 10	75	1	1000
			150	0.5	
			300	0.5	1000
BG sand		0.05, 0.1, 0.5, 1, 0.5, 1	75	1	1000
			150		
			300		
		5	75	1	1000
			150	0.5	1000
			300	0.5	1000
YF		0.1, 0.5, 1, 5	50	1	1000
			100		
			200		
			300		
YC		0.1, 0.5, 1, 5	50	1	1000
			100		
			200		
			300		

The effect of shear strain (γ) on the stress-strain response of cohesionless soils is investigated in this section. Cyclic stress-strain responses of BG sand at 150 kPa constant effective vertical stress (σ'_n) condition for the first (N=1) and the 100th loading cycles (N=100), are presented in Fig. 4.16 and Fig. 4.17, respectively. Stress-strain response of soils thus obtained follows a typical hysteretic behaviour. An important observation can be drawn based on the response: increase in shear strain increases the stresses induced in the specimen, meaning, higher stresses will be required to mobilize the higher displacements.

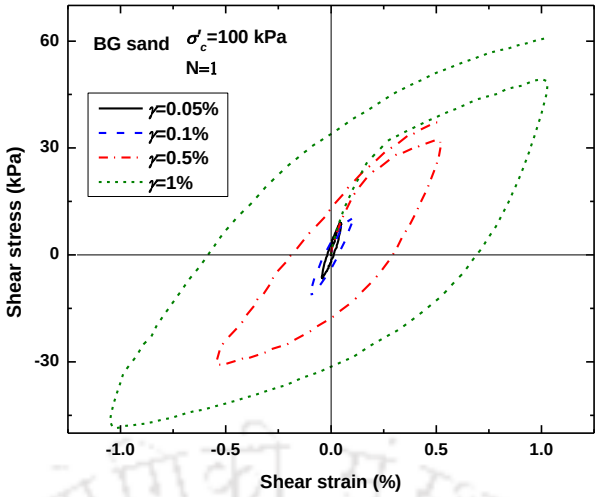

Fig. 4.16 Stress-strain response of BG sand at 150 kPa effective vertical stress condition for the first loading cycle

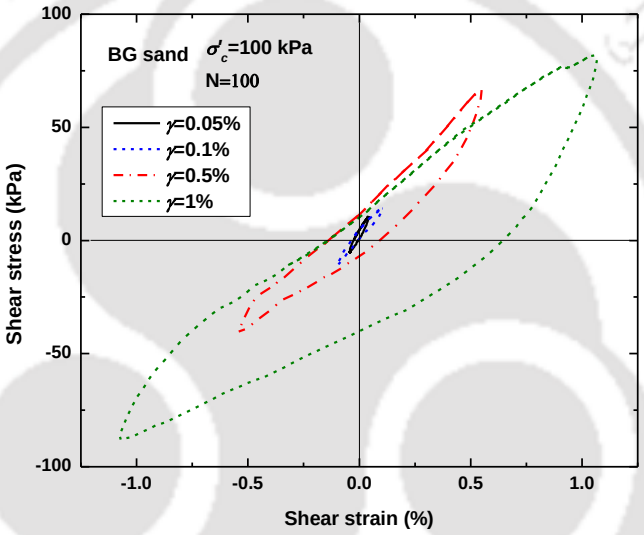

Fig. 4.17 Stress-strain response of BG sand at 150 kPa effective vertical stress condition for the 100th loading cycle

The effect of loading cycles (N) on the high strain behaviour of BG sand is shown in Fig. 4.18, Fig. 4.19, and Fig. 4.20 at shear strain amplitudes of 0.1%, 0.5%, and 1%, respectively. An interesting observation can be noted, with increase in the number of loading cycles, peak shear stress (τ_{peak}) increases and this is more pronounced at large shear strain amplitudes. In case of 0.1% strain (Fig. 4.18), first loading cycle showed a τ_{peak} of 10 kPa while 100th and 1000th cycles, τ_{peak} of 14 kPa and 14.6 kPa was noted, respectively. This amounts to 46% rise in the τ_{peak} for 1000 loading cycles. Similarly, in case of 0.5% (Fig. 4.19) and 1% (Fig. 4.20) strains, high τ_{peak} magnitudes were observed. This increase in τ_{peak} for large loading cycles in dry granular soils is attributed to the relative increase of compactness (due to particle rearrangement) with increasing loading cycles. Similar high stresses for large loading cycles were observed for granular soils by Drenvich et al. (1967).

Normal settlement variation with loading cycles provides an insight in to this observation. Fig. 4.21 presents the normal settlement of BG sand specimens at different strain amplitudes. In case of 1% strain amplitude, settlement of 0.4 mm was observed for 600 cycles while the same is reduced to 0.2 mm, 0.025 mm and 0.01 mm in case of 0.5%, 0.1% and 0.05% amplitudes, respectively. This means that intense seismic events induce excessive soil settlements. In soil dynamics applications, large (multiples of hundreds and thousands) loading cycles are expected in case of machine foundations and offshore wind turbines. Adhikari and Bhattacharya (2011) and Nikitas et al. (2016) reported similar increase of shear stiffness with loading cycles for granular soils in case of offshore wind turbine foundations.

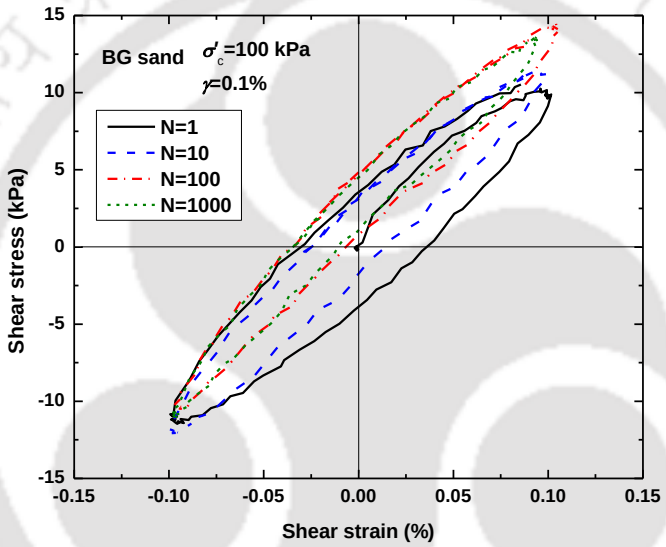

Fig. 4.18 Stress-strain response of BG sand at 0.1% shear strain for different loading cycles

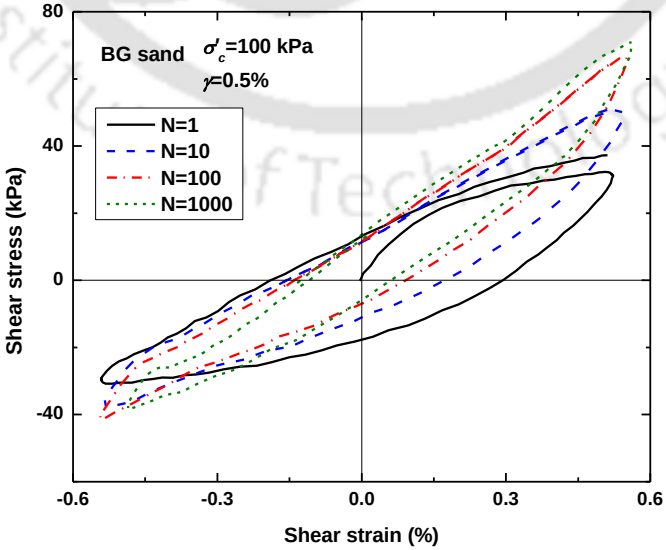

Fig. 4.19 Stress-strain response of BG sand at 0.5% shear strain for different loading cycles

Another important observation can be made based on the stress-strain response: asymmetricity of the loops increases with the loading cycles and such increase is more prominent at high shear strains and large loading cycles (Fig. 4.19 and Fig. 4.20). A positive τ_{peak} (loading) of 72 kPa can be noted for 1000th cycle in case of 0.5% shear strain (Fig. 4.19) while a negative τ_{peak} (unloading) of 40 kPa was observed for the same loading cycle. Similarly, from Fig. 4.20, positive τ_{peak} of 115 kPa was noted for the 1000th loading cycle, while it reduced to 91 kPa in the negative side. Similar asymmetric loops at strains≥0.15% have been reported by Kumar et al. (2017) for granular soils. This asymmetricity is basically attributed to the plastic nature of the granular soils at high shear strains, meaning: that the high strains induce permanent plastic deformations during the loading phase (positive stress-strain) and during the unloading phase, the specimen offers less shear resistance.

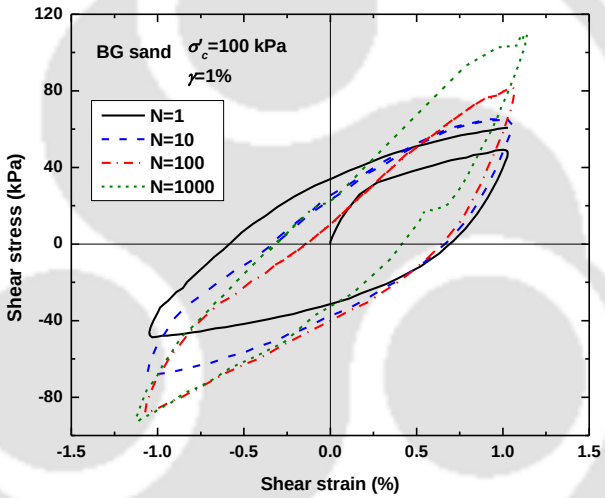

Fig. 4.20 Stress-strain response of BG sand at 1% shear strain for different loading cycles

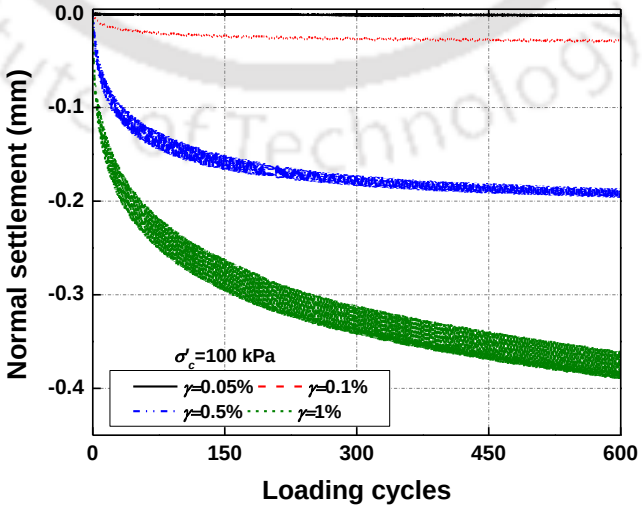

Fig. 4.21 Effect of loading cycles on normal settlement of BG sand at different strain amplitudes

The effect of constant effective vertical stress (σ'_n) on high strain dynamic response of BG sand is illustrated through Fig. 4.22 and Fig. 4.23 at 0.5% and 1% shear strains, respectively. The increase in effective vertical stress increased the stiffness (slope) as well as the τ_{peak}. The slope refers to the secant modulus (G_{sec}) of the soil. At 0.5% strain (Fig. 4.22), at 75 kPa effective vertical stress condition, G_{sec} of 408 kPa is noted while the same is increased to 644 kPa and 1152 kPa under 150 kPa and 300 kPa effective vertical stress conditions, respectively. Similar high G_{sec} can be observed at 1% shear strain condition (Fig. 4.23). Similar responses were observed for other tested sands at the investigated loading conditions. This means that the deep granular deposits exhibit high modulus than that of surficial soils, keeping all other conditions same (i.e. similar void ratio, loading cycles, strain level, etc.).

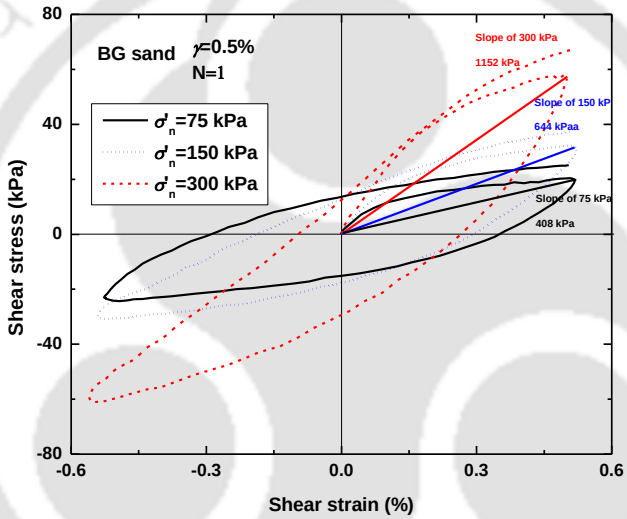

Fig. 4.22 Stress-strain response of BG sand at 0.5% shear strain for different effective vertical stress conditions

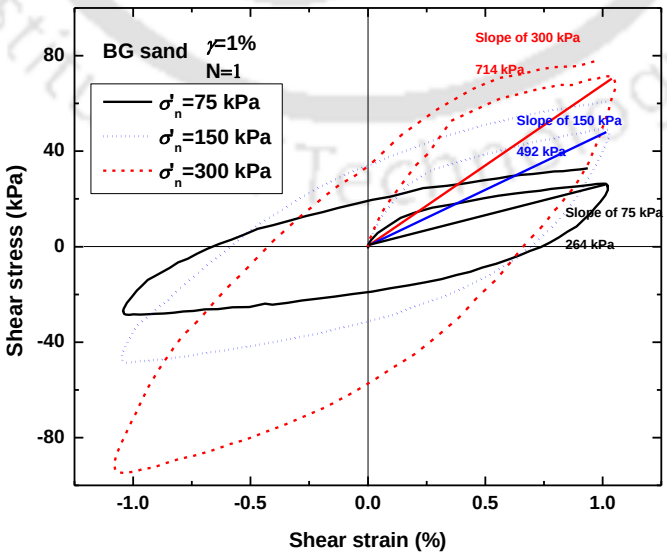

Fig. 4.23 Stress-strain response of BG sand at 1% shear strain for different effective vertical stress conditions

The obtained hysteresis loops are then adopted to determine the dynamic soil properties (*G* and *D*) at different strain amplitudes. Many researchers adopted different loading cycles to determine the dynamic properties: 10th cycle (Iwasaki et al. 1978; Kokusho 1980), 5th cycle (Seed et al. 1986), 3rd cycle (Okur and Ansal 2007), 1st cycle (Govindaraju 2005; Vucetic et al. 1998; Kumar et al. 2017). As the initial state of the specimen is expected to be altered/strained by increasing loading cycles, present study considers the first loading cycle (N=1) for *G* and *D* determination.

Regarding the shape of the hysteresis loop, traditionally symmetric loop (similar in shape in both loading and unloading) has been in use for evaluating *G* and *D* for a particular strain (ASTM D3999 2013). However, with the asymmetrical stress-strain response observed for the granular soils at high strains, a modified approach proposed by Kumar et al. (2017) as depicted in Fig. 4.24, has been adopted here for the determination of *G* and *D*.

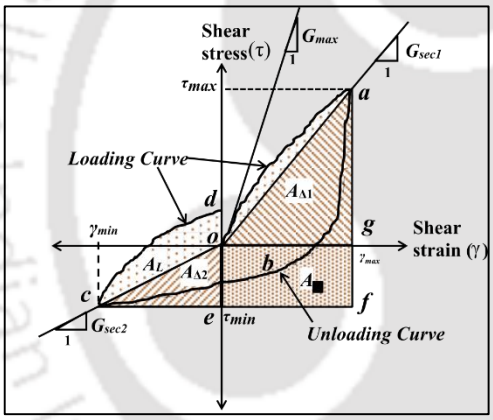

$$G = \frac{G_{sec1} + G_{sec2}}{2}$$

$$D = \frac{1}{\pi} \cdot \frac{A_{L(o-a-b-c-d)}}{A_{\Delta1} + A_{\Delta2} + A_{\blacksquare}}$$

Fig. 4.24 Methodology adopted for determination of *G* and *D* (modified after Kumar et al. 2017)

Fig. 4.25 (a, b and c) presents the variation of *G*, G/G_{max} and *D* with γ for BP sand at different effective confining pressures. The G_{max} values obtained from BE tests have been utilised to obtain G/G_{max}. The effect of effective confining pressure can be noted in *G* and this effect diminishes at high strains reaching almost zero stiffness. Similarly, G/G_{max} also approaches a minimal value at high strains, with insignificant effect of effective confining pressure. This is due to the loss of inter-particle contact under high strains, leading to uniform shear modulus. An interesting trend of damping ratio can be observed at high strains (Fig. 4.25c): increase and decrease of *D* with γ. Such trend at high strains is attributed to the dilative behaviour of sands resulting from S shaping of the stress-strain response (Matasovic and Vucetic 1994). Similar trends were observed for sands by

Matasovic and Vucetic (1994), Kiku and Yoshida (2000), Chiaradonna et al. (2015), Pagliaroli et al. (2018) and for clays by Chehat et al. (2018).

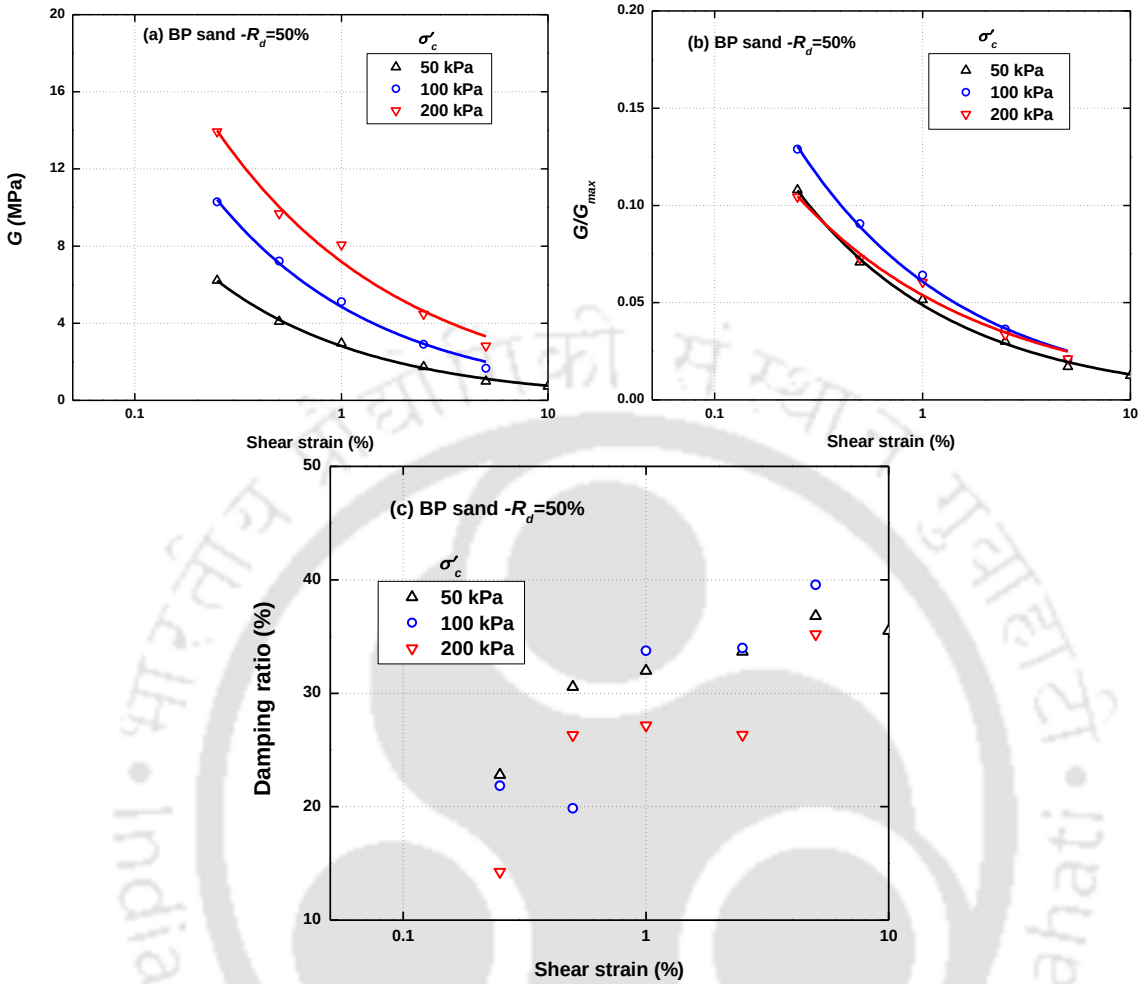

Fig. 4.25 Variation of **(a)** G **(b)** G/G_{max} and **(c)** D with γ for BP sand at high shear strains

4.4 COMPREHENSIVE G/G_{max} AND DAMPING RATIO CURVES

Results obtained from the three equipment (RC and DSS) are compiled together to provide comprehensive data of G/G_{max} and damping ratio for all the chosen soils. For low to intermediate strains range (0.001% to 0.1%), RC test results were used. The DSS test results were adopted for high strain range (strains>0.1%). Fig. 4.26, Fig. 4.27, Fig. 4.28, and Fig. 4.29 present the combined G/G_{max} and D of all the chosen sandy soils. Boundaries of G/G_{max} and D for sands proposed by Seed and Idriss (1970) and Darendeli (2001) were also presented in the figures. As can be observed, G/G_{max} data of all the sands have plot on higher to the curves proposed by both Seed and Idriss (1970) and Darendeli (2001) up to 0.1% strain that are typically the engineering strains prevail during dynamic loading. It must be mentioned that Darendeli (2001) limits shown in Fig. 4.26, Fig. 4.27, Fig. 4.28, and Fig. 4.29 are for 25 kPa and 400 kPa effective confining pressures and the present test

data still do not fall in the range. Similar stiff G/G_{max} and soft damping properties (in comparison with Seed and Idriss (1970) and Darendeli (2001) have been reported for Germany sands by Bai (2011) and for Kasai river sand by Chattaraj and Sengupta (2016). This means that the damping of the soil during dynamic loading may be overestimated if standard curves are used for the analysis while the stiffness may be underestimated. The differences in the G/G_{max} and D of investigated soils from the literature sands could possibly due to many reasons, which may be classified into major and minor. The major parameters include compositional, index and shear characteristics while the minor possibilities include sample preparation, testing type and loading conditions. Hinged on these observations, it may be realized that a mere adoption of standard/available stiffness curves in seismic design of structures may lead to inappropriate design and hence, availing region-specific soil data is imperative. Further section provides a continuity to this framework by providing the best-fit parameters for G/G_{max} and damping functions based on regression analysis for all the chosen soils.

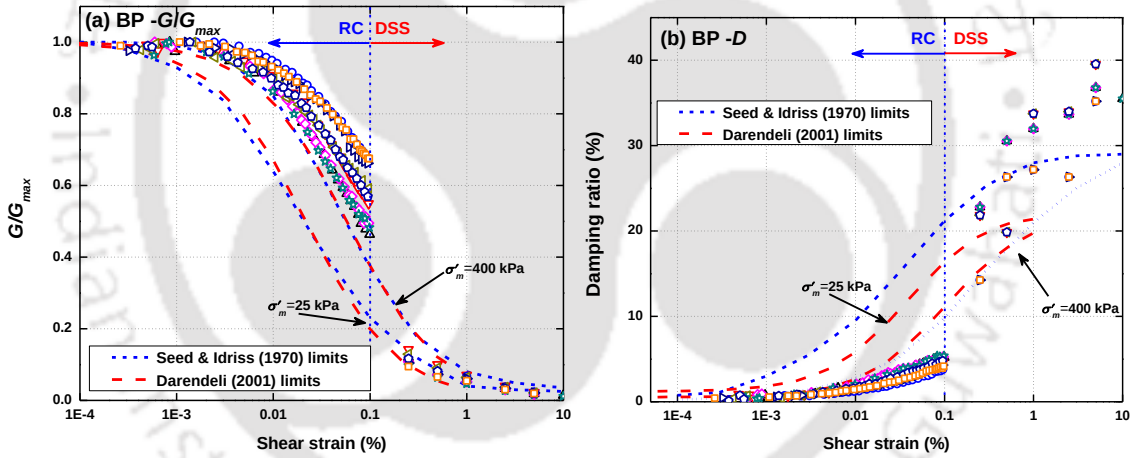

Fig. 4.26 (a) G/G_{max} and (b) damping ratio of BP sand

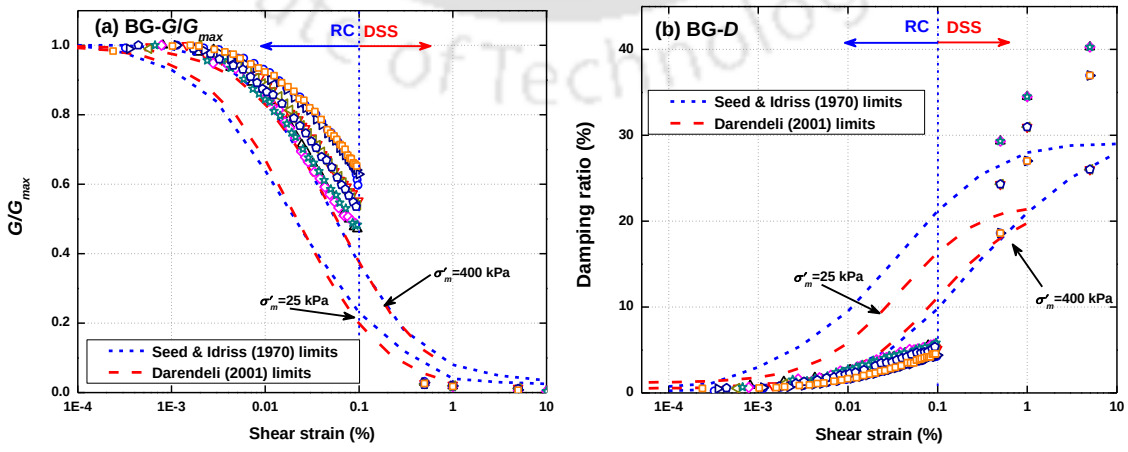

Fig. 4.27 (**a**) G/G_{max} and (**b**) damping ratio of BG sand

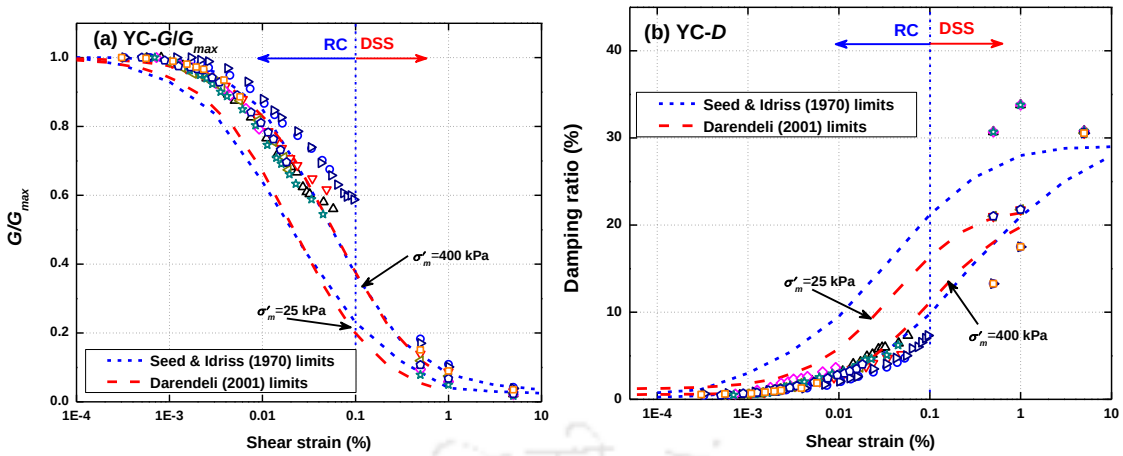

Fig. 4.28 (a) G/G_{max} and (b) damping ratio of YC sand

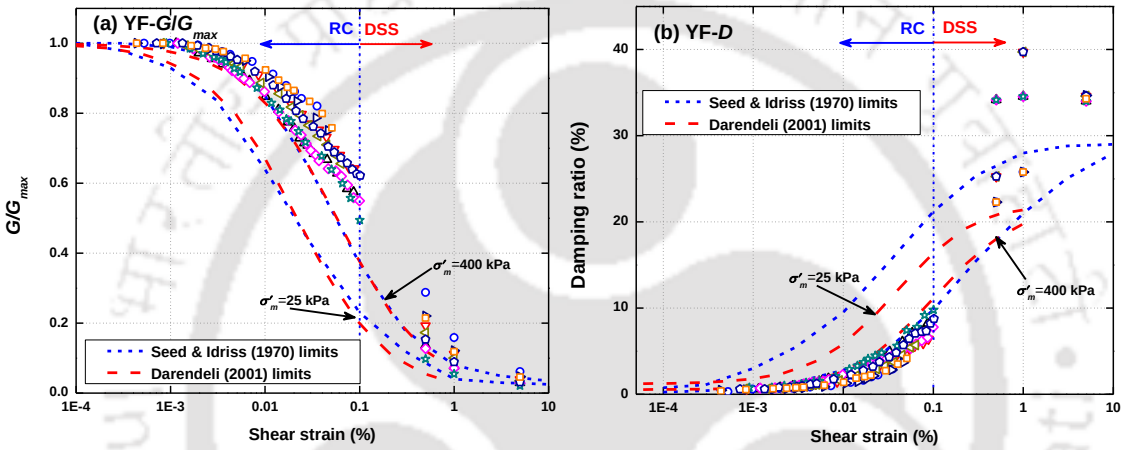

Fig. 4.29 (a) G/G_{max} and (b) damping ratio of YF sand

4.5 EMPIRICAL FORMULATIONS

The tested soils were sampled from the shores of two rivers (Brahmaputra and Yamuna) which are essentially the major rivers of the country and huge infrastructure development (such as road cum rail bridges, etc.) is planned over these two rivers. Since most of the soils in these regions are river sediments, the bore log data of these regions indicate soils of similar properties as that of tested soils. Therefore, whenever typical soils are encountered, the determined properties can be used based on the σ'_c and density condition. However, in cases of other σ'_c and density conditions, the empirical formulations will be handy. Simplified empirical formulations are primarily needed for modelling the constitutive behaviour of soils in numerical modelling techniques. This section describes the regression analyses performed on element test results for providing generalized models for G_{max}, G/G_{max} and D with appropriate fitting parameters, which can be directly used for the soil dynamics applications. In case of G/G_{max} and D curves, data from published literature for other Indian sandy soils have also been considered.

4.5.1 Maximum Shear Modulus (G_{max})

Several forms of G_{max} functions are available in the literature, which were listed in Table 2.4 of *Chapter II*. Present study considers the formulation proposed by Hardin (1978) as shown in Eqn. 4.1. This function has been in wide use for many geotechnical applications (Saxena and Reddy 1989; Bai 2011; Chattaraj and Sengupta 2016) due to its dimensional consistency and application validity to soils of even larger void ratio (Chung et al. 1984).

$$G_{max} = \frac{A \cdot (P_a)^{1-m} \cdot (\sigma_c')^m}{(0.3+0.7 \cdot e^2)} \quad (4.1)$$

where P_a is atmospheric pressure (101 kPa), A is a constant depending on the type of soil (625 as proposed by Hardin 1978), σ'_c is the mean effective confining pressure, and m is a stress dependent factor (0.5 according to Hardin 1978).

Several researchers made use of Hardin's equation as a basic form and provided the best-fit parameters for the soils of interest (as shown in Table 4.5). The values of A range from 520 to 750 while the values of m range between 0.46 and 0.60. This shows the necessity of determination of soil-specific best-fit parameters for an efficient dynamic analysis. Hence, the aforementioned formulation (Eqn. 4.1) has been used for regression analysis. The G_{max} data determined from both RC and BE tests has been used independently for the regression analysis, for a comparison purpose.

Fig. 4.30 presents the regression results of BP sand in terms of normalized G_{max} (G_{max}×F(e)/P_a) with normalized effective stress (σ'_c/P_a) for the BE and RC G_{max} data independently. The function of void ratio (F(e)) in the regression analysis refers to the form 0.3+0.7e^2 as deduced from the Eqn. 4.1. It is evident that a power law ($y = Ax^m$) can adequately model the G_{max} data with a high correlation coefficient (R^2). It can also be noted that the both the experimental data (BE and RC) falls in the narrow range and so does the best-fit parameters. Therefore, data from both the tests (RC and BE) have been combined to provide the best-fit parameters for the sands chosen. Fig. 4.31 depicts the combined regression data for BP sand. A satisfactory simulation of experimental data can be noted using Hardin's formulation with an R^2 of 0.987.

Table 4.6 lists the best-fit parameters for the tested sands. It can be noted that the values of A (range between 588 and 615) and m (0.47 to 0.54) of the chosen sands (BP, BG, YF and YC) are consistent with the literature (Table 4.5). Fig. 4.32 presents the efficiency of

the proposed best-fit parameters, which shows that the estimated values are within the satisfactory range (± 10%) from the measured data.

Table 4.5 List of fitting parameters for various sands using Hardin's formulation

Author/s	Soil	*A* value	*m*
Hardin (1978)	Clean sand	625	0.5
Chung et al. (1984)	Monterey No. 0 sand	523	0.48
Saxena and Reddy (1989)	Monterey No. 0 sand	428	0.57
Bai (2011)	Berlin sand	751	0.50
Bai (2011)	Braunschweig fine sand	654	0.48
Bai (2011)	Braunschweig coarse sand	523	0.60
Bai (2011)	Cuxhaven fine sand	736	0.49
Bai (2011)	Cuxhaven medium sand	658	0.47
Chattaraj and Sengupta (2016)	Kasai River sand	612	0.46

Table 4.6 Fitted parameters for Eqn. 4.1

Soil	*A* value	*m*	R^2
BP	588	0.48	0.987
BG	608	0.47	0.958
YF	609	0.46	0.982
YC	615	0.53	0.970

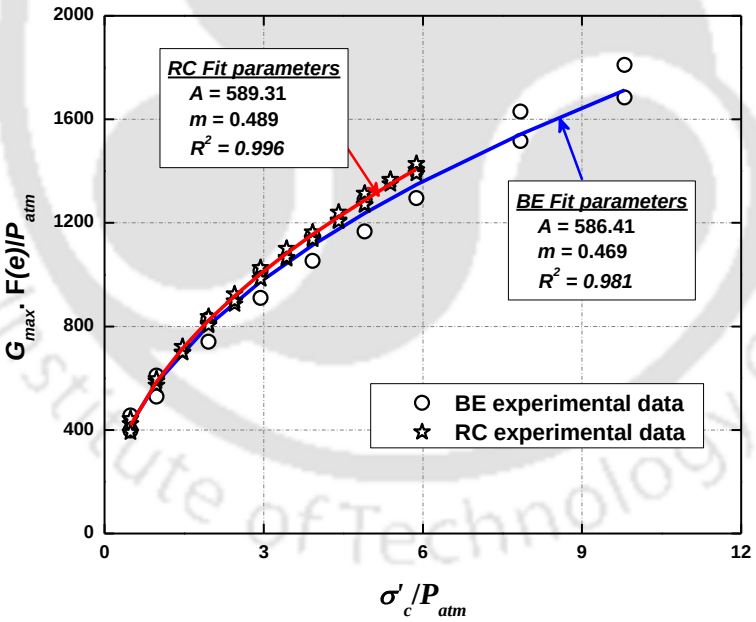

Fig. 4.30 Regression results of BP sand using Eqn. 4.1 independently for RC and BE data

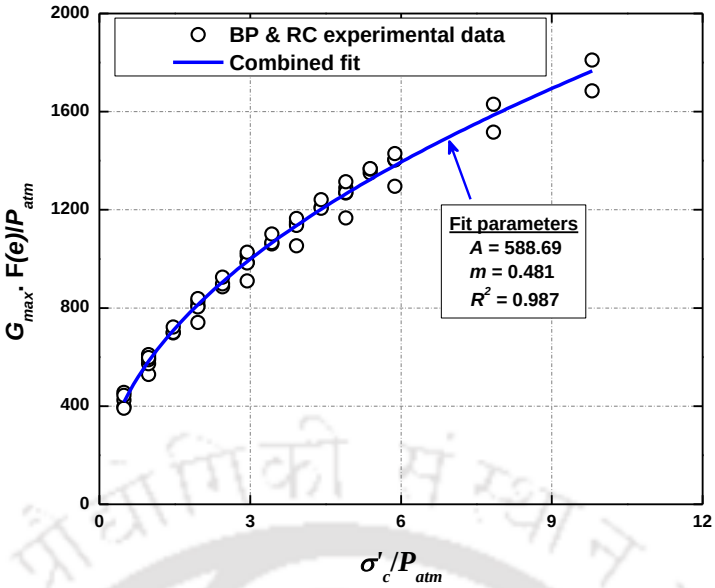

Fig. 4.31 Regression results of BP sand using Eqn. 4.1 combined for RC and BE data

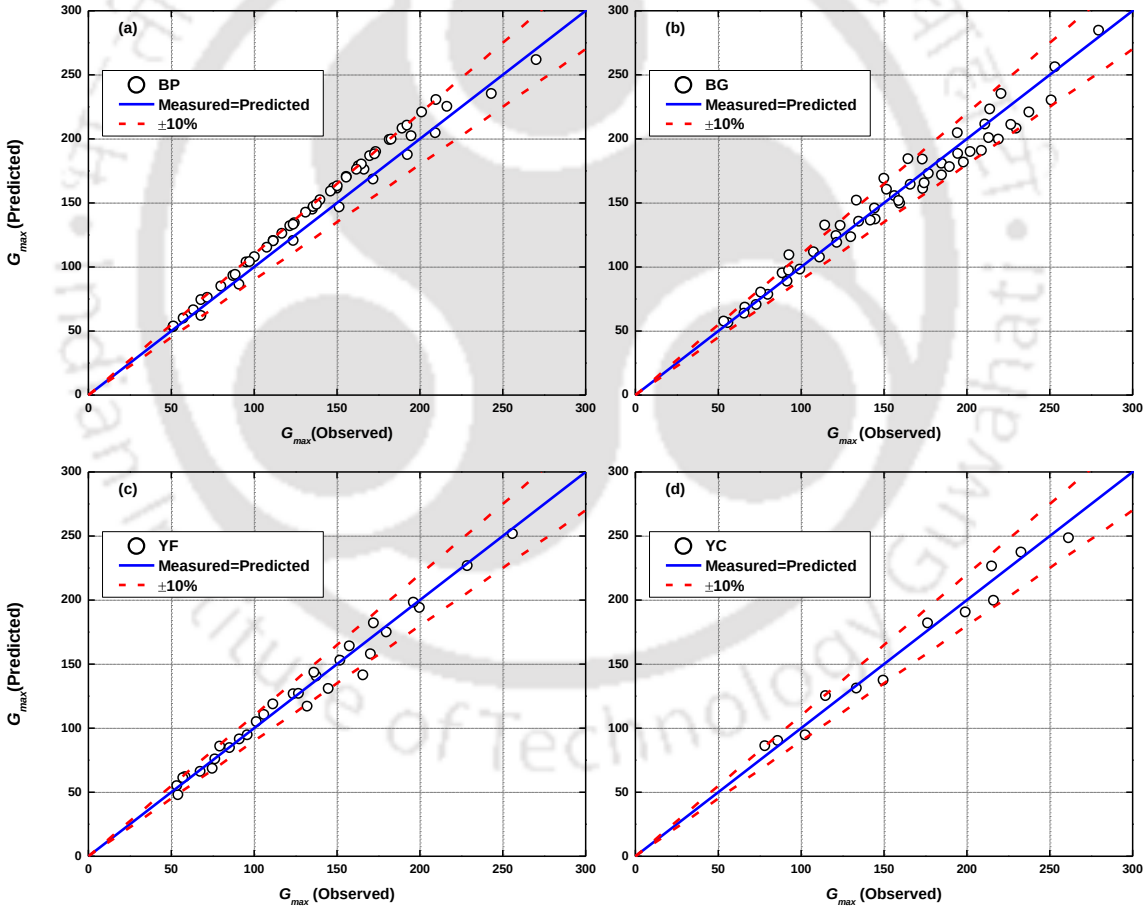

Fig. 4.32 Efficiency of proposed best-fit parameters for the sands chosen

4.5.2 Normalized Shear Modulus (G/G_{max})

Several forms of G/G_{max} have been employed by various researchers, which are presented in Section 2.1.3 of Chapter II. Chapter II also presents the data of G/G_{max} and D of cohesionless soils of India. The modified hyperbola form of equation proposed by

Matasovic and Vucetic (1994) as described through Eqn. 4.3, has been adopted here for modelling G/G_{max}.

$$\frac{G}{G_{max}} = \frac{1}{1+\beta\cdot\left[\frac{\gamma}{\gamma_{ref}}\right]^{\alpha}} \tag{4.3}$$

where γ_{ref} is the reference shear strain, τ_{max}/G_{max}; α and β are the curve fitting parameters obtained through regression analysis on the experimental data. Darendeli (2001) considered γ_{ref} as the shear strain corresponding to 50% of the maximum shear modulus (G/G_{max}=0.5), which was considered appropriate and also makes the entire function simple (Zhang et al. 2005). The same form of γ_{ref} has been adopted here. The soils of interest (both tested and data from literature-KS; SL; HS) are considered to provide the curve fitting parameters (α and β).

For the purpose of comparison, Matasovic and Vucetic (1994) model's efficiency in capturing the experimental G/G_{max} trends has been compared with that of Darendeli (2001) model (presented in Table 2.4) for BP sand at 50% R_d and 50 kPa effective confining pressure (Fig. 4.33). It can be observed that the gentle curvature existing between RC and DSS results has been effectively simulated using the Matasovic and Vucetic (1994) model with high correlation coefficient (R^2=0.988) than Darendeli's model (R^2=0.946).

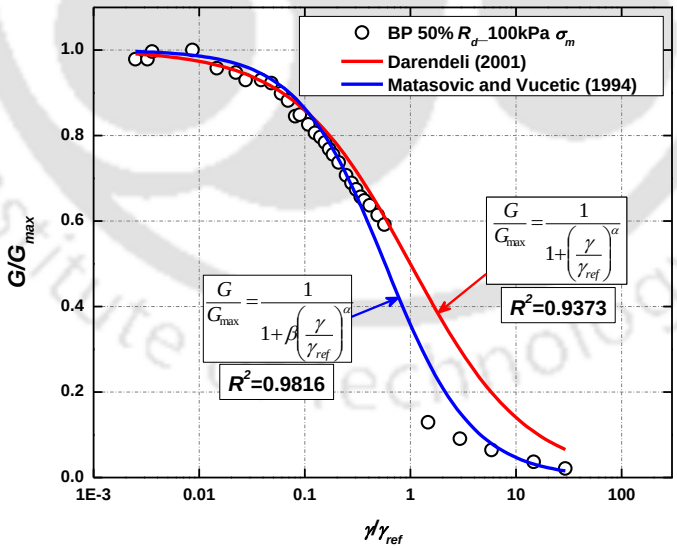

Fig. 4.33 Comparison of Matasovic and Vucetic (1994) and Darendeli (2001) in modelling G/G_{max} of sands

Regression analysis has been performed for the experimental results of all the sands (tested sands and literature collected data of Indian sands). The γ_{ref} values have been considered from the test results at G/G_{max} of 0.5 as suggested by Darendeli (2001) and Zhang et al.

(2005). The values of γ_{ref} vary with σ'_c significantly and their relationship is required to find γ_r. Stokoe et al. (1995) formulated the following equation (Eqn. 4.4) to determine the reference shear strain value at a given σ'_c.

$$\gamma_{ref} = \gamma_{r1} \cdot \left(\frac{\sigma'_c}{P_a}\right)^k \tag{4.4}$$

where γ_{r1} is the reference shear strain for a effective confining pressure of 100 kPa and k is the stress correction exponent, suggested a value of 0.5 for non-plastic soils by Zhang et al. (2005). For validation of this expression to tested soils, a normalized curve has been drawn (Fig. 4.34) and this yields a k value of 0.374 with a reasonable correlation coefficient (R^2=0.751). The Eqn. 4.4 has been used to determine γ_{ref} in conjunction with a k value of 0.374, in cases where experimental data is scarce.

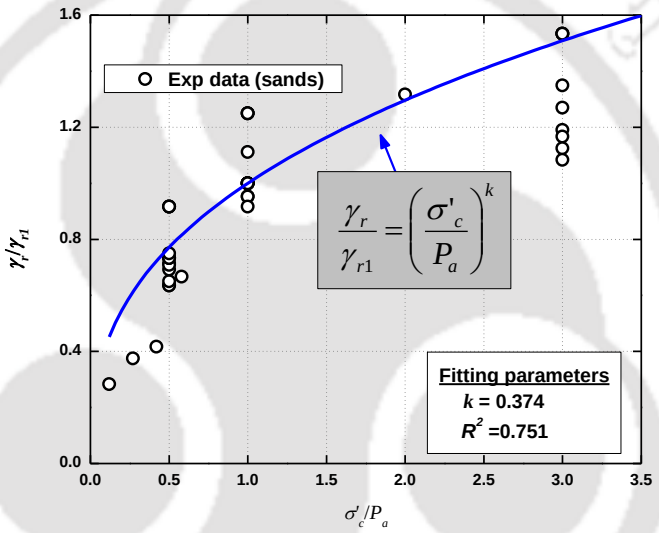

Fig. 4.34 Normalized reference shear strain for the tested sands

In addition to the tested sands, data from literature pertaining to other Indian soils have also been collated for providing best-fit parameters for the considered hyperbolic function. The soils include Kasai River (KS) sand reported by Chattaraj and Sengupta (2016), Saloni (SL) sand by Kirar and Maheswari (2017) and Hyderabad (HS) sand by Dutta and Saride (2016). All the soils are river bed sands and classified as poorly graded (SP) sands based on their GSD characteristics. The C_u of the sands range from 2.0 to 2.7 which is in range of the currently tested sands.

Table 4.7 presents the regression data and the best-fit parameters for all the sands. It can be observed that the G/G_{max} of all the sands has been reasonably modelled using the Matasovic and Vucetic (1994) function. Fig. 4.36 compares the predicted and measured G/G_{max} values with ±10% error. The efficiency of the proposed formulations is obvious from the comparison.

Table 4.7 Regression results for G/G_{max} and D

		G/G_{max} - Matasovic and Vucetic (1994)			Damping ratio- Darendeli (2001)	
Soil	γ_{r1}	α **value**	β **value**	R^2	***b value***	R^2
BP	0.12	1.090	1.184	0.965	0.653	0.702
BG	0.12	1.014	1.097	0.976	0.698	0.680
YF	0.14	0.906	1.241	0.991	0.794	0.924
YC	0.13	0.872	2.070	0.994	0.731	0.810
SL	0.12	1.081	1.247	0.922	0.294	0.866
KS	0.13	0.963	1.686	0.97	0.361	0.912
HS	0.10	0.898	0.706	0.991	0.740	0.942

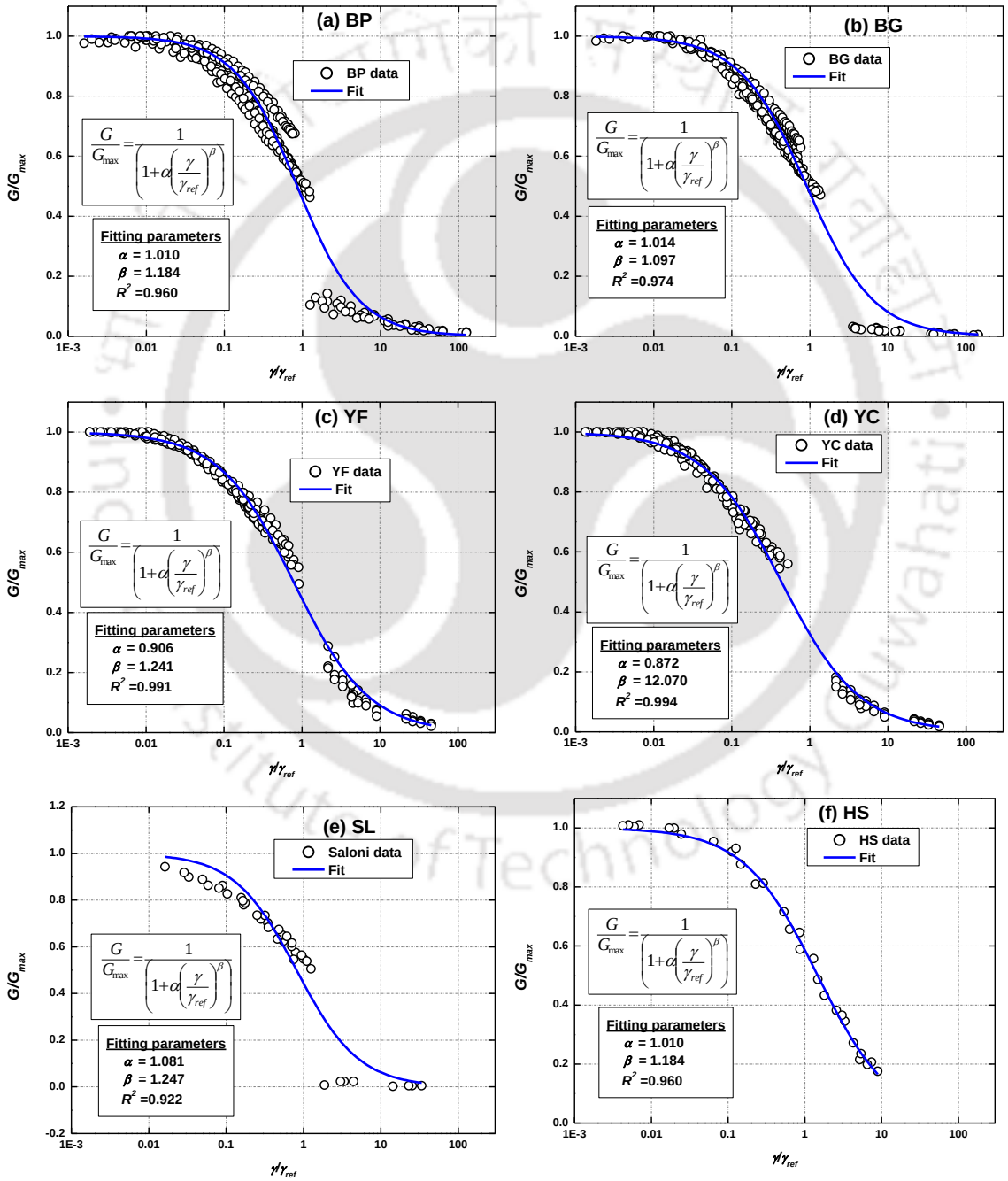

Fig. 4.35 Regression analysis for G/G_{max} of sands

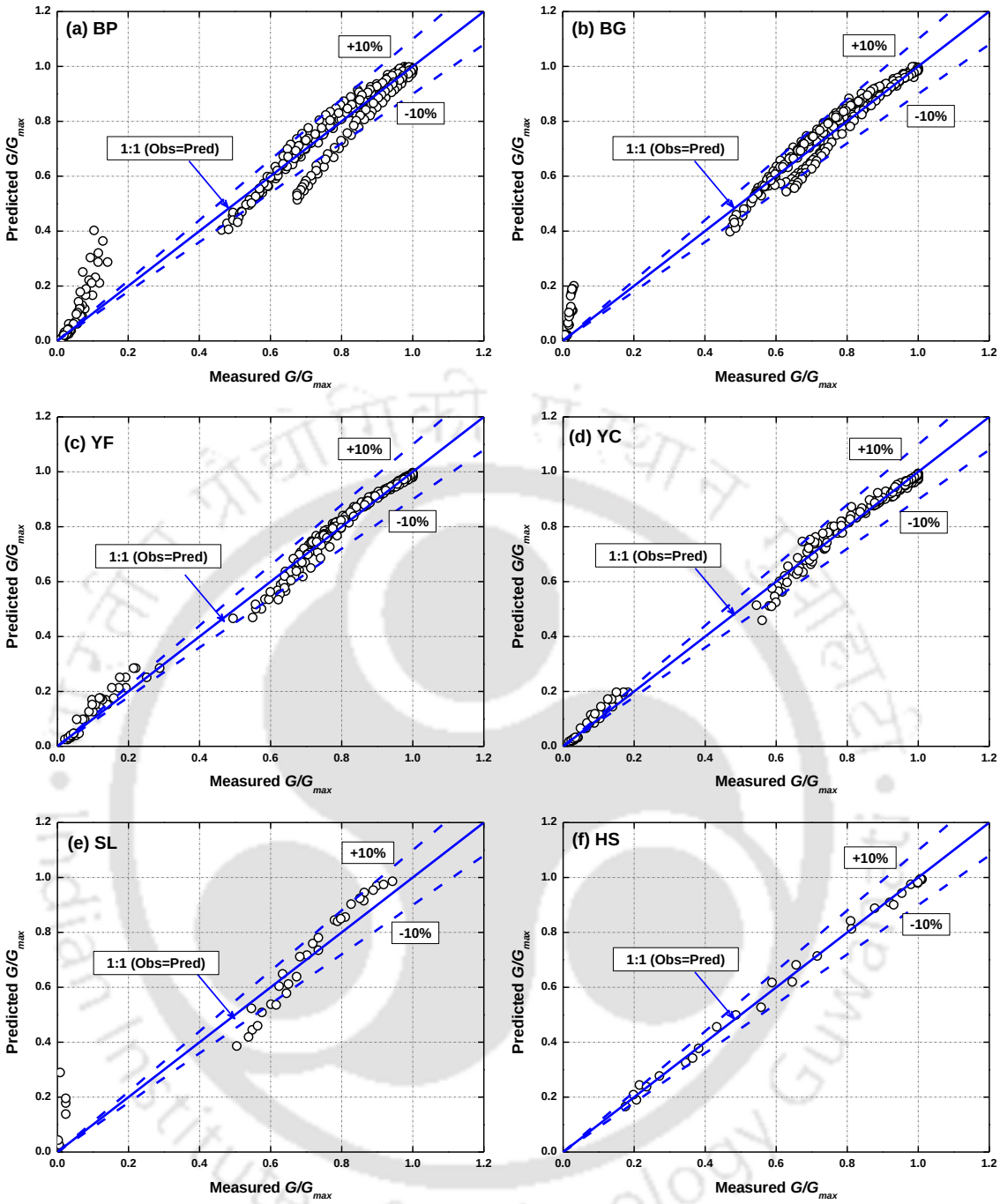

Fig. 4.36 Efficiency check of the proposed best-fit parameters of G/G_{max}

4.5.3 Damping Ratio (*D*)

Studies pertaining to the empirical expressions for the evaluation of material damping are reviewed briefly and presented in the section 2.1.3 of *Chapter II.* As the damping ratio is a function of nonlinear stress strain behaviour, and it is appropriate to relate the material damping to the G/G_{max}. Several damping models (Seed and Idriss 1970; Hardin and Drenvich 1972; Ishibashi and Zhang 1993; Zhang et al. 2005) have been tried to understand their efficacy in modelling the damping behaviour of the chosen sandy soils.

However, the untraditional high strain damping response as witnessed in DSS tests was only captured using the Darendeli (2001) model. Therefore, Darendeli (2001)'s model has been adopted for the present study.

A strategic procedure has been proposed by Darendeli (2001) for estimating *D* based on the Masing damping behaviour, while relating it to G/G_{max}. The steps are described here briefly and further discussion on these parameters can be found elaborately in Darendeli (2001). According to Darendeli (2001), damping based on Masing rules (D_{mas}) for any given strain amplitude is a function of: (a) Masing damping at that strain for a curvature coefficient (α) of 1.0, and (b) the value of curvature coefficient independently. The form of damping ratio (*D*) is given through Eqn. 4.5.

$$D = b \cdot \left(\frac{G}{G_{max}}\right)^{0.1} \cdot D_{mas} + D_{min} \tag{4.5}$$

where Masing damping (D_{mas}) is illustrated through Eqn. 4.6.

$$D_{min} = C_1 \cdot D_{mas@\alpha=1.0} + C_2 \cdot {D_{mas@\alpha=1.0}}^2 + C_3 \cdot {D_{mas@\alpha=1.0}}^3 \tag{4.6}$$

where C_1, C_2 and C_3 are functions of curvature coefficient (α) given as Eqns. 4.7, 4.8 and 4.9, respectively; $D_{mas@\alpha=1.0}$ is the Masing damping at unity curvature coefficient estimated using Eqn. 4.10.

$$C_1 = -1.1143 \cdot \alpha^2 + 1.8618 \cdot \alpha + 0.25223 \tag{4.7}$$

$$C_2 = 0.0805\alpha^2 - 0.0710 \cdot \alpha - 0.0095 \tag{4.8}$$

$$C_3 = -0.0005 \cdot \alpha^2 + 0.0002 \cdot \alpha + 0.0003 \tag{4.9}$$

$$D_{mas@\alpha=1.0}(\%) = \frac{100}{\pi} \cdot \left[4 \cdot \left\{\frac{\gamma - \gamma_{r \cdot ln\left(\frac{\gamma+\gamma_r}{\gamma_r}\right)}}{\left(\frac{\gamma^2}{\gamma+\gamma_r}\right)}\right\} - 2\right] \tag{4.10}$$

Scaling coefficient (*b*) controls the characteristics of the Eqn. 4.5 and needs to be estimated for different soils using regression analysis, based on the G/G_{max} and damping correlation. The values of best-fit scaling coefficients (*b*) are estimated for all the soils through regression analysis. Fig. 4.37 presents normalized procedure in determining the scaling coefficient, *b*. Based on the experimental results, the value of minimum damping ratio (D_{min}) has been chosen as 0.5% for all the soils. It can be seen from Fig. 4.37 that a reasonable estimate of *D* was achieved with a reasonable correlation coefficient (R^2=0.952). The value of *b* and correlation coefficients for all the soils have been determined and plotted in Fig. 4.38 and also listed in Table 4.7.

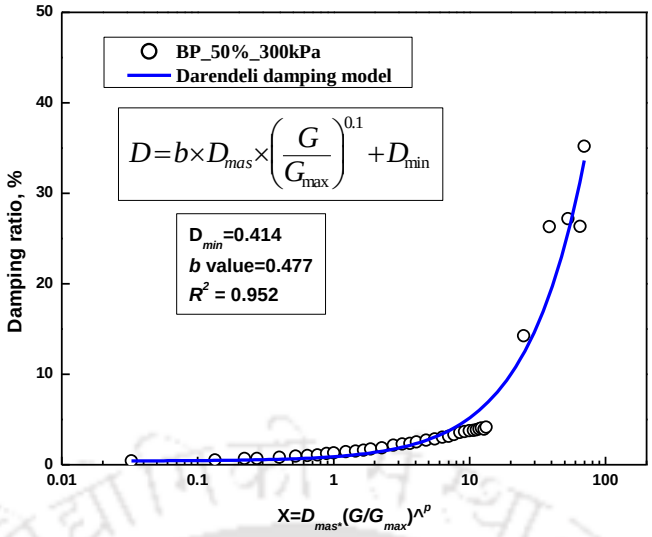

Fig. 4.37 The *b* value determination for BP sand at 50% R_d and 300 kPa effective confining pressure

4.5.4 Design G/G_{max} and D Curves

After the successful analysis of the element test results and determining the regression coefficients, it is necessary to provide the design curves (G/G_{max} and damping ratio variation curves) for carrying out dynamic analysis. These curves are useful for design engineers, especially while carrying out soil dynamics applications such as site/region - specific GRA, liquefaction analysis, seismic foundation analysis, slope stability and settlement problems. For sandy soils, curves at different effective confining pressures (p') are required as only effective confining pressure was found to be the significant contributor for G/G_{max} and D variation. Therefore, curves at practical range of p' magnitudes are established based on the regression analysis coefficients (starting from 25 kPa to extending up to 400 kPa). Fig. 4.39 presents the developed G/G_{max} and D curves for the chosen sandy soils at different levels of p'. These effective confining pressures represent the overburden depths of 5 m to 150 m, beyond which a typical rock or hard stratum is found.

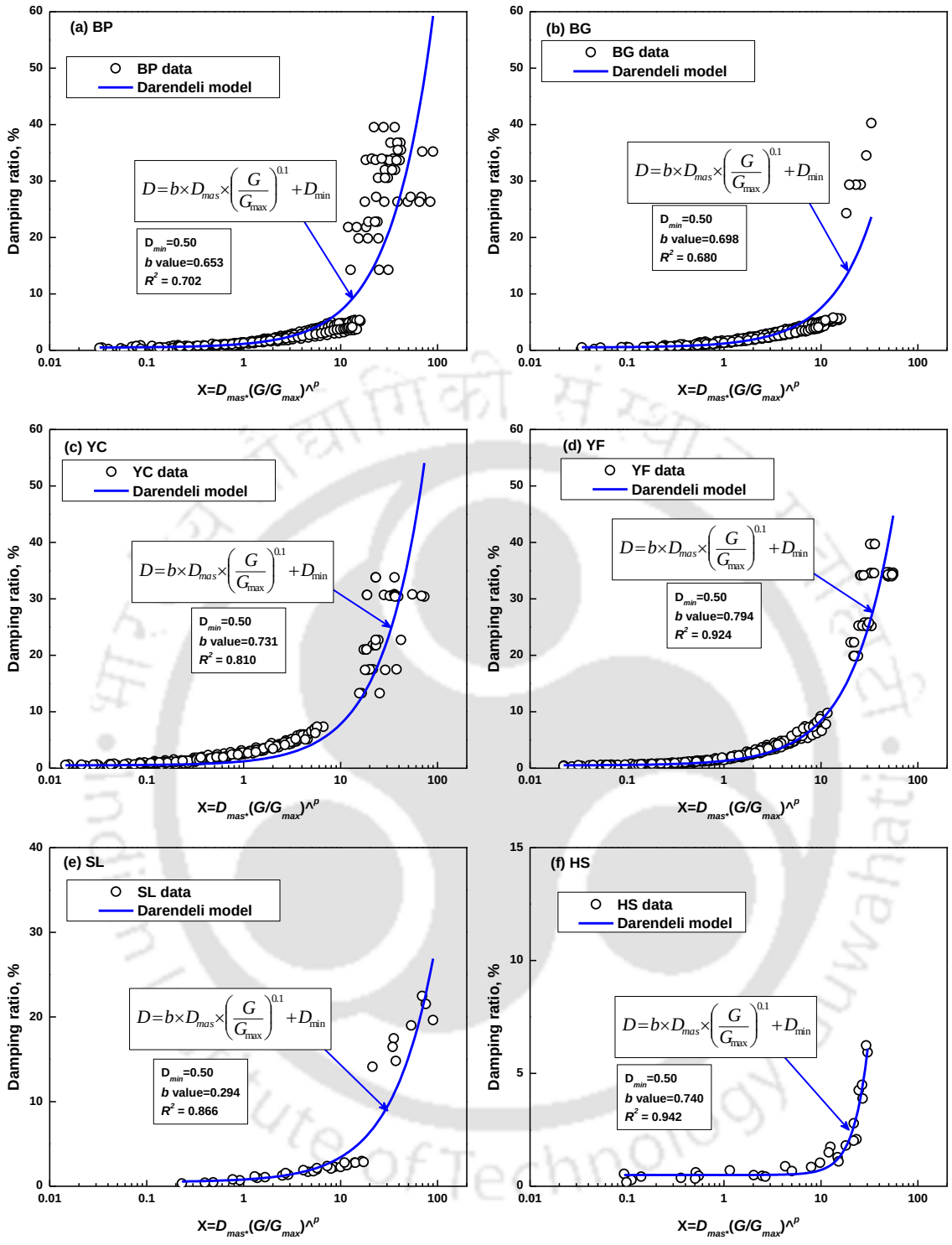

Fig. 4.38 Regression analysis for damping ratio of all the sands

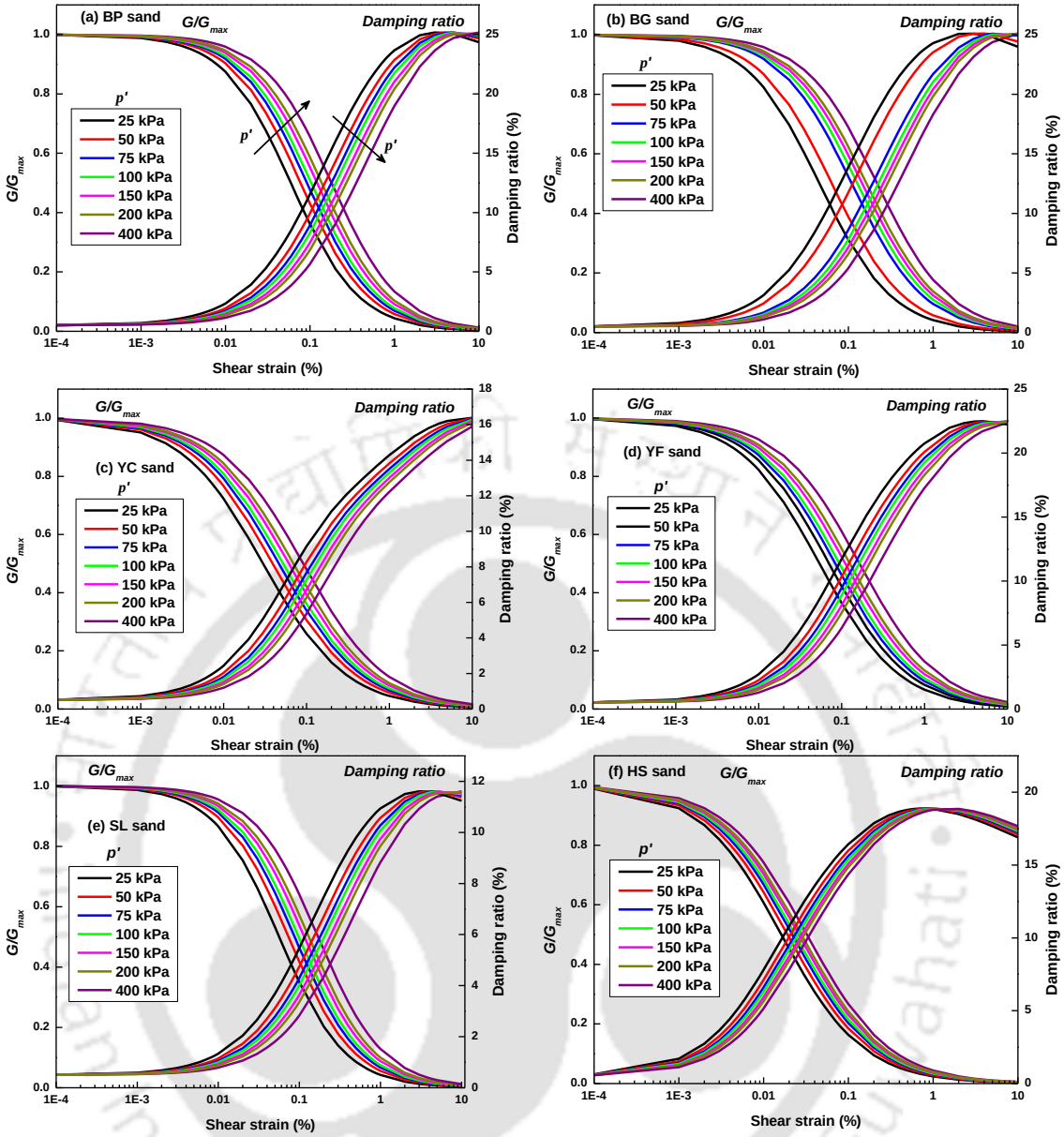

Fig. 4.39 Design stiffness curves for all the sands

4.6 LIQUEFACTION ANALYSIS (CTX TEST RESULTS)

Multi-stage stress-controlled triaxial tests have been conducted on BP sand specimens in undrained conditions to understand the liquefaction behaviour. Three stages are employed in the testing: isotropic consolidation, stress-controlled undrained cyclic shearing and strain-controlled monotonic shearing. The tests have been conducted at three different cyclic stress ratio (CSR) conditions (0.15, 0.225, and 0.30) and three initial relative density conditions (30%, 60% and 90%) with a constant effective confining pressure (σ'_c) of 100 kPa. It is to reiterate that the relative density mentioned is the initial bulk density and consolidated densities are not considered. As the CSR is a ratio of single amplitude deviatoric stress (q_{cyc}) to the twice of σ'_c, the q_{cyc} thus obtained for the three chosen CSR

magnitudes of 0.15, 0.225 and 0.30 are 30, 45 and 60 kPa, respectively. Table 4.8 presents the list of CTX tests and loading conditions. The chosen CSR magnitudes are in the range of typical stress ratios (0.15 to 0.30) induced during moderate seismic events (Seed and Idriss 1971; Sitharam et al. 2004). The obtained test results are presented in terms of variation of pore water pressure ratio (r_u), stress-path (q and p') and accumulated axial strains.

Table 4.8 Summary of the CTX tests performed on BP sand specimens

R_d (%)	σ'_c (kPa)	q_{cyc} (kPa)	CSR=[q_{cyc}/(2σ'_c)]
30	100	30	0.15
		45	0.225
		60	0.30
60		30	0.15
		45	0.225
		60	0.30
90		30	0.15
		45	0.225
		60	0.30

The typical results of an undrained CTX test in terms of PWP ratio variation with loading cycles and the corresponding stress-path (q-p') are shown in Fig. 4.40 a and b, respectively, for BP sand in loose (30% R_d) condition. Pore water pressure (PWP) ratio (r_u) which is the ratio of excess PWP to the σ'_c, is traditionally used to represent the liquefaction state at r_u of unity (r_u≈1.0). Similarly, Fig. 4.41 (a and b) depicts the response for a medium dense (60% R_d) BP sand specimen. It can be seen that under undrained cyclic loading, loose sand specimens (Fig. 4.40) tend to contract, however, due to the prevailing undrained (no volume change) conditions, pore pressures gradually rise (Fig. 4.40a) resulting in the reduction of p' (Fig. 4.40b). As a result, effective stress path progressively moves towards the state of p'≈0, and at such instance, induced excess pore water pressures equals the initial applied confining stress (σ'_c) representing a state of complete liquefaction (r_u≈1.0). In case of medium dense to dense sand specimens (Fig. 4.41), the progressive decrease of p' towards zero takes relatively longer duration than that of loose specimens which can be explained by ability of the dense granular packing to resist the cyclic shearing. The post liquefaction monotonic response of dense sands (Fig. 4.41b) shows an increased strength in comparison to the loose sands (Fig. 4.40b).

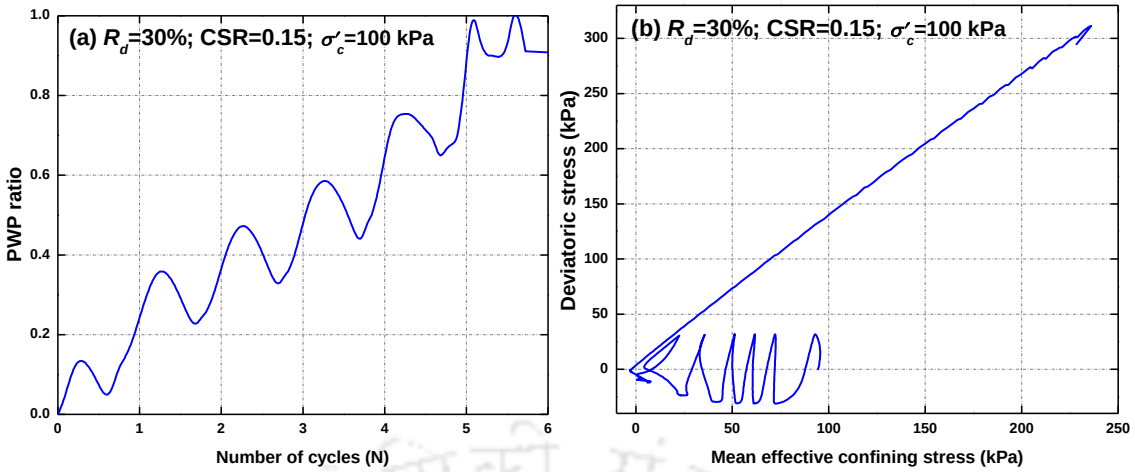

Fig. 4.40 (a) Plot of PWP ratio and **(b)** stress-path for loose (30% R_d) BP sand specimens

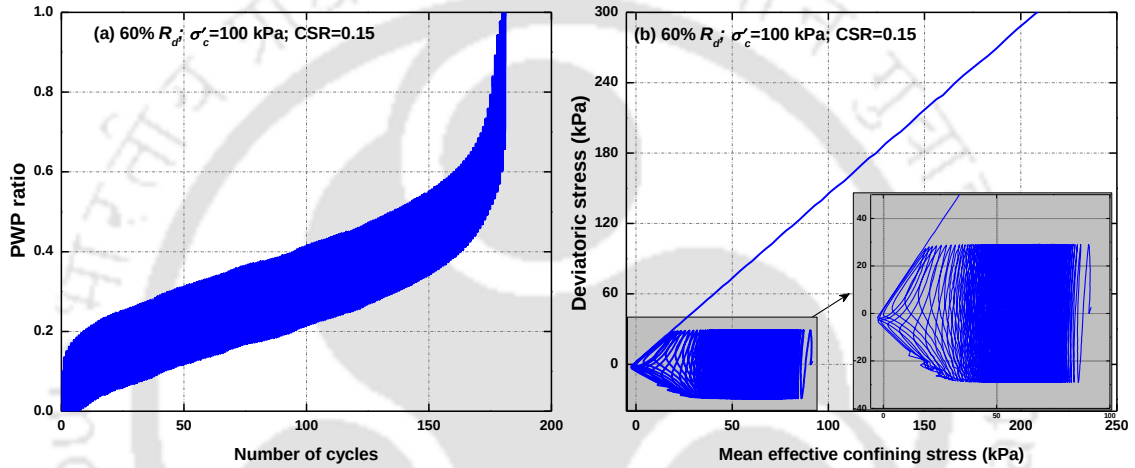

Fig. 4.41 (a) Plot of PWP ratio and **(b)** stress-path for medium dense (60% R_d) BP sand specimens

Fig. 4.42 (a-c) presents the variation of r_u and axial strain with loading cycles for BP sand, in three R_d (30%, 60% and 90%) conditions at CSR of 0.15. Two important observations can be drawn based on Fig. 4.42. With increase in the R_d of the specimen (denseness of the granular particle packing), the liquefaction resistance increases. The loose specimen of 30% R_d (Fig. 4.42a) takes only 5 cycles to reach r_u of unity while the medium dense of 60% R_d (Fig. 4.42b) sand requires 181 cycles and the dense specimen of 90% R_d (Fig. 4.42c) did not liquefy even at 350 cycles. Another interesting observation is that remarkable axial strains (>1% and up to 4%) were induced in loose and medium dense samples, with significant pore pressures ($r_u \geq 0.5$). However, in case of denser specimens (90% R_d), liquefaction was not observed even with 350 loading cycles ($r_u << 1.0$) the strains were in the range of 0.1% for CSR 0.15 test condition. This points out to the fact that significant pore pressure generation ($r_u \geq 0.5$) may lead to remarkable strain accumulation (as high as 2%) in cohesionless soils.

The stress-strain response (axial strain and deviatoric stress) of BP sand at loose and medium dense conditions is shown in Fig. 4.43 (a and b). In loose conditions (Fig. 4.43a), specimen rapidly compressed while reaching full liquefaction state while the medium dense specimen (52% R_d) shown in Fig. 4.43b, gradual strain accumulation. The magnitude of strains induced in loose specimen (60% R_d from Fig. 4.42a and Fig. 4.43a) at the onset of liquefaction ($r_u \approx 1.0$) are close to 1.5% while that of medium dense specimen (60% R_d from Fig. 4.42b and Fig. 4.43b) counts to 3%. This shows that dense granular soils require relatively large strains to be developed for complete liquefaction condition. This phenomenon of significant amount of strain softening in case of medium dense to dense sands (and also in soft clays) is termed as cyclic mobility (Castro 1985). Lombardi et al. (2014) and Rouholamin et al. (2017) observed similar response for saturated Toyoura sand.

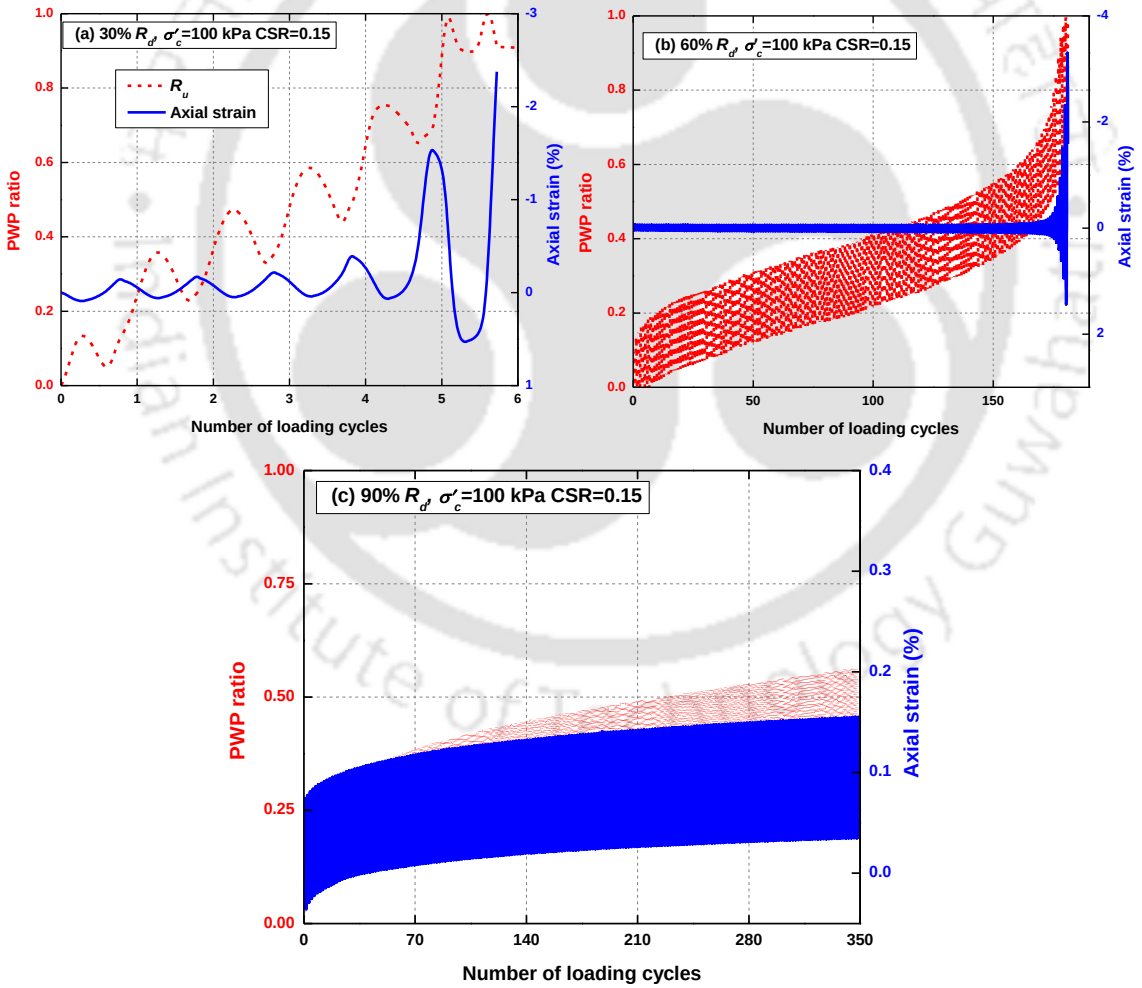

Fig. 4.42 Variation of r_u and axial strain with loading cycles for BP sand in **(a)** loose-33% R_d **(b)** medium dense-52% R_d and **(c)** dense- 90% R_d conditions at CSR of 0.15

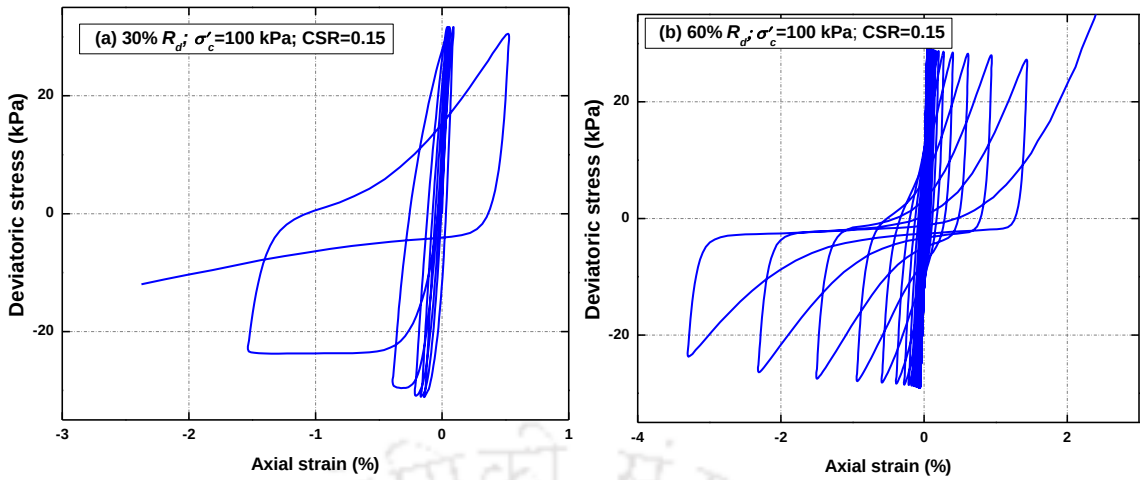

Fig. 4.43 Stress-strain response of BP sand in **(a)** loose and **(b)** medium dense conditions

The effect of R_d on the liquefaction resistance of BP sand at CSR of 0.225 is shown in Fig. 4.44, plotted in terms of r_u and loading cycles. The loose specimen experienced liquefaction in the very second cycle of shearing while the medium dense and dense specimens took 4 and 8 cycles, respectively, to liquefy. This shows that even highly dense granular soils may be prone to liquefaction at high CSR loading conditions. Fig. 4.45 depicts the effect of CSR on the r_u plotted at 30% R_d condition. It can be noted that high CSR (high deviatoric stress) conditions induce pore pressures rapidly compared to the lower CSR and hence, earthquakes of high intensity are expected to liquefy the granular soils quicker than the lower intensity motions at similar R_d and overburden conditions.

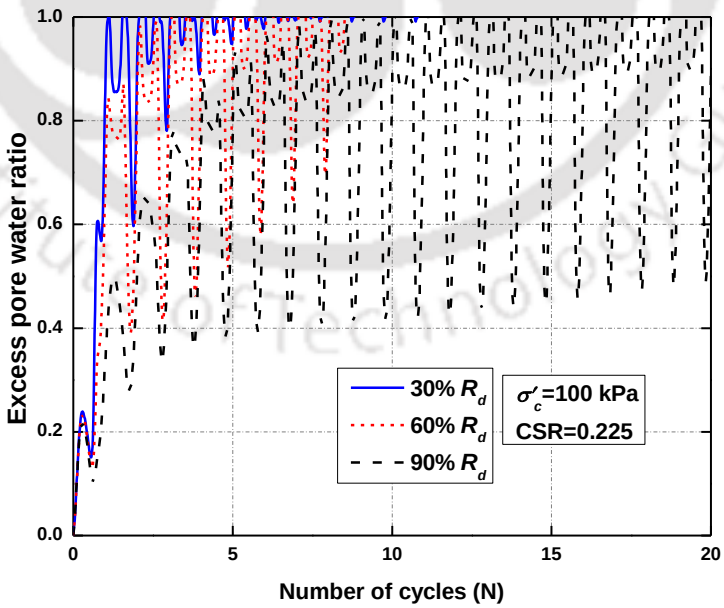

Fig. 4.44 Effect of R_d on the PWP generation in BP sand

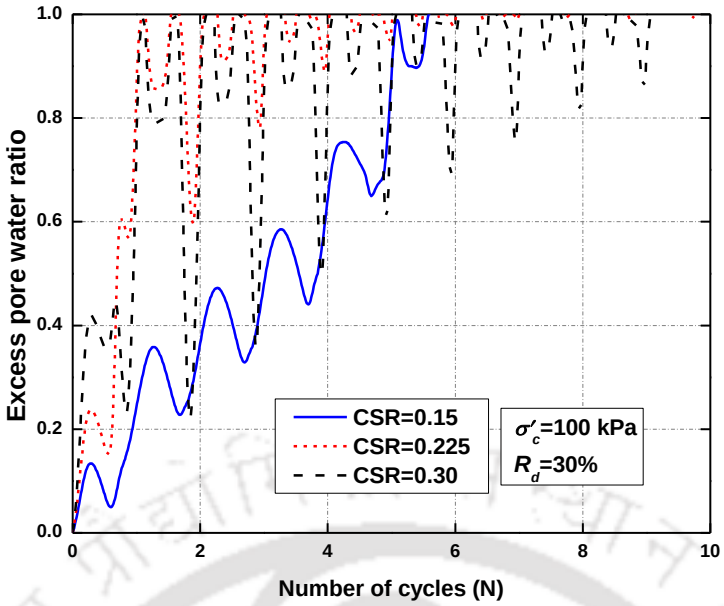

Fig. 4.45 Effect of CSR on the PWP generation in BP sand

To conclude the liquefaction assessment of granular soils, the variation of CSR and the corresponding loading cycles to cause liquefaction (r_u=1.0) is shown in Fig. 4.46, for different R_d conditions. It can be seen that the loose BP sand specimens (30% R_d) were liquefied under 10 cycles of loading while medium dense (60% R_d) and dense specimens (90% R_d) require relatively large number of loading cycles, manifesting the well-known trend of increase of cyclic resistance of sands with R_d. Also the liquefaction data of some Indian sands are collated from literature (Ahmedabad sand-Sitharam et al. 2013; Kaveri sand-Balreddy et al. 2015; Kasai sand-Chattaraj and Sengupta 2016) at different R_d conditions and presented in the Fig. 4.46. It is to be mentioned that the presented literature data of liquefaction curves are based on stress-controlled CTX tests. It can be seen that the BP sand data (at the tested R_d conditions) plots in similar trend of data as reported in literature for Indian sands and also reasonably matches with that of Kasai sand at comparable R_d conditions. The established chart can be used for understanding the liquefaction characteristics of BP sand under severe cyclic loading conditions at a σ'_c of 100 kPa.

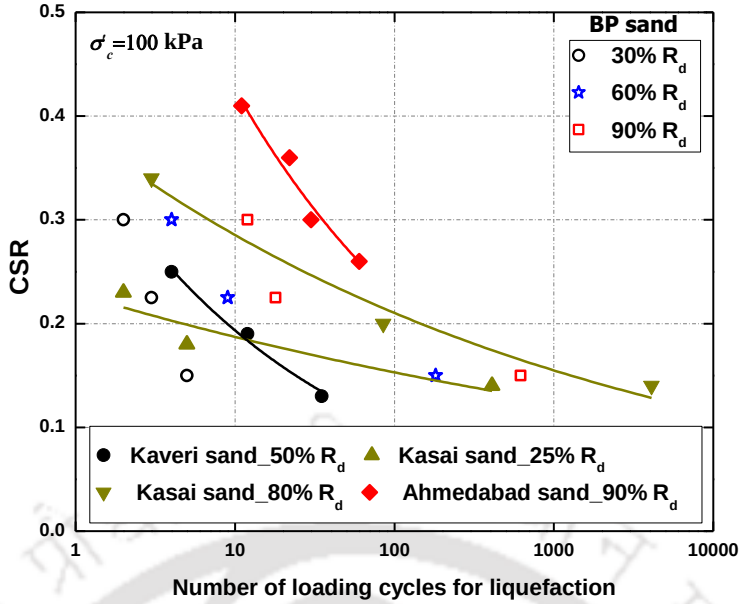

Fig. 4.46 CSR versus number of cycles for liquefaction for BP sand and other Indian sands

Pore Water Pressure (PWP) Generation Model

Pore water pressure (PWP) models facilitate the calculation of generation of excess pore pressures during cyclic loading. Numerous PWP models, ranging from simple to complex nature, are available in the literature (Seed et al. 1975; Dobry et al. 1985; Ivsic 2006; Park et al. 2015; Chiaradonna et al. 2018). A brief review of available PWP models has been presented in section 2.1.4 of Chapter II. Present study utilises the Vucetic and Dobry (1988) PWP model which is a modified form of the Dobry et al. (1985) model. The model is based on the strain accumulation at the onset of liquefaction with number of loading cycles (Eqn. 4.11).

$$r_{u,N} = \frac{P \cdot N \cdot F \cdot (\gamma - \gamma_t)^S}{1 + N \cdot F \cdot (\gamma - \gamma_t)^S} \quad (4.11)$$

where $r_{u,N}$= excess PWP ratio at N number of cycles (equivalent loading cycles are estimated based on Idriss and Boulanger (2008) recommendation); γ= cyclic shear strain amplitude; p, F and s are the curve fitting parameters; γ_t is the threshold shear strain below which no significant PWP is generated or shear strain below which no significant permanent volume changes are observed (also called volumetric threshold shear strain). The value of γ_t was established at a G/G_{max} value of 0.80 as suggested by Vucetic (1995). The magnitude of γ_t increases with increasing effective confining pressure which means that the depth of overburden increases the strain required for the volume changes or significant pore pressure generation. Therefore, for the three tested effective confining

pressures of 50, 100 and 150 kPa of BP sand (considered from Fig. 4.13), the values of γ_t established are 0.02%, 0.03% and 0.035%, respectively. The adopted γ_t values are consistent with the literature suggested range for sands: 0.01% to 0.04% (Hsu and Vucetic 2004; Heshmati et al. 2015).

The PWP model curve fit parameters (*p*, *F* and *s)* are obtained by performing regression analysis on the experimental data. In addition to the present CTX test results which are performed only at one σ'_c condition (100 kPa), strain-controlled CTX tests performed on BP sand by Kumar (2018) have also been considered for the regression analysis. Fig. 4.47 (a-c) depicts the obtained results of PWP model with the fitting parameters, at three σ'_c. Having the curve fitting parameters at three σ'_c levels, a confining pressure dependent PWP model for BP sand is attempted, however, a general trend could not be obtained.

These proposed best-fit parameters will be helpful in performing nonlinear effective stress ground response studies (incorporating liquefaction characteristics) of the region, with soils of similar index and geotechnical properties, at the mentioned σ'_c conditions (50-150 kPa).

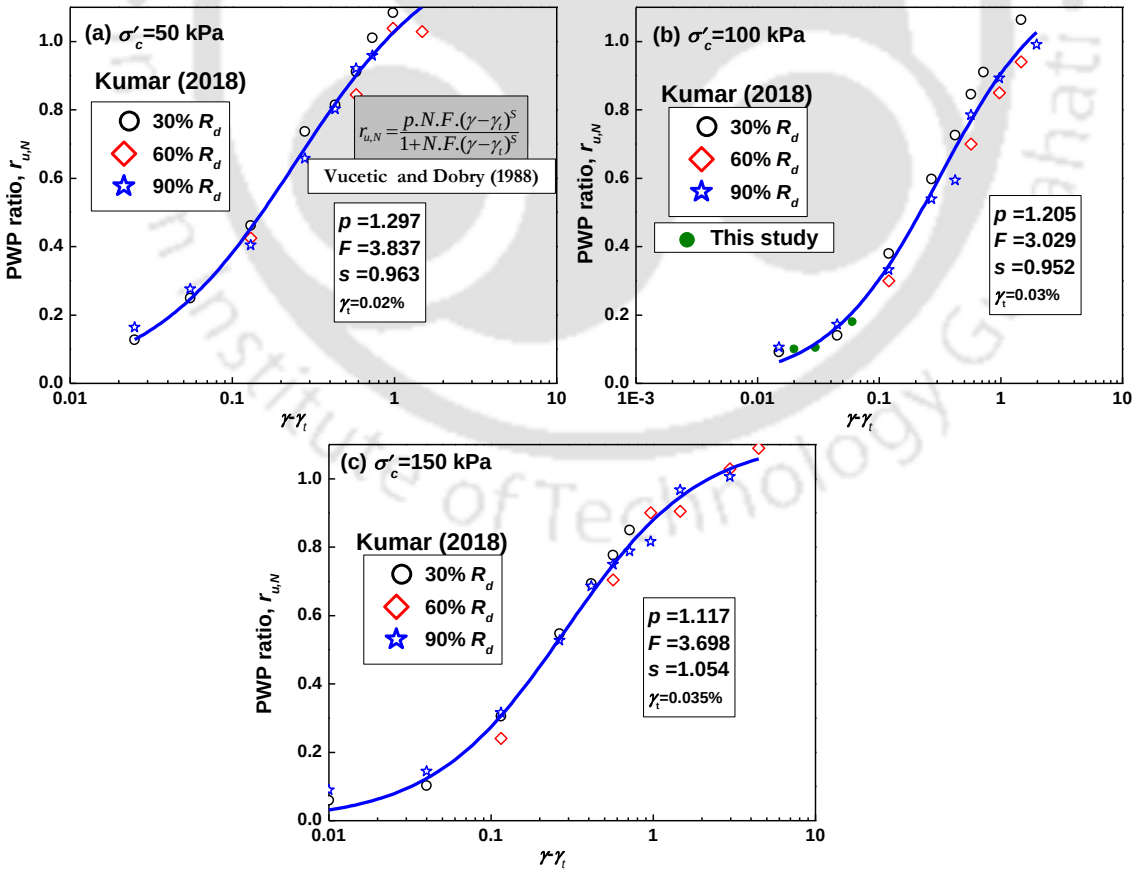

Fig. 4.47 Pore water pressure ratio variation of BP sand at **(a)** 50 kPa, **(b)** 100 kPa and **(c)** 150 kPa σ'_c

4.7 SUMMARY

The chosen sandy soils have been dynamically characterised using four independent element testing techniques (bender element, resonant column, dynamic simple shear and cyclic triaxial). The obtained results are presented in terms of dynamic soil properties (G_{max}, G/G_{max} and damping ratio), liquefaction potential, and the corresponding analysis and discussions are presented. In order to provide a comprehensive data of G/G_{max} and damping ratio over wide strain range, results obtained from individual apparatus are combined and compared with the existing widely used G/G_{max} and damping curves. It has been understood that the existing curves may overestimate the damping ratio and underestimate the G/G_{max} of the soils. Empirical formulations have been presented for all the sandy soils based on regression analysis on the experimental data. In addition, data from literature pertaining to other Indian sandy soils have been collated and best-fit parameters were provided. To provide design engineers with the readymade charts, design G/G_{max} and damping ratio curves at varying range of mean effective confining pressures (σ'_c) of practical interest are proposed.

Liquefaction potential of BP sand at different cyclic stress conditions and R_d states has been studied and results are presented in terms of pore water pressure ratio, effective stress path and stress-strain responses. The data presented in this chapter (G/G_{max}, damping curves and liquefaction parameters) will be helpful in performing nonlinear effective stress (incorporating PWP) ground response studies of the region with the soils of typical characteristics.

CHAPTER V. DYNAMIC CHARACTERISATION OF COHESIVE SOILS

5.0 INTRODUCTION

Dynamic behaviour of cohesive soils investigated through the four element testing techniques is presented in this chapter. Two cohesive soils, namely Pachoria Cohesive (PC) soil and Redsoil (RS) which were collected from the Guwahati city of northeastern India, have been tested at different loading conditions. Test results from each testing technique are described independently followed by combining the results for comprehensive dynamic soil characterisation. Empirical formulations are provided based on the experimental data. Liquefaction behaviour of the clays is analysed under different loading conditions.

5.1 BENDER ELEMENT TEST RESULTS

Two bender element tests have been performed on clays to determine the maximum shear modulus (G_{max}). In case of PC, specimens were prepared at field density and in case of Red soil (RS), specimens were prepared at maximum dry density (MDD) conditions. Both the densities mentioned are initial bulk densities. Effective confining pressures (σ'_c) ranged from 50 kPa to 600 kPa. Table 5.1 lists the BE tests performed on both the clays.

Table 5.1 BE tests and their loading conditions

Soil	Density (g/cc)	σ'_c (kPa)
PC	1.60	50-600
RS	1.78	50-600

Typical input and output from a BE test on PC specimen in presented in Table 5.2. The arrival time of the wave (T_s) is used to determine the shear wave velocity (V_s) using the effective sample height (L_{eff}). The G_{max} is then correlated using the initial bulk density (ρ). It can be seen from the Table 5.2 that the increase in σ'_c on the specimen, decreases the arrival time of the input wave at the receiver. This is due to the relative increase in particle contact with increase in σ'_c and thereby quicker propagation of waves.

Table 5.2 Output and G_{max} determination from a typical BE test on PC specimen

Input			Output	Correlation	
σ'_c (kPa)	L_{eff} (mm)	ρ (g/cc)	T_s (ms)	V_s (m/s)	G_{max} (MPa)
50	96	1.60	0.782	121.4	25.5
100			0.699	135.9	31.9
200			0.588	161.5	45.1
300			0.520	182.6	57.6
400			0.484	196.0	66.4
600			0.409	231.9	93.1

Fig. 5.1 depicts the variation of G_{max} with effective confining pressure for both the cohesive soils. It can be seen that with increasing effective confining pressure on the specimen, G_{max} is increased. This shows that irrespective of type of soil (cohesive or cohesionless), low strain dynamic shear modulus would always increase with the depth of overburden with all other conditions keeping constant. Red soil showed significantly higher G_{max} values compared to PC due to the MDD condition used in the testing of RS.

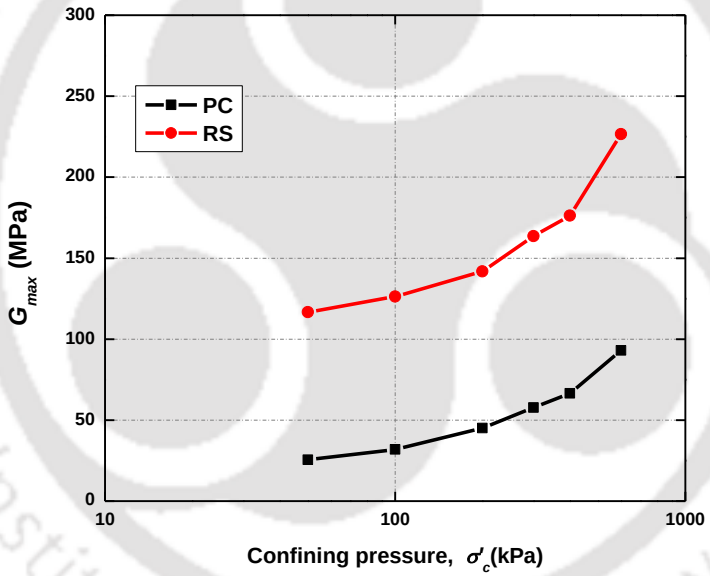

Fig. 5.1 G_{max} variation with effective confining pressure for clays

5.2 RESONANT COLUMN TEST RESULTS

Six RC tests have been conducted on both the cohesive soils at different loading conditions to obtain the low to intermediate strain dynamic behaviour. Table 5.3 lists the RC tests performed on the clays. Similar to the BE testing conditions, PC samples were prepared at field density while RS specimens were prepared at MDD conditions. Three isotropic effective confining pressures were chosen to investigate the effect on G and D at various strain levels. Only the approach of incremental strains was adopted, where the same specimen will be sheared further by increasing the voltage and monitoring the response and thereby determining the dynamic properties.

Table 5.3 RC testing programme and loading conditions

Soil	Density (g/cc)	Cell pressure (kPa)	Results
PC	1.60	50	*G-γ, D-γ*
		100	
		200	
RS	1.78	50	
		100	
		200	

Fig. 5.2 (a and b) presents the variation of shear modulus (G) with shear strain (γ) for both the clays at different effective confining pressures. It can be noted that the increase in effective confining pressure increases G for both the soils which means that the depth of overburden increases the dynamic stiffness of the cohesive soils with other parameters being constant. The RS soil showed relatively high G at comparable σ'_c condition when compared to that of PC soil, due to the difference in tested density conditions (MDD for RS and field density for PC) of both the soils. As MDD is the maximum density of a soil, it is expected that PC would yield high G values. It is also evident from Fig. 5.2 (a and b) that clays exhibit constant G up to a certain strain level (≤0.04%) beyond which a non-linear response is noted.

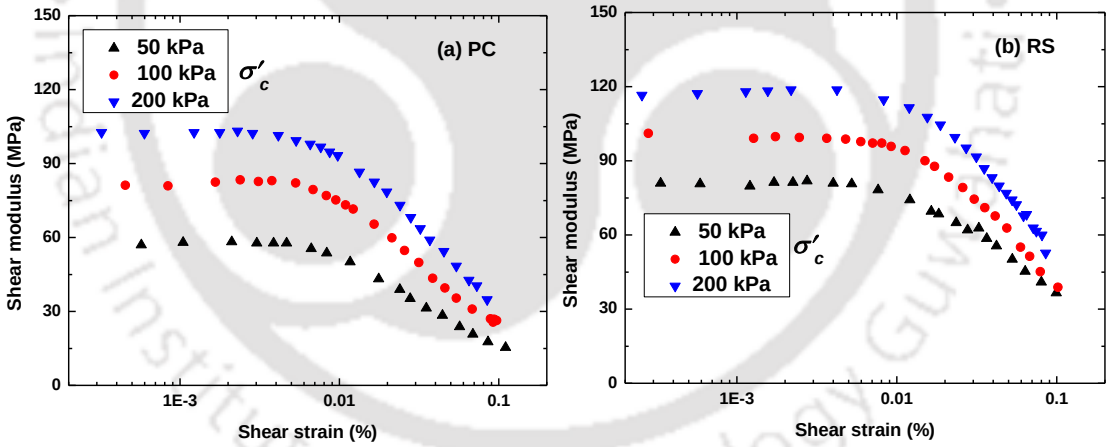

Fig. 5.2 Variation of shear modulus with shear strain for (**a**) PC and (**b**) RS

In order to understand the reduction rate of dynamic stiffness, normalized shear modulus reduction (G/G_{max}) of both the clays at different effective confining pressures is presented in Fig. 5.3 (a and b). It is evident that an elastic region exists with a constant G/G_{max} up to a strain level of 0.005%. This strain level is referred as elastic threshold shear strain (γ_{tl}), below which the soil essentially behaves as a linear elastic material (Vucetic 1995). Several researchers determined γ_{tl} of various clays around the globe and proposed the range as 0.001% to 0.01% (Hsu and Vucetic 2006; Tabata et al. 2010; Mortezaie et al. 2016). The γ_{tl} of cohesive soils is relatively larger in comparison to that of sands and gravels

(Vucetic 1995; Mortezaie et al. 2016). The establishment of γ_{tl} range is essential as it can facilitate the effective selection of constitutive model for dynamic analysis. For example, in a low seismic prone region (with only possibility of low intensity seismic motions), the soils are expected to subject to low level of strains and in such cases, based on the established soil threshold limits (γ_{tl}), the appropriate stress-strain model (simple elastic) can be adopted for the seismic analysis, without the need of complex nonlinear models.

Another important observation from Fig. 5.3 (a and b) is the insignificant effect of effective confining pressure on G/G_{max} of both the clays in the tested pressure range. It is worth mentioning that the plasticity index (PI) is the key factor controlling the reduction rate of clays (Seed and Idriss, 1970; Sun et al. 1988; Vucetic and Dobry 1991). The PI of PC is 19 while RS has a PI of 22. Lanzo and Doroudian (1997) and Vucetic et al. (1998) based on DSS tests concluded that the effect of effective confining pressure on G/G_{max} and D diminishes with increasing PI of clays. The plastic nature and cohesive properties of soils enlarge the elastic bounds of the G/G_{max} and hence, when compared to sandy and gravelly soils, cohesive soils tend to show higher G/G_{max} values.

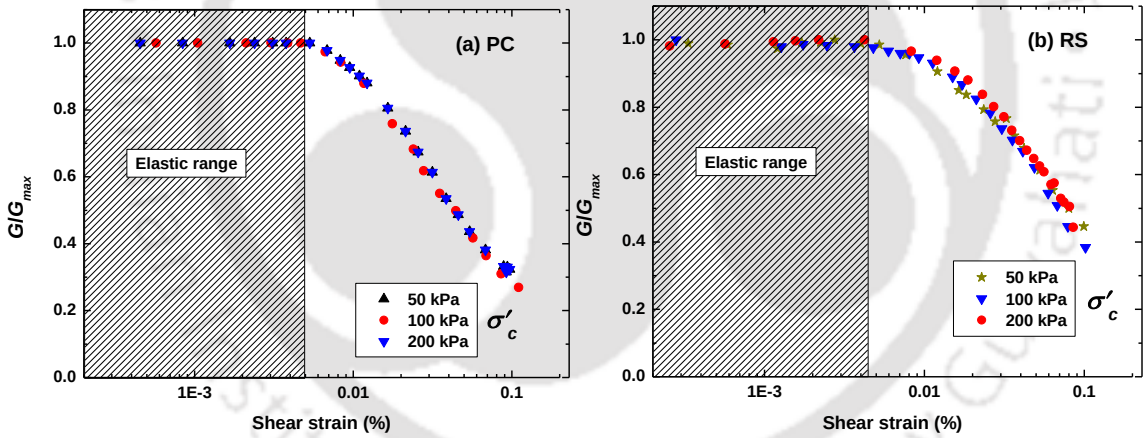

Fig. 5.3 Variation of G/G_{max} with shear strain for **(a)** PC and **(b)** RS

Fig. 5.4 (a and b) presents the damping ratio variation of both the clays evaluated from RC tests. Similar to the G/G_{max} response, no significant effect of effective confining pressure was found on damping behaviour of the cohesive soils. However, the expected increasing trend of damping ratio with increased shear strain is observed.

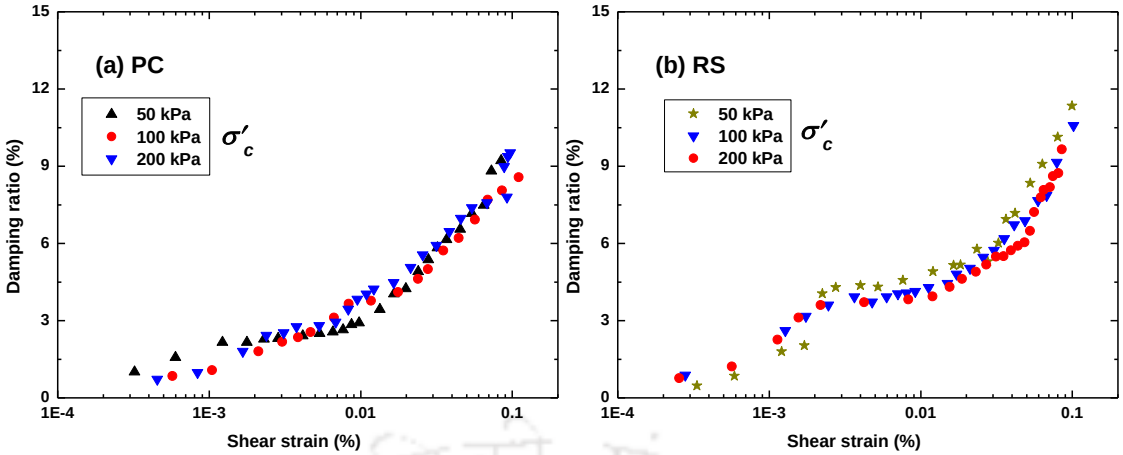

Fig. 5.4 Variation of damping ratio with shear strain for **(a)** PC and **(b)** RS

5.3 DYNAMIC SIMPLE SHEAR TEST RESULTS

Dynamic simple shear tests have been conducted on cohesive soils in strain-controlled mode, at strain range of 0.1% to 5%. Table 5.4 presents the DSS testing programme on both the cohesive soils. Six tests have been performed in total on both the clay specimens. All the tests were performed for 1000 loading cycles to investigate the effect of loading cycles. The results are presented in terms of stress-strain loops at different shear strain amplitudes and loading cycles, to facilitate a comparison of dynamic response of cohesive soils.

Table 5.4 DSS testing programme and loading conditions

Soil	Density	Shear strain (%)	Effective vertical stress (kPa)	Frequency (Hz)	Number of cycles
PC clay	Field density	0.1, 0.25, 0.5, 1	100	1	1000
		2.5		0.5	
		5		0.5	
RS clay	MDD	0.1, 0.25, 0.5, 1		1	
		2.5		0.5	
		5		0.5	

Fig. 5.5 (a-d) presents the stress-strain (shear stress and shear strain) response of Redsoil (RS) at varying shear strain amplitudes of 1st, 10th, 100th and 1000th loading cycles, respectively. It can be noted that increase in shear strain flattens the stress-strain loops at any loading cycle, which means that high intensity excitations (inducing high strains in the soil) result in low initial stiffness of cohesive soils. Similar observation was also drawn for sands. This means that irrespective of soils, strains are inversely related to the stiffness of soils. The effect of loading cycles on the dynamic stress-strain response of RS is shown in Fig. 5.6 (a-f) at different shear strain amplitudes (0.1% to 5%). With increase in the loading

cycle number, the stress-strain loops move upwards with relatively high initial slope, testifying the increase in compactness of the soil. Relative compactness of the specimens can also be represented using the normal settlement. Fig. 5.7 shows the variation of normal settlement of RS specimen for different strain amplitudes. Similar to the response in case of cohesionless soils, increased normal settlement can be observed with increased shear strain amplitudes. A normal settlement of >1 mm was observed for high strain amplitude tests (2.5% and 5%) while the same is reduced to <0.5 mm for relatively lower strain amplitudes. This testifies that the high amplitude motions induce higher normal settlements in the cohesive soil deposits.

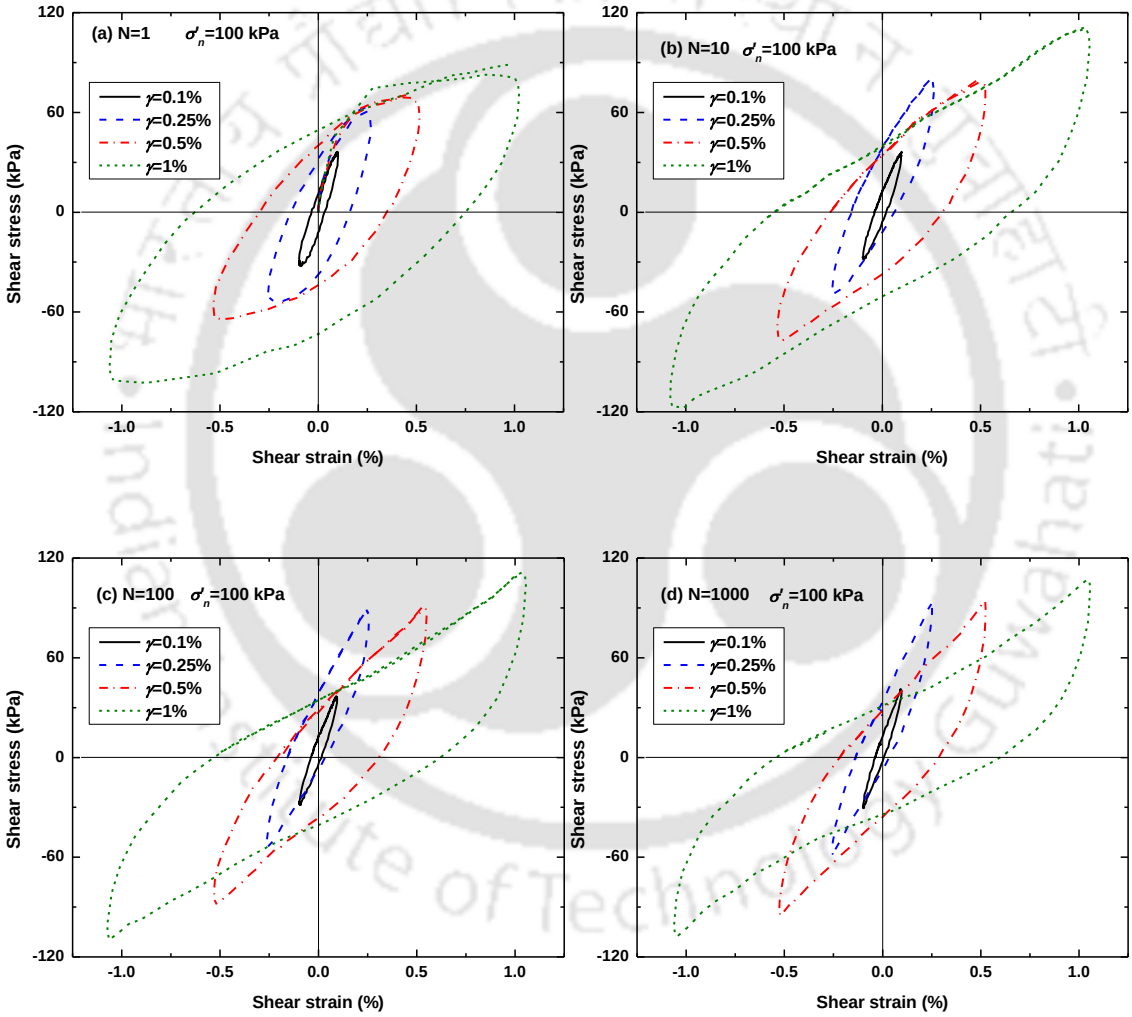

Fig. 5.5 Stress-strain response of RS at different loading cycles (**a**) N=1 (**b**) N=10 (**c**) N=100 and (**d**) N=1000

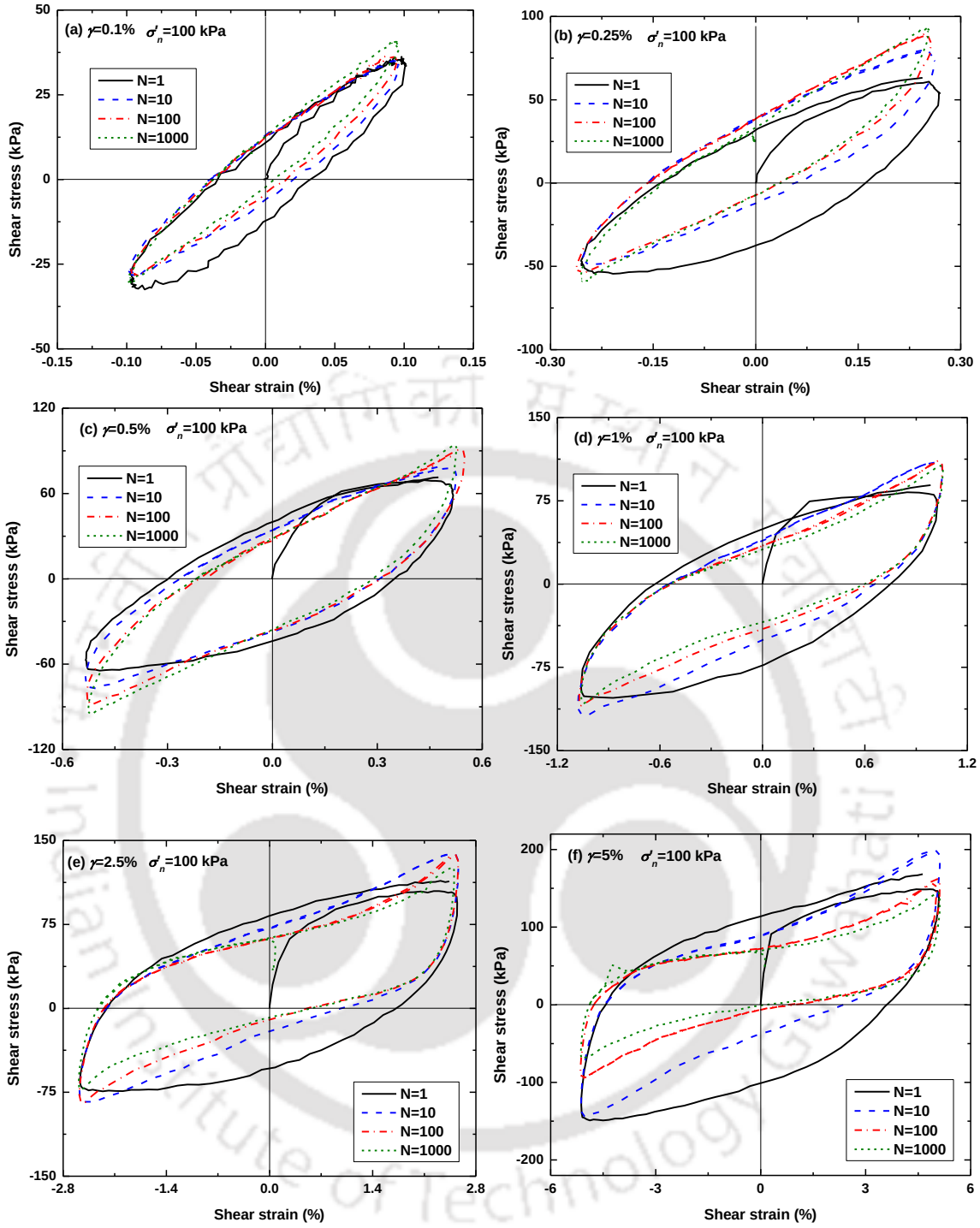

Fig. 5.6 Stress-strain loops of RS at shear strains of (**a**) 0.1% (**b**) 0.25% (**c**) 0.5% (**d**) 1% (**e**) 2.5% (**f**) 5%

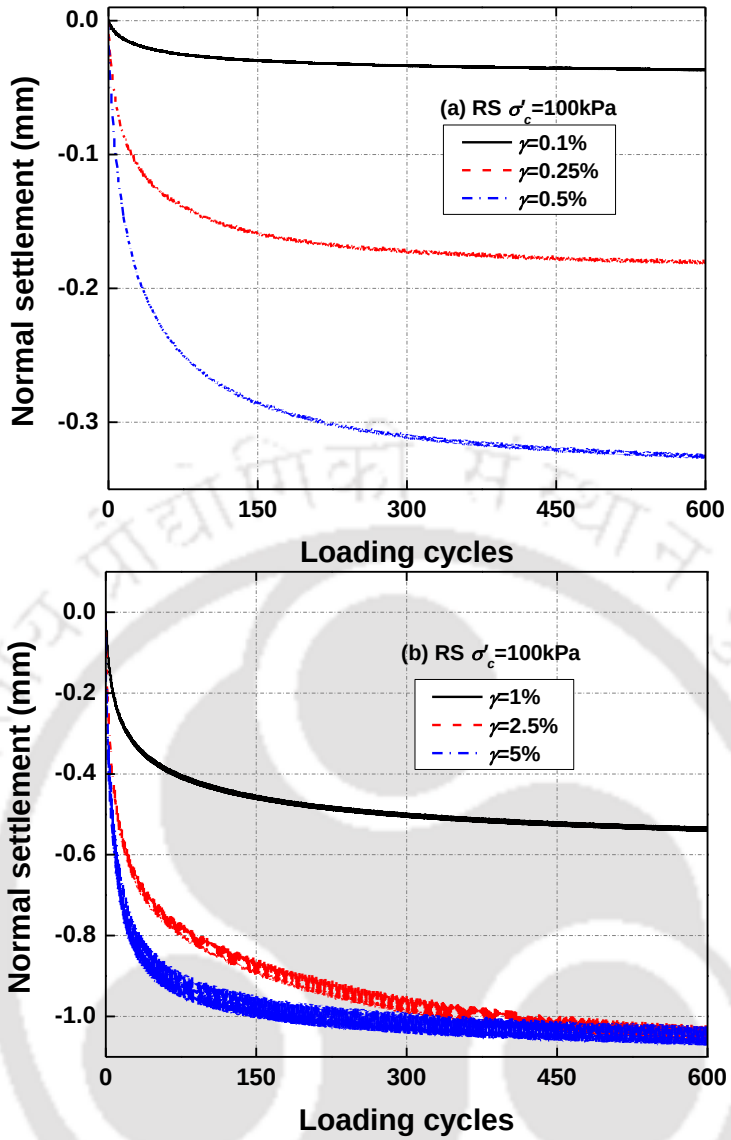

Fig. 5.7 Variation of normal settlement for RS specimen in DSS test conditions at 100 kPa effective vertical stress

The shear stress- shear strain loops are utilised to determine the *G* and *D* of cohesive soils using the asymmetrical loop approach suggested by Kumar et al. (2017).

5.4 COMPREHENSIVE G/G_{max} AND DAMPING RATIO CURVES

Results obtained utilising the RC and DSS have been combined together in order to provide the comprehensive shear modulus reduction and damping ratio curves. Fig. 5.8 and Fig. 5.9 (a and b) present the comprehensive data of G/G_{max} and damping ratio of both the clays. In order to define G/G_{max} data from DSS tests, G_{max} values obtained through BE tests have been used. Similar to the G/G_{max} and damping ratio of sands, data up to 0.1% have been considered directly from RC tests, while the remaining data (from 0.1% and beyond) have been adopted from DSS tests. It can be seen that the values of *D* at high strains (>0.1%) obtained from DSS tests are significantly higher (as high as 35%) than the

RC test results, which is possibly due to the differences in type of testing adopted-RC and DSS (such as frequency of loading, type of sample straining, sample geometry, etc.). Similar differences were also reported for cohesionless soils by Chattaraj and Sengupta (2016) and for cohesive soils by Subramaniam and Banerjee (2016). Most cyclic studies on dynamic properties of cohesive soils (Seed and Idriss 1970; Vucetic and Dobry 1991; Darendeli 2001; Zhang et al. 2005; Torabi and Rayhani 2017; Park and Kishida 2018; Subramaniam and Banerjee 2016) were limited to strain range of 1% and reported maximum D values up to 35%. As the present DSS tests were performed for strains across 5%, the reported maximum D values range between 35% and 40%, which seems reasonable. It must be mentioned that both the soils have PI close to 20 and therefore the G/G_{max} and damping ratio curves of cohesive soils (for PI 10 and 20) proposed by Vucetic and Dobry (1991) are also shown in Fig. 5.8 and Fig. 5.9 (a and b). It can be noted that present data plots within the range proposed by Vucetic and Dobry (1991) up to shear strains of 0.1%.

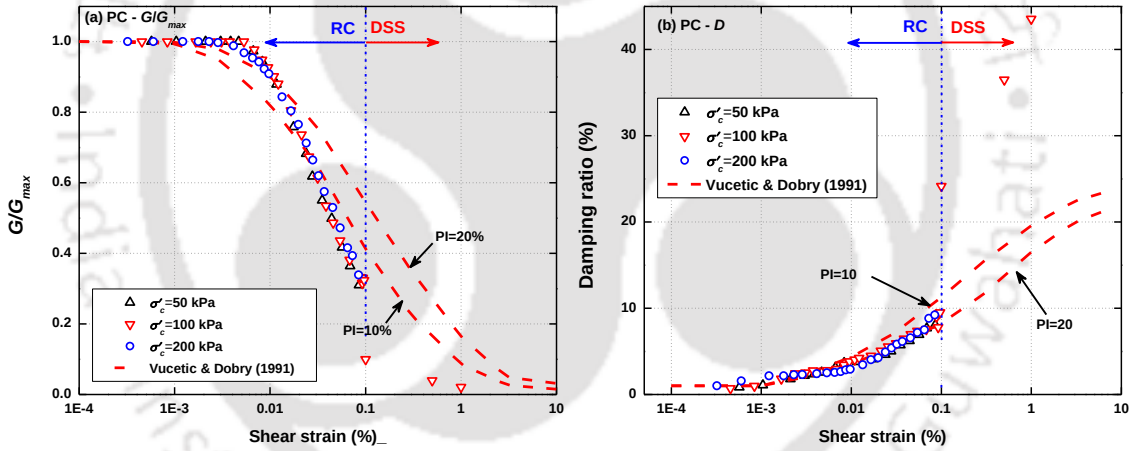

Fig. 5.8 (a) Modulus reduction and **(b)** damping ratio of PC soil

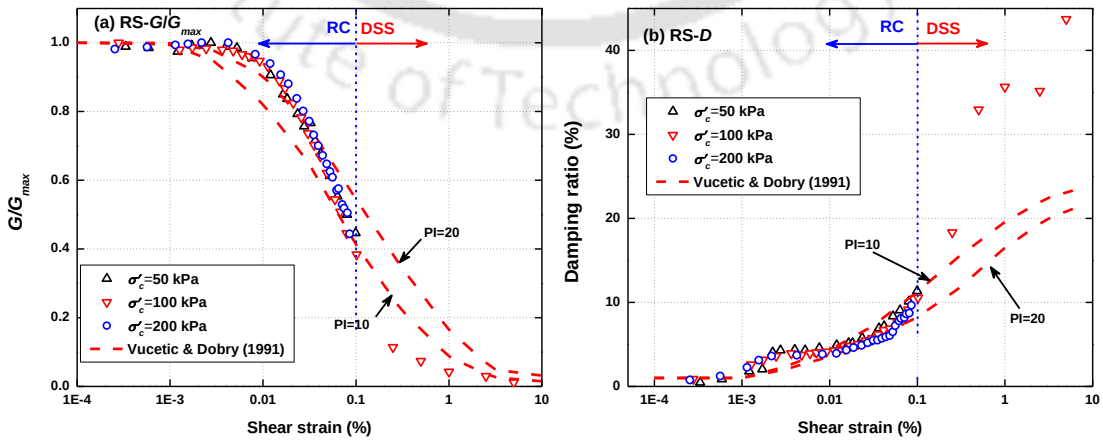

Fig. 5.9 (**a**) G/G_{max} and **(b)** Damping ratio of RS soil

5.4.1 Empirical Formulations (G_{max})

Empirical formulations for the estimation of G_{max} of tested cohesive soils have been presented. Fig. 5.10 depicts the G_{max} regression analysis fitted using a power law (Eqn. 5.1).

$$G_{max} = A \cdot (\sigma_c')^m \tag{5.1}$$

where A is the value of G_{max} (MPa) at an isotropic effective confining pressure of 1 kPa and m is the slope of the best fit curve (stress-dependent factor) as suggested by (Hoyos et al. 2011; Dutta et al. 2017). The obtained coefficients are presented in Fig. 5.10. It can be noted that m values are different for both the soils (0.285 for RS and 0.584 for PC) due to the difference in the tested density conditions of both the soils (field density for PC and maximum dry density for RS).

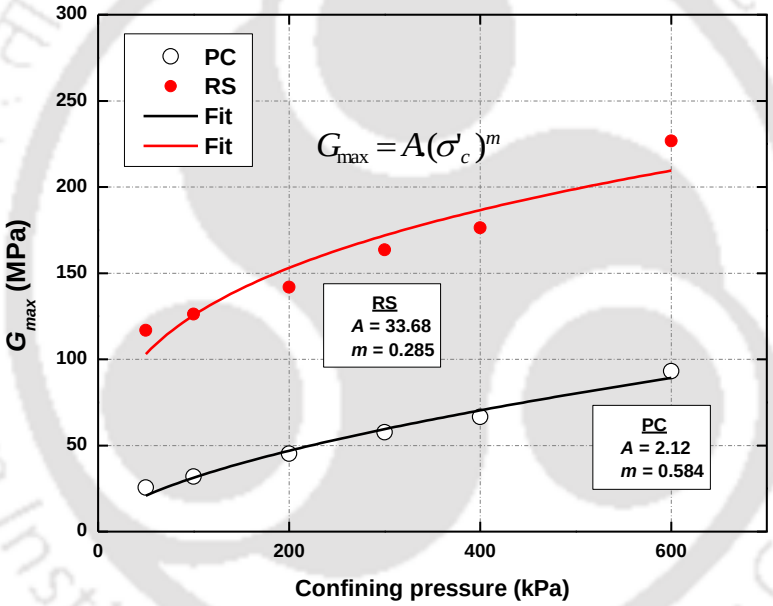

Fig. 5.10 Regression analysis of G_{max} of both cohesive soils

5.4.2 Empirical Formulations (G/G_{max})

In case of normalized shear modulus reduction (G/G_{max}) function, Matasovic and Vucetic (1994) model which was adopted for the sandy soils in *Chapter IV* (as represented through Eqn. 5.2), has been utilised herein.

$$\frac{G}{G_{max}} = \frac{1}{1+\beta \cdot \left[\frac{\gamma}{\gamma_{ref}}\right]^{\alpha}} \tag{5.2}$$

where the values of γ_{ref} for PC and RS are deduced from the comprehensive G/G_{max} curves at a G/G_{max} value of 0.5 (as suggested by Darendeli (2001)). As noted from Fig. 5.3 (a and

b), that the effect of effective confining pressure is minimal in case of tested clays and therefore the values of γ_{ref} established for PC and RS are 0.06% and 0.08%, respectively. Using the γ_{ref} and experimental G/G_{max} data, regression analysis has been performed with the Eqn. 5.2 for determining the best-fit parameters of both the clays. Fig. 5.11 (a and b) presents the variation of G/G_{max} with the normalized shear strain (γ/γ_{ref}). It can be observed that the model can reasonably match the experimental data with best-fit coefficients of α=1.392, β=1.029 for PC and α=1.310, β=1.039. Table 5.5 list the best-fit parameters of both the clays.

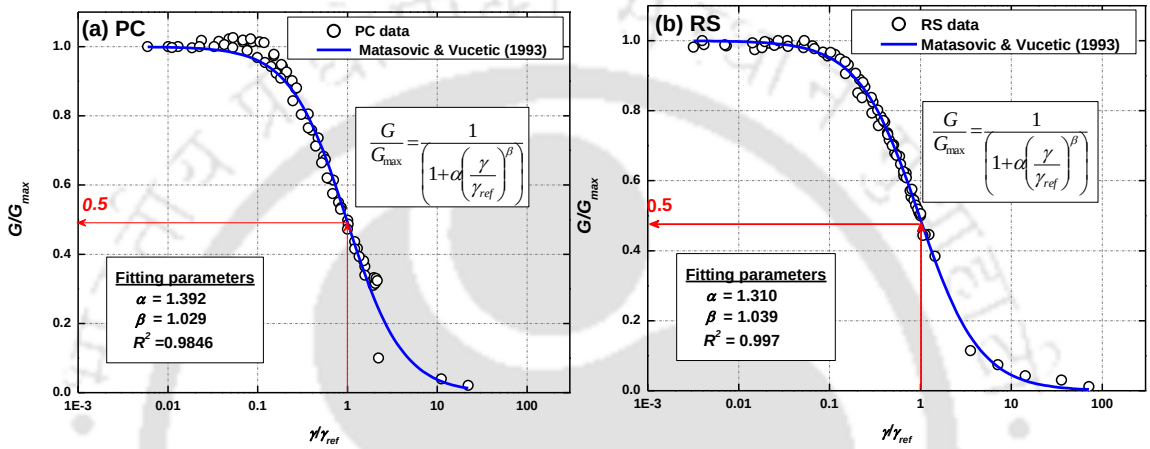

Fig. 5.11 Regression analysis for G/G_{max} of clays

Table 5.5 Best fit parameters for G/G_{max} and D of tested clays

		G/G_{max}			Damping ratio		
Soil	γ_{ref}	**α value**	**β value**	R^2	D_{min}	***b* value**	R^2
PC	0.06	1.392	1.029	0.9846	1.00	0.268	0.921
RS	0.08	1.310	1.039	0.9968	0.764	0.310	0.906

5.4.3 Empirical Formulations (Damping Ratio)

Darendeli (2001) Masing damping criteria (as represented through Eqn. 5.3) adopted for the sandy soils has been utilised herein for the modelling of cohesive soils damping ratio at varying strain levels.

$$D = b \cdot \left(\frac{G}{G_{max}}\right)^{0.1} \cdot D_{mas} + D_{min} \qquad (5.3)$$

The value of scaling coefficient (b) has been evaluated through regression analysis on the experimental data. The D_{min} has been considered from the RC test results: 1% for PC and 0.764% for RS. Fig. 5.12 (a and b) present the regression analysis data for the damping ratio and the obtained coefficients are listed in Table 5.5. It can be noted that the Darendeli (2001) Masing model could reasonably model the damping behaviour of clays (R^2>0.90).

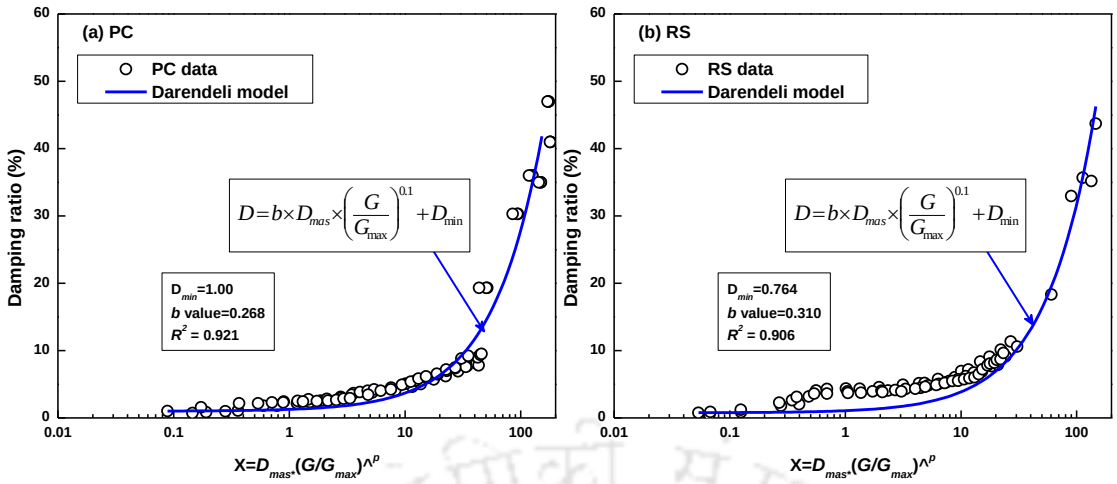

Fig. 5.12 Regression analysis for damping ratio of clays

The design G/G_{max} and damping ratio curves for both the cohesive soils, using the achieved best-fit parameters are shown in Fig. 5.13. It can be noted that their curves are different since their tested densities were different. The G/G_{max} curve of RS showed stiffer response and softer D values compared to that of PC, since the maximum dry density condition was adopted in the tests for RS. A comparison is made for the developed curves and the data from Vucetic and Dobry (1991) and Darendeli (2001) for cohesive soils at PI 20 in Fig. 5.14 and Fig. 5.15 for G/G_{max} and D, respectively. It must be noted that at the comparable PI of 20, the literature suggested G/G_{max} curves are reasonably matching. However, the untraditional D trend observed at high strain level is only being simulated through Darendeli (2001) D curves. The data presented here can be used for the seismic analysis of cohesive soils of similar index properties, density conditions and plasticity levels. For cohesive soils with indices other than the tested soils, Darendeli (2001) curves are suggested to be adopted.

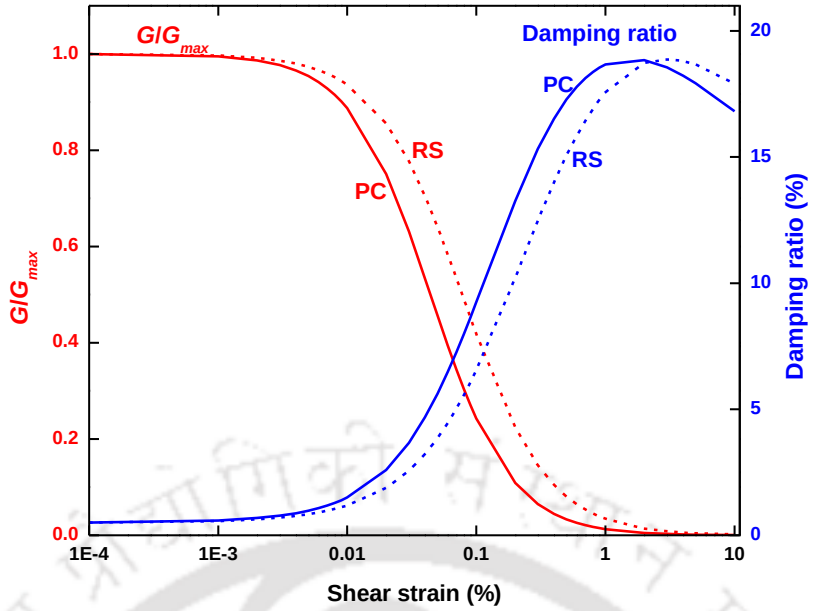

Fig. 5.13 Design G/G_{max} and D curves of both the cohesive soils

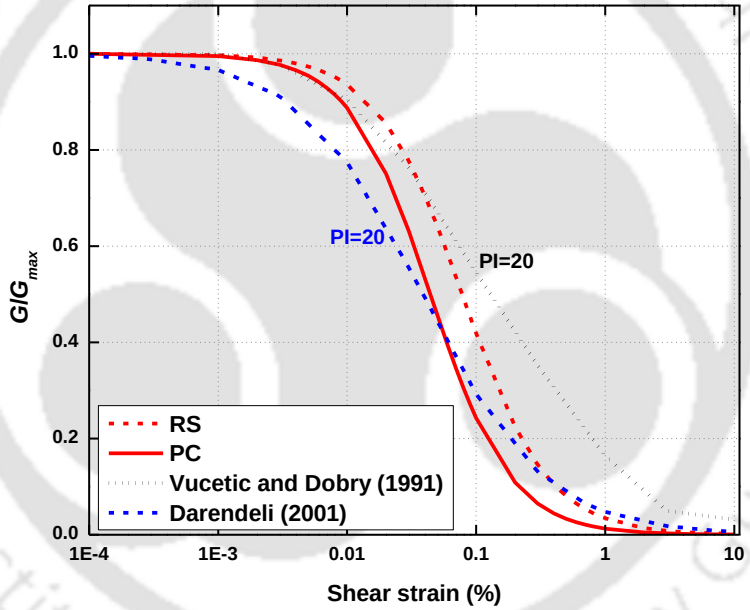

Fig. 5.14 Comparison of developed G/G_{max} curves of PC and RS with literature curves at PI=20

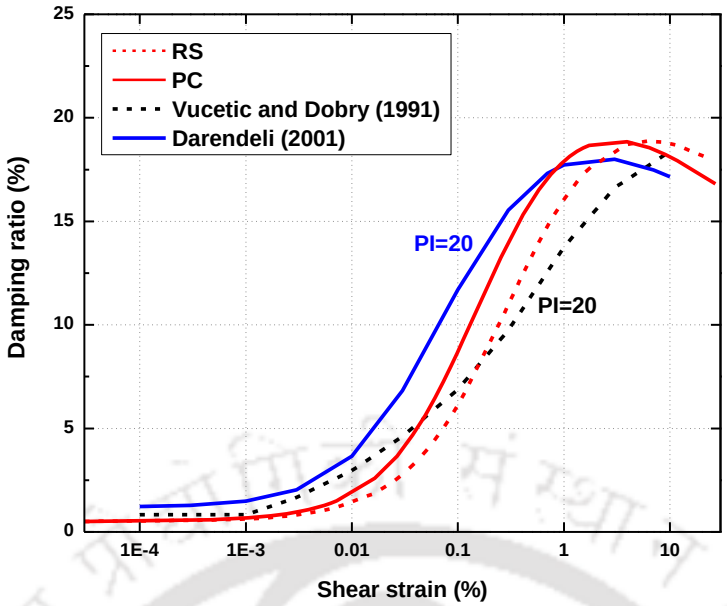

Fig. 5.15 Comparison of developed *D* curves of PC and RS with literature curves at PI=20

5.5 CYCLIC TRIAXIAL TESTS RESULTS

Cyclic triaxial tests have been performed on PC samples at stress-controlled conditions, at two different cyclic stress ratios. Typically, cohesive soils do not exhibit liquefaction phenomenon for low intensity motions and require high induced stresses for significant pore pressure generation (Youd et al. 2001; Kumar et al. 2018c). Therefore, two relatively high CSRs have been considered for the CTX testing (0.2 and 0.4). Both the tests were performed at an effective confining pressure of 100 kPa, which gives a deviatoric stress of 40 kPa and 80 kPa for CSR of 0.20 and 0.40, respectively. The chosen CSR of 0.2 represents moderate events while the 0.4 CSR represents the intense event based on the deviatoric stress condition. Table 5.6 lists the tests and the parameters of investigation. Tests on RS samples were not performed as Kumar et al. (2018b) has already reported the same.

Table 5.6 Summary of the CTX tests performed on PC

Soil	σ'_c (kPa)	f (Hz)	q_{cyc} (kPa)	$[q_{cyc}/2\sigma'_c]$
PC	100	1	40	0.20
			80	0.40

The typical undrained CTX results in terms of pore water pressure variation and stress-plot (q vs p') are presented in Fig. 5.16 a and b, respectively for PC specimen at CSR 0.2. A gradual increase of pore water pressure and consequent decrease of mean effective stress can be noted. It must be noted that up to first 40 loading cycles, as noted from Fig. 5.16 b, no significant reduction of p' is observed (p' reduced to 60 kPa from 100 kPa). This is also

evident from pore pressure variation plot (Fig. 5.16 a), where only 40 kPa of PWP is developed (r_u=0.40). Typically, most intense earthquake events contain less number of loading cycles, and cohesionless soils in loose state tend to liquefy in the very first few cycles as observed in the section 4.6 of Chapter IV. However, dense granular soils require relatively large loading cycles for significant pore pressure generation. The present PC specimen at CSR 0.2 represent the response of typical dense granular soil. Fig. 5.17 (a and b) presents the excess pore water pressure variation and q vs p' for PC specimen at CSR of 0.4. A rapid increase of pore pressure within the first 10 cycles of loading (Fig. 5.17 a) (pore water pressures as high as 100 kPa) and consequent decrease of p' can be observed (Fig. 5.17 b). This means that even soils of cohesive nature can be prone to significant pore pressures at high cyclic stress conditions or in case of intense seismic events, such as the cyclic softening cases of soft clays reported during 1985 Mexico City earthquake (Seed et al. 1988), in 1999 Kocaeli earthquake (Bray et al. 2000) and 2001 Bhuj earthquake in India (Dash et al. 2009).

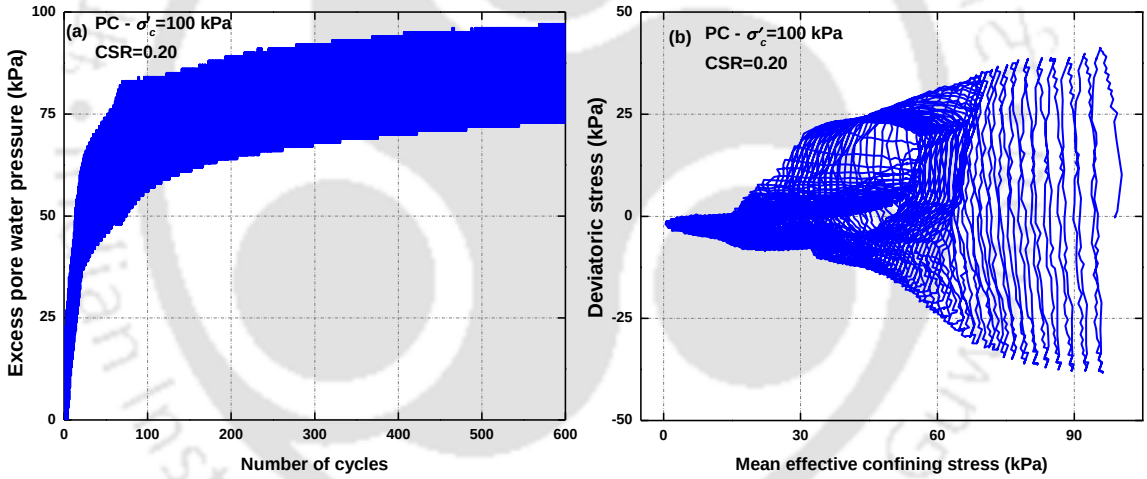

Fig. 5.16 (a) Plot of excess PWP and **(b)** stress-path for PC specimen at 0.2 CSR

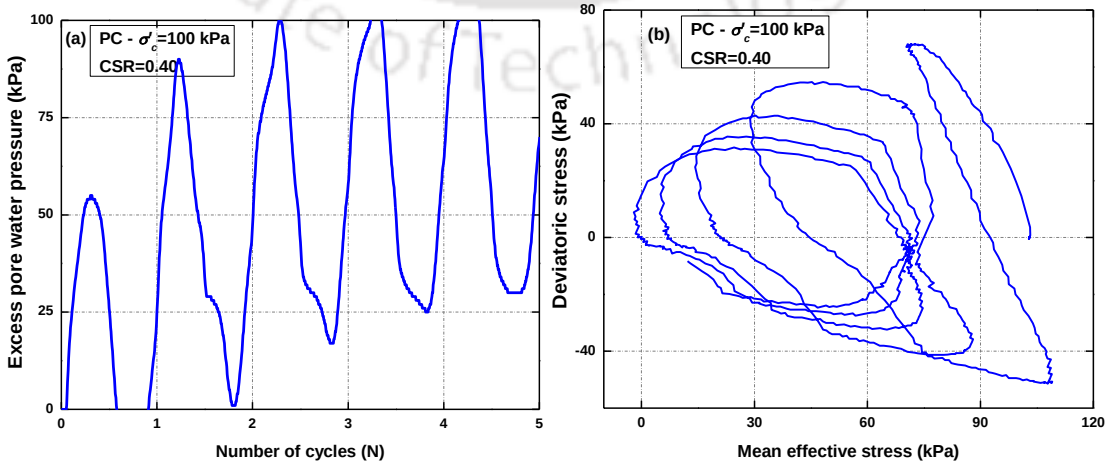

Fig. 5.17 (a) Plot of excess PWP and **(b)** stress-path for PC specimen at 0.4 CSR

Fig. 5.18 a and b present the variation of pore water pressure ratio (r_u) and axial strain with loading cycles for CSR of 0.20 and 0.40 conditions, respectively. It can be understood that both the loading conditions on PC specimens yield liquefaction (r_u=1.0). Large strain accumulation (as high as 10%) can be depicted at both the CSR conditions upon reaching liquefaction. Compared to the sandy specimen axial strain accumulations in undrained conditions, the strains induced in clay specimens at testing conditions are significantly large. In case of loose BP sand specimen (Fig. 4.40a), under CSR of 0.15, at liquefaction condition, the maximum strains induced are around 2%, while at CSR of 0.20, the PC specimen showed a strain accumulation of 10%. This means that although cohesive soils tend to resist pore pressure generation in the first few cycles, once liquefaction initiates, large strains (cyclic mobility phenomenon) may be induced which will be a concern for settlement of foundations.

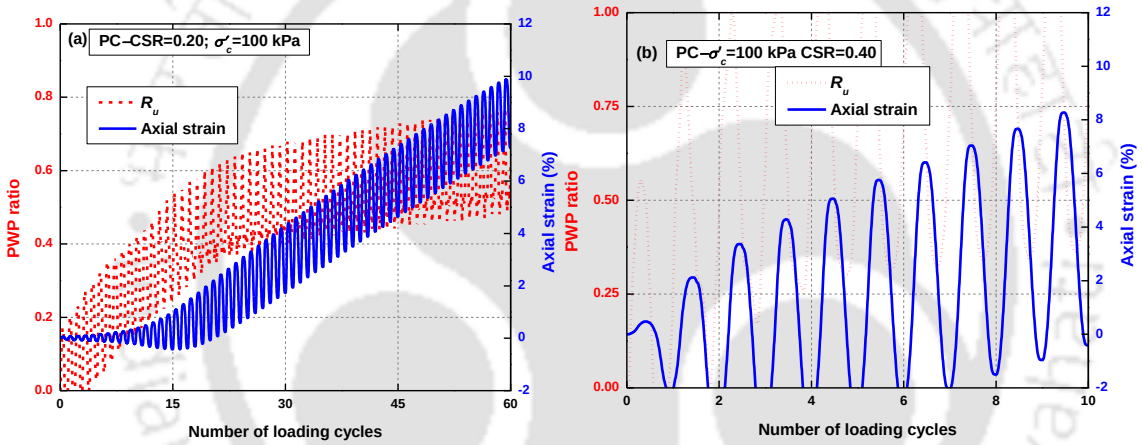

Fig. 5.18 PWP ratio and axial strain variation of PC for (**a)** CSR 0.20 and **(b)** CSR 0.40

The deviatoric stress-axial strain variation for both the CSR conditions is shown in Fig. 5.19 (a and b). Interesting observation can be drawn based on the stress-strain response: significantly large compressional displacements can be noted in both the cases. This means that the cohesive soils may exhibit contractive response upon undrained shearing conditions. Similar response for soft clay specimens was also reported by Hyde et al. (2006) and Kumar et al. (2018b).

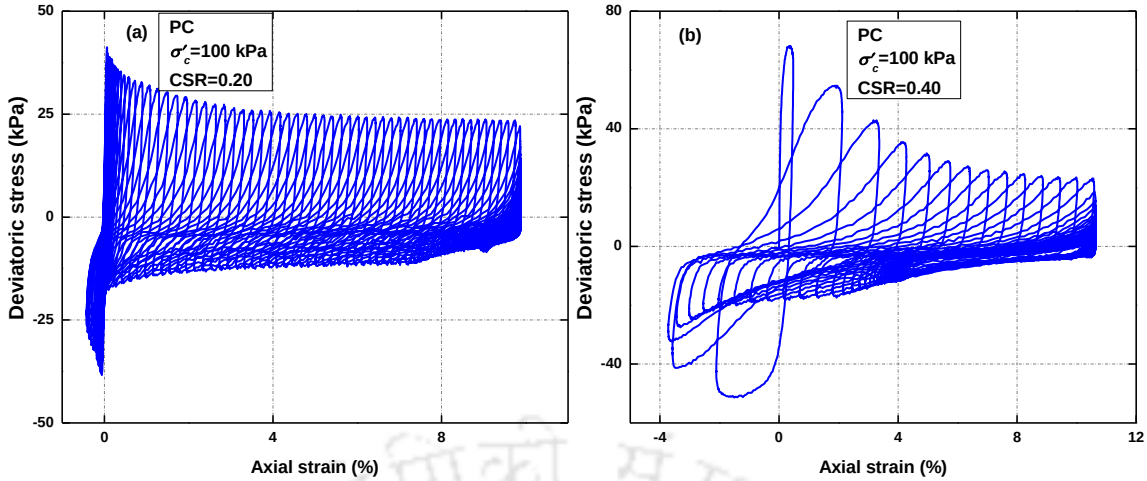

Fig. 5.19 Stress-strain response of PC at (a) CSR 0.20 and (b) CSR 0.40

5.6 SUMMARY

The chosen cohesive soils are characterised under dynamic loading conditions, using four element testing techniques. Results obtained from each testing technique and the corresponding analysis have been presented. Bender element tests provided the maximum shear modulus while resonant column and dynamic simple shear tests were used to obtain the low to high strain dynamic characteristics. Results are presented in terms of dynamic soil properties such as shear modulus, normalized shear modulus and damping ratio variation with shear strain. Results from independent tests are combined to provide the comprehensive data of dynamic soil properties over wide strain range. Empirical formulations have been proposed for the soils based on the regression analysis of the experimental data. Triaxial tests performed on the cohesive soils showed resistance to liquefaction for in the first set of loading cycles in case of moderate events. However, with intense loading, even the cohesive soils showed rapid rise of pore pressures and large strain accumulation. The undrained response of PC specimens duplicates the response of dense granular soils and large strain accumulation in comparison with sandy soils has been observed.

CHAPTER VI. SEISMIC GROUND RESPONSE ANALYSIS

6.0 INTRODUCTION

Seismic ground response analysis (GRA) studies are performed to understand the response of soil deposit (in terms of accelerations, stresses and strains) during earthquakes. The main aim of this chapter is to demonstrate the applicability of established strain dependent dynamic soil properties and liquefaction parameters, obtained from the experimental programme in the seismic GRA studies. One dimensional equivalent linear and nonlinear effective stress GRA studies are performed, using commercial ground response evaluation programme (DEEPSOIL v6.1). The input parameters required for performing GRA studies are discussed and the obtained responses are presented in terms of peak ground acceleration (PGA), peak spectral acceleration (PSA), stress-strain response, and pore water pressure variation.

6.1 METHOD OF ANALYSIS

One dimensional (1D) method of analysis is adopted for the present study utilising the DEEPSOIL v6.1 program (Hashash et al. 2016). The 1D GRA deals with the vertical propagation of shear waves through a linear viscoelastic system and the soil behaviour is approximated using Kelvin-Voigt (KV) solid, governed by the linear elastic G and D (Kramer 1996). Two basic assumptions are involved in 1D analysis: (a) subsoil boundaries are horizontal and all the layers of soil and rock are infinitely long (b) the soil domain is subjected to vertically propagating shear waves.

Three basic approaches are available for performing any GRA studies: linear, equivalent linear and fully nonlinear methods. The complexity of the problem increases towards linear-equivalent linear-fully nonlinear approach as it requires more input parameters. For example, soil dynamics problems involving very small strains (in case of low intensity earthquakes in stiff soils), only low strains are expected in the soil deposit and in such cases, use of linear or equivalent approaches are accepted. However, problems dealing with moderate to large strains (with high intensity motions and soft soils), plastic strains may induce in the soil column and such nonlinearity can only be simulated using nonlinear

approaches. Despite the simulation of full dynamic soil behaviour in nonlinear approach, design engineers adopt the equivalent linear approach often due to its simplicity. The present study utilises both the equivalent and nonlinear approaches for the GRA studies.

6.1.1 Equivalent Linear (EQL) Approach

Frequency domain equivalent linear (EQL) approach is a sandwiched method combining principles of both the elastic and non-linear approaches. In this approach, non-linearity of the soil is approximated using equivalent strain dependent dynamic soil properties (*G* and *D*) at an effective shear strain value using iterative procedure (Kramer 1996). The dynamic response of soil (stress-strain) is simulated using the stress-strain response of Kelvin-Voigt (KV) solid elements subjected to shear as per Eqn. 6.1.

$$\tau = G \cdot \gamma + \eta \cdot \frac{\partial \gamma}{\partial t} \tag{6.1}$$

where, τ is the shear stress, G is the shear modulus, $\gamma=\frac{\partial \gamma}{\partial t}$ is the shear strain and η is the coefficient of viscous damping. One-dimensional equation of motion for vertically propagating shear waves (in vertical direction) is represented as Eqn. 6.2.

$$\rho \cdot \frac{\partial^2 u}{\partial t^2} = \frac{\partial \tau}{\partial z} \tag{6.2}$$

where, ρ is the mass density of medium, and u is the displacement of the medium along lateral direction.

$$\rho \cdot \frac{\partial^2 u}{\partial t^2} = G \cdot \frac{\partial^2 u}{\partial z^2} + \eta \cdot \frac{\partial^3 u}{\partial z^2 \cdot \partial t} \tag{6.3}$$

Solving Eqn. 6.1 and Eqn. 6.2, using the adopted iteration technique in EQL approach, the equation of motion presented in Eqn. 6.3 yields the one-dimensional ground response.

6.1.2 Non Linear (NL) Approach

Despite EQL approach being computationally convenient and yielding reasonable results of ground response, it remains an approximation to the actual nonlinear soil response. The nonlinear response can be effectively estimated by adopting fully nonlinear approach using direct numerical integration in the time domain (Garala and Madhabushi 2018). Assumptions considered in the EQL approach (approximation of *G* and *D* and neglecting the soil yielding) can be avoided by employing NL approach. In addition, NL approach can be used for estimating the effective stress response of the soil deposit, incorporating pore water pressures.

The computer program *DEEPSOIL* (Hashash et al. 2016) has been used for the NL analysis since it is a widely used nonlinear site response analysis software (Kumar et al. 2018b; Garala Madabhushi 2018; Basu et al. 2019). The program utilises a discretized multi-degree-of-freedom lumped parameter model of the 1D soil column. Briefly, in the NL effective stress analysis, dynamic equation of motion (Eqn. 6.4) is solved numerically following the Newmark β method (Newmark 1959).

$$[M] \cdot \{\ddot{u}\} + [C] \cdot \{\dot{u}\} + [K] \cdot \{u\} = -[M] \cdot \{I\} \cdot \ddot{u}_g \quad (6.4)$$

where $[M]$ is the mass matrix, $[C]$ is the viscous damping matrix, $[K]$ is the stiffness matrix, is $\{\ddot{u}\}$ the vector of nodal accelerations, $\{\dot{u}\}$ is the vector of nodal relative velocities, u is the vector of nodal relative displacements, $\ddot{u_g}$ is the acceleration at the base of soil column and $[I]$ is the unit vector. The chosen constitutive relationship (stress-strain behaviour of soil) will be utilised during the small time steps involved in the NL analysis. At the beginning of each time step, the stress-strain relationship adopted is used to obtain the strain dependent dynamic soil properties to be employed in that particular time step.

6.2 SITES OF INTEREST

Four sites were chosen to perform the seismic ground response analysis, out of which three are located in Assam, a northeastern state in India and the other site is located in Rohtak region of Haryana, northern state of India. Fig. 6.1 presents the location of chosen sites in northeastern India. Selection of these profiles is motivated by the presence of different layers of soils and properties of soils represent the investigated soil gradation and strength characteristics based on the borehole details supplied by the local consultancy firms (SPAN Consultants 2005; Experto Geotechnical Consultants 2015). Table 6.1 list the sites chosen for the GRA study and site classification based on Eurocode of practice (EN 1998-1 2004). The characteristic site period using the thickness of layers and V_s has been determined as suggested in Kramer (1996) and reported in Table 6.1.

Table 6.1 Sites chosen for the study

Site	Location	Predominant soil layering	$V_{s\text{-}30}$, m/s	Site Class-EC8	Characteristic site period, sec
Site 1 (Saraighat Bridge)	Shore of BP river, Guwahati	Sand-clay	212	C	0.80
Site 2 (Pachoria)	Pachoria, North Guwahati	Clay-sand	270	C	0.40
Site 3 (Tezpur)	Tezpur	Sand-clay-sand	390	B	0.31
Site 4 (Rohtak)	Rohtak, Haryana	Sand-clay-sand	260	C	0.46

On comparison with the borehole details obtained from local consultancy firms for the four chosen sites, it is understood that although the sampled soils appear slightly different to the tested soils, their gradation and shear strength properties reasonably match. Based on this, author feels that the applicability of established soil properties may be justifiable in representing the seismic response of soils at chosen sites as an illustration.

In brief, the first site (Site-1), predominantly consists of loose to dense fine sand up to a depth of 42 m from the surface. The second site (Site-2) has predominant layers of clay (top 12m) and sand. The third site (Site-3) consists of soft clay layer of 5 m thickness sandwiched between loose and dense sand stratum. The fourth site (Site-4) consists of dense silty sand up to a depth of 15 m from the surface, followed by a coarse sand for 5 m and stiff clay for 13m. Further explored depth of Site-4 consists of dense gravel. Fig. 6.2 depicts the geotechnical details of the chosen sites based on borehole data provided by local consultancy agencies (SPAN Consultants 2005; Experto Geotechnical Consultants 2015).

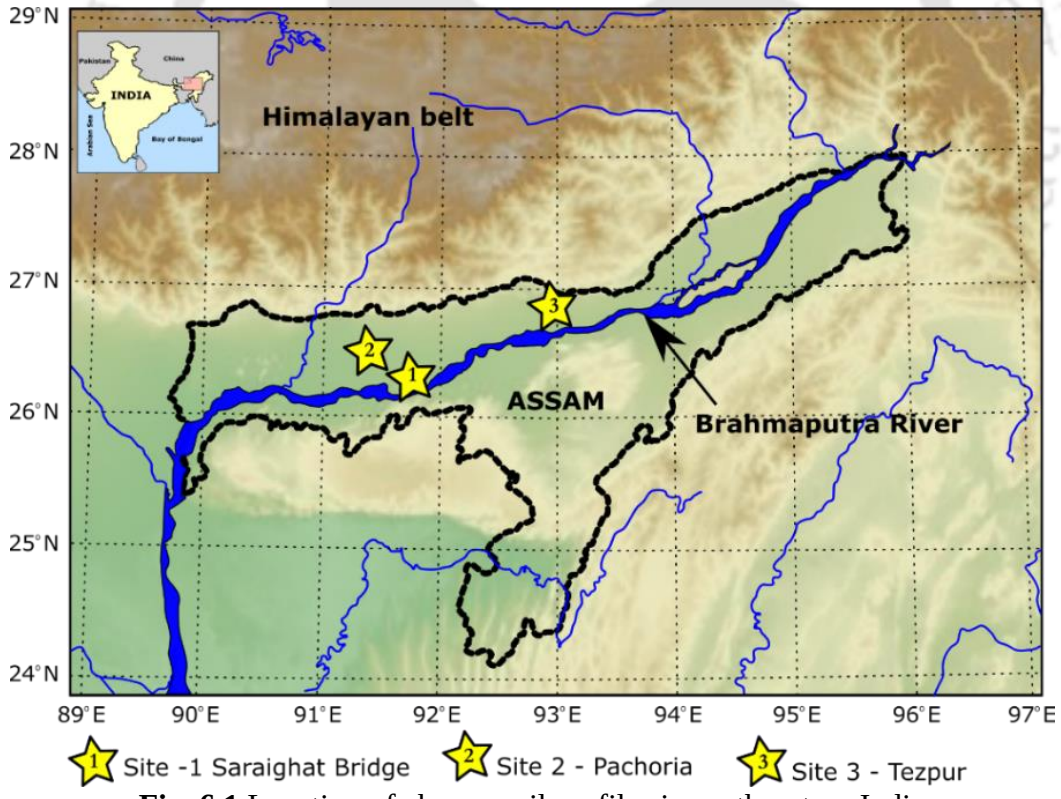

Fig. 6.1 Location of chosen soil profiles in northeastern India

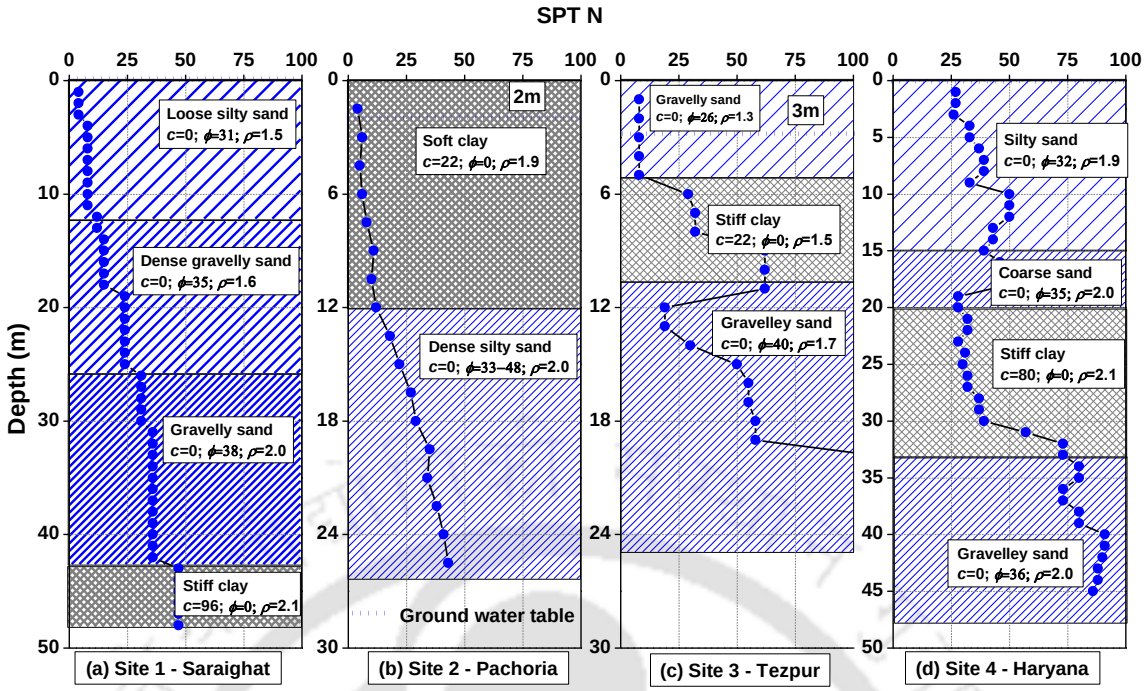

Fig. 6.2 Bore log data of the chosen sites (***Note:*** Units of c are in kPa; ϕ in deg and ρ are in g/cc) availed from local consultancy firms (SPAN Consultants 2005; Experto Geotechnical Consultants 2015)

6.3 GROUND MOTIONS CONSIDERED

The primary requirement of any GRA study is the input ground motions and the selection of ground motions should be guided by the regional seismicity. The region under consideration (northeastern India) witnessed two great earthquakes (moment magnitude, $Mw > 8.0$) and more than 15 large seismic events ($6.0 < Mw < 8.0$) since the first recorded event in the country (1897). Such high seismicity of the region is attributed to the proximity of Himalayan arc in the north and the presence of many active faults in and around the region. Fig. 6.3a presents the seismic intensity of the region with IS:1893 (2016) classified seismic zones and Fig. 6.3b depicts the past seismic events of the region superimposed on the identified seismic faults. Seismologists (Khattri 1999; Kayal et al. 2006) are of the opinion that this region is prone to an impounding earthquake of M_w>8.0, in the near future due to the accumulated energy in the region since the last great event in 1950. Therefore, based on the recurring warnings of the seismologists, ground motions that could emanate from Shillong plateau in case of a future event of M_w>8.0, are considered for the present study.

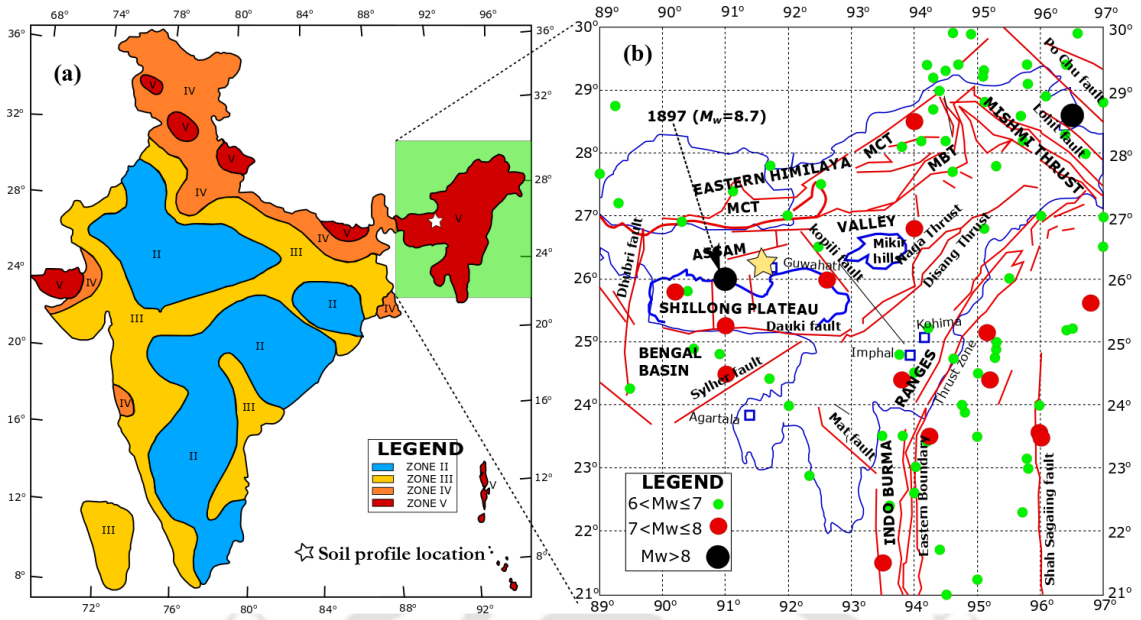

Fig. 6.3 (a) Indian seismic zone map (IS 1893-2002) **(b)** Seismotectonic map of northeastern India (redrawn after Raghu Kanth et al. 2008)

Multiple ways of ground motion selection exist: direct use of recorded ground motions, simulation of artificial ground motions based on seismicity of the region, matching of recorded motions to an available response spectrum and hybrid approaches combining two or more of the above. Bommer and Acevedo (2004) recommended the use of recorded ground motions, if available for the site of interest as they essentially contain the seismic source and path characteristics. However, for the considered source (Shillong plateau) and the expected seismic event (M_w>8.0), no such recordings were available in the region. Artificially generated ground motions are a viable option in such cases. In the present study, artificially generated ground motions for Guwahati city for 1897 Shillong earthquake, by Raghu Kanth et al. (2008) have been utilised. Raghu Kanth et al. (2008) developed rock outcrop motions for Guwahati city, based on stochastic finite-fault simulation algorithm proposed by Hanks and McGuire (1981); Boore (1983). The peak bedrock acceleration (PBRA) of the developed motions for Guwahati city, range from 0.14g to 0.19g for the considered event (1897 Shillong earthquake). Fig. 6.4 depicts the generated motions by Raghu Kanth et al. (2008) for Guwahati city and the corresponding frequency content of the motions. The predominant frequency of the motions ranges from 5 Hz to 6.25 Hz (Fig. 6.4b). In case of Site-4 (Rohtak region of Haryana), a recorded motion for the 1999 Chamoli earthquake (Fig. 6.5) with a PBRA of 0.36g has been considered for the GRA study.

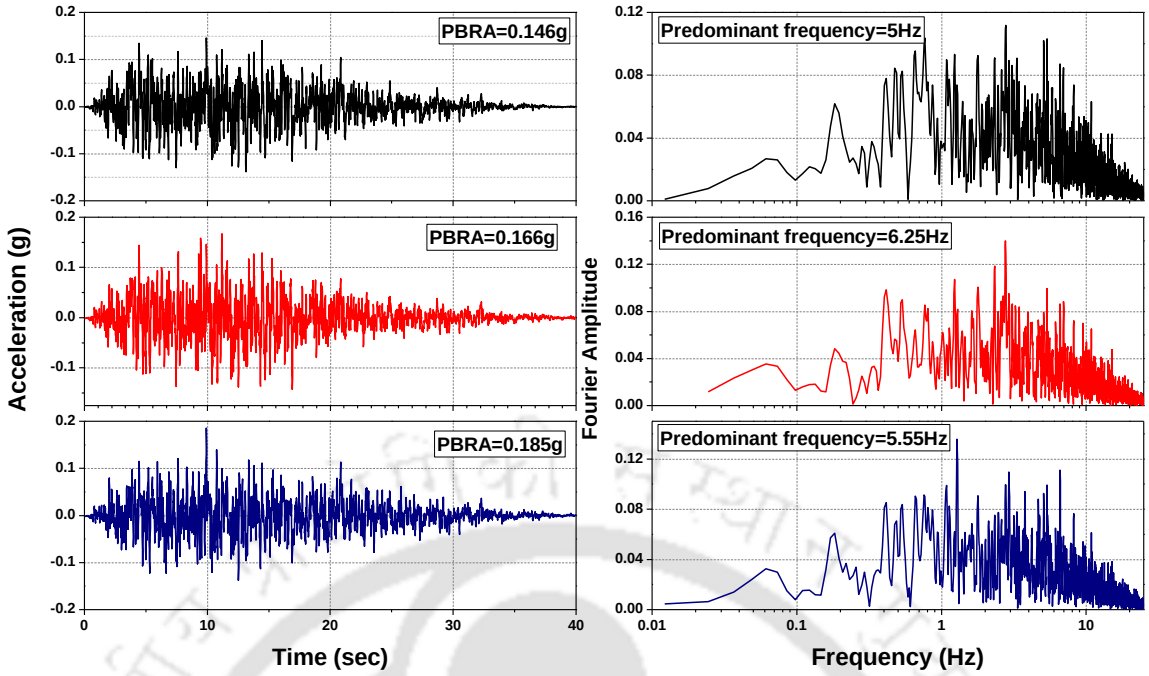

Fig. 6.4 Artificial ground motions for Guwahati city (redrawn after Raghu Kanth et al. 2008)

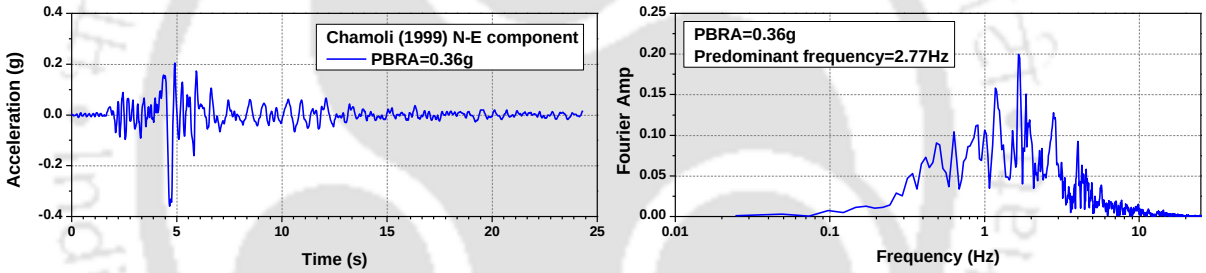

Fig. 6.5 Recorded Chamoli (1999) motion (Source:COSMOS)

The acceleration response spectrum (S_a/g) of chosen ground motions is compared to the rock spectrum for 5% damping, recommended by IS 1893 (2016) and Eurocode 8 (Fig. 6.6). It can be observed that the spectra of chosen motions for Guwahati city is higher than the codal spectrum at shorter periods (<0.4 sec), and reasonably consistent at longer periods (>0.4s).

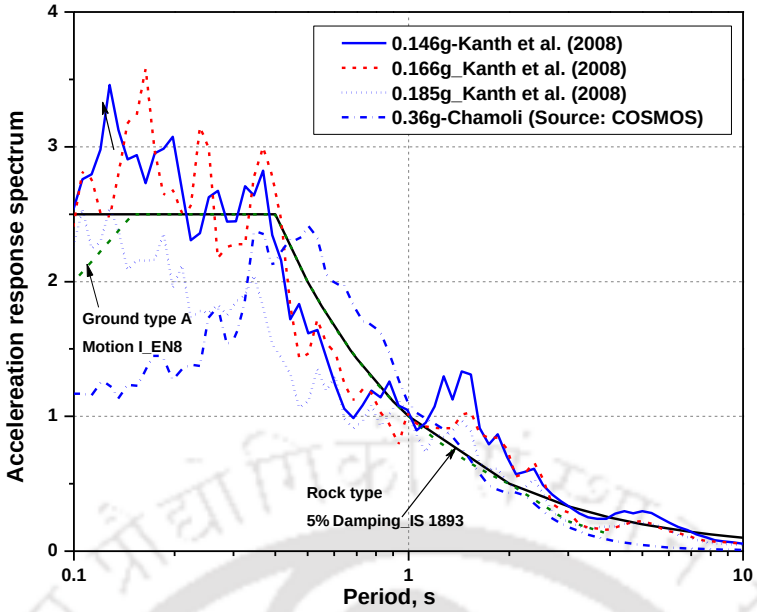

Fig. 6.6 Comparison of acceleration spectrum of chosen motions to the global spectrum

6.4 SUBSOIL PROPERTIES REQUIRED

The input parameters of soil required for GRA study are the layer thickness, unit weight, and strain dependent dynamic soil properties (G_{max}; G/G_{max} and D curves). As the direct measurements of V_s of the chosen profiles is not available, SPT N (measured) data obtained from the borehole surveys (Fig. 6.2) were used to obtain the V_s profile, employing the correlation proposed by Imai and Tonouchi (1982) –Eqn. 6.5.

$$V_s = 97 \cdot N^{0.314} \tag{6.5}$$

The G_{max} values are then determined using the V_s and density (ρ) of each layer.

Efficiency of seismic wave propagation depends on the element size (maximum thickness of each layer) in case of finite element models as it would govern the maximum frequency that can be propagated through the layer. In this regard, Kuhlemeyer and Lysmer (1973) recommended that the size of element (thickness of each layer) must be less than one sixth to one eighth of the minimum wavelength ($\lambda=V_s/f_{max}$), (where f_{max} is the predominant frequency of the input motion) for accurate wave transmission. However, recent study by Ramirez et al. (2018) suggested that the maximum size of element should be less than $\lambda/16$ for soils of soft or liquefiable nature. The results of EQL approach do not generally depend on element sizes as they essentially are based on solving mathematical formulations in frequency domain. However, in case of time domain analysis, coarser mesh leads to the obstruction of high frequencies. Therefore, for the present study, the discretization of soil layers has been carried out following the recommendation of Ramirez et al. (2018) for both

EQL and NL approaches. In this way, thickness of layers increases towards the depth of the stratum. Table 6.2 depicts the discretization of Site- 1 and the corresponding subsoil properties.

6.4.1 G/G_{max} and Damping Ratio Curves for EQL Analysis

Concerning the strain dependent dynamic soil properties, ideally, each layer should have its own modulus and damping curves depending on the mean effective confining pressure of that particular layer (p'_i). Instead of having unique curves for each sub-layer (every p'_i), curves for major units (with p') are adopted. Stokoe et al. (1995) suggested that the estimated p' should be within about ±50% of the actual values when selecting the curves for design. To elaborate this, Site-1 is considered. The profile is divided in to seven major units (51 minor layers) with mean effective confining pressure (p') assigned for each major unit. Similar approach was used by Zhang et al. (2005) for performing an equivalent linear GRA study in Charleston site, US. Based on this, p'_i for each layer is calculated assuming the coefficient of at-rest earth pressure (K_o) as 0.5. The p' adopted for the bigger units is shown in Table 6.2. Based on the considered p' magnitudes, G/G_{max} and damping ratio curves which were established based on the laboratory investigations have been utilised. It must be mentioned that although the soils from the chosen sites do not exactly represent the tested soil characteristics, the tested soils are from the nearby locations and approximate the index properties of the soils as observed from the sampled bore log data supplied by the local consultancy firm. Therefore, for fine/silty sands form northeastern India, data of BP sand have been used and for coarse/gravelly sands, BG data have been adopted. Similarly, in the northern India, YF and YC sands data have been employed for silty and gravelly sands.

In case of Site-1, the surficial loose silty sand has been modelled using BP sand curves while the gravelly sand has been modelled using BG sand with varying p' conditions. For the bottom most clay stratum of 6 m thickness (43 m to 48 m), the developed curves for Pachoria Cohesive (PC) soil are adopted. Fig. 6.7 depicts the adopted G/G_{max} and damping ratio curves for Site-1, considered from the experimental investigations. The stratum underlying the stiff silty clay layer is a highly dense gravel with SPT N value of 110. Therefore, the bedrock is assumed as an elastic (deformable) rock with a SPT N correlated shear wave velocity of 425 m/s.

For the remaining chosen sites (Sites-2 to 4), the G/G_{max} and D curves are generated based on the mean effective confining pressure of each layer. In case of Site-2 (Pachoria), for surficial (0 to 11 m) soft clay, PC data have been adopted while for the dense sand layers from 12 m to 26 m, BP sand data were employed for generating G/G_{max} and D curves (Fig. 6.8). In case of Site-3 (Tezpur), loose surficial gravel layer (0 to 5 m) has been assigned with BG sand of 25 kPa p', while the clay layer (6 m to 10 m) was modelled with RS soil and subsequent deep dense gravelly sand layers are modelled using BG sand of varying p' as 50 and 100 kPa (Fig. 6.9). In case of Site-4, surficial loose sand layers are modelled using the Yamuna fine (YF) sand with varying p' (25, 50 and 75 kPa) while the deep dense sand is modelled using coarse Yamuna sand of 100 and 300 kPa p'. The sandwiched clay layer in case of Site-4 was modelled using Redsoil curves (Fig. 6.10), since no data of cohesive soils of northern India are available. The chosen data of G/G_{max} and D curves is inputted for the major units as discrete points in the program for EQL approach.

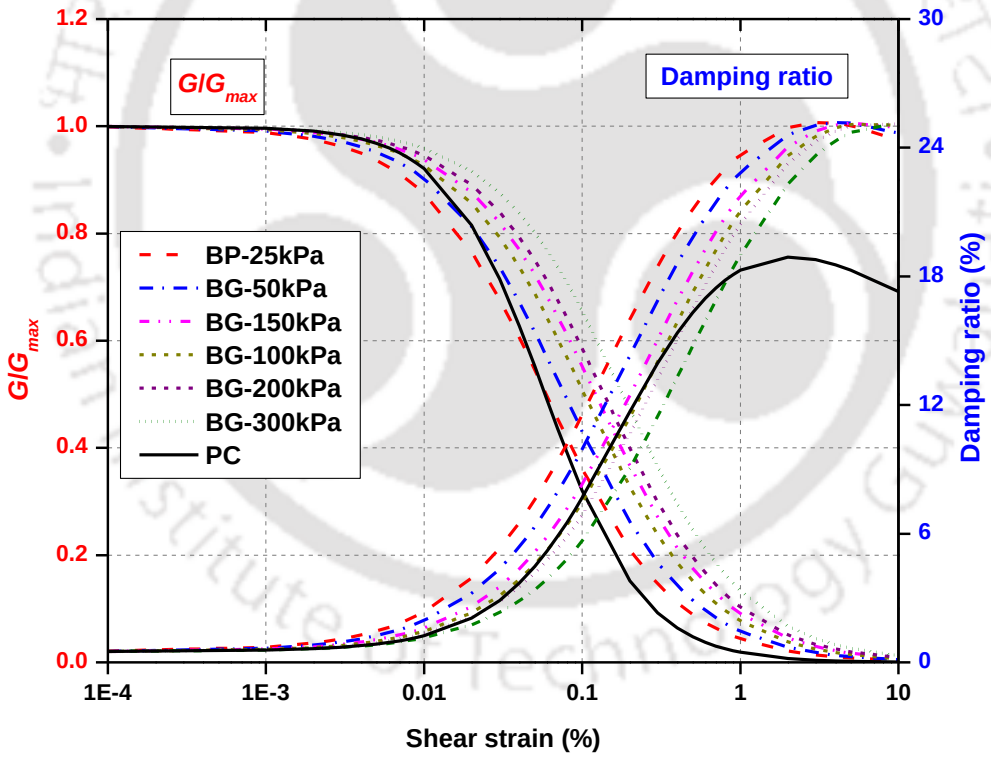

Fig. 6.7 G/G_{max} and damping curves for Site-1

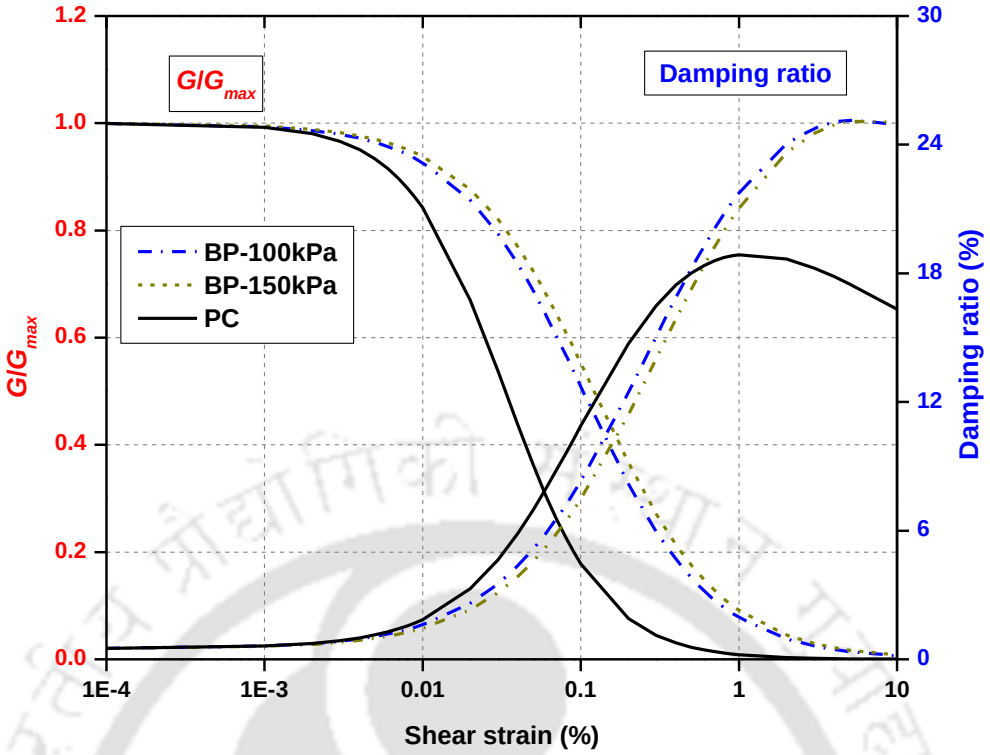

Fig. 6.8 G/G_{max} and D curves adopted for Site-2

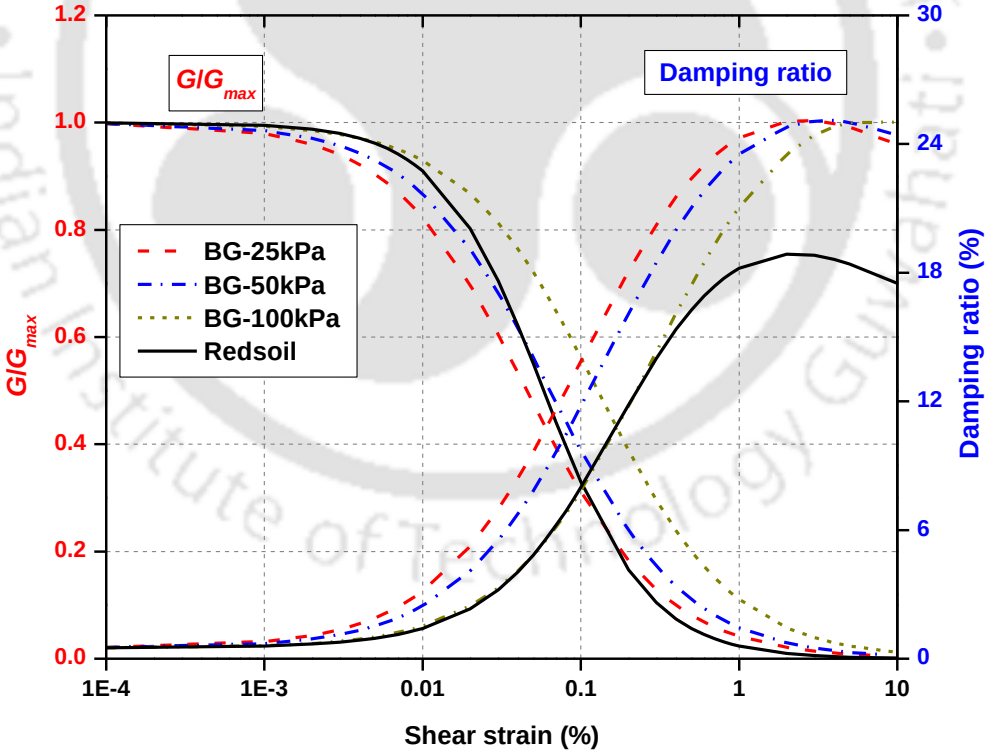

Fig. 6.9 G/G_{max} and damping curves for Site-3

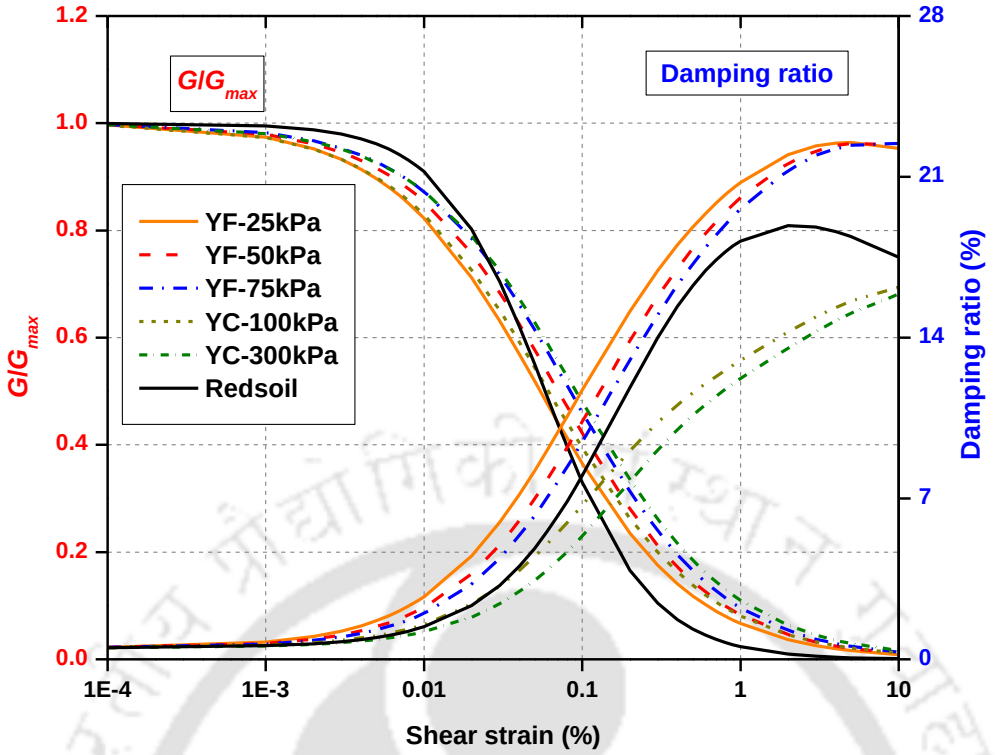

Fig. 6.10 G/G_{max} and damping curves for Site-4

Table 6.2 Design soil profile of Saraighat Bridge site (Site-1)

Soil type	Thickness, m	Cumulative depth, m	Unit weight, kN/m^3	V_s, m/s	Total stress, kPa	PWP, kPa	Eff Vertical stress, kPa	p'_i, kPa	G/G_{max} and D Curves adopted (p')
Loose and fine silty sand	0.5	0.5	15.1	149	7.55	4.905	2.645	1.77	BP sand (25 kPa)
	0.5	1	15.1	149	15.1	9.81	5.29	3.54	
	0.5	1.5	15.1	149	22.65	14.715	7.935	5.31	
	0.5	2	15.1	149	30.2	19.62	10.58	7.08	
	0.5	2.5	15.1	149	37.75	24.525	13.225	8.86	
	0.5	3	15.1	149	45.3	29.43	15.87	10.63	
	1	4	15.7	178	62.8	39.24	23.56	15.78	
	1	5	15.7	178	78.5	49.05	29.45	19.73	
	1	6	15.7	178	94.2	58.86	35.34	23.67	
	1	7	15.7	178	109.9	68.67	41.23	27.62	
	1	8	15.7	178	125.6	78.48	47.12	31.57	
	1	9	15.7	178	141.3	88.29	53.01	35.51	
	1	10	15.7	178	157	98.1	58.9	39.46	
	1	11	15.7	178	172.7	107.91	64.79	43.4	
Highly dense sand	1	12	16.2	211	194.4	117.72	76.68	51.37	BG sand (50kPa)
	1	13	16.2	211	210.6	127.53	83.07	55.65	
	1	14	16.5	226	231	137.34	93.66	62.75	
	1	15	16.5	226	247.5	147.15	100.35	67.23	
	1	16	16.5	226	264	156.96	107.04	71.71	
	1	17	16.5	226	280.5	166.77	113.73	76.19	BG sand (100kPa)
	1	18	16.5	226	297	176.58	120.42	80.68	
	1	19	17.8	262	338.2	186.39	151.81	101.71	
	1	20	17.8	262	356	196.2	159.8	107.06	
	1	21	17.8	262	373.8	206.01	167.79	112.41	
	1	22	17.8	262	391.6	215.82	175.78	117.77	

Soil type	Thickness, m	Cumulative depth, m	Unit weight, kN/m^3	V_s, m/s	Total stress, kPa	PWP, kPa	Eff Vertical stress, kPa	p'_i, kPa	G/G_{max} and D Curves adopted (p')
	1	23	17.8	262	409.4	225.63	183.77	123.12	BG sand (150kPa)
	1	24	17.8	262	427.2	235.44	191.76	128.47	
	1	25	17.8	262	445	245.25	199.75	133.83	
Highly dense deep sand mixed with greyey silt	1	26	19.4	284	504.4	255.06	249.34	167.05	
	1	27	19.4	284	523.8	264.87	258.93	173.48	
	1	28	19.4	284	543.2	274.68	268.52	179.9	BG sand (200kPa)
	1	29	19.4	284	562.6	284.49	278.11	186.33	
	1	30	19.4	284	582	294.3	287.7	192.75	
	1	31	20.6	298	638.6	304.11	334.49	224.1	
	1	32	20.6	298	659.2	313.92	345.28	231.33	
	1	33	20.6	298	679.8	323.73	356.07	238.56	
	1	34	20.6	298	700.4	333.54	366.86	245.79	
	1	35	20.6	298	721	343.35	377.65	253.02	
	1	36	21.7	298	781.2	353.16	428.04	286.78	BG sand (300kPa)
	1	37	21.7	298	802.9	362.97	439.93	294.75	
	1	38	21.7	298	824.6	372.78	451.82	302.71	
	1	39	21.7	298	846.3	382.59	463.71	310.68	
	1	40	21.7	298	868	392.4	475.6	318.65	
	1	41	21.7	298	889.7	402.21	487.49	326.61	
	1	42	21.7	298	911.4	412.02	499.38	334.58	
Deep hard silty clay	1	43	22	324	946	421.83	524.17	351.19	Pachoria Cohesive soil
	1	44	22	324	968	431.64	536.36	359.36	
	1	45	22	324	990	441.45	548.55	367.52	
	1	46	22	324	1012	451.26	560.74	375.69	
	1	47	22	324	1034	461.07	572.93	383.86	
	1	48	22	324	1056	470.88	585.12	392.03	

6.4.2 NL Soil Parameters

Nonlinear analysis requires the stress-strain behaviour of soil to be modelled using the nonlinear stress strain response, along with the pore pressure parameters. One of the oldest and widely acceptable models for cyclic loading of soils is the Masing (1926) model, which describes the stress-strain path of the soil during loading, unloading, and reloading cycles. Two basic assumptions exist in the Masing formulations: cyclic stress-strain (loading and unloading) path can be represented using the monotonic stress-strain path (also called backbone curve) of the soil and hysteresis loops for two-way cyclic loading can be obtained by scaling the backbone curve by a factor of two. Upon the initial loading, the scaled curve is flipped on the horizontal and vertical axes, respectively, and placed at the end of the unloading path. As the cycles continue, unloading and reloading continues and the loading and unloading paths during any cycle would not intersect (Darendeli 2001). As the forcing function during an earthquake is non-sinusoidal, few more rules must have to be followed in order to consider this approach in modelling the cyclic loadings which are non-harmonic. Therefore, extended Masing rules have been brought-in with subsequent modifications and are being implemented in soil dynamics applications by various researchers (Kondner and Zelasko 1963; Matasovic and Vucetic 1994; Phillips and Hashash 2009).

In the present analysis, modified Kondner and Zelasko (MKZ) hyperbolic stress-strain model (Matasovic and Vucetic 1994) has been used to represent the constitutive behaviour of the soil using the Eqn. 6.6.

$$\frac{G}{G_{max}} = \frac{1}{1+\beta\cdot\left[\frac{\gamma}{\gamma_{ref}}\right]^{\alpha}} \tag{6.6}$$

Where τ is the shear stress, γ is the shear strain, γ_{ref} is the reference shear strain, G_o is the initial shear modulus (or G_{max}), β and α are the parameters defining the shape of the stress-strain curve. In the present study, pressure-dependent MKZ model (Matasovic and Vucetic 1994) has been chosen for the backbone formulation and non-Masing Re/Unloading criteria was adopted for the hysteretic cyclic response simulation (Hashash et al. 2016). Further details about the theoretical background of the methodology can be found in Park and Hashash (2008) and Phillips and Hashash (2009).

Once the soil profiles are discretized with an appropriate thickness (based on the maximum frequency propagation principle) and assigned with the unit weight and associated V_s

properties (based on SPT *N* correlation), each minor layer should be provided with the data of the constitutive model either in terms of parameters of Eqn. 6.6 or the data directly inputted. The experimentally obtained G/G_{max} and *D* curves were inputted as discrete data points to the program to act as a targeted G/G_{max} and damping ratio. The provided data points were then fitted using the available MRDF-UIUC pressure dependent, hyperbolic procedure implemented in DEEPSOIL (Phillips and Hashash 2009). The primary reason for fitting the established soil properties is due to the efficient hyperbolic representation of the fitted damping ratio as well as for a better representation of high strain damping ratio.

Table 6.3 PWP model parameters for sand layers of four chosen sites

Site	Depth and stress range	*p*	*F*	*s*	γ_t
Site-1	<16m (p'=50 kPa)	1.297	3.837	0.963	0.02
	17 to 22m (p'=100 kPa)	1.205	3.029	0.952	0.03
	23 to 42m (p'=150 kPa)	1.117	3.698	1.054	0.035
Site-2	13 to 19m (p'=100 kPa)	1.205	3.029	0.952	0.03
	20 to 26m (p'=150 kPa)	1.117	3.698	1.054	0.035
Site-3	<5m (p'=50 kPa)	1.297	3.837	0.963	0.02
	11 to 19m (p'=100 kPa)	1.205	3.029	0.952	0.03
	20 to 26m (p'=150 kPa)	1.117	3.698	1.054	0.035
Site-4	<10m (p'=50 kPa)	1.297	3.837	0.963	0.02
	11 to 20m (p'=100 kPa)	1.205	3.029	0.952	0.03
	33 to 45m (p'=150 kPa)	1.117	3.698	1.054	0.035

DEEPSOIL program incorporates the variation of pore water pressure during cyclic loading through various models depending on the type of soil (sand or clay). The PWP model of Vucetic and Dobry (1988) has been used for sands, which can be represented through the Eqn. 6.7. The same model has been employed for PWP variation modelling of BP sand in section 4.6.1 of Chapter IV.

$$u_N = \frac{p \cdot f \cdot N \cdot F \cdot (\gamma - \gamma_t)^s}{1 + f \cdot N \cdot F \cdot (\gamma - \gamma_t)^s} \qquad (6.7)$$

where, u_N=normalized pore water pressure (PWP ratio-r_u); N_c=number of loading cycles which is a function of M_w, based on Boulanger and Idriss (2008) recommendation, adopted as 3 cycles; γ_c=current reversal shear strain; γ_t=threshold shear strain for PWP generation (considered at a G/G_{max} of 0.80 according to Vucetic 1995); *f*=dimensionality factor (assumed as 1 considering the 1D wave propagation); *p*, *F* and *s* = curve fitting parameters (can be obtained from undrained tests on saturated specimens). Since, CTX tests were only conducted on BP sand specimens and with the availability of PWP model parameters for only BP sand, for all the sandy layers, PWP parameters of BP sand were utilized. The values of *p*, *F* and *s* are considered at p' values close to that of the tested σ'_c conditions

from the experimental investigations presented in Chapter IV. Table 6.3 lists the PWP model parameters chosen for sandy layers of all the four sites.

In case of clayey soil layers, pore pressure variation is modelled using Matasovic and Vucetic (1995) model (Eqn. 6.8).

$$u_N = A \cdot N_c^{-3s(\gamma_c-\gamma_t)^r} + B \cdot N_c^{-2s(\gamma_c-\gamma_t)^r} + C \cdot N_c^{-s(\gamma_c-\gamma_t)^r} + D \quad (6.8)$$

Where, *r*, *s*, *A*, *B*, *C*, and *D* are the curve fitting parameters, which can be obtained by best fitting the results of undrained tests on clay specimens. As the undrained CTX tests conducted on clay samples are limited in number, formulations proposed by Carlton (2014) have been adopted to estimate the PWP parameters of clay layers (Eqns. 6.9-6.10).

$$s = 1.6374 \cdot PI^{-0.802} \cdot OCR^{-0.417} \quad (6.9)$$

$$r = 0.7911 \cdot PI^{-0.113} \cdot OCR^{-0.147} \quad (6.10)$$

where, *PI*=plasticity index (22 for PC and 19 for RS), *OCR*=over consolidation ratio (1.0 for both the clays). Other parameters have been adopted from the study of Matasovic and Vucetic (1995) for OCR of 1.0: *A*=7.6451, *B*=-14.7174, *C*=6.38, and *D*=0.6922. In order to model the PWP dissipation characteristics of the soil column, the consolidation characteristics (coefficient of consolidation) of the soil layers were calculated based on the empirical formulation proposed by Sridharan and Nagaraj (2004).

6.5 ANALYSES PERFORMED

Total of five series of analysis (three NL and two EQL) are performed with different objectives. The first series involves the EQL analysis of Site-1 to understand the effect of adopting different G/G_{max} and damping ratio curves in the seismic GRA studies. The artificial motions developed for Guwahati city shown in Fig. 6.4, have been used for the first set of analysis. Different G/G_{max} and damping ratio curves used in the analysis are: Seed and Idriss (1970) different ranges (lower range for $p' \leq 25$ kPa; mean curves for $75 \leq p' \geq 25$ kPa; and upper range $p' \geq 100$), Darendeli (2001) curves for sands and the experimentally obtained curves for different layers (Fig. 6.7). The literature review chapter depicts the data of Seed and Idriss (1970) and Darendeli (2001). Selection of these particular literature curves is motivated by their wide utilisation in GRA studies (Boulanger et al. 1999; Desai and Choudhury 2015; Chatterjee and Choudhury 2016; Kumar 2018). Fig. 6.11 presents the adopted G/G_{max} and *D* curves at 25 kPa of p'. All the

considered strain dependent dynamic soil properties (G/G_{max} and D curves) are inputted as discrete points in the DEEPSOIL program for first series of analysis. Table 6.4 lists the analysis program and the targeted investigations.

The second and third series involves NL analysis for all the four sites with varying level of intensity of PBRA. For the sites in northeastern India (Sites: 1-3), Rock outcrop motion shown in Fig. 6.4 (PBRA=0.146g) has been baseline corrected and linearly scaled to different intensities of PBRA (0.05g, 0.138g, 0.24g and 0.36g). The maximum PBRA chosen justifies the expected maximum seismic intensity in the region (0.36g as per IS 1893-2016). Linear scaling of the motion is performed to check the effect of varying intensity of motion (keeping other ground motion parameters constant) on the nonlinear response of soil. Similarly, for the Site-4 (Rohtak, Haryana), the chosen motion (Fig. 6.5) has been linearly scaled to achieve ground motions of varying intensity (0.05g, 0.10g, 0.24g and 0.36g) with the maximum intensity matching the maximum expected seismic intensity of the region (0.36g according to IS 1893-2016).

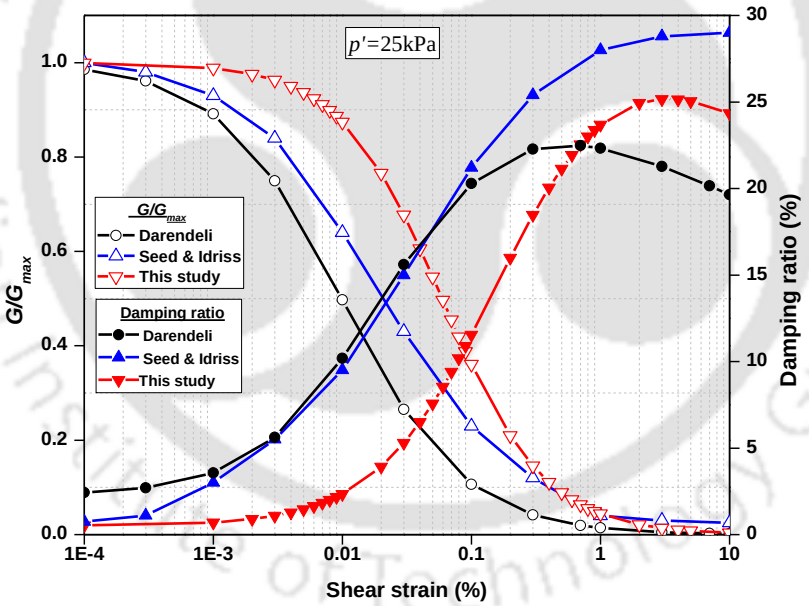

Fig. 6.11 Various curves used at 25 kPa overburden depth for first series of analysis

Table 6.4 List of analysis performed and parameters of investigation

Series	Approach	Site	Ground motions	Investigations
I	EQL	Site-1	Simulated motions for Guwahati (0.146g, 0.166g, 0.185g)-Fig. 6.4	Effect of using different G/G_{max} and D curves
II	NL	Sites 1-3	Scaled ground motions of Guwahati (0.05g, 0.138g, 0.24g, 0.36g)	Effect of PBRA on accelerations, stresses, strains and liquefaction characteristics of soil deposits
III	NL	Site-4	Scaled ground motions of recorded Chamoli event-Fig. 6.5(0.05g, 0.10g, 0.24g, 0.36g)	Effect of PBRA on accelerations, stresses, strains and liquefaction characteristics of soil deposits
IV	EQL	Sites 1-3	Scaled ground motions of Guwahati (0.05g, 0.138g, 0.24g, 0.36g)	For comparison of EQL results to NL in terms of PGA, stresses and strains
V	EQL	Site-4	Scaled ground motions of recorded Chamoli event-Fig. 6.5(0.05g, 0.10g, 0.24g, 0.36g)	

The fourth and fifth set of analysis involve EQL approach for the four chosen sites for similar ground motions as in set II and set III of analysis. This has been done essentially to understand the differences of the methodology on the nonlinear soil response due to the increasing motion's intensity. The base of the four chosen sites is simulated as deformable strata with appropriate V_s as derived from SPT N- V_s relationship (Eqn. 6.5). The selected ground motions are then applied at the base of the soil column.

6.6 RESULTS AND DISCUSSIONS

The results section is divided in to four major subsections with different objectives. The first subsection discusses the importance of site-specific soil properties in GRA studies using the first set of analysis (EQL for Site-1). The second section provides a comparative study on the EQL and NL approaches for varying PBRA motions. Third section discusses the effect of increased PBRA intensity on nonlinear response of soils. The last subsection provides a discussion on the response of soil deposits in northeastern India for different levels of seismic intensity.

6.6.1 Significance of Site-Specific Properties in GRA

Fig. 6.12 presents the PGA variation along the depth for different soil curves, for the three ground motions considered. It can be noted that the experimentally obtained curves predict higher values of PGA than the response estimated by the standard curves over the entire depth, especially in the loose surficial layers (top 11 m). The PGA at surface from the curves developed experimentally for 0.146g input bedrock motion is 0.24g while it is 0.171g and 0.158g for Seed and Idriss (1970) curves and Darendeli (2001) curves, respectively. Similar trend of acceleration amplifications has been observed for all the

ground motions considered. Table 6.5 summarizes the surface acceleration amplifications for the soil curves for all the ground motions considered. It is clear that the surface accelerations are being under estimated by almost 30 to 40% with the standard empirical soil curves. In order to examine the reason for such amplification, effective shear strain profiles along the depth for all the considered soil models are presented in Fig. 6.13. It may be observed that the soil column experienced maximum effective strains up to 0.1%, with highest occurring at 10 m from the surface. The modulus and damping curves at 10 m location (at $p' \approx 25$ kPa) for the three soil models are shown in Fig. 6.11. Although the strains induced in the soil column for experimentally derived curves are narrowly less than those of the other three models, at such strain levels, the soil curves obtained from experimental investigations furnish higher modulus ratio (less non-linearity) and lower damping ratio, due to which such acceleration amplifications are witnessed.

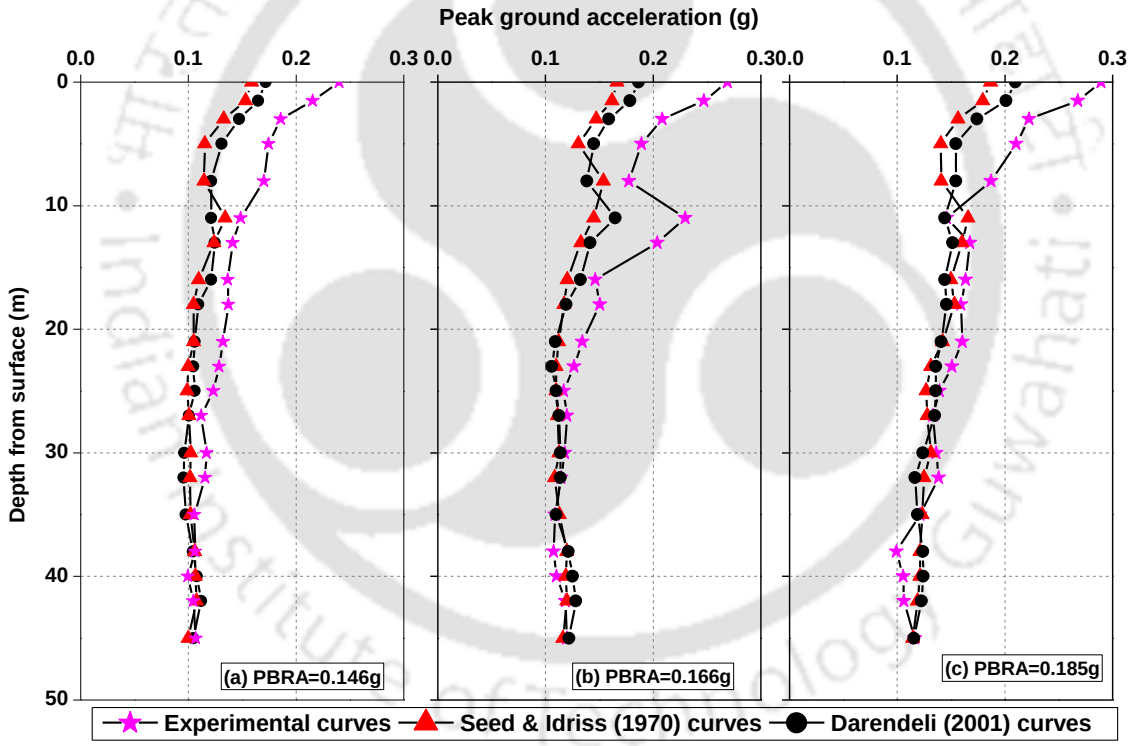

Fig. 6.12 PGA profiles from EQL study for Site-1

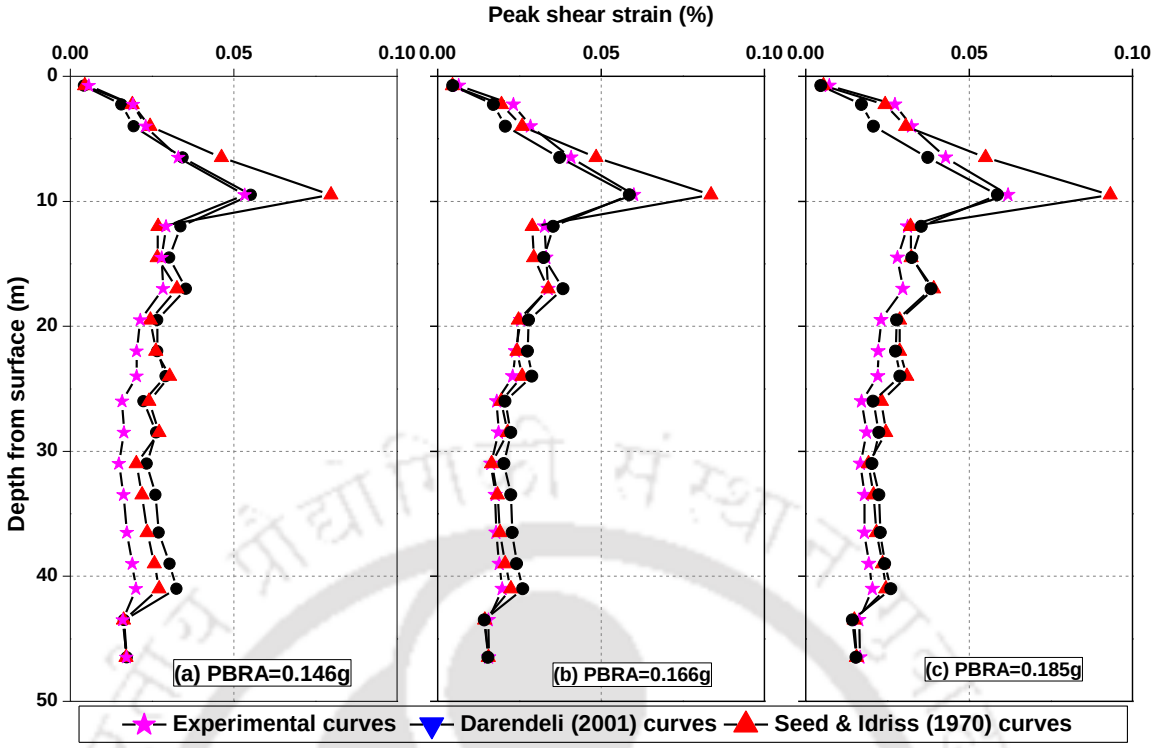

Fig. 6.13 Effective shear strain profile for Site-1 based on EQL GRA

Table 6.5 Comparison of percentage difference in surface PGA using different soil curves

Input bedrock PGA, g	Surface PGA, g (experimental curves)	Darendeli (2001) curves		Seed and Idriss (1970) curves	
		PGA, g	% difference	Surface PGA, g	% difference
0.146	0.240	0.171	-28.75	0.158	-34.16
0.160	0.274	0.169	-38.32	0.157	-42.70
0.166	0.268	0.186	-30.59	0.166	-38.05
0.185	0.289	0.192	-33.56	0.186	-35.64

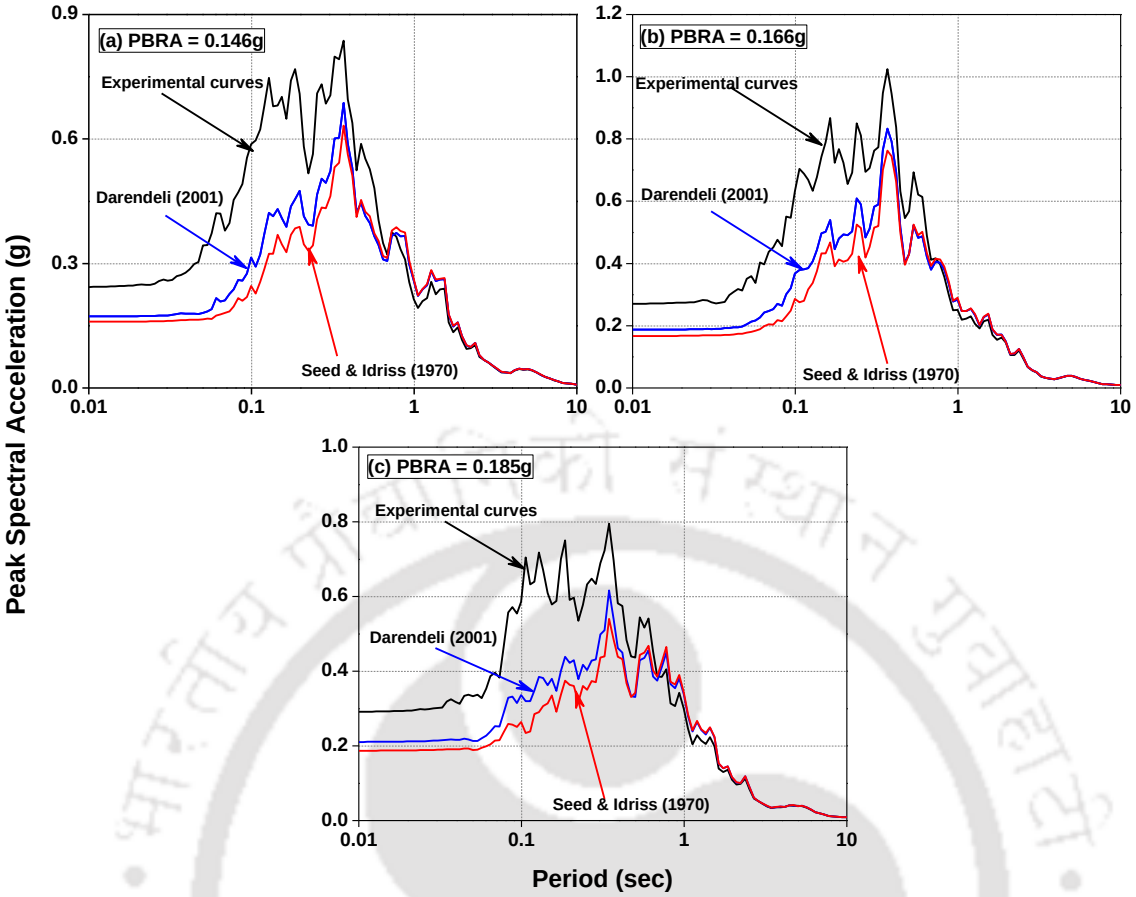

Fig. 6.14 PSA response obtained for Site-1 based on EQL GRA

Fig. 6.14 presents the peak spectral accelerations (PSA) at the surface using different modulus and damping curves for all the input ground motions considered. A similar trend of higher amplification in spectral accelerations can be observed for all the ground motions for the experimentally obtained soil curves. The higher amplifications in the PGA values and the corresponding spectral accelerations are attributed to the wide variation in the G/G_{max} and damping characteristics of the soils. Similar findings were also reported by Hwang and Lee (1992), Zhang et al. (2005) and Kumar et al. (2018a). This may infer that the utilisation of standard curves from literature would often underestimate the seismic demands and therefore, the use of experimentally obtained curves is strongly suggested.

6.6.2 Comparison of Soil Response from EQL and NL Analysis

A comparison is made in Fig. 6.15 and Fig. 6.16 for the ground responses of all four sites obtained using both the EQL and NL approaches for four ground motions of increasing intensity. It can be seen that the PGA response of low intensity motions (0.05g and 0.138g as seen in Fig. 6.15) show similar response for both the approaches for all the sites. However, as the intensity of ground motion increases (0.24g and 0.36g as shown in Fig.

6.16), variation in PGA along the depth differs for both the approaches. Such negligible variations for the low intensity motions and significant differences for high intensity motions can be explained by the induced strains in the soil. Fig. 6.17 and Fig. 6.18 present the peak shear strains induced for both the approaches along the depth, for both the approaches. As it can be noted that the induced strains are consistent for both the approaches for low intensity motions (Fig. 6.17), while the high intensity motions yielded significant strain differences for all the chosen motions (Fig. 6.18). For both the approaches, the low intensity motions yielded low shear strains, requiring only the elastic nature of the soil to be in action, for which the response is expected to be same for EQL and NL approaches (Garala and Madabhushi 2018). Despite using the same G/G_{max} and D curves in both the approaches, high intensity motions yielded high strains in case of NL approach due to the plastic deformations induced by the pore water pressures. Such soil yielding is not considered in EQL approach as it is an approximated nonlinear approach without fully capturing the dynamic nonlinearity of the soil.

In order to understand the stress-strain response obtained using EQL and NL approaches, the shear strain history for all the chosen motions at 10 m depth for Site-1 is shown in Fig. 6.19 and Fig. 6.20. It can be clearly seen that for the low intensity motions (Fig. 6.19), magnitude of shear strain is reasonably consistent for both the approaches. However, for high intensity motions (Fig. 6.20 a and b), significant variation in magnitudes prevail along with a plastic soil deformation in case of NL approach. A peak shear strain of 0.065% can be noted in case of 0.24g event for NL approach along with some plastic deformations at the end of excitation (Fig. 6.20 a), while less shear strains and no permanent deformations are observed in EQL results. Similarly, in case of 0.36g event (Fig. 6.20 b), 0.05% of peak shear strain and 0.016% permanent deformation of soil is observed in NL approach, while EQL approach yielded relatively less magnitude of shear strains with no traces of plastic deformation.

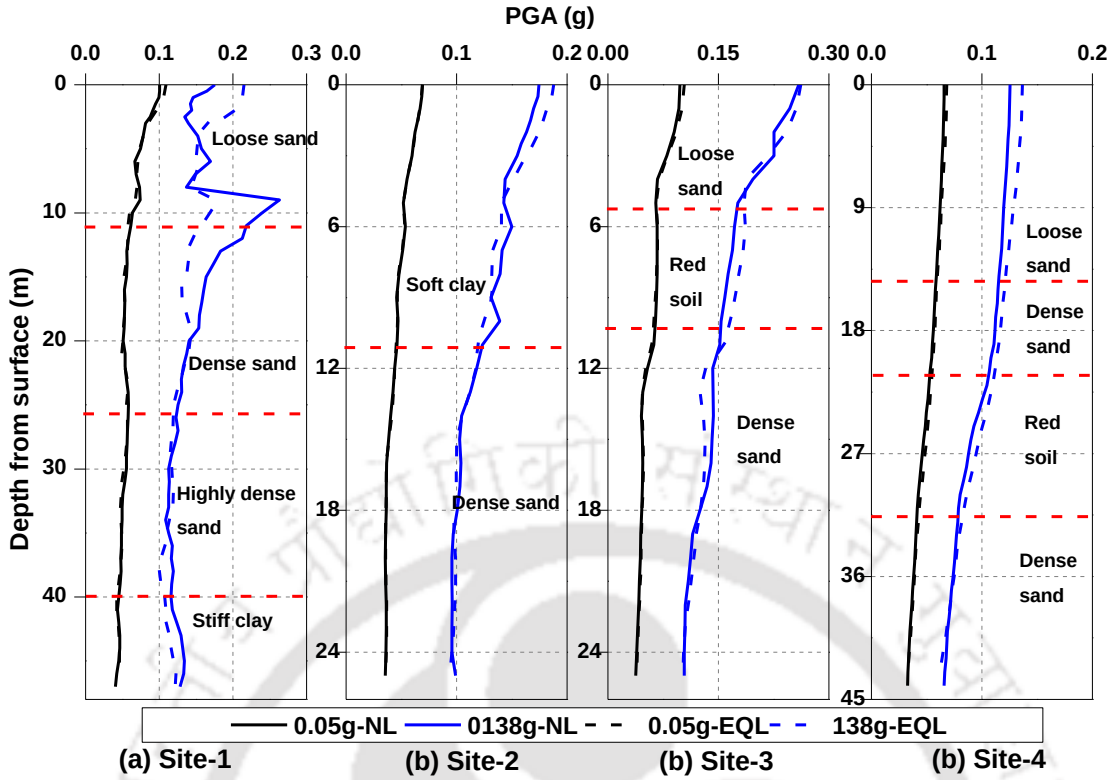

Fig. 6.15 PGA profiles for 0.05g and 0.138g ground motions

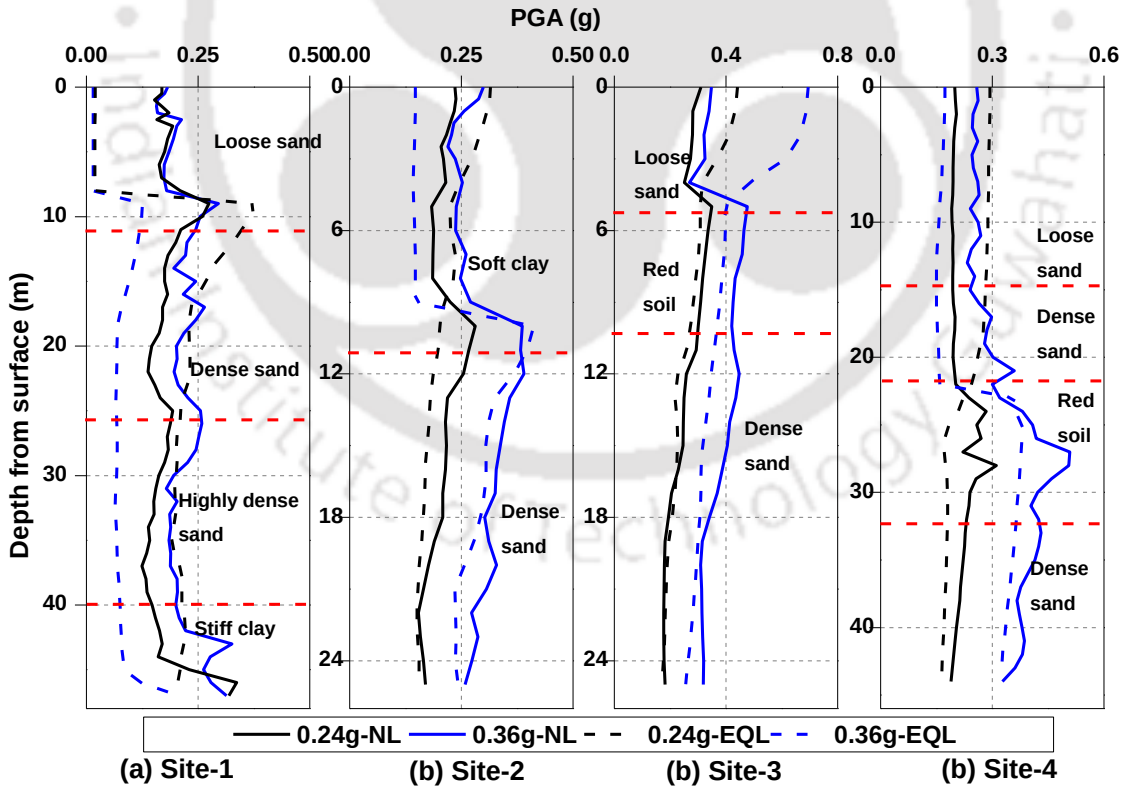

Fig. 6.16 PGA profiles for 0.24g and 0.36g ground motions

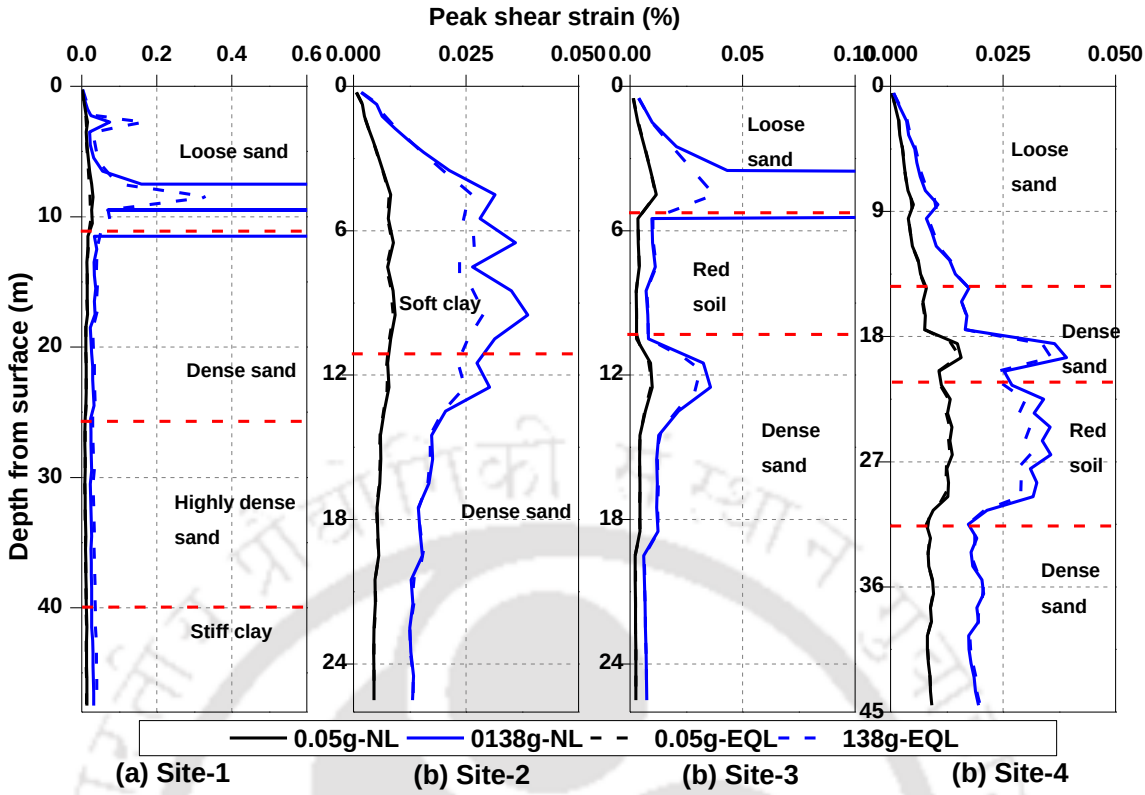

Fig. 6.17 Peak strain profiles for 0.05g and 0.138g ground motions

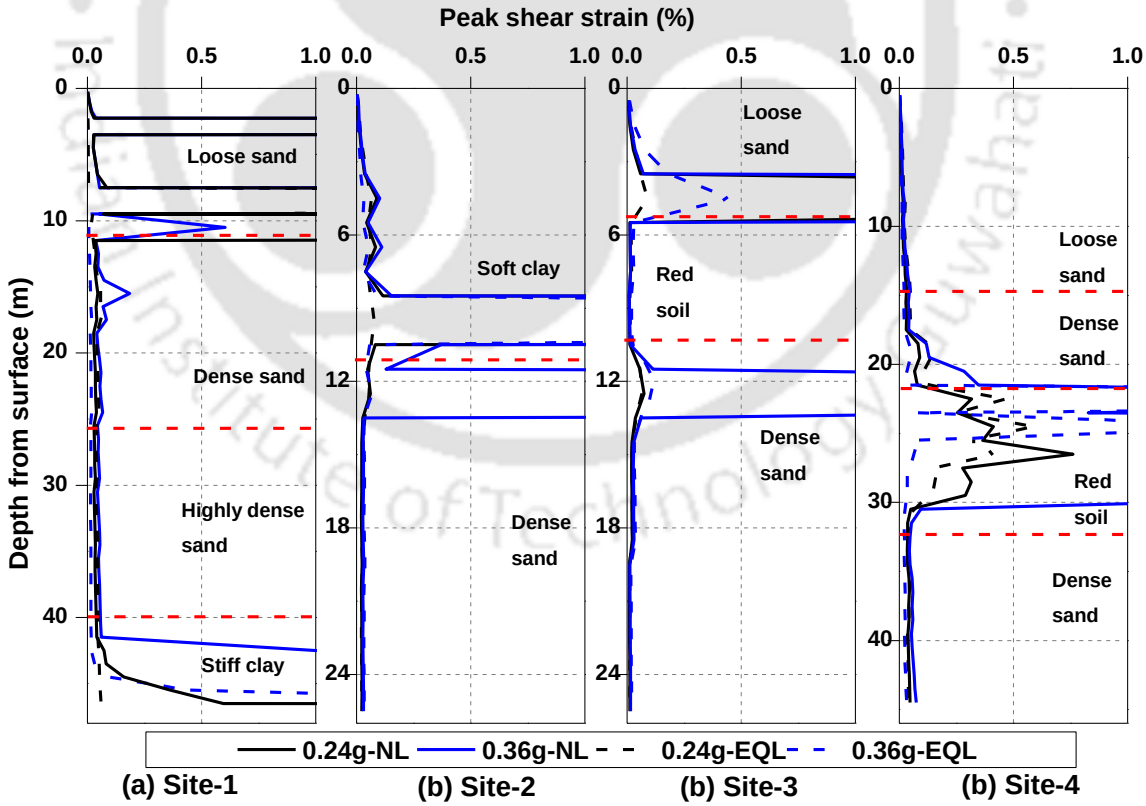

Fig. 6.18 Peak strain profiles for 0.24g and 0.36g ground motions

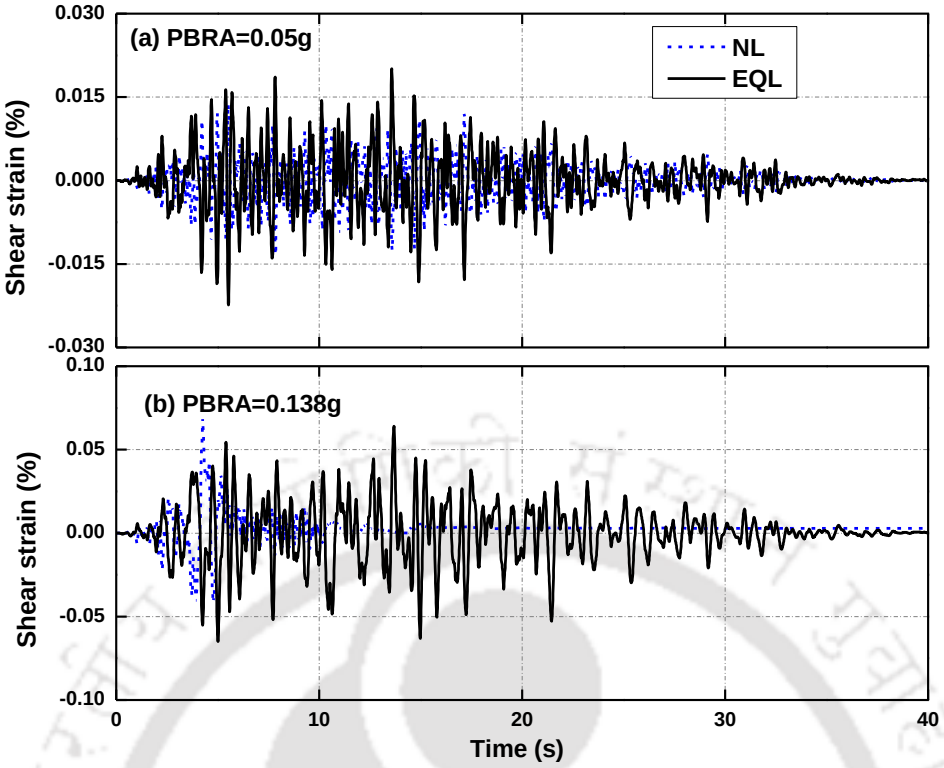

Fig. 6.19 Shear strain histories of **(a)** 0.05g and **(b)** 0.138g motions at 10 m depth for Site-1

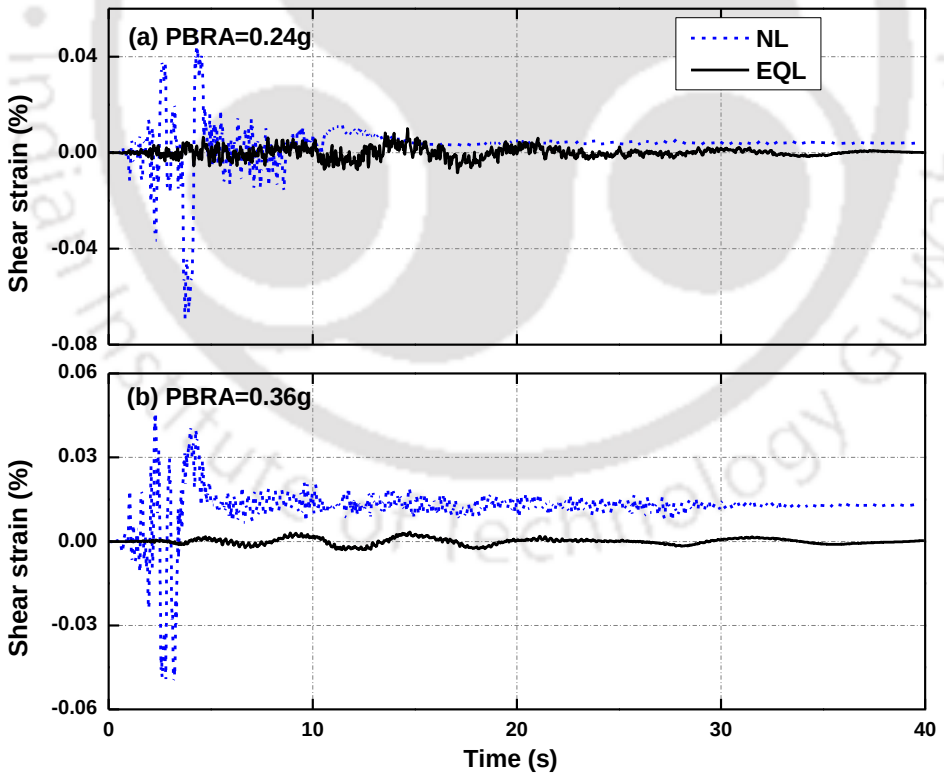

Fig. 6.20 Shear strain histories of **(a)** 0.24g and **(b)** 0.36g motions at 10 m depth for Site-1

The shear stress-strain response of the soil deposit at 10 m depth for Site-1 for the four motions is depicted in Fig. 6.21. It can be noted that the EQL analysis showed almost linear

response even at high shear strains for high intensity motions. As mentioned, EQL approach is a simplified approach and cannot incorporate the realistic in-situ characteristics of soil, such as pore water pressures and corresponding plastic strains, which are necessary properties in case of soft soils subjected to intense seismic events. This discussion therefore highlights the necessity of nonlinear approach for intense seismic events, in effectively simulating the complex dynamic soil characteristics such as soil yielding and liquefaction characteristics.

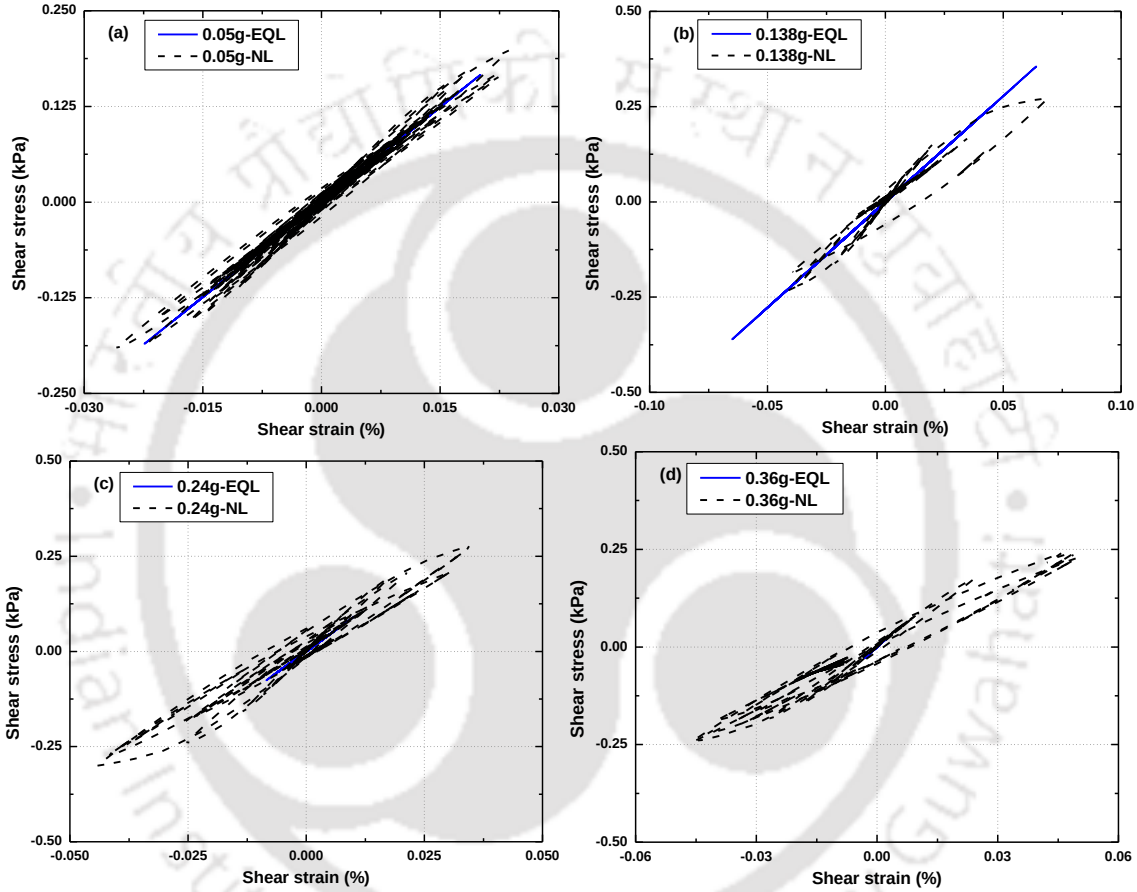

Fig. 6.21 Shear stress-shear strain response obtained from EQL and NL approaches at 10 m depth for Site-1 for **(a)** 0.05g **(b)** 0.138g **(c)** 0.24g and **(d)** 0.36g motions

6.6.3 Nonlinear Analysis Results

Results obtained from the NL GRA are presented in terms of accelerations, stresses, strains and pore water pressure variations for the four sites. As the chosen sites have different layers of stratification (Table 6.1), effects of varying intensity (PBRA) of ground motion (GM) on the seismic response of layered soils are highlighted.

Acceleration Response

The acceleration variations induced in the soil column at different depths for Sites-1, 2, and 3 for the four considered ground motions, are shown in Fig. 6.22, Fig. 6.23, and Fig.

6.24, respectively. It can be seen that the induced accelerations vary significantly along the depth with a pattern of increasing intensity towards the surface for relatively low intensity motions (0.05g and 0.138g motions). In contrast, a decreasing trend of accelerations towards the surface can be noted, for high intensity motions (0.24g and 0.36g events). For site-1, 0.05g motion induced a surface acceleration of 0.10g (twice that of base intensity) and while 0.175g, 0.168g and 0.182g of surface accelerations were noted for 0.138g, 0.24g and 0.36g PBRA motions. Such phenomenon of high surface accelerations for low intensity motions and vice-versa can be justified by the high viscous damping of the soft soils at the surface at high strains. Seismic events with increasing intensity induce high shear strains in the soil leading to high damping ratio, which will dampen the accelerations upon reaching the surface. Similarly, the low intensity motions induce lower shear strains leading to only low viscous damping and increased accelerations towards the surface. An important observation can be drawn from the acceleration response along the depth (Fig. 6.22, Fig. 6.23, and Fig. 6.24), with increase in the PBRA of the input motion, accelerations towards the surface are damped (ceased to cycle) after certain duration of the motion. This trend of acceleration ceasing (reduction of energy content of the motion) is predominantly visible in the loose sand and soft clayey soils. Existence of loose fine sand for top 11m depth at Site-1, presence of soft clay up to 11m from surface of Site-2, and surficial 5m loose sandy stratum at Site-3 are the examples of this observation. Such acceleration dampening (for high intensity motions) in the loose soils may be due to the pore pressure generation, causing the loss of particle-to-particle contact and ceasing of seismic energy movement between the soil particles. However, for stiff layers of soil (deeper stratum) where complete loss of contact is not expected, such acceleration dampening may not be visible.

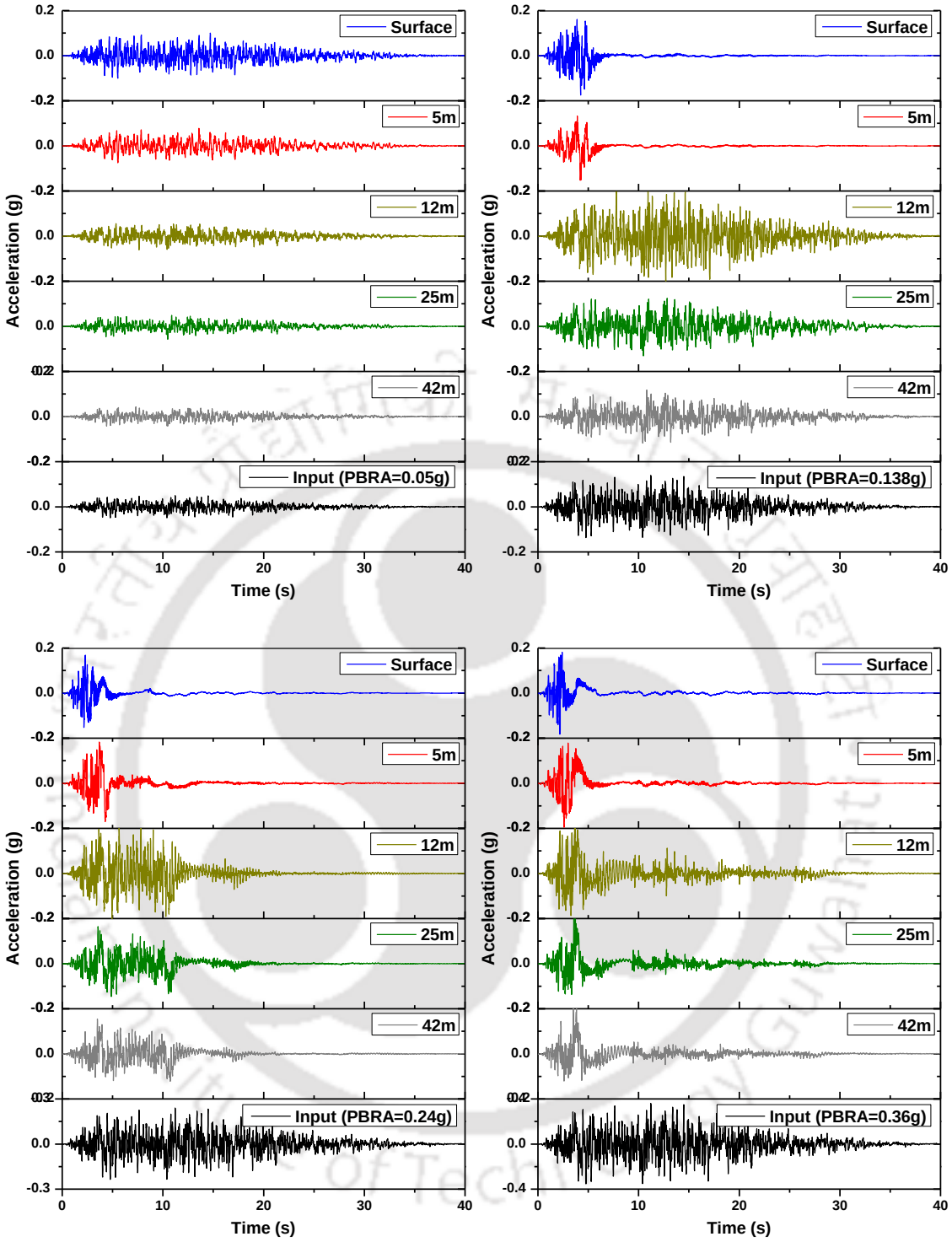

Fig. 6.22 Acceleration histories along the depth for four motions at Site-1

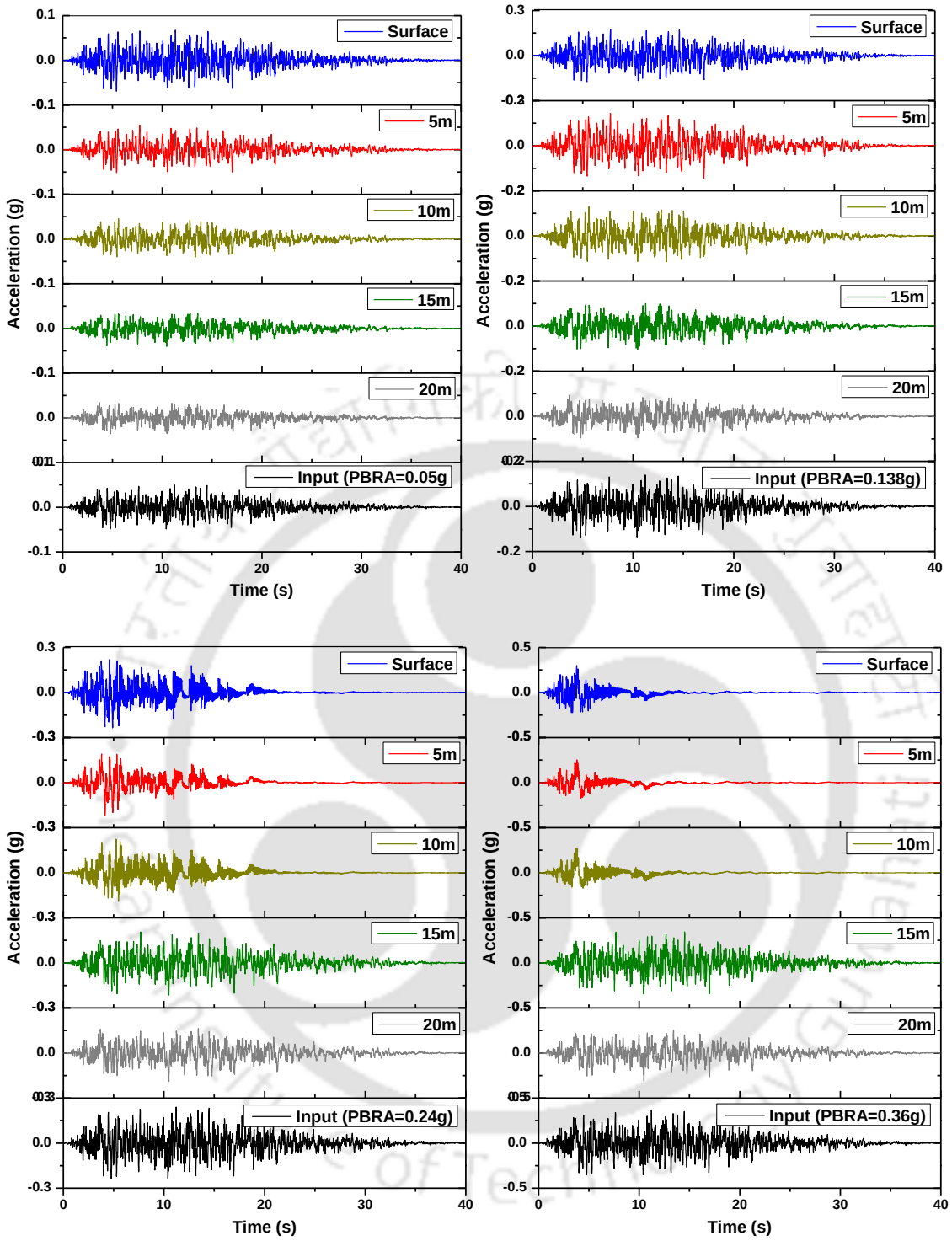

Fig. 6.23 Acceleration histories along the depth for four motions at Site-2

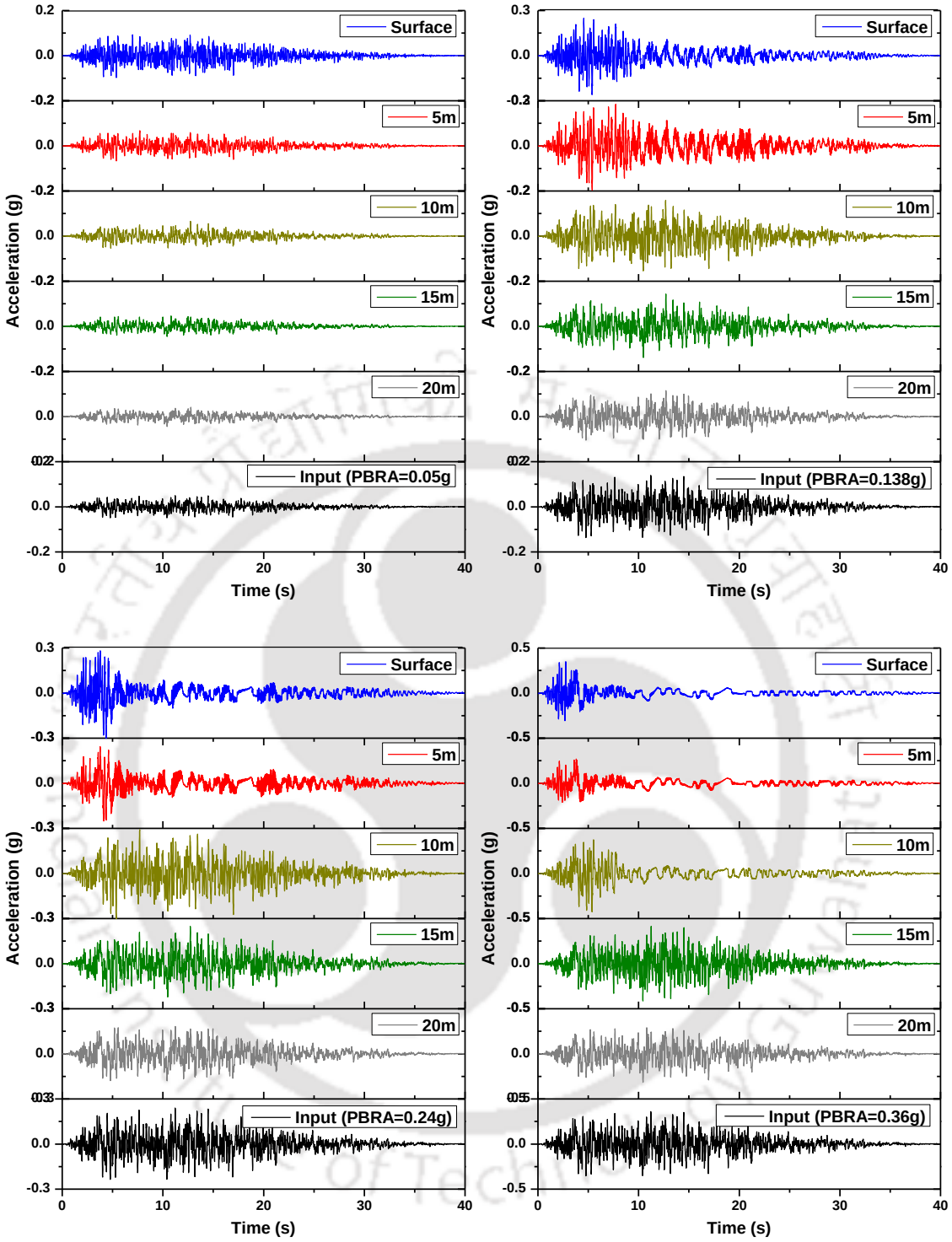

Fig. 6.24 Acceleration histories along the depth for four motions at Site-3

The variation of PGA, percentage change in PGA and pore water pressure ratio (r_u) along the depth are shown in Fig. 6.25, Fig. 6.26, Fig. 6.27, and Fig. 6.28, respectively, for the four ground motions in all the four sites. The percentage change in PGA is the difference of PGA at any depth to the input PBRA, represented as percentage. As noted in the acceleration response along the depth, the PGA increased towards the surface for 0.05g

motion while decrease of PGA can be observed for high intensity motions. An amplification of 100% can be observed for 0.05g motion while +27%, -30% and -50% of change in PGA was observed for the 0.138g, 0.24g and 0.36g motions, respectively (Fig. 6.25b). Fig. 6.29 (a-d) presents the peak spectral acceleration (PSA) in the soil column at different depths. Increased PSA towards the surface for 0.05g and 0.138g motions can be seen, while decreased PSA for 0.24g and 0.36g is witnessed. Such amplification or attenuation (deamplification) can be justified by the relatively high damping of the loose soils. It can also be seen that the surficial 11m (loose sandy stratum) of Site-1 experienced liquefaction ($r_u \approx 1.0$ in Fig. 6.25c) for the three motions (0.138g, 0.24g and 0.36g) leading to loss of particle contact, thereby resulting in dampening of the acceleration response at the surface for the three motions (Fig. 6.25a). The profiles (PGA, % change in PGA and r_u) in the dense stratum (12m to 42m) did not show abrupt changes due to the presence of dense sandy stratum.

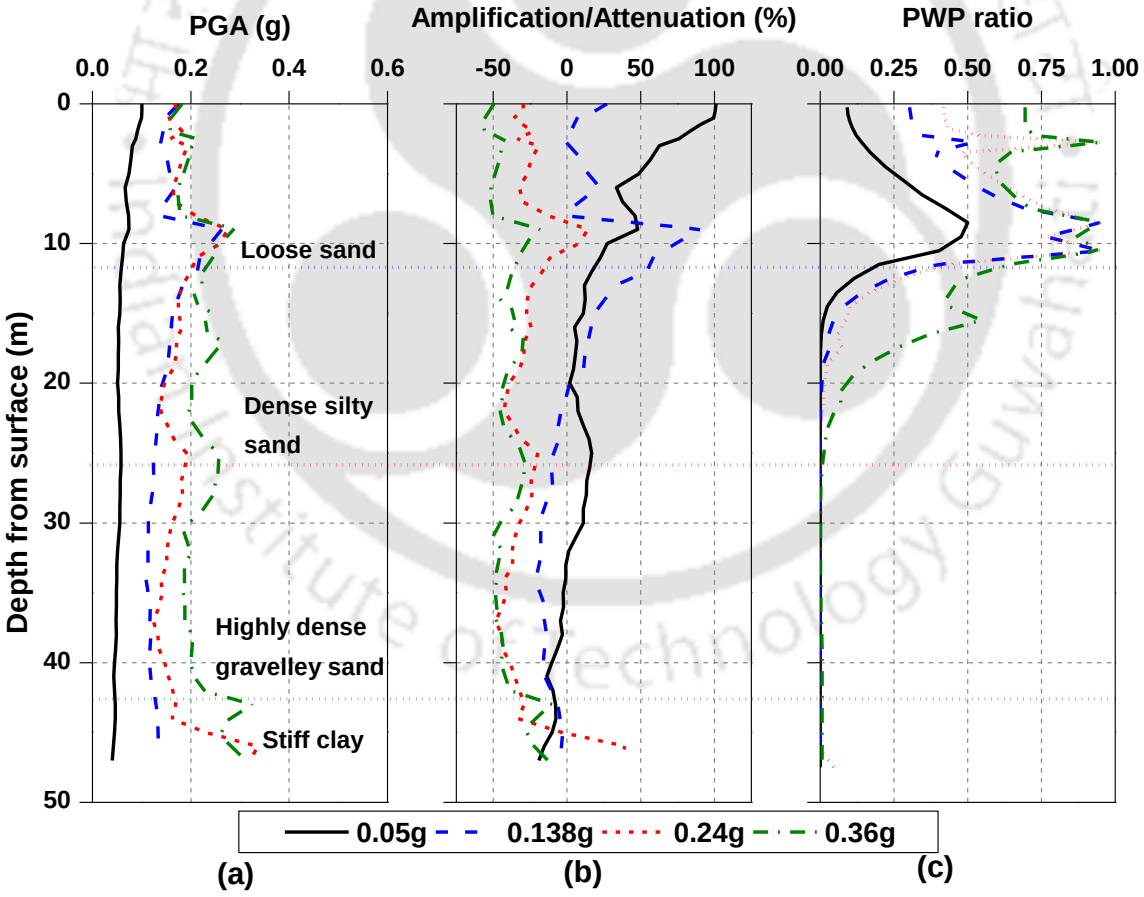

Fig. 6.25 Profiles of **(a)** PGA **(b)** Amplification/attenuation **(c)** r_u for Site-1

In case of Site-2 (soft clay stratum followed by dense sand), similar amplification of PGA at surface (in the range of 30 to 40%) was observed for 0.05g and 0.138g motions and

attenuation (in the range of 5% to 30%) was noted for high intensity motions (0.24g and 0.36g). The surficial soft clay stratum of Site-2 (Pachoria Cohesive soil with cohesion of 20kPa) showed significantly lower PGA and high attenuation, due to the liquefaction triggering of the clayey stratum (Fig. 6.26c). The maximum stress ratio (ratio of induced shear stress to the p') obtained from NL GRA for low intensity motions is less than 0.20 and ranges from 0.30 to 0.60 for high intensity motions. As described in the section 5.5 of Chapter V, PC samples (in CTX tests) did not generate significant pore pressures for CSR 0.20 till 40 cycles of loading, and for CSR of 0.40, liquefaction triggered in the first 20 cycles of loading, which is consistent with the NL GRA results obtained (Fig. 6.26c). Similarly, the surficial loose fine sand of Site-3 experienced liquefaction (Fig. 6.27c) for the high intensity motions, thereby causing acceleration attenuation in the liquefied stratum. This confirms the phenomenon of attenuation of accelerations in liquefiable soils due to the loss of particle contact and resulting ceasing of seismic energy movement and high viscous damping of the liquefied crest (Lombardi and Bhattacharya 2016).

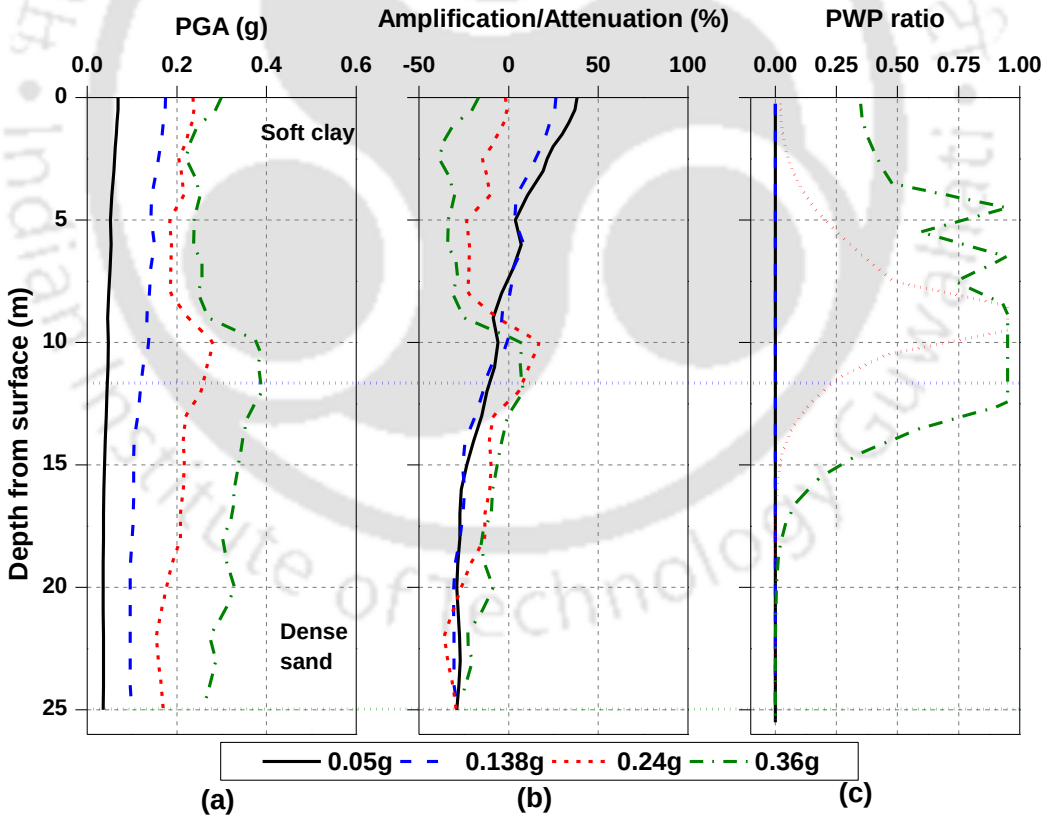

Fig. 6.26 Profiles of **(a)** PGA **(b)** Amplification/attenuation **(c)** r_u for Site-2

No traces of liquefaction were seen at Site-4 from the PWP ratio variation (Fig. 6.28c) although r_u values are close to 0.50 in the clayey stratum (20m to 32m). At such depth, significant % PGA change can be observed (Fig. 6.28b) showcasing the possible shift of

liquefaction triggering on the acceleration response of the soil deposits. As observed in the northeastern sites (Sites-1 to 3), amplifications were observed for low intensity motions while attenuations are noted for high intensity motions at Site-4.

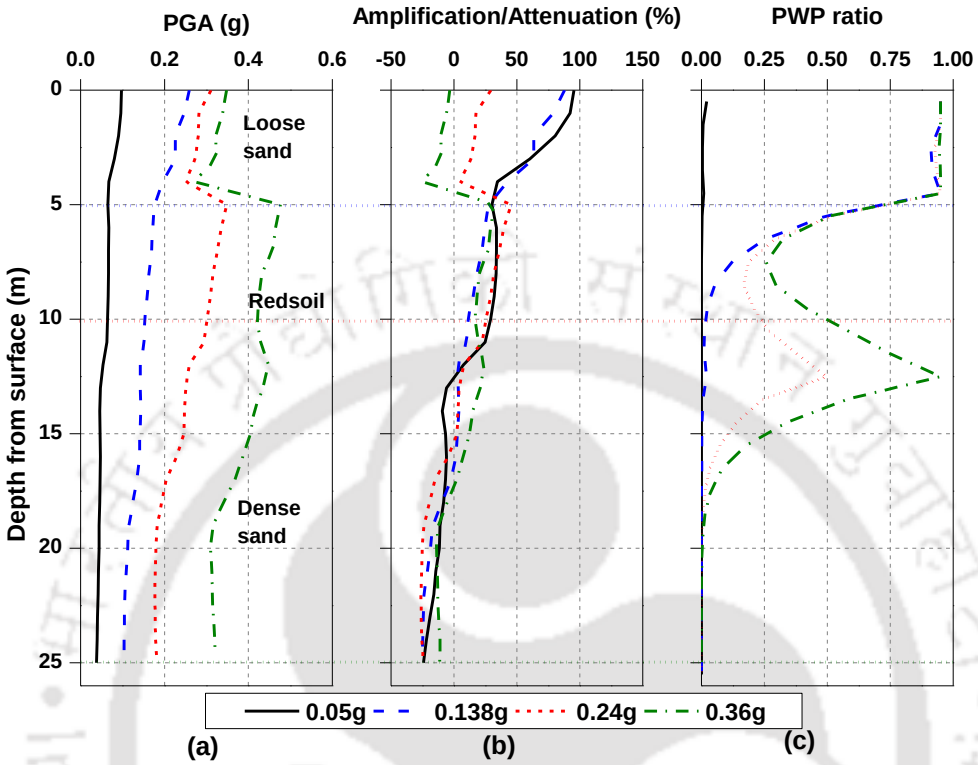

Fig. 6.27 Profiles of **(a)** PGA **(b)** Amplification/attenuation **(c)** r_u for Site-3

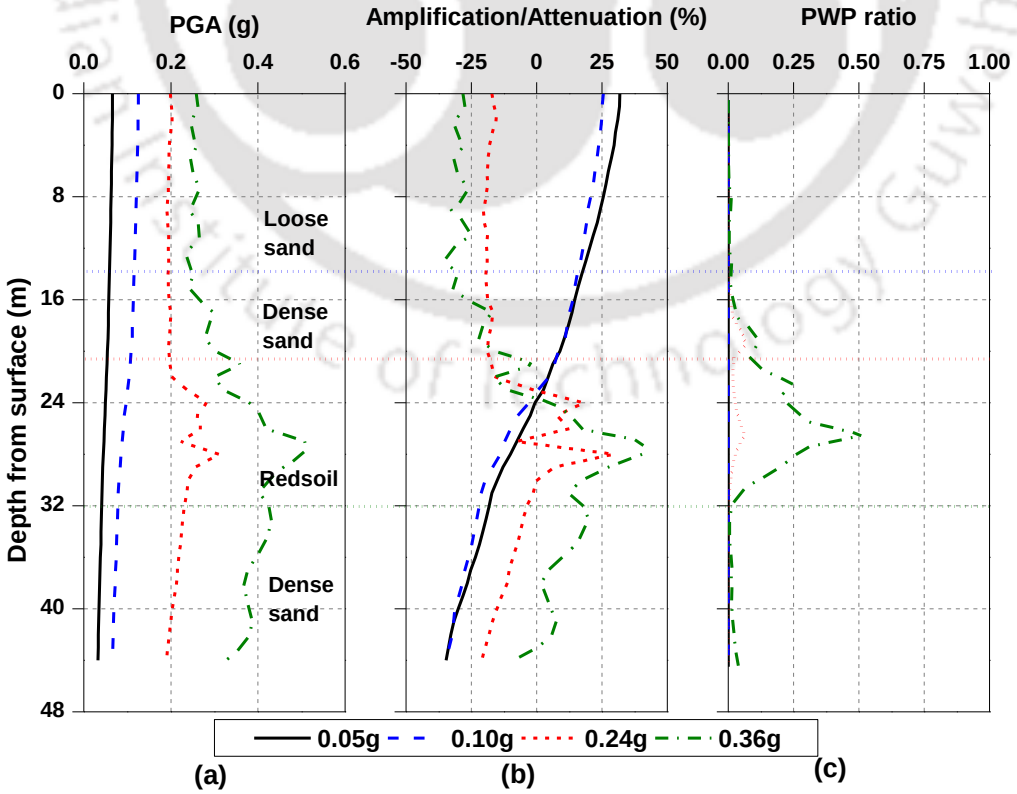

Fig. 6.28 Profiles of **(a)** PGA **(b)** Amplification/attenuation **(c)** r_u for Site-4

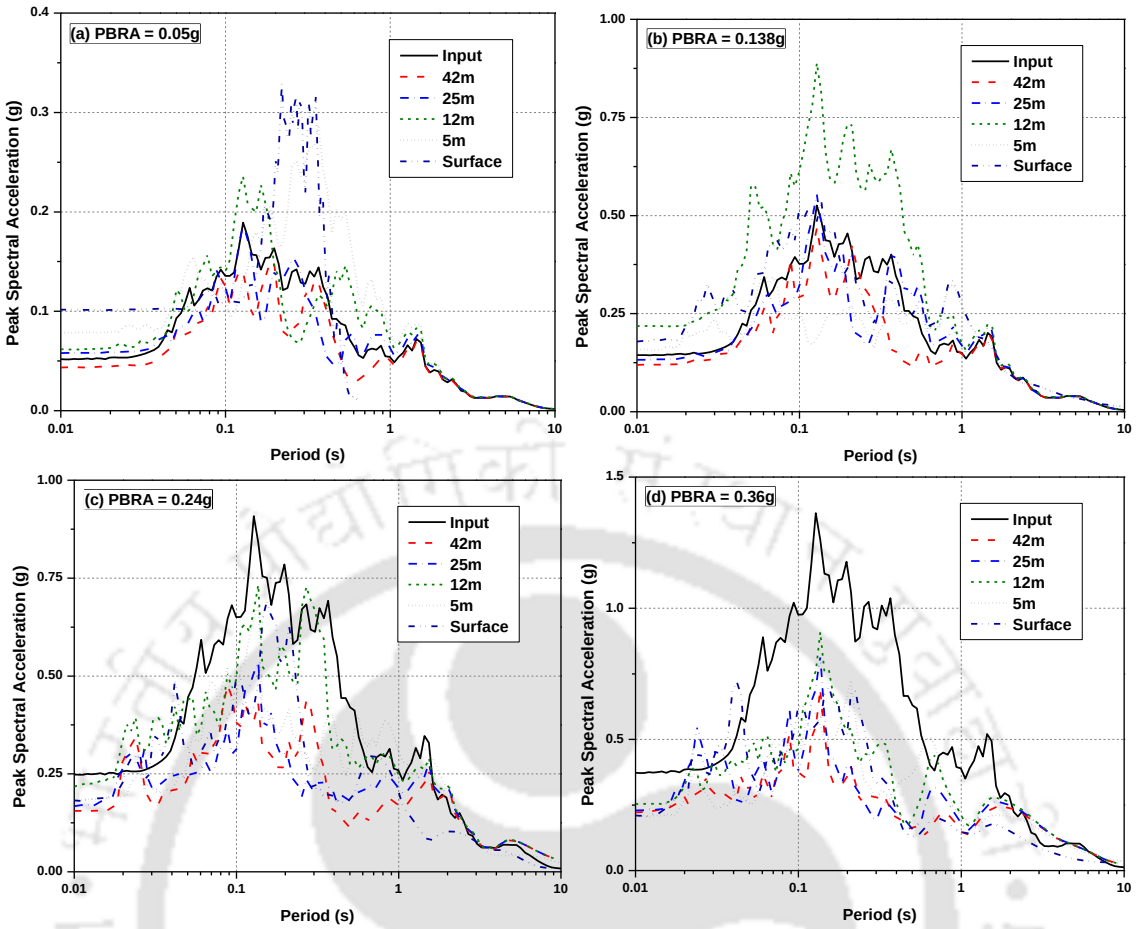

Fig. 6.29 PSA response for Site-1

Liquefaction Analysis

The influence of ground motion intensity on the pore water pressure variation at different depths for Site-1 is shown in Fig. 6.30. The smallest intensity motion (0.05g) chosen did not induce liquefaction (Fig. 6.30a), while remaining motions liquefied the loose stratum (top 11m). Similarly, Site-2 and 3 also showed increased tendency of liquefaction with increased intensity of motion (Fig. 6.31 and Fig. 6.32).

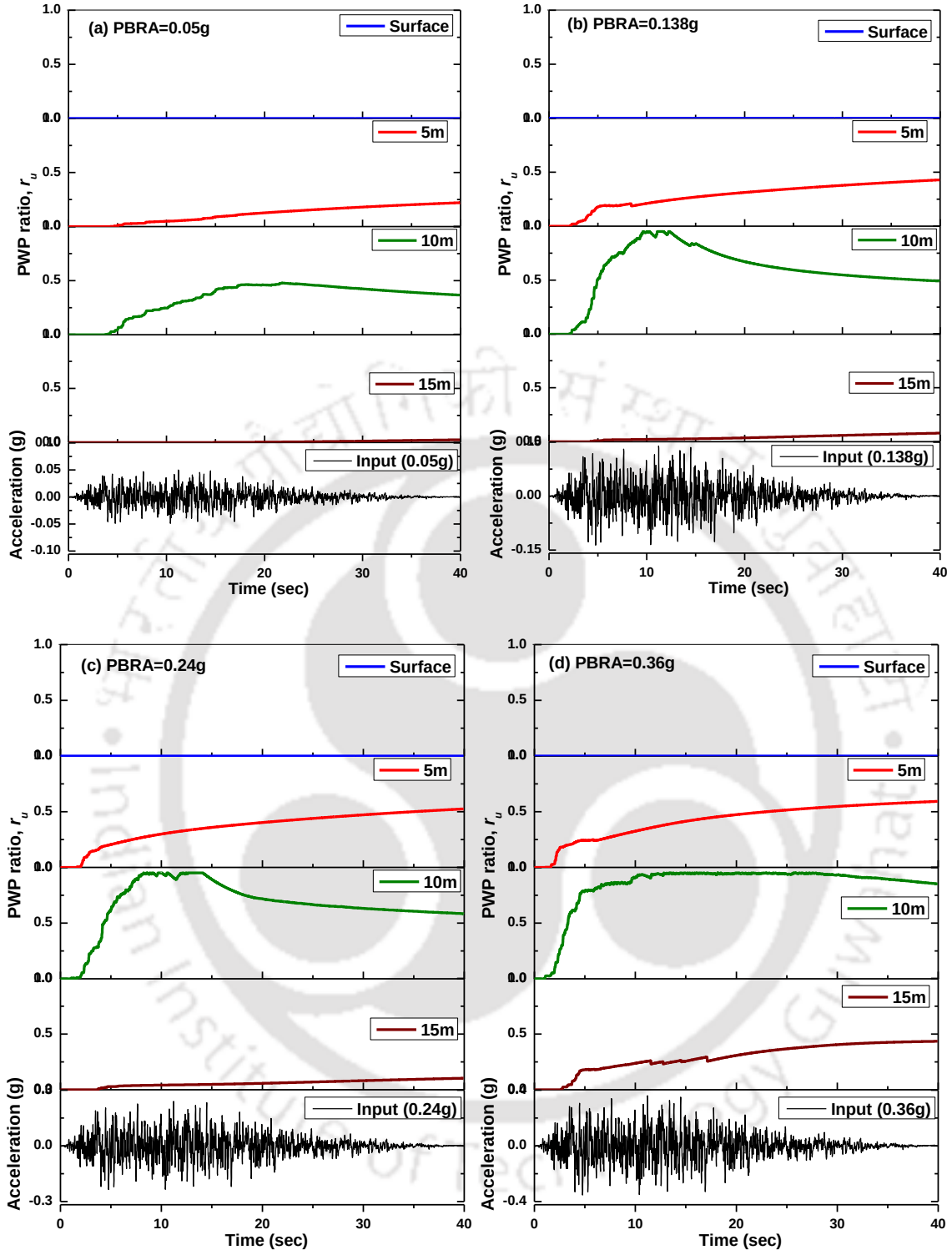

Fig. 6.30 The r_u histories for four chosen motions at Site-1

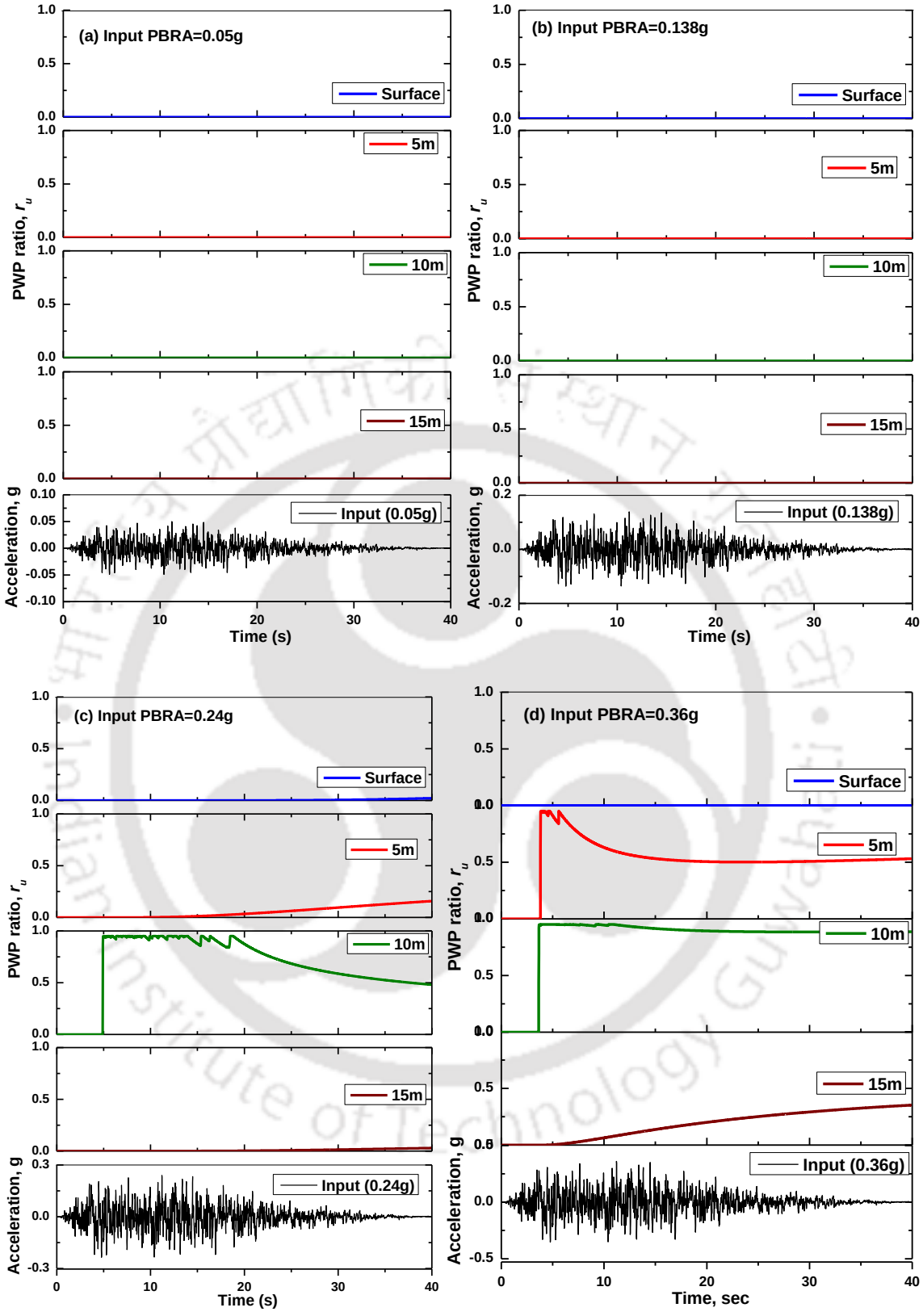

Fig. 6.31 The r_u histories for four chosen motions at Site-2

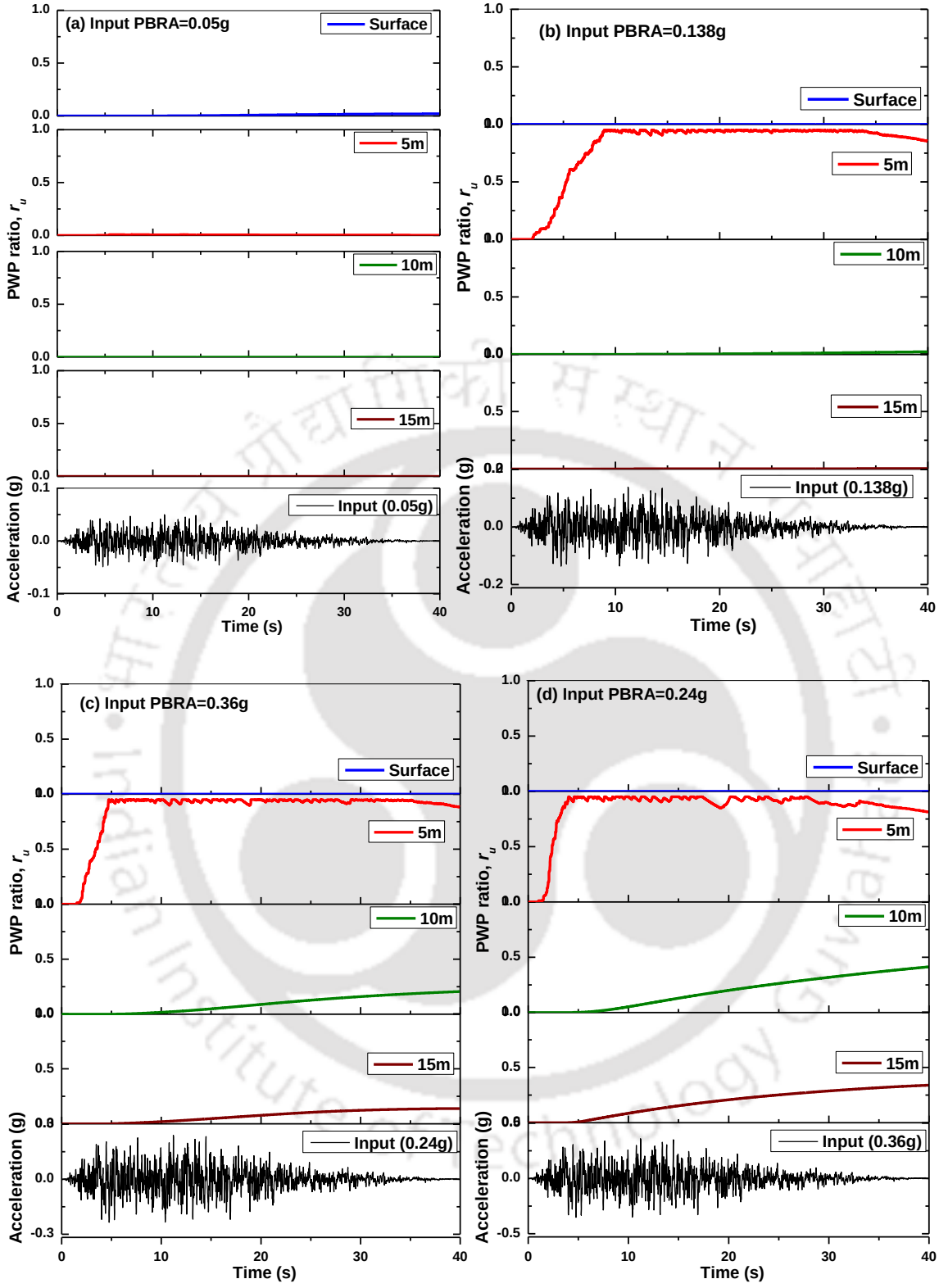

Fig. 6.32 The r_u histories for four chosen motions at Site-3

Effect of intensity of ground motion on the initiation and duration of liquefaction is discussed here. Fig. 6.33 presents the r_u histories for the four ground motions at 10 m and 3 m depth (loose sandy stratum) at Site-1. At 10m depth (Fig. 6.33a), PWP started

increasing at 4sec for 0.05g, while the same is 3sec, 2sec and 1.4 sec for 0.138g, 0.24g and 0.36g motions. Similarly, at 3m depth (Fig. 6.33b), pore pressures initiated at 5sec for 0.05g,while the motions 0.138g, 0.24g, and 0.36g took 2.5sec, 2sec and 1.6sec respectively to initiate the pore pressures in the soil column at a particular depth. This shows that the initiation of liquefaction quickens with the increase in intensity of ground motions. Fig. 6.34 presents the r_u variation at 5 m and at 0.5 m from the ground surface, for the chosen motions at Site-3. At 5 m depth (Fig. 6.34a), the total time taken for the soil to liquefy (duration of liquefaction-DU_{liq} from r_u of 0.05 to 0.95) in case of 0.138g is 5.69 sec which reduced to 2.64 sec and 2.14 sec for 0.24g and 0.36g motions respectively. Similarly at 0.5 m depth of Site-3 (Fig. 6.34b), decreased duration of liquefaction was noted with increased intensity of ground motion. This confirms that the intensity of input motion decreases DU_{liq} due to the high energy content of the high intensity motions.

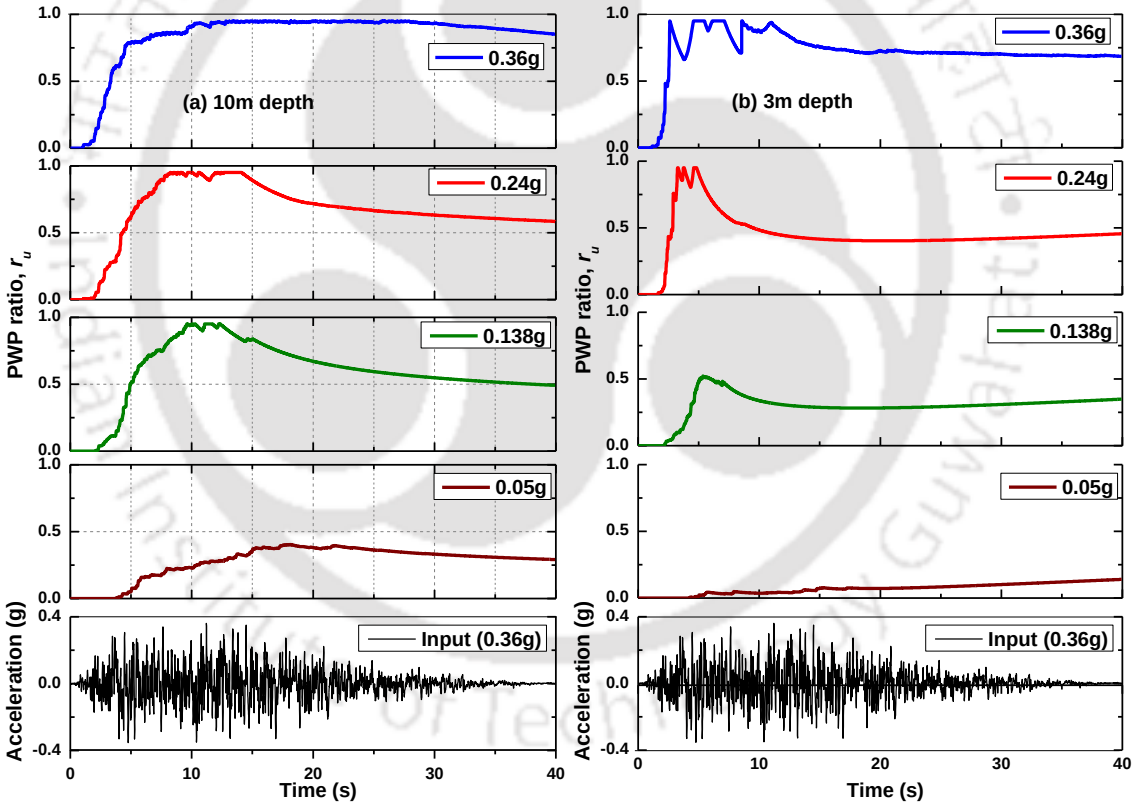

Fig. 6.33 r_u histories for different motions at Site-1 at **(a)** 10 m and **(b)** 3 m depth

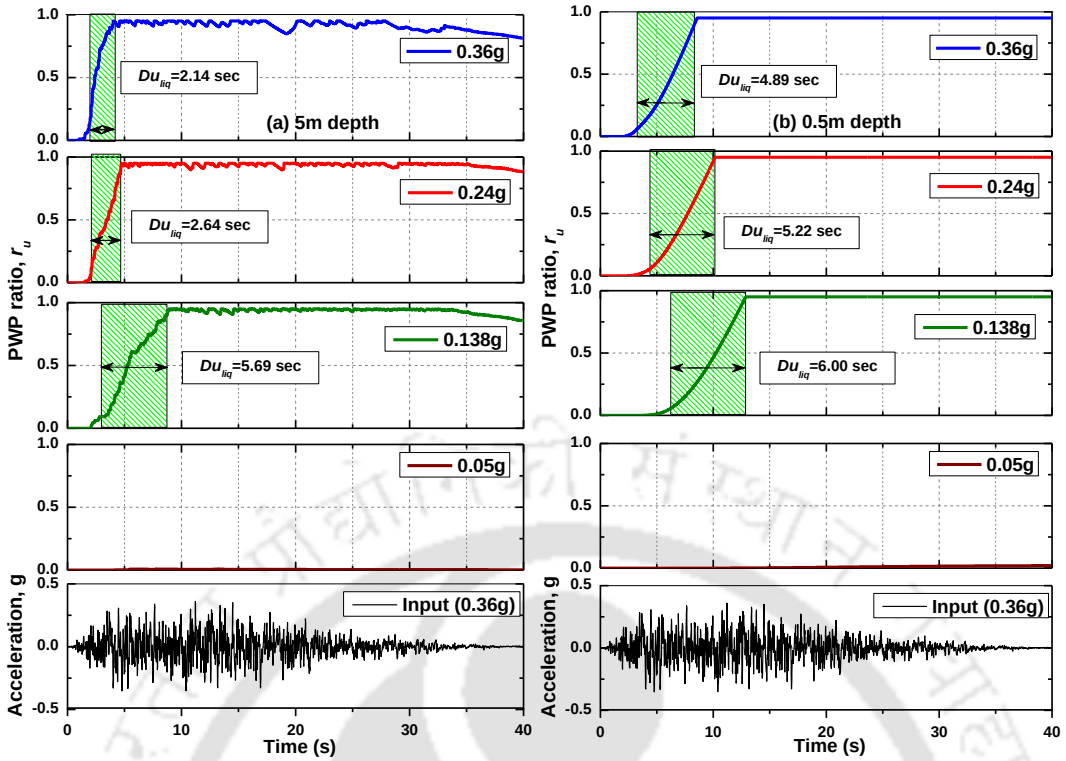

Fig. 6.34 r_u histories for different motions at Site-3 at **(a)** 5 m and **(b)** 0.5 m depth from surface

Stress-Strain Response of Soils

Influence of intensity of ground motion on the stress-strain response of liquefiable soils is discussed in this section. Fig. 6.35, Fig. 6.36, Fig. 6.37, and Fig. 6.38 present the shear stress history and r_u variation along with shear stress-shear strain response (hysteresis loops) at different depths, respectively, for the four ground motions at Site-1. As the low intensity motion (0.05g) did not develop any significant pore pressures in the soil column and also the induced strains are less than 0.02% at all the layers shown (Fig. 6.35), the stress-strain response seems linear elastic. Based on the undrained CTX tests on BP specimens, it was also observed that the threshold for pore pressure initiation is close to 0.02% at the lowest effective confining pressure which validates the non-liquefaction of Site-1 for 0.05g motion.

With the intensity of motion increased to 0.138g (Fig. 6.36), significant pore pressures were induced in the soil deposit at 5 m depth (loose sand) of Site-3, and subsequently strains reached as high as 2% (Fig. 6.36c). This strain level is higher than the threshold strain level of 0.02% and at such strains liquefaction can be expected. A nonlinear (and notably asymmetric) hysteretic response was also observed at the liquefiable depth and in addition, plastic yielding of the soil was observed.

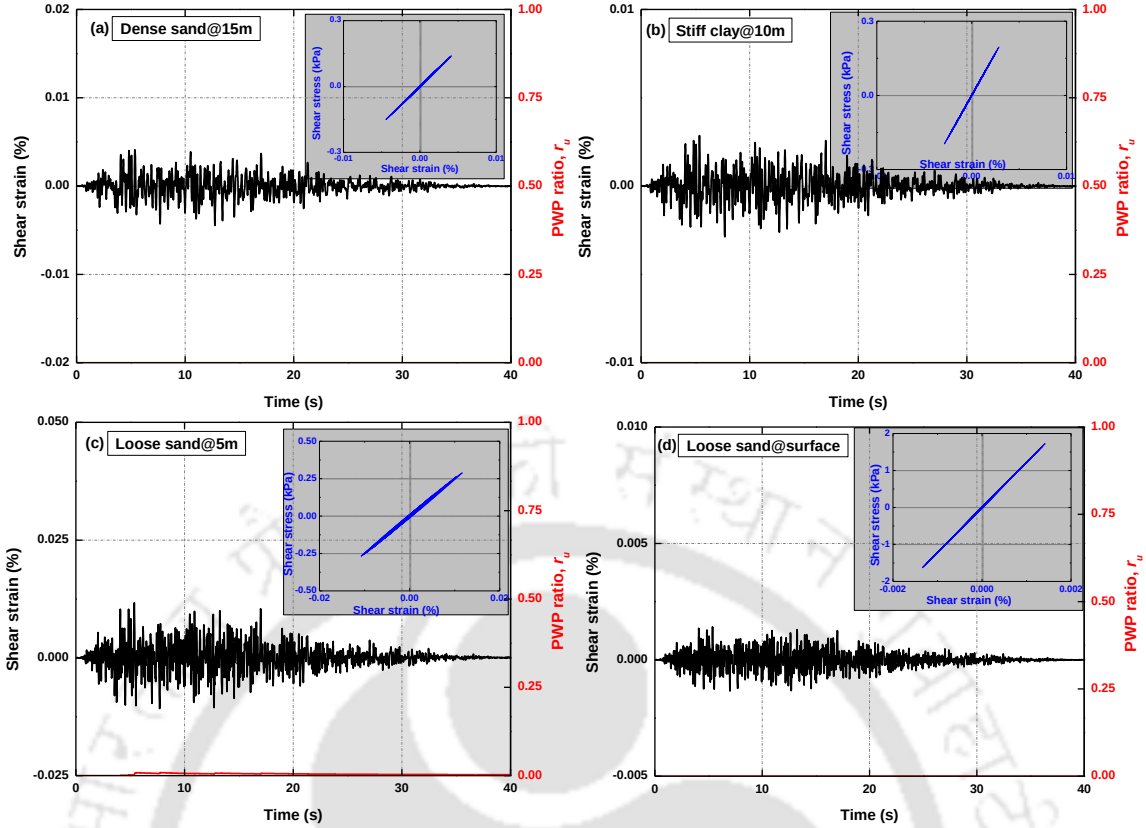

Fig. 6.35 Shear strain variation and stress-strain response at different depths **(a)** 15m **(b)** 10m **(c)** 5m and **(d)** surface, for 0.05g motion at Site-3

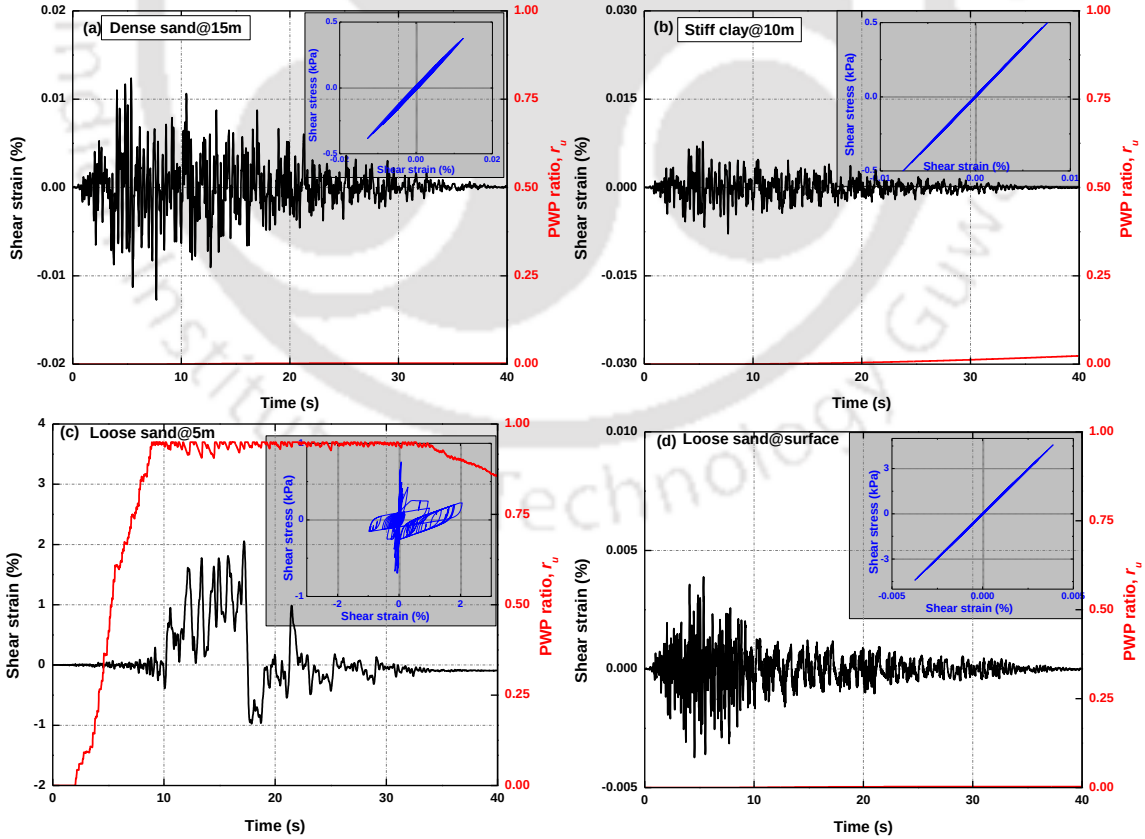

Fig. 6.36 Shear strain variation and stress-strain response at different depths **(a)** 15m **(b)** 10m **(c)** 5m and **(d)** surface, for 0.138g motion at Site-3

Fig. 6.37 and Fig. 6.38 present the response of soil deposit at different depths for 0.24g and 0.36g ground motions, respectively for Site-3. It can be noted that the liquefied stratum exhibited nonlinear stress-strain response and plastic deformations. It must be noted that the intensity of the motion increased the magnitude of plastic strains in soil deposits. For example, at 5 m depth in case of 0.24g motion (Fig. 6.37c), plastic strains in the soil is close to 8% while the same is increased to 30% in case of 0.36g motion (Fig. 6.38c). This shows that although soil deposits show similar depth of liquefaction for particular ground motions, magnitude of plastic deformations may increase with the intensity of motion.

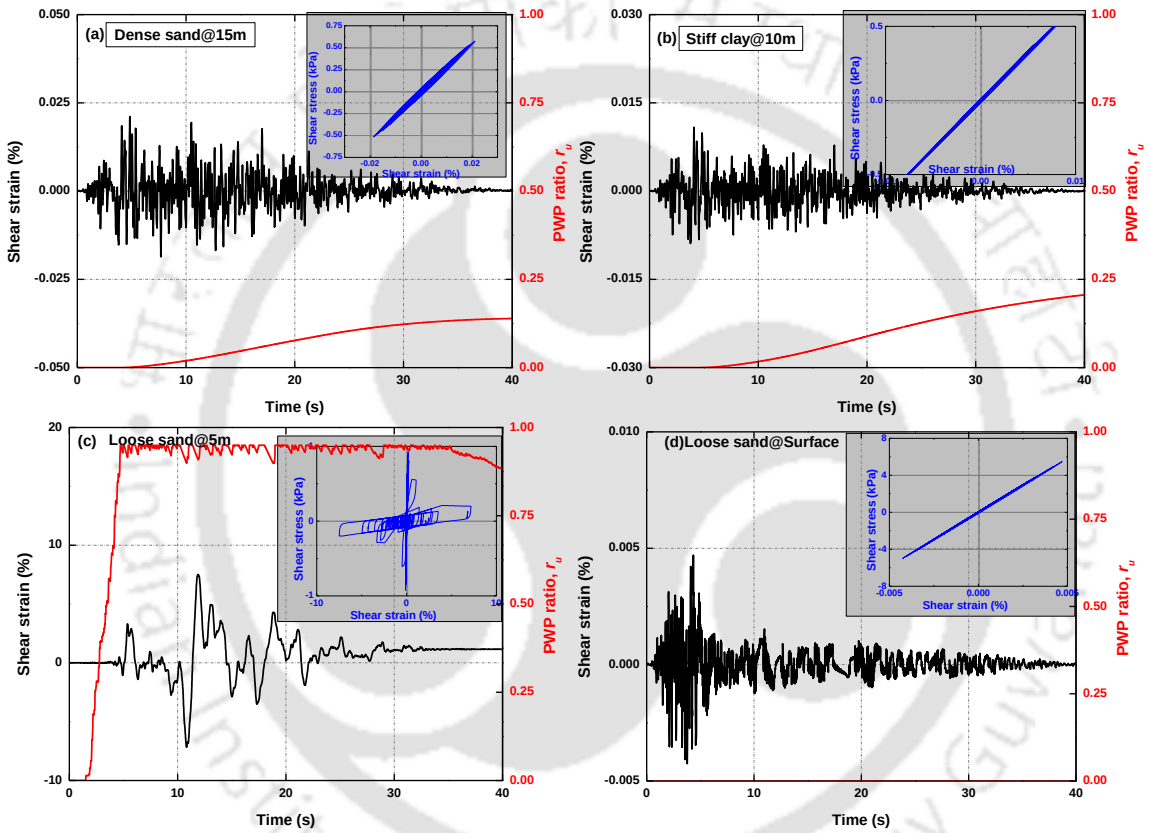

Fig. 6.37 Shear strain variation and stress-strain response at different depths **(a)** 15m **(b)** 10m **(c)** 5m and **(d)** surface, for 0.24g motion at Site-3

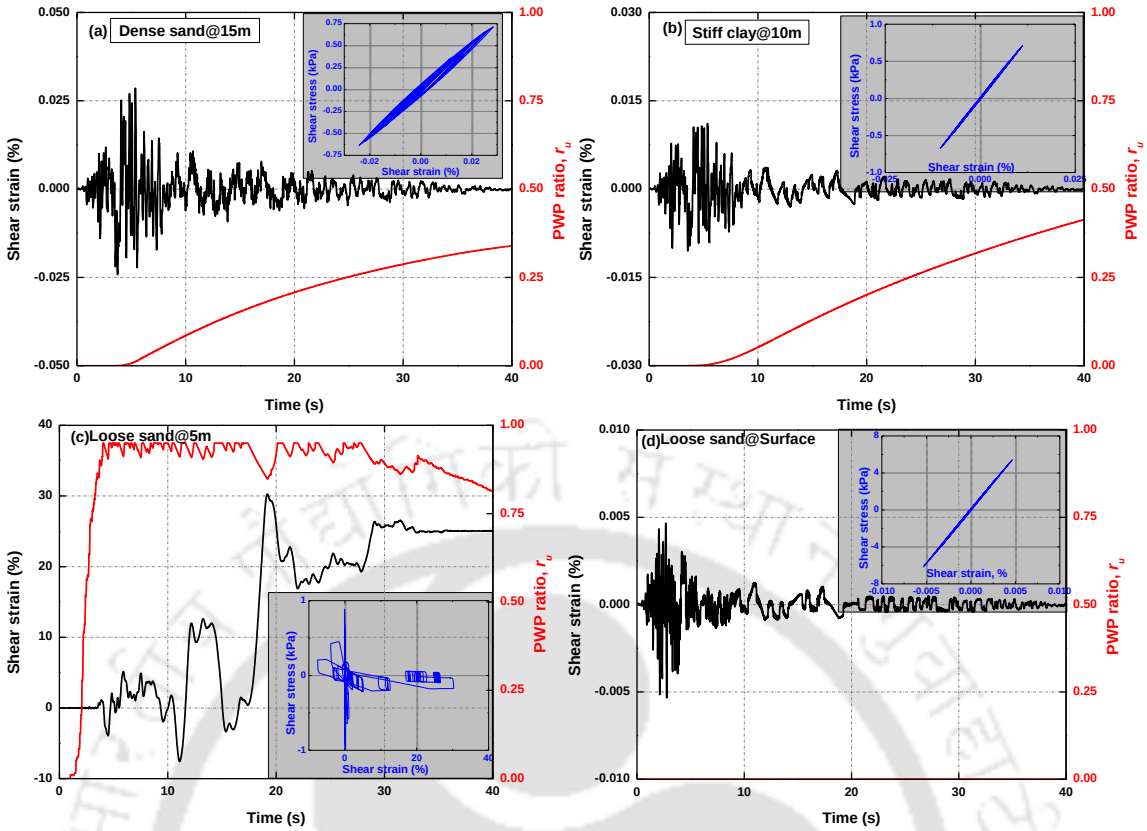

Fig. 6.38 Shear strain variation and stress-strain response at different depths **(a)** 15m **(b)** 10m **(c)** 5m and **(d)** surface, for 0.36g motion at Site-3

6.6.4 Comparison of Northeast Site Response

Results of NL GRA performed on the sites chosen in northeastern India (Sites-1 to 3) are combined so as to systematically understand the critical intensity at which the typical soil profiles in the region may be prone to seismic induced failures. Fig. 6.39, Fig. 6.40, Fig. 6.41, and Fig. 6.42 present the comparison of PGA, % change in PGA and r_u variation along the depth for the four considered motions at the three chosen sites (Sites: 1 to 3). It can be noted that the 0.05g exhibited amplification at all the three sites with the surface amplification ranging from 50 to 100%. Significant pore pressures representing liquefaction triggering were not exhibited by the 0.05g motion at any of the chosen three sites (Fig. 6.39c).

For 0.138g motion (Fig. 6.40), Sites 2 and 3 (Pachoria and Tezpur sites) showed amplification of the PGA while Site-1 (Saraighat bridge location) showed abrupt change in PGA amplification at the interface of liquefiable and non-liquefiable crust (at 11 m form surface). Also, Sites 1 and 3 (Saraighat bridge and Tezpur) showed liquefaction of the surficial loose sand while Site-2 (Pachoria) did not show any traces of liquefaction (Fig.

6.40c). Finally, 0.24g and 0.36g motions (Fig. 6.41 and Fig. 6.42) yielded attenuation of seismic waves towards the surface and significant liquefaction depths for the three sites.

High intensity PBRA motions are rarely witnessed in the northeastern Indian region, however, occurrence of mild to moderate events of PBRA ranging from 0.02g to 0.10g is very common due to the proximity of several seismic faults and their continuous deformations. As this study confirms high amplification of low intensity motions in the region and possible seismic liquefaction for high intensity motions, therefore it is strongly recommended to perform seismic NL GRA studies (with PWP incorporation) for efficient seismic resistant design of structures in the region.

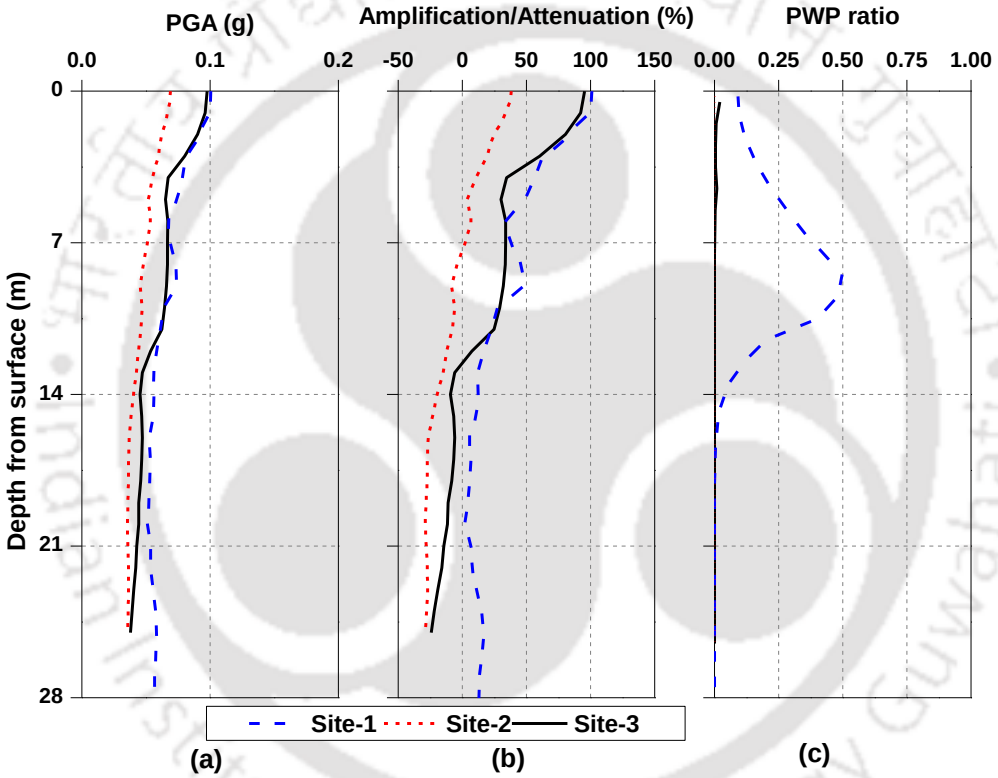

Fig. 6.39 Comparison of **(a)** PGA **(b)** Amplification/attenuation and **(c)** r_u profiles for northeastern India region for 0.05g motion

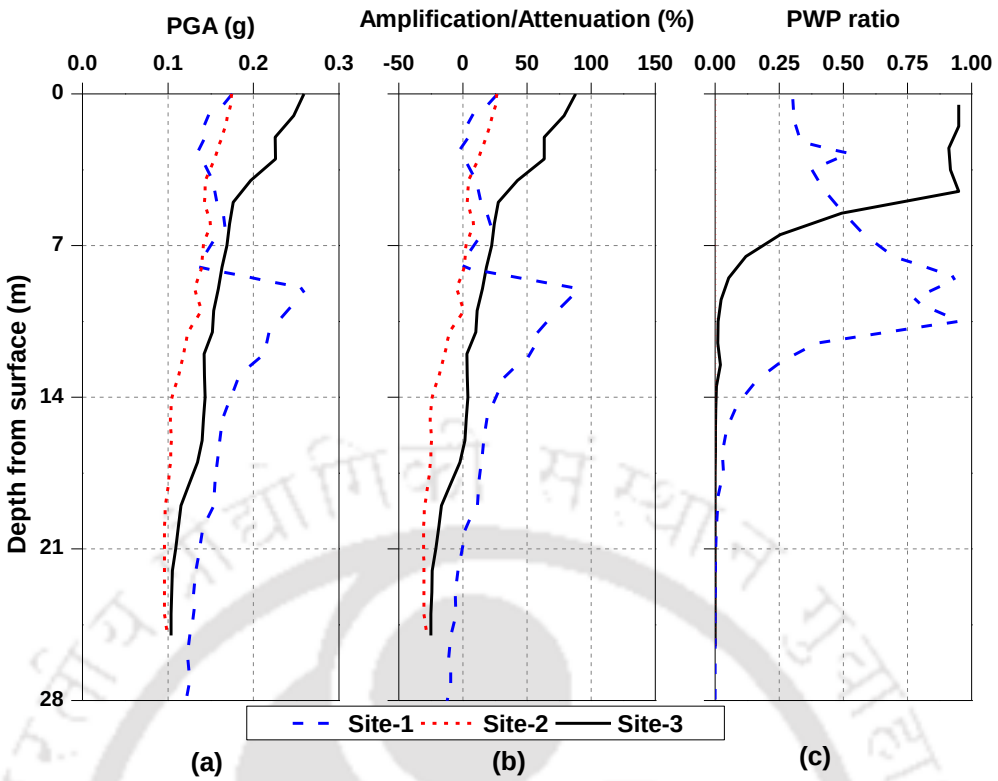

Fig. 6.40 Comparison of **(a)** PGA **(b)** Amplification/attenuation and **(c)** r_u profiles for northeastern India region for 0.138g motion

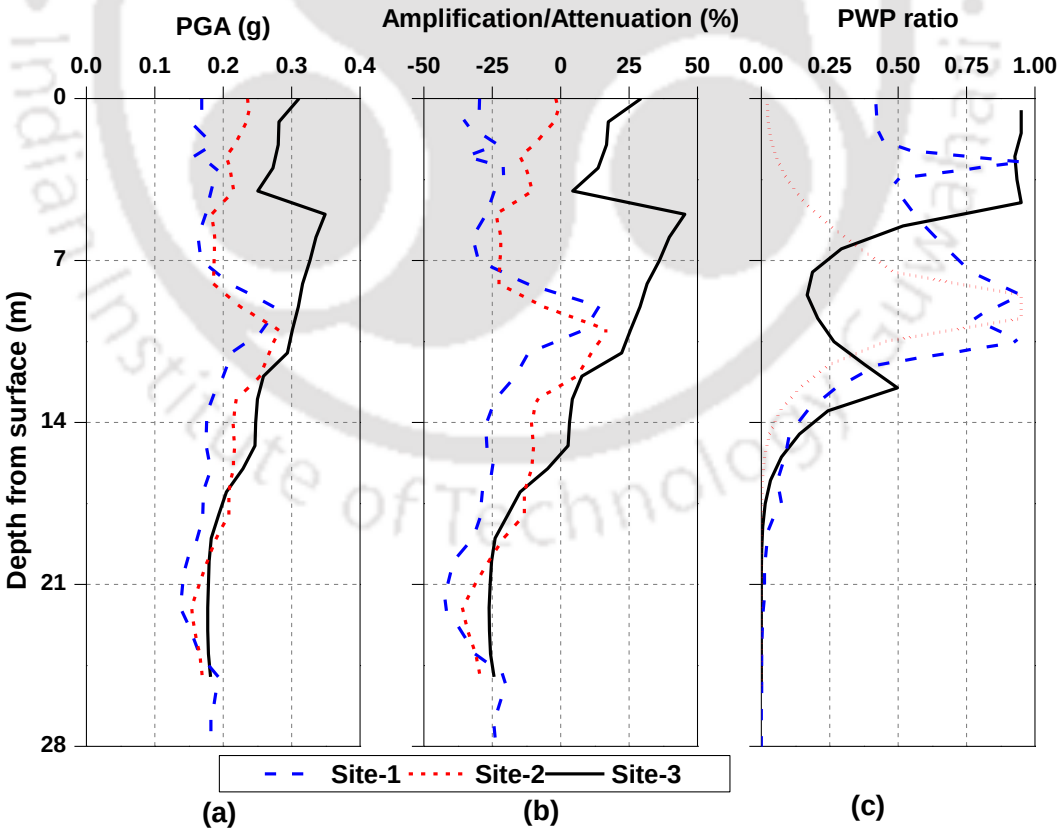

Fig. 6.41 Comparison of **(a)** PGA **(b)** Amplification/attenuation and **(c)** r_u profiles for northeastern India region for 0.24g motion

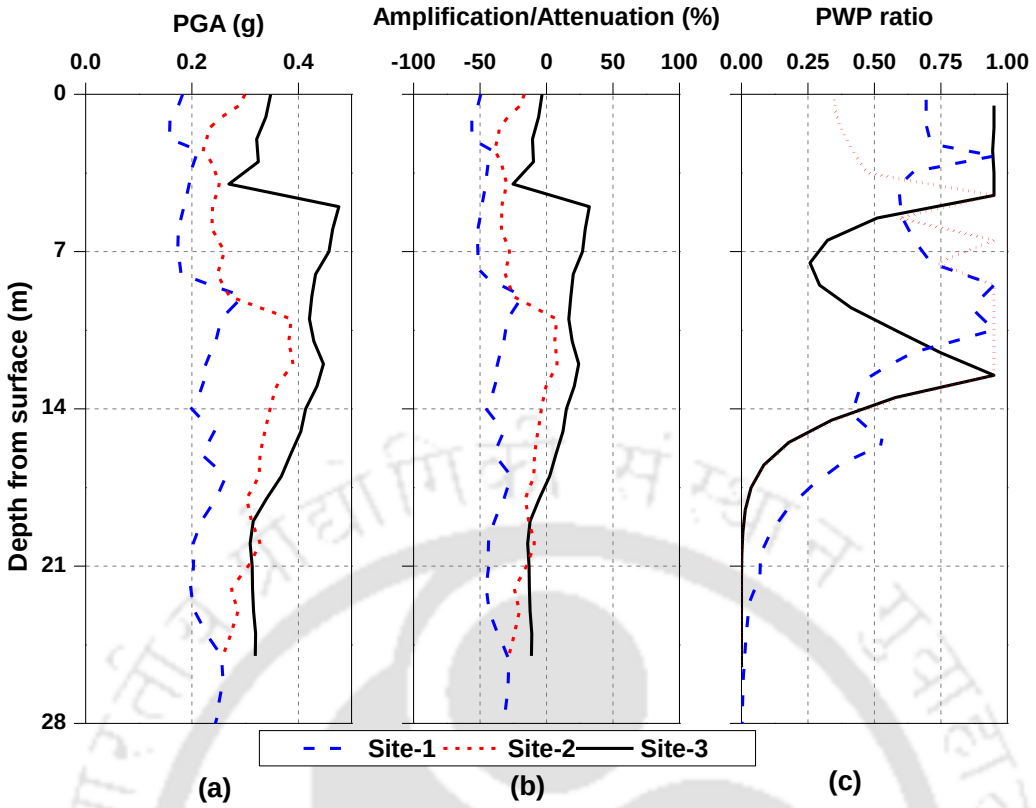

Fig. 6.42 Comparison of **(a)** PGA **(b)** Amplification/attenuation and **(c)** r_u profiles for northeastern India region for 0.36g motion

6.7 SUMMARY

Application of the established strain dependent dynamic soil properties and pore water pressure parameters from the experimental investigations is demonstrated through one dimensional ground response analysis. Four sites with varying layers of stratification were chosen from northeastern and northern India. Equivalent linear analysis has been performed initially to demonstrate the significance of experimentally derived stiffness curves for GRA studies. Nonlinear effective stress GRA studies (incorporating pore water pressure generation and dissipation) have been conducted for the chosen sites by utilising the established PWP parameters and by using ground motions of varying intensity (increasing PBRA). The results are presented in terms of accelerations, stresses, strains and pore water pressure characteristics. Analysis and discussions pertaining to the effects of intensity of ground motion on various liquefaction parameters have been highlighted. The nonlinear effective stress approach compared with the EQL analysis yielded realistic soil response. Results obtained in this chapter will be utilised for performing seismic analysis of deep foundations in the subsequent chapters.

CHAPTER VII – SEISMIC ANALYSIS OF PILE FOUNDATIONS

7.0 INTRODUCTION

Pile foundations are the widely used deep foundations supporting heavy superstructure loads and in case of problematic (loose or soft) surficial soils. In case of seismic conditions, kinematic and inertial interactions play a crucial role in the stability of pile foundations. This chapter presents the seismic analysis of pile foundation considering the kinematic interaction effects, investigated via dynamic Winkler beam approach. A multi-layered soil stratum with a probable liquefiable layer is chosen and the bilinear Winkler model (Lombardi et al. 2017) has been adopted in order to simulate the soil-structure-interaction in liquefiable soils. The required free field soil displacements are considered from the nonlinear effective stress GRA studies presented in the previous chapter. Nonlinear analysis is performed in time domain. Details about the adopted numerical program (SAP2000) and methodology is initially presented, followed by the description of validation of the program and the considered pile configurations. The results achieved are presented in terms of pile displacements and bending moments and the corresponding analysis is described. The chapter is intended to act as demonstration of the final step in seismic requalification framework of pile foundations (as briefed in the Chapter-I) in liquefiable soils, by making use of the data available from previous chapters (Chapters IV, V and VI). The chapter concludes with summary and significant conclusions from the study.

7.1 DYNAMIC BNWF MODEL

The present study adopts Beams on nonlinear Winkler foundation (BNWF) approach (Nogami et al. 1992), which is a widely used method (also called *p-y* approach) for the seismic analysis of pile foundations. In this approach, seismic soil-pile-structure-interaction (SPSI) arising due to the incoming waves is modelled through discrete spring element (*p-y* element, where *p* is the soil resistance offered for a unit pile horizontal displacement, *y*), manifesting the nonlinear behaviour of SPSI during dynamic loading. Bending response of pile foundations in seismic conditions which arise due to the

kinematic and inertial interactions, have been reasonably simulated using the nonlinear time history analysis of BNWF approach (Nogami et al. 1992; Wang et al. 1998).

7.1.1 Components Involved in Dynamic BNWF Approach

The dynamic BNWF method of pile foundations (Nogami et al. 1992) involves three main components, which are presented step-wise below. Fig. 7.1 briefly illustrates the dynamic BNWF approach.

Step 1: The first step involves the independent ground response analysis whereby the soil displacements (without structure) caused by the seismic waves along the depth are determined using 1D or advanced models (step-1 in Fig. 7.1).

Step 2: The SPSI is modelled through closely spaced nonlinear *p-y* elements. A *p-y* element is a combination of both linear and nonlinear behaviour and can also simulate the far field effects adequately. Various standard empirical forms (based on the shear strength properties of soils) are available to develop the *p-y* element properties, such as API (2014) and DNV (2013) etc. (step-2 in Fig. 7.1).

Step 3: Final component involves the nonlinear time history analysis of developed soil-pile model by inputting the free field soil displacements at various elevations. This step requires an analytical or numerical program (SAP2000) which can apply the free field motions along the depth.

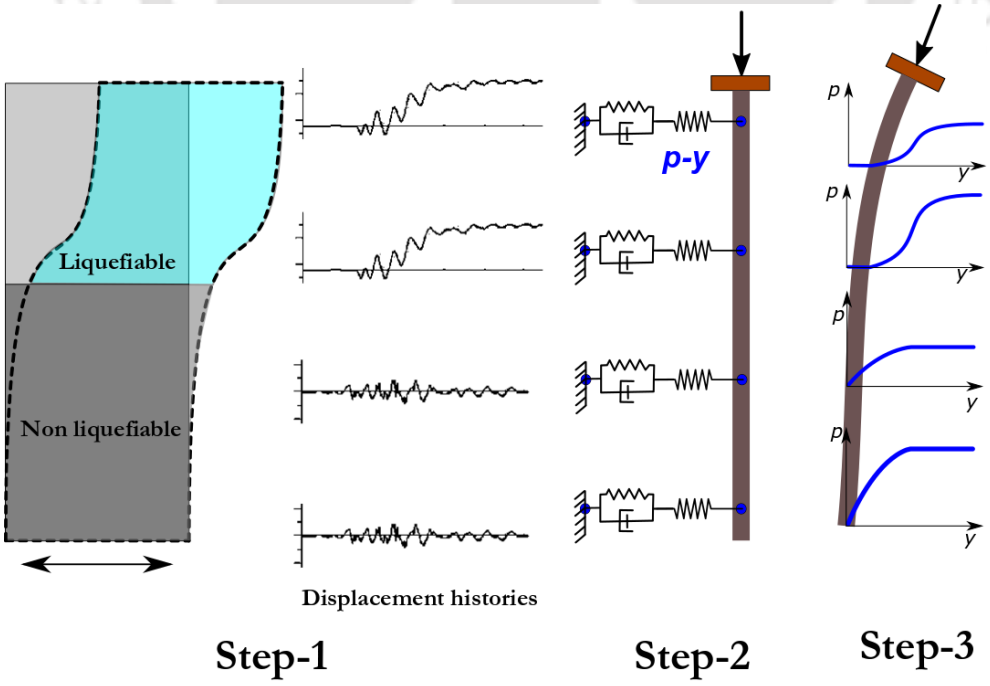

Fig. 7.1 Overview of dynamic BNWF approach for seismic analysis of pile foundations in liquefiable soils

7.1.2 Numerical Program – SAP2000

The commercially available numerical program-SAP2000 (CSI Inc. 2011) has been used for performing the nonlinear time history analysis (step 3 shown in Fig. 7.1) of pile foundations. The program can effectively simulate both the static and seismic loading conditions on pile foundations. In SAP2000, pile is typically modelled using straight frame elements discretized along the depth and assigned with the appropriate mass and stiffness properties. Surrounding soil is modelled by closely spaced two-joint link elements (*p-y*), with six degrees of freedom. Response of the spring is governed by the defined properties (linear, nonlinear or frequency dependent) and the element local coordinate system (defined by 1, 2 and 3 for global axes of X, Y and Z directions, respectively). These two-joint link elements must be zero-length elements to avoid any self-imposed additional shearing effects on the pile foundation. Once the properties are defined to the spring elements at different depths, each spring is assigned along the depth at various depths of the pile. One end of the spring must be grounded while the other end should be connected to the node point in the pile (Fig. 7.1). The achieved displacement time histories at different depths from GRA are defined using different load patterns and applied at the grounded nodes of the two-joint elements (in lateral direction) simultaneously using the multi-support excitation option available in SAP2000.

The nonlinear time history analysis in SAP2000 is performed through Hilbert-Hughes-Taylor direct time integration method whereby the equation of motion (Eqn. 7.1) is solved numerically.

$$K \cdot u(t) + C \cdot \frac{du(t)}{dt} + M \cdot \frac{d^2u(t)}{dt^2} = F(t) \qquad (7.1)$$

where *K*, *C* and *M* are the stiffness, damping and mass matrices while *u* and *F* are the deformation and external forces, respectively.

7.2 VALIDATION OF DYNAMIC BNWF MODEL

The methodology of dynamic BNWF approach has been validated against the centrifuge test results of dynamic behaviour of a single pile, reported by Boulanger et al. (1999). Fig. 7.2 (a) presents the schematic view of the experimental setup. Only the results of SP1 (Fig. 7.2a) are considered for validation. The tested pile is of 20.81 m in length with 3.81 m projection above the ground level and the rest is embedded in a two layered soil stratum. The surficial stratum is a reconstituted Bay Mud (PI=48, liquid limit 88 and water content 140%) of 6 m depth while the base layer is a uniformly graded Nevada sand (C_u=1.5 and

D_{50}=0.15 mm) of 11 m. The pile is of hollow aluminium section equivalent to a steel pipe pile of external diameter 670 mm with 19 mm thickness and is installed at 1g. An axial load of 49.1 Mg (481 kN) is present at the top of the pile to represent the mass of superstructure. The centrifuge model with the pile configuration was shaken with several earthquake events. The recorded and filtered acceleration histories of 1995 Kobe earthquake event was chosen and linearly scaled to achieve motions of varying seismic intensity (0.055g, 0.20g and 0.58g). Earthquake event with the smallest intensity was first applied and the response of the soil pile system has been recorded, followed by exciting with the increased intensity of the event. Displacement and bending moment developed in the pile have been monitored using displacement transducers and strain gauges, respectively. The obtained dynamic response of the pile foundations was also simulated by dynamic BNWF approach (Boulanger et al. 1999), using finite element program (GeoFEAP).

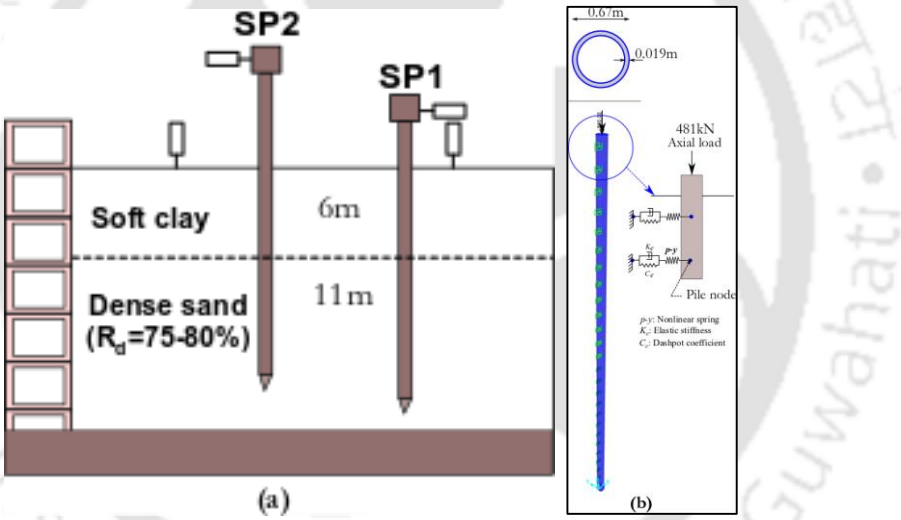

Fig. 7.2 (a) Schematic view of centrifuge setup for the dynamic testing of pile foundations (Boulanger et al. 1999) **(b)** SAP2000 model adopted for validation

The pile was modelled using 17 number of liner-elastic beam elements (1m spacing below the ground and 3m above the ground). Nonlinear behaviour of soil was modelled using two-joint dynamic *p-y* elements at various depths of the pile (Fig. 7.2b). Elasto-plastic *p-y* properties were defined based on the recommendations of Matlock and Reese (1970) for the surficial soft clay layer and API (2014) recommendations for the underlying dense sand layer (Boulanger et al. 1999). Elastic stiffness and radiation damping were modelled using the parallel spring and dashpot system (as shown in Fig. 7.2b) based on Gazetas and Dobry (1984) formulations.

For the present validation study, *p-y* curves for both the clay and sand are established following the API (2014) standards as they are essentially developed based on the Matlock and Rees (1970) analogy. Gapping elements were considered by Boulanger et al. (1999) to model the probable gap formation at high strains due to plastic deformations of the soil. However, the sensitivity analysis carried out by Boulanger et al. (1999) confirmed the negligible effect of gapping elements on the dynamic response of piles and therefore, gap elements are neglected in the present validation.

The required soil displacements for the nonlinear time history analysis were obtained by performing GRA for the design soil profile. Boulanger et al. (1999) performed equivalent linear GRA using SHAKE91, however in the present validation, equivalent GRA is performed using DEPSOIL program. Soil layers are discretized with a thickness of 1 m and the low strain shear modulus (G_{max}) for the upper clay layer was established by correlating it with the shear strength properties (Boulanger et al. 1999). Similarly, for the lower sandy stratum, G_{max} values were established following the Seed and Idriss (1970) empirical correlation. The strain dependent dynamic soil properties (G/G_{max} and D curves) for the upper clay layer are chosen from the work of Vucetic and Dobry (1991) for a PI of 50. In case of dense sand, upper range of data proposed by Seed and Idriss (1970) have been adopted as they are expected to contain high effective confining pressures. Base of the soil domain was assumed as rigid rock so as to represent the non-deformable base of the centrifuge container. The chosen ground motions for GRA study are the recorded motions of Kobe (1995) event with varying PBRA intensity – 0.055g, 0.20g, and 0.58g. Upon acquiring the displacement histories along the depth from free field EQL GRA, each of them are defined as load patterns in the developed soil pile model in SAP2000. A nonlinear direct time history analysis load case is defined whereby all the load patterns are given together. Each of the load patterns are assigned to the far ends of *p-y* springs (grounded joint) along the depth. The superstructure mass on the pile head (481 kN) is assigned as a live load and is present during the analysis and the corresponding *p-Δ* effects are incorporated through large strain *p-Δ* option available in the program. It must be mentioned that the base of pile is given a hinged support. Once the load cases are defined, nonlinear time history analysis is performed using multi-support excitation option based on Hilbert-Hughes-Taylor direct time integration method.

Fig. 7.3 and Fig. 7.4 present the peak displacements and bending moments of the pile respectively, for the considered ground motions. The centrifuge and FE results of

Boulanger et al. (1999) are also superimposed (Fig. 7.3 and Fig. 7.4). It is interesting to note that the results from current study are in close match with that of FE model of Boulanger et al. (1999) as the parameters of *p-y* curves adopted are similar. Both the dynamic *p-y* models (current study and Boulanger's) underestimate the peak displacements of the pile for high intensity motions. However, the bending responses of pile (Fig. 7.4) are reasonably simulated using the adopted approach. Therefore, based on the obtained results, it can be conveniently presumed that the adopted dynamic model can reasonably simulate the dynamic behaviour of pile foundations reasonably.

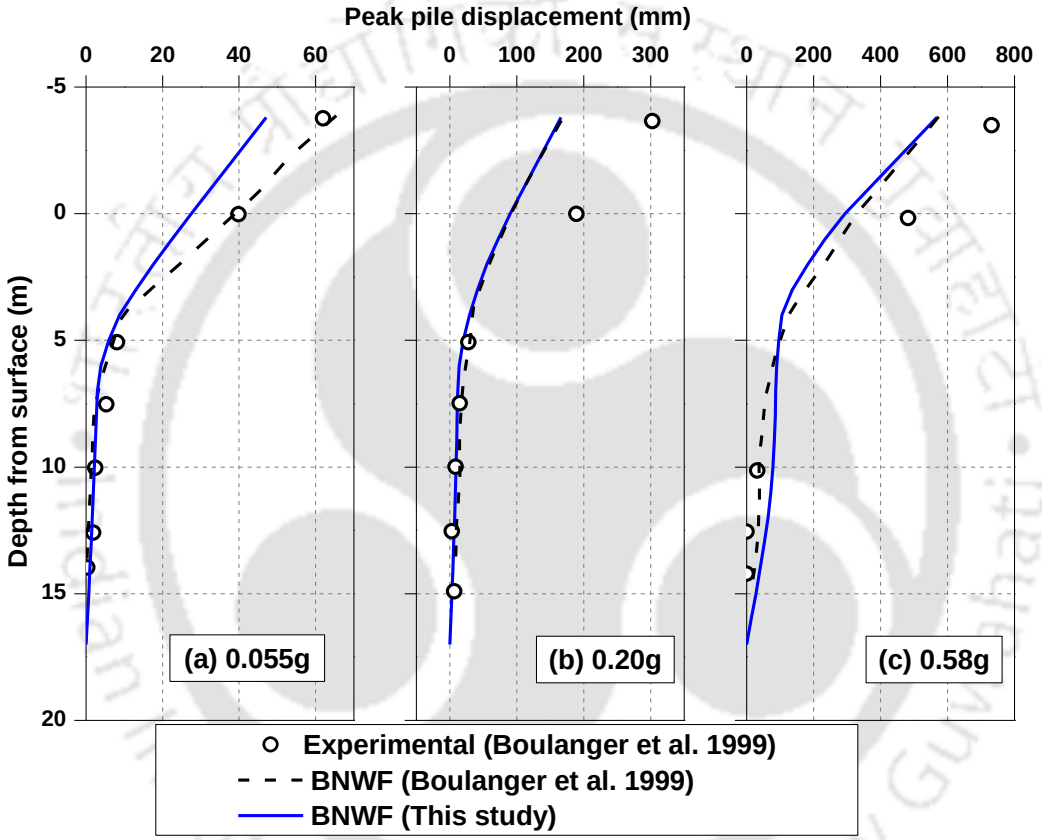

Fig. 7.3 Peak displacements of pile for Kobe (1995) motions **(a)** 0.055g **(b)** 0.20g and **(c)** 0.58g

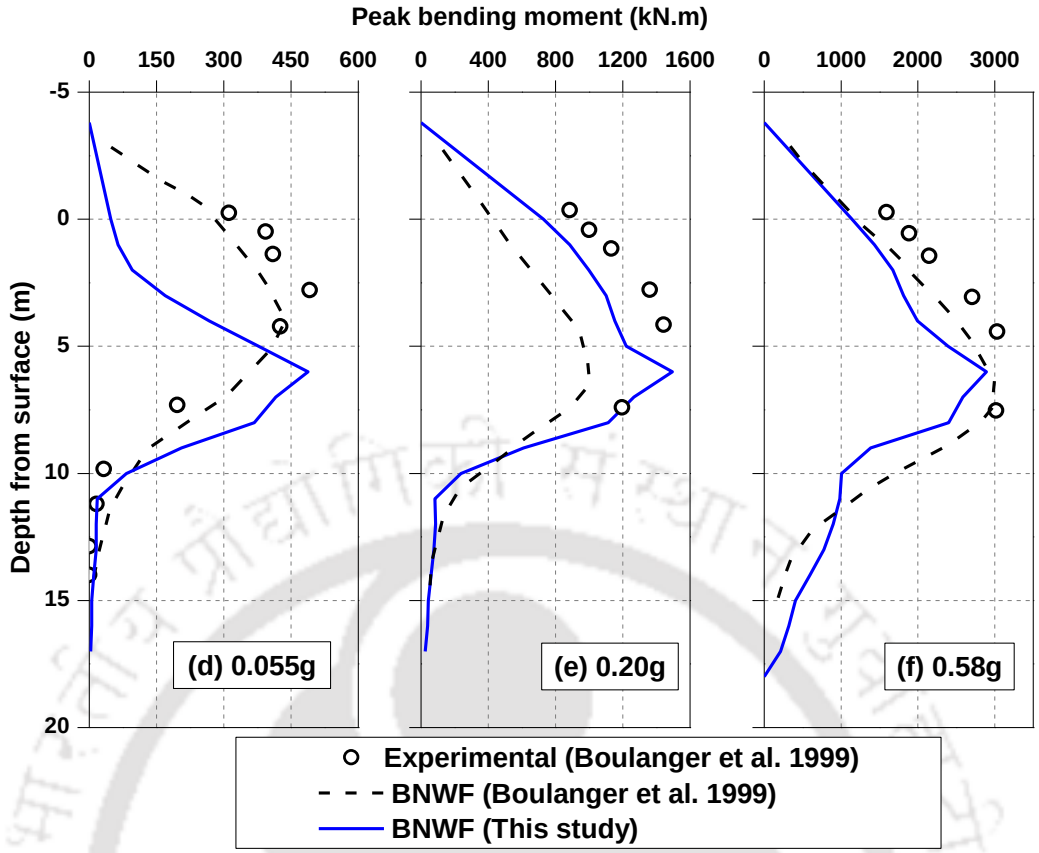

Fig. 7.4 Peak bending moments of pile for Kobe (1995) motions **(a)** 0.055g **(b)** 0.20g and **(c)** 0.58g

7.3 PROBLEM STATEMENT

In the current study, two pile configurations (single pile and 2×2 pile group) have been chosen to assess their seismic stability against different intensities of earthquake motions simulated for Guwahati city (0.05g, 0.138g, 0.24g and 0.36g). A liquefiable soil stratum is chosen, so as to check the effect of liquefaction on the dynamic response of the chosen pile configurations. The validated dynamic *p-y* approach is adopted with consideration of liquefaction implications. Fig. 7.5 (a and b) depicts the schematic view and numerical model of chosen pile configurations. Single pile and all the piles in the group are solid members of 600 mm diameter and are 26 m in length. The configuration details are considered from a local pile supported building and such geometry is typical in the north-eastern region of India. The piles and pile cap for the group are made of M25 concrete. Pile cap for the 2×2 group is of square section with 2.8m×2.8m geometry and of 900 mm thickness. The centre to centre spacing of the piles in the group is maintained at 1.6 m with a cover of 0.4 m on all the sides. All the four piles are rigidly connected to the pile cap.

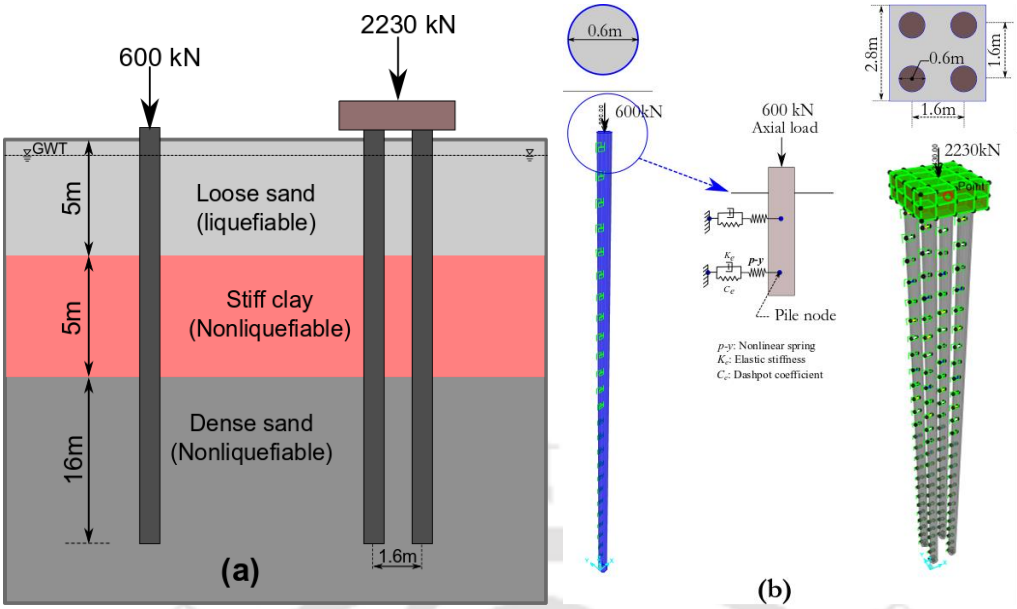

Fig. 7.5 (a) Schematic view and **(b)** numerical model of single pile and 2×2 pile group

Table 7.1 Design soil profile of Site-3 (Tezpur)

Soil type	R_d (%)	Unit weight (kN/m^3)	Undrained cohesion (kPa)	Friction angle (degree)
Loose sand	25	10.39	00	26
	25	14.71	00	26
	25	14.71	00	29
	25	14.71	00	32
	25	14.71	00	32
Clay	NA	14.81	22	00
	NA	14.81	22	00
	NA	14.81	22	00
	NA	14.81	22	00
	NA	14.81	22	00
Dense sand	75	16.15	00	39
	75	16.15	00	39
	75	16.15	00	39
	75	16.15	00	39
	75	16.15	00	39
	75	16.15	00	39
	75	16.15	00	39
	75	16.15	00	39
	75	16.15	00	39
	90	16.77	00	41
	90	16.77	00	41
	90	16.77	00	41
	90	16.77	00	41
	90	16.77	00	41
	90	16.77	00	41
	90	16.77	00	41

Both the single pile and 2×2 pile group are assumed to be embedded in Site-3 (Tezpur soil profile), Fig. 7.5a. Stratification details and shear strength characteristics of the site are presented in Table 7.1. Selection of Site-3 is motivated by the presence of multiple layers of stratification and surficial loose liquefiable stratum (top 5 m based on nonlinear effective stress GRA presented in the previous chapter). The single pile and pile cap in 2×2 pile group are at the same bed level, with the piles extending below the ground level to 26 m from the surface. As the chosen pile configurations will be analysed for the four artificial ground motions developed for Guwahati city (Raghu Kanth et al. 2008) using the nonlinear time history analysis, results from the previous chapter (NL GRA section) for the chosen site are utilised here.

7.4 NUMERICAL MODEL

SAP2000 (CSI Inc. 2011) has been utilised for the numerical modelling of chosen pile configurations. Pile is modelled as solid straight frame element with 27 number of nodes (26 frame elements of each 1 m depth) and M25 concrete properties are assigned to it. Table 7.2 lists the assigned properties to the pile. Base of the pile is given a hinged condition which restricts the lateral movement with no restraint on rotation and the top of the pile is considered to be a free condition to represent a free-headed pile (Fig. 7.5).

Table 7.2 Pile geometry and material properties

Property	Value
Diameter, m	0.6
Length of embedment, m	26
Modulus of elasticity, kPa	25×10^6
Unit weight, kN/m^3	24
Poisson ratio	0.20
Shear modulus, kPa	10.41×10^6

In case of 2×2 pile group, piles are modelled as frame elements and a pile cap of 0.9 m thick, modelled as thick shell element representing a rigid body with M25 properties. Piles are taken to the half of the depth of pile cap to represent the full fixity condition. The pile cap is given a rotation fixity and translation possibility which represents the typical pile cap support condition. Soil pile interaction is modelled using two-joint link elements (representing *p-y* behaviour). One end of the *p-y* elements is grounded and fixed against all degrees of freedom while the other end is connected to the pile node at different depths. The nonlinear *p-y* properties are defined based on the formulations presented in the subsequent section.

Each chosen pile configuration has been excited using four ground motions of increasing PBRA intensity (0.05g, 0.138g, 0.24g and 0.36g). Hinged on the NL GRA study, the surficial loose sandy stratum of chosen site (top 5 m of Site-3) is prone to liquefaction beyond a PBRA of 0.138g and is non-liquefiable for 0.05g motion. As Winkler approach is a decoupled analysis, *p-y* curves must be developed independently to consider the effects of liquefaction (and resulting soil yielding) in case of events greater than 0.138g PBRA for the chosen site. Table 7.3 lists the numerical analysis program. In case of 0.05g event (nonliquefiable), standard API (2014) formulations have been employed to generate *p-y* curves for the layers. In case of other events (liquefiable), bilinear strain-hardening model proposed by Dash et al. (2017) has been adopted to model the *p-y* curves of liquefiable stratum (top-5m).

Table 7.3 Nonlinear analysis programme in SAP2000

Pile configuration	**PBRA of event (g)**	***p-y* curves adopted**
Single pile	0.05	API (2014) curves full depth
	0.138	Bilinear *p-y* curves for top 5m and API (2014) curves for the rest of the depth
	0.24	
	0.36	
2×2 pile group	0.05	API (2014) curves full depth
	0.138	Bilinear *p-y* curves for top 5m and API (2014) curves for the rest of the depth
	0.24	

7.4.1 *P-Y* Curves for Non-Liquefiable Soils

In case of 0.05g event, *p-y* curves can be conveniently developed based on the standard recommendations. Current study adopts the API (2014) *p-y* curves for the three type of soils of the chosen site (top 5m sand, 6-10m clay and 11 to 26m dense sand) in case of 0.05g event. The *p-y* function in case of sand layers is represented through Eqn. 7.2 and for clays, the formulations are based on undrained cohesion (API 2014).

$$p = A \cdot P_u \cdot tanh\left[\frac{k \cdot Z \cdot y}{A \cdot P_u}\right] \qquad (7.2)$$

where A is a factor accounting for cyclic loads (0.9); P_u is the ultimate lateral bearing capacity at depth, Z; k is the initial modulus of subgrade reaction; and y is the lateral displacement. API (2014) recommended design charts to determine the parameters involved. Fig. 7.6 (a-c) depicts the developed *p-y* curves at different depths based on API (2007) formulations. It can be observed that in case of sandy stratum (Fig. 7.6 a and c), *p-y* curves are stiffened with depth as their shear strength increases with depth. However, as

the clay layer (6 to 10m) possess similar undrained cohesion (Table 7.1), curves from 6 to 10 m are superimposed over one another (Fig. 7.6b).

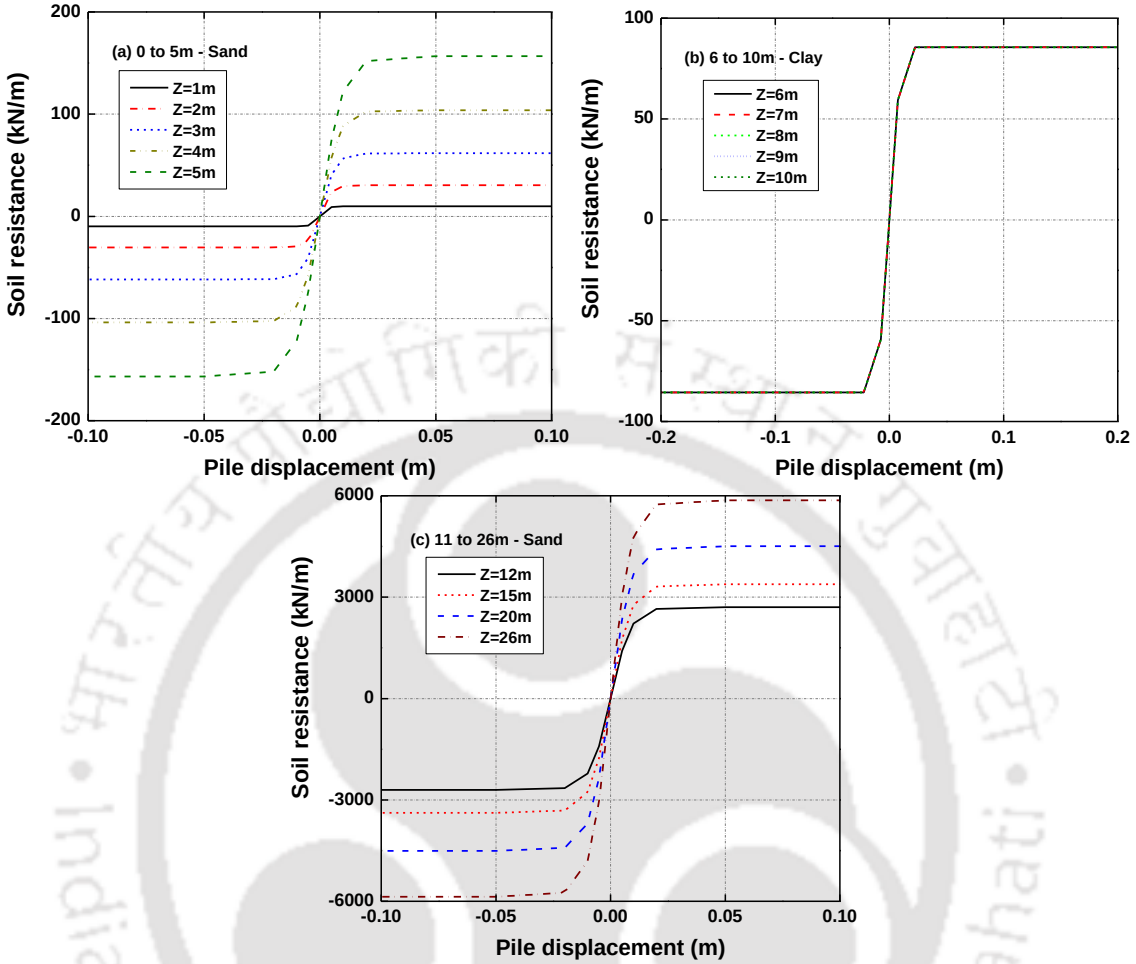

Fig. 7.6 *p-y* curves for non-liquefiable soils based on API (2014) recommendations

7.4.2 *P-Y* Curves for Liquefiable Soils

Dash et al. (2017) and Lombardi et al. (2017) based on extensive experimental program (both element and model tests), formulated a strain-hardening bilinear *p-y* model which can efficiently simulate the dynamic behaviour of pile foundations in liquefiable soils. Fig. 7.7 presents the schematic representation of bilinear *p-y* curve development for liquefiable soils. Present study adopts the model for simulating the SPSI of pile foundations in liquefiable soils.

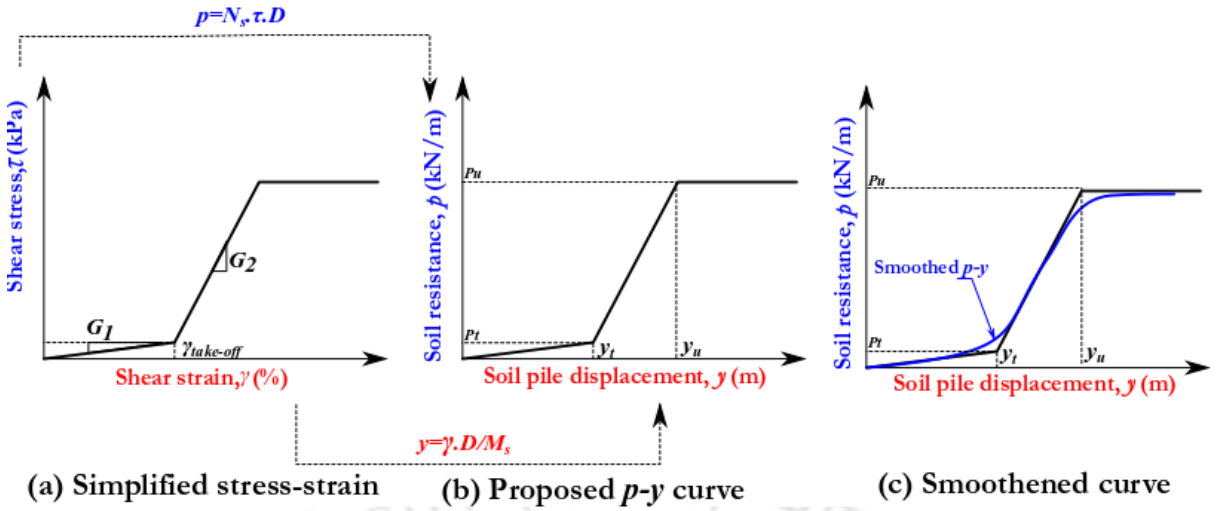

Fig. 7.7 Schematic representation of obtaining liquefied *p-y* curve (redrawn after Dash et al. 2017)

In case of liquefiable events (0.138g, 0.24g and 0.36g) for the surficial 5 m loose sand, liquefiable *p-y* curves (Dash et al. 2017) are utilised. Effectively, the procedure of developing liquefied *p-y* curves involves two main components (Fig. 7.7): development of stress-strain response based on residual soil strength (Fig. 7.7a) and scaling of the stress-strain using validated scaling factors to form a smooth *p-y* curve (Fig. 7.7c). The methodology is briefly summarized below.

Step 1: Calculation of take-off shear strain ($\gamma_{take\text{-}off}$) for the discretized soil layers based on the relative density (R_d). The $\gamma_{take\text{-}off}$ is the shear strain required for liquefied soils to initiate strength mobilization.

$$\gamma_{take-off} = 74.34 - 17.71 \cdot \ln(R_d) \text{ in \%} \quad (7.3)$$

Step 2: Initial shear modulus (G_1) determination through Eqn. 7.4

$$G_1 = 1/\gamma_{take-off} \quad \text{in kPa} \quad (7.4)$$

Step 3: Critical state shear modulus (G_2) should be determined as per Eqn. 7.5

$$G_2 = G_{max}/\left(5 \cdot \sqrt{\sigma_c'}\right) \quad \text{in kPa} \quad (7.5)$$

Step 4: Estimation of ultimate shear strength (S_r) of liquefied soils based on residual shear strength of the liquefied soil. A design chart has been provided by Cubrinovski and Bradley (2008) for the upper and lower limits of the residual shear strength in correlation to the SPT N value and the same chart can be used as it includes the data of soils from many parts of the world.

Step 5: Identification of proper scaling factors for conversion of the stress-strain response (Steps 1-4) to *p-y* curves for liquefied soils. A stress scaling factor (N_s) of 11.94 was suggested for rough interface (ideal for concrete piles) and a strain scaling factor (M_s) of 1.87 was recommended for fully liquefied soils (Lombardi et al. 2017; Dash et al. 2017).

Step 6: Calculation of initial lateral resistance (p_1) corresponding to take-off shear strain from Eqn. 7.6

$$p_1 = N_s \cdot 1.25 \cdot \gamma_{take-off} \cdot G_1 \cdot D \qquad \text{in kN/m} \qquad (7.6)$$

Where D is the external diameter of the pile

Step 7: Calculation of initial lateral displacement (y_1) corresponding to take-off shear strain from Eqn. 7.7

$$y_1 = \frac{1.25 \cdot \gamma_{take-off} \cdot D}{M_s} \qquad \text{in m} \qquad (7.7)$$

Step 8: Ultimate lateral resistance (p_u) estimated from the residual shear strength through Eqn. 7.8

$$p_u = N_s \cdot S_r \cdot D \qquad \text{in kN/m} \qquad (7.8)$$

Step 9: The ultimate lateral displacements (y_u) is estimated using Eqn. 7.9

$$y_u = \left[\left(1.25 \cdot \gamma_{take-off}\right) + \left(\frac{S_r - \left(G_1 \cdot 1.25 \cdot \gamma_{take-off}\right)}{G_2}\right)\right] \cdot \left(\frac{D}{M_s}\right) \qquad (7.9)$$

Step 10: Finally, the obtained p-y curve is smoothed to represent the behaviour in a pragmatic way using Eqn. 7.10

$$p = w \cdot \frac{p_1}{y_1} \cdot y + A \cdot (1 - w) \cdot \left[\frac{p_u + p_1}{2} + \frac{p_u - p_1}{2} \cdot tanh \frac{2 \cdot \pi}{3(y_u - y_1)} \left(y - \frac{y_u + y_1}{2}\right)\right] \qquad (7.10)$$

Where A=0 for y=0, and A=1 for $y \neq 0$ and w is the weight function given by Eqn. 7.11

$$w = \frac{1}{2} \cdot \left[1 - tanh\left(\frac{6\pi}{y_u} \cdot \left(y - \frac{4 \cdot y_1 + y_u}{6}\right)\right)\right] \qquad (7.11)$$

Based on these formulations (Eqn. 7.3-7.11), the smoother *p-y* curves for the liquefied soil stratum (top 5m) have been developed. For a comparison purpose to show the difference between a liquefied *p-y* curve and a standard *p*-y curve (API 2014), both the curves at 3m depth are shown in Fig. 7.8a. It can be seen that the initial slope of the liquefied *p-y* curve is almost negligible and the strength increased with the strain (strain-hardening

phenomenon). Fig. 7.8b presents the developed *p-y* curves for the liquefied stratum and the corresponding non-liquefied curves.

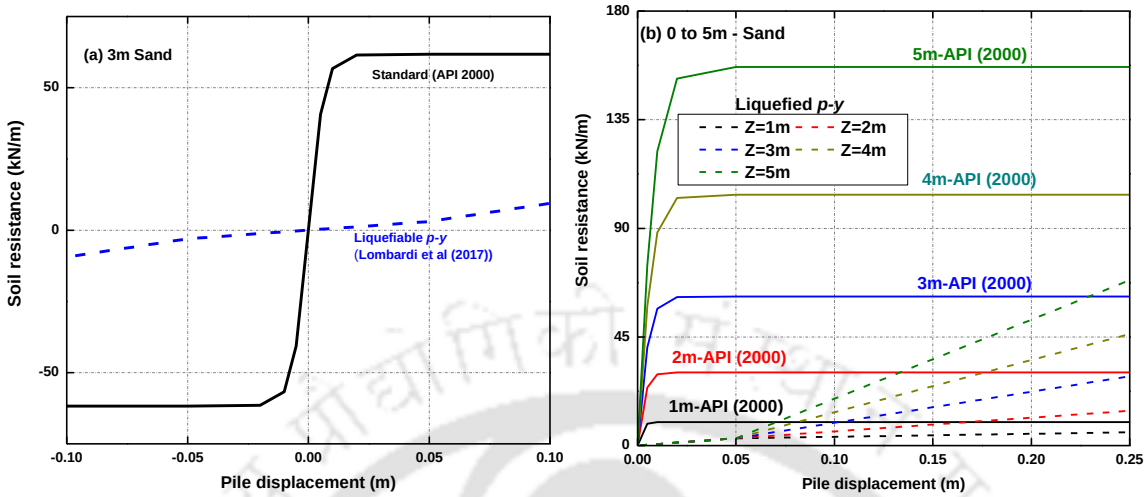

Fig. 7.8 (**a**) Comparison of liquefied and standard *p-y* curve at 3m depth (**b**) developed p-y curves for liquefied soil for the Site-3

For the *p-y* curves in case of group piles, due to the possibility of pile-soil-pile interaction (typically called shadowing effects), a multiplication factor of 0.5 as suggested by Brown et al. (1988) and Rollins et al. (2005) has been considered so as to reduce the strength of *p-y* curves. Traditionally in static cases, the multiplication factor is high for the rear row of piles and less for the front row, however in cyclic loads, during the stress reversals, both the rows act as front and rear rows simultaneously and therefore, a consistent factor of 0.5 has been chosen.

The chosen configurations were analysed under four ground motions of varying PBRA (0.05g, 0.138, 0.24g and 0.36g) for which the ground response analysis was presented in the previous chapter. From the NL GRA performed for Site-3, free field soil displacement histories are obtained at depths of 1m spacing for 26 m depth of the profile. Fig. 7.9 presents the typical displacement histories at different depths for the 0.05g PBRA event. As observed, soil displacements are amplified towards the surface. Fig. 7.10 presents the displacement response for 0.24g PBRA motion. It can be seen that the severe amplification is witnessed in case of high intensity motion. In addition, plastic yielding (permanent displacements) of the soil close to 15 mm at the surficial layers is seen. Such plastic yielding is attributed to the complete loss of shear strength of the surficial layers due to the induced seismic liquefaction at the surficial loose stratum.

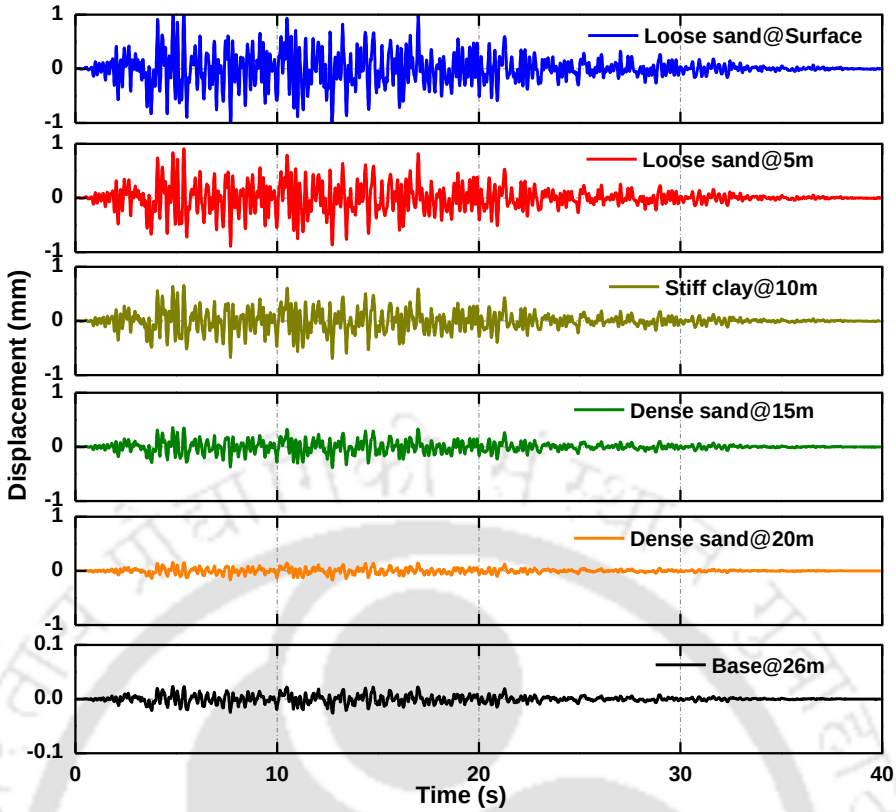

Fig. 7.9 Free field soil displacements along the depth for 0.05g PBRA motion

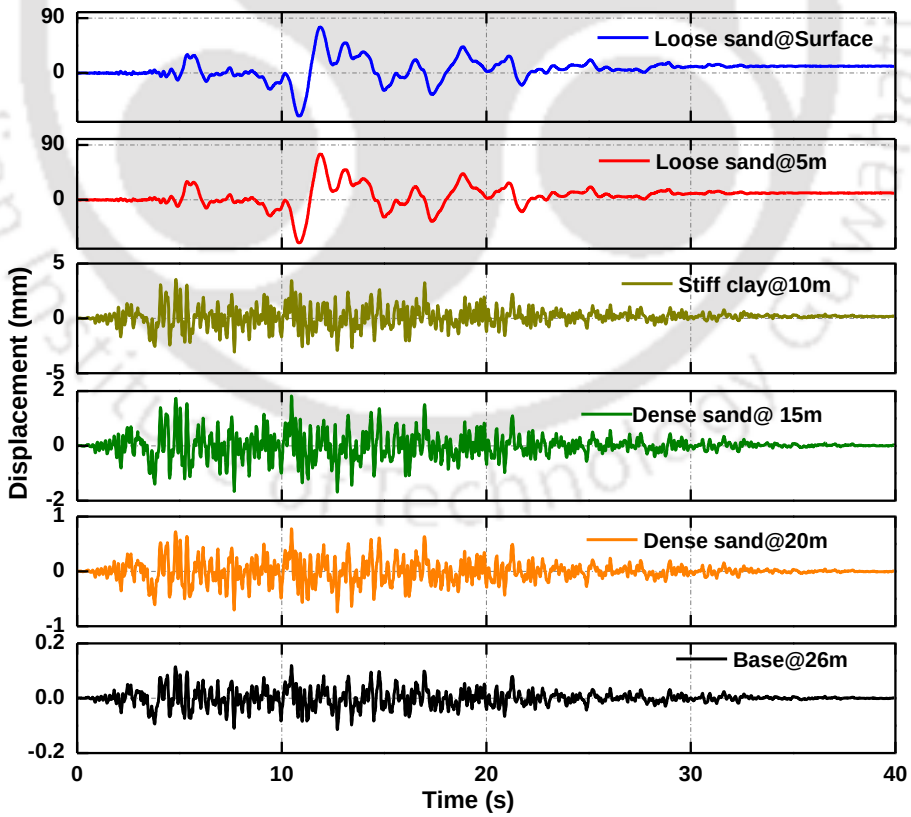

Fig. 7.10 Free field soil displacements along the depth for 0.24g PBRA motion

These ground displacements are assigned at the far end of the *p-y* elements for the nonlinear time history analysis through multi-support excitation. A global frequency-dependent damping ratio of 5% has been allotted for the analysis.

7.5 RESULTS AND DISCUSSIONS

Analysis have been performed independently for single pile and 2×2 pile group configurations for different ground motions of increasing PBRA intensity. Results obtained for single pile and pile group are presented separately to facilitate the understanding on the effect of earthquake intensity on the chosen configurations. Responses of single and group piles are presented in terms of displacement histories, peak displacement profiles, shear force and bending moments. Also, comparison is made between the response of single pile and a pile in the 2×2 pile group to understand the seismic performance of the pile foundations.

7.5.1 Single Pile Response

Fig. 7.11 presents the lateral displacement history of single pile at various depths (pile head, 2.5 m below GL, 5.5 m below GL and 10.5 m below GL). Similar to the free field soil response, pile response is also amplified towards the surface. A peak displacement of 1.5 mm can be noted at the surface, however, no excessive yielding is witnessed at any depth of the pile for 0.05g motion. The displacement response of single pile for 0.24g motion at different depths is shown in Fig. 7.12. As depicted from the field response of liquefiable soil deposits, significant deformation of the pile foundation is visible and such deformations exist only in the liquefiable zones. This is due to the fact that the liquefied crust exerting high lateral pressures resulting in large strains, often exceeding the plastic limit of liquefied soil. Similar large lateral displacements for pile have been observed experimentally by Wilson et al. (2000) and numerically by Haldar and Babu (2010) and Saeedi et al. (2018). Such large deformations in the pile are primarily the effect of kinematic interaction of liquefied soil and pile foundation.

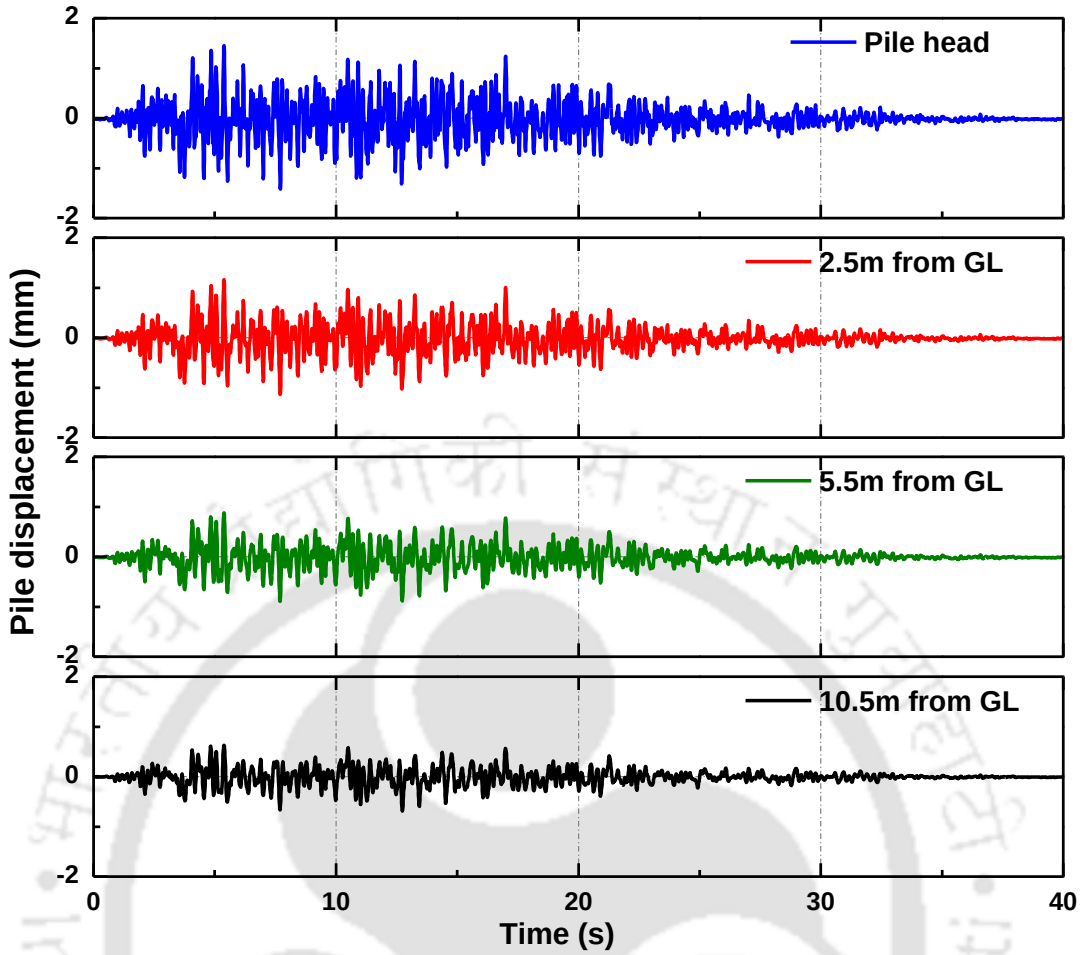

Fig. 7.11 Pile foundation displacement response along the depth for 0.05g PBRA motion

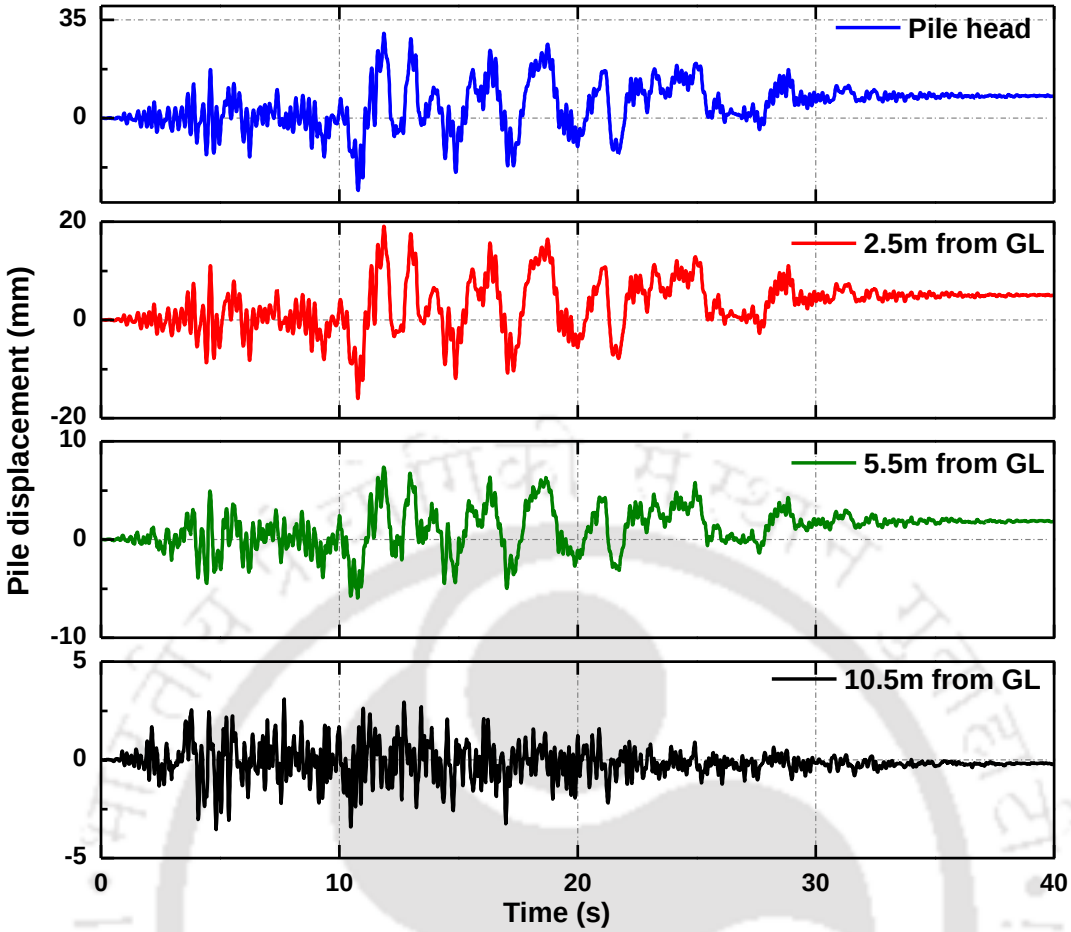

Fig. 7.12 Pile foundation displacement response along the depth for 0.24g PBRA motion

The peak free field soil displacements along the depth are compared to the peak pile displacements of single pile for all the chosen ground motions in Fig. 7.13 and Fig. 7.14. The pile typically is following the displacement of soil up to a certain depth, beyond which the differences are noticeable. In case of 0.05g motion which did not liquefy the profile (Fig. 7.13a), pile experienced narrowly higher displacement than that of soil. However, in cases of surficial liquefiable stratum (top 5 m) for the remaining three motions (Fig. 7.13b and Fig. 7.14 a and b), pile exhibited lower displacement and it is attributed to the higher relative soil-pile stiffness. As soil is relatively softer compared to the pile, and in liquefaction cases, soil flows like a fluid. However, pile being a relatively stiff member does not always follow the soil displacement trend. Another interesting phenomenon can be observed from the pile displacement response: sudden shift of significant pile deformations can be witnessed at the interface of liquefiable and non-liquefiable stratum. This is due to the sharp stiffness contrast prevailing at the juncture of the different soil strata (Mylonakis 2001).

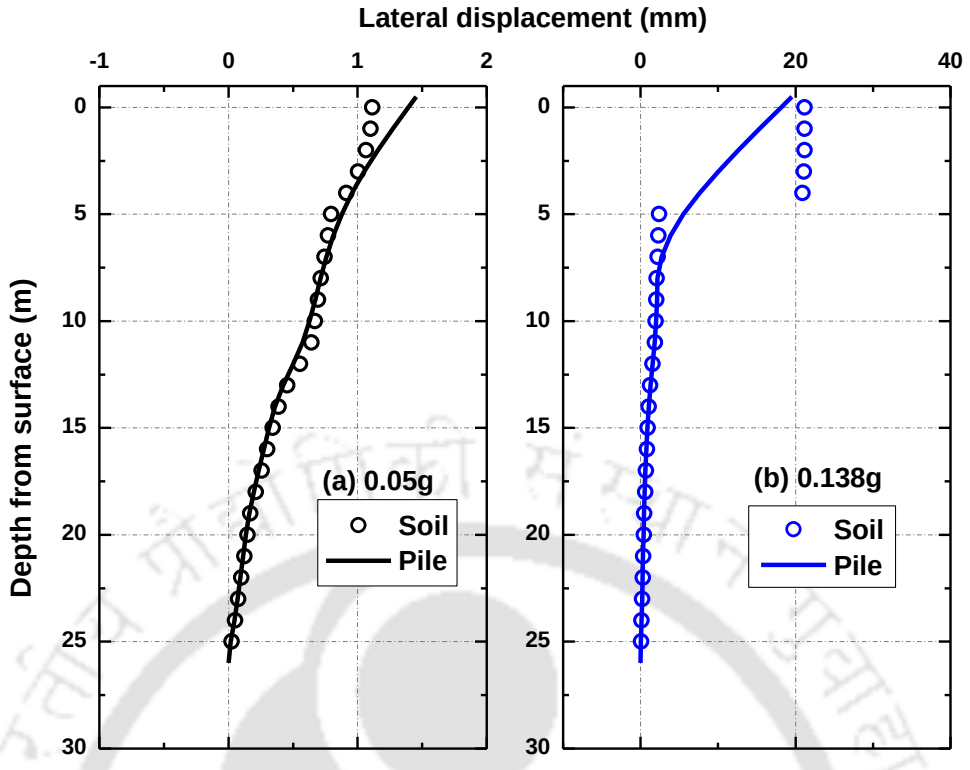

Fig. 7.13 Comparison of free field and single pile displacements for (**a**) 0.05g (**b**) 0.138g events

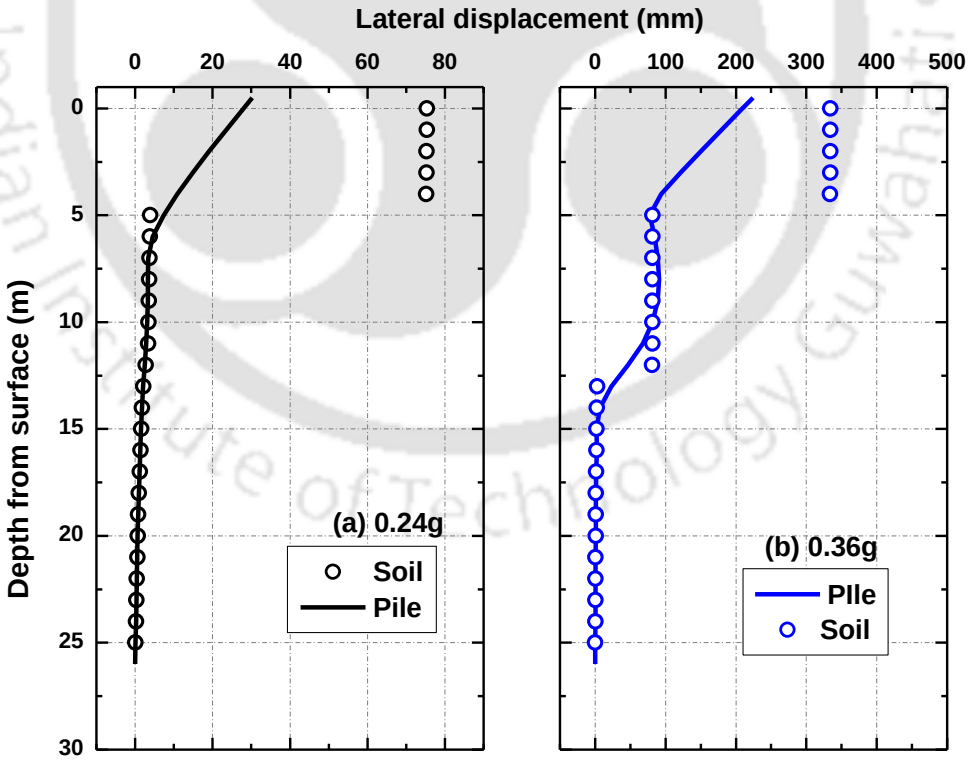

Fig. 7.14 Comparison of free field and single pile displacements for (**a**) 0.24g (**b**) 0.36g events

In order to understand the effect of varying seismic intensity on the pile foundation behaviour in liquefiable soils, peak magnitudes of displacement, shear force (SF) and bending moments (BM) of single pile are presented in Fig. 7.15, Fig. 7.16, and Fig. 7.17, respectively. The first obvious observation is the increase of magnitudes of displacement, shear force and bending moment with increase in PBRA of motions. As the single pile is free headed, peak displacement is observed at the pile top in all the cases. Another interesting observation is that the pile experiencing severe response shift (displacements, shear forces and bending moments) at the interface of liquefiable and non-liquefiable strata (close to 5 m from surface) for events which can cause liquefaction (0.138g, 0.24g and 0.36g). This is attributed to the kinematic response and can be understood by considering the bending moment profile (Fig. 7.17). At the interface of two layers (be it non-liquefiable or liquefiable), a strong stiffness (V_s or G_{max}) contrast exists resulting in discontinuous strains at the interfaces. This imposes relatively large curvature (inverse of strain) on piles at the juncture of two layers. Such excessive curvature at the interfaces leads to high bending possibilities in the piles, which was also reported by Nikolaou et al. (2001) and Mylonakis (2001).

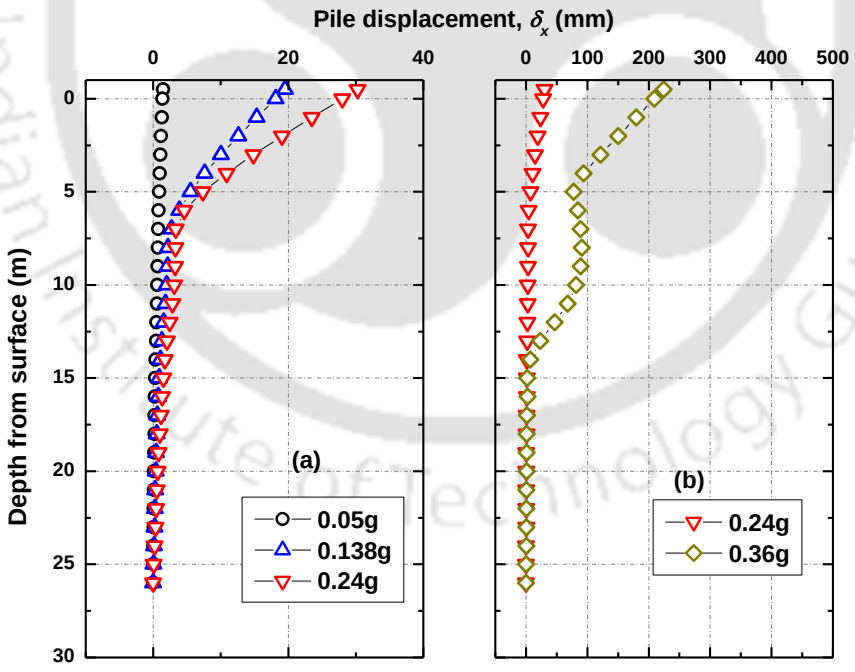

Fig. 7.15 Peak displacements in the single pile for different seismic events

Recent reported failures of pile foundations in liquefiable soils highlighted the issue of severe bending moments and resulting plastic hinge formation at the interface of two layers (Hamada and O'Rourke 1992). In lieu of this, global seismic codes (NEHRP 1997; JRA

2002; EN 1998-1 2004; IS:2911 2010) strongly suggests to incorporate the kinematic effects due to seismic induced soil deformations over entire length of pile to avoid any plastic hinge formation at the interface of the stiffness contrasting layers. As it can be seen from Fig. 7.16a and Fig. 7.17a, magnitudes of peak SF and BM are less than 50 kN and 120 kN.m, respectively for events up to 0.24g, however, for the event 0.36g (Fig. 7.16and Fig. 7.17b), excessive magnitudes of SF (close to 2000 kN) and BM (as high as 1800 kN.m) were observed.

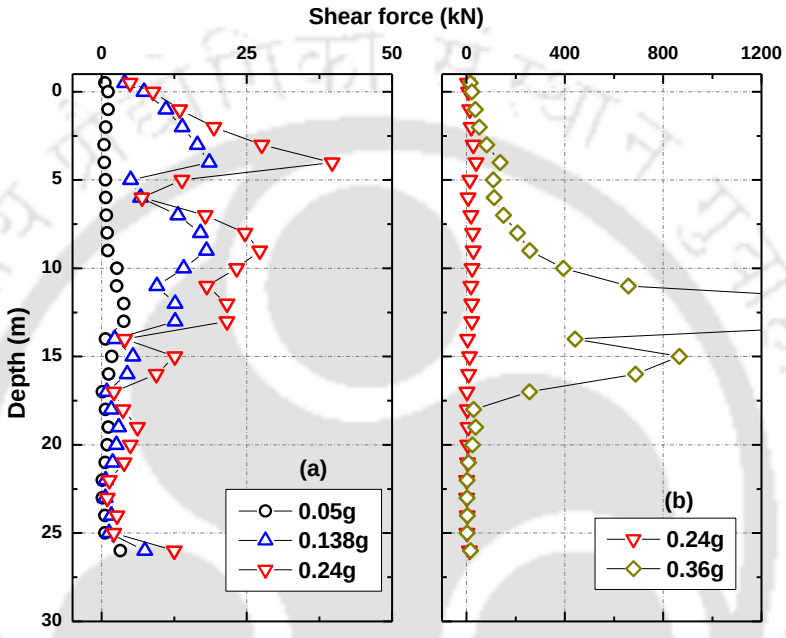

Fig. 7.16 Peak shear forces in the single pile for different seismic events

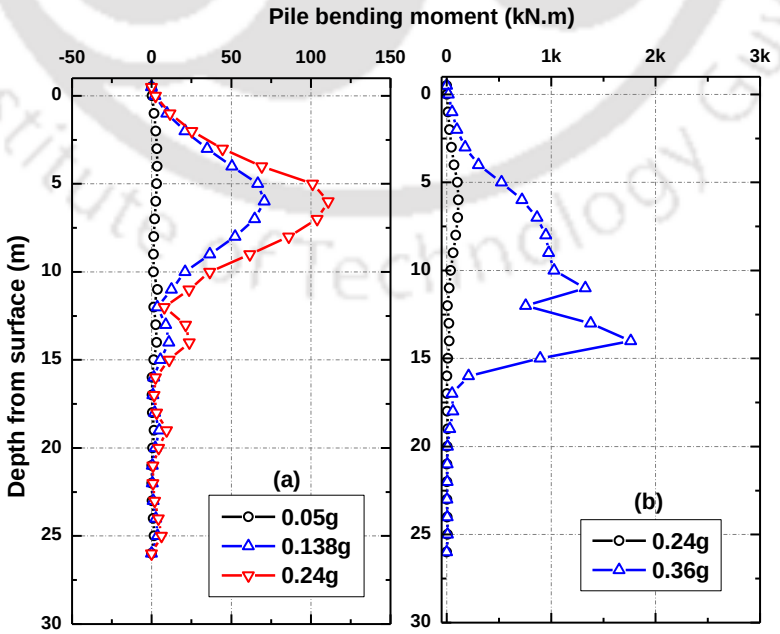

Fig. 7.17 Peak bending moments in the single pile for different seismic events

7.5.2 Group Pile Response

The chosen pile group configuration was also subjected to the similar seismic events. Response of all the four piles in the group are monitored after the analysis was run and identified that all of them gave similar results as the same *p-y* curves (with 0.5 multiplication factor) have been utilised. This means that response considered for any single pile from the group should represent behaviour of the group. Therefore, only the response from one pile is considered here to understand the effect of increasing PBRA on the seismic performance of pile group in liquefiable soils. Fig. 7.18 (a and b) presents the profiles of peak pile displacements and peak BM along the depth for the three considered ground motions. It must be mentioned that the support condition at the pile cap is given a rotation fixity and translation allowed (typical pile cap restraint condition). Therefore, from Fig. 7.18 a, peak displacements are observed at the pile head, while peak BM are also noted at the pile head due to the rotation fixity condition, unlike the bending response of free-headed pile. It can be observed that pile group also exhibited similar response of high displacement and BM with increasing intensity of PBRA. The 0.05g event yielded 5 mm pile displacement at the pile cap while 8 mm and 12.5 mm of displacements were noted for 0.138g and 0.24g events, respectively. The magnitude of BM at the pile head for the three events almost remained unaffected even with significant increase in the PBRA of the motions. This has been explained by Nikolaou et al. (2001) that for fixed head piles, the effect of seismic loads on kinematic interaction are more pronounced in the deeper soil layers and practically unaffected at the pile head.

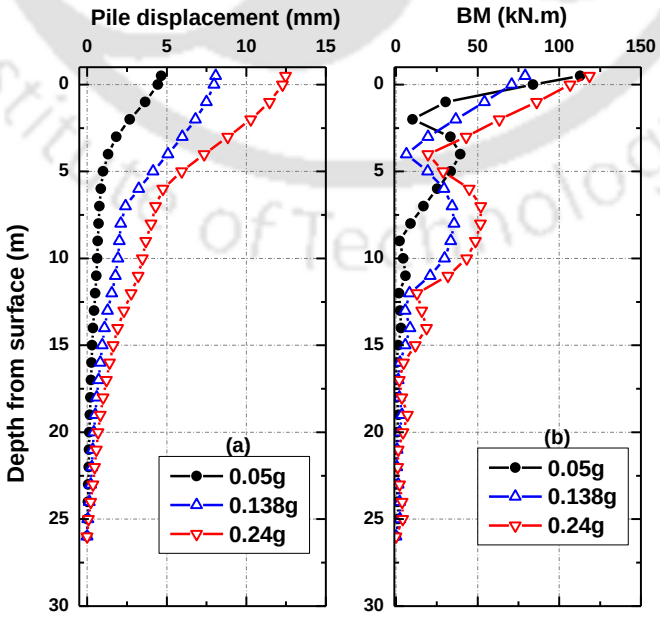

Fig. 7.18 Single pile and 2×2 pile group performance comparison in terms of **(a)** peak displacement **(b)** peak bending moment

To facilitate a comparison between the seismic performance of single pile and 2×2 pile group at the chosen site and analysed conditions, displacements and BM are plotted together for each event (Fig. 7.19(a-c) and Fig. 7.20(a-c) respectively). Few interesting observations can be made from these: first is the similar displacement profiles up to 5 m from the base of the pile for all the motions (Fig. 7.19); and similar BM response up to 10 m from the base of the pile for the chosen motions (Fig. 7.20). Considering the pile group response to be a fixed head (rotation fixity) pile and the single pile to be free-headed pile, such (similar) response can be explained by the bending moment profile. Such depth up to which both the free and fixed headed piles show similar bending response is termed as active length (or the depth beyond which a head-loaded pile behaves as an infinitely long beam) (Poulos and Davis 1980; Randolph 1981).

Another important observation from the comparison of single and pile group is that in case of nonliquefiable event (0.05g) as observed from Fig. 7.19a and Fig. 7.20a, pile group yielded relatively higher than the single pile. A peak pile displacement of 1.5 mm was observed for single pile for 0.05g event while the same is increased to 4.5 mm in case of the group. Similarly, increased BM for the pile group in case of 0.05g event can be noted (Fig. 7.20a). However, in case of liquefiable events (0.138g and 0.24g), single pile yielded relatively higher and pile group showed lower magnitudes of displacement and BM.

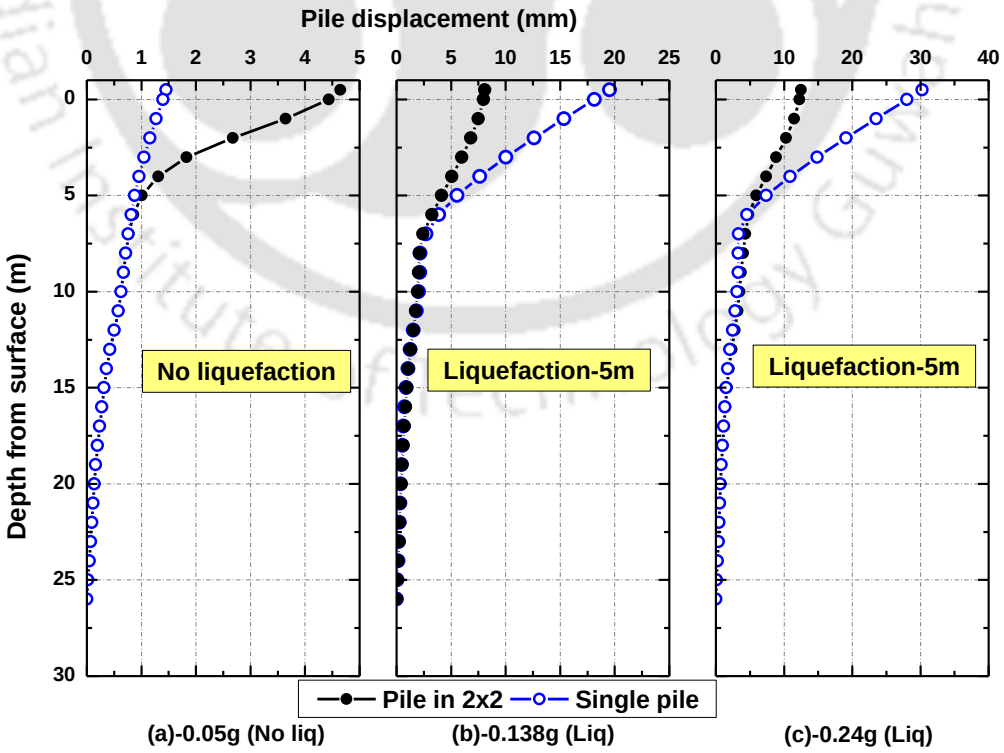

Fig. 7.19 Peak pile displacements comparison for single and 2×2 pile group

Such phenomenon of higher response (displacements and BM) of pile group in nonliquefiable soils and lower response in liquefiable soils can be attributed to the presence of shadowing effects in nonliquefiable soils. In case of nonliquefiable soils (or in typical static cases), it is expected that pile group would yield higher response compared to a single pile of similar loadings due to the interference of strain contours from pile to soil to pile (pile-soil-pile) as reported experimentally by Brown et al. (1988). However, in case of liquefiable events due to the loss of surrounding soil support and resulting absence of shadowing effect, pile group is in beneficial condition and yields relatively lesser response compared to the single pile of similar loading conditions. Kumar et al. (2016) noted similar lower response of combined pile raft foundation in liquefiable soils in comparison to a single pile of similar loading.

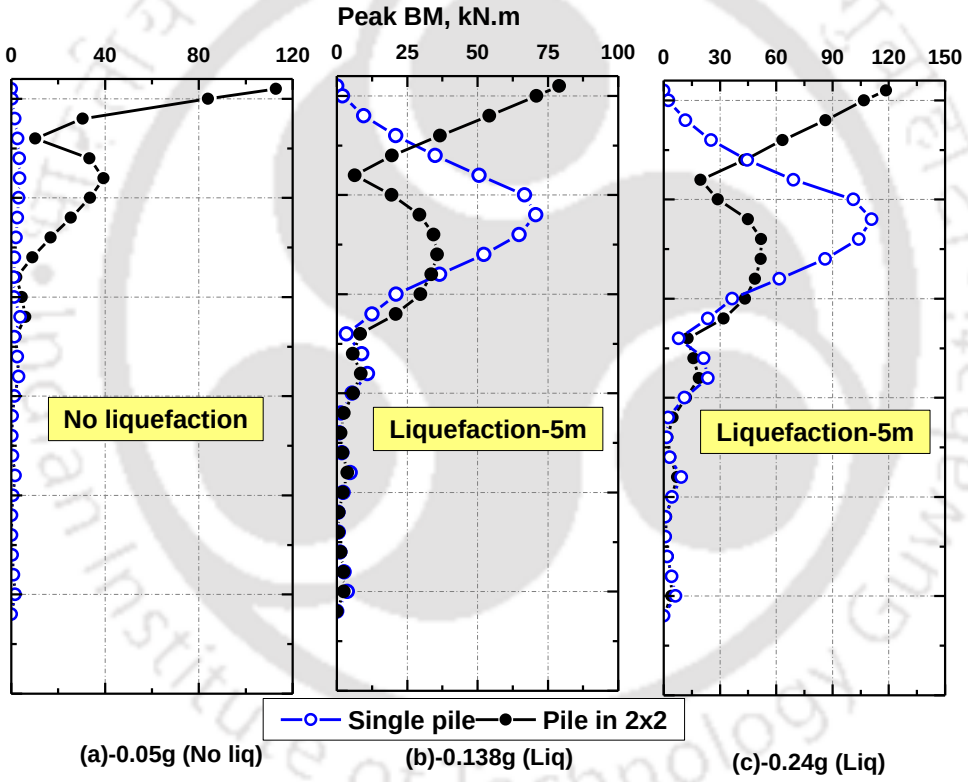

Fig. 7.20 Peak pile bending moments comparison for single and 2×2 pile group

Based on the performed seismic analysis of pile foundations, design engineers may consider some of the alluded recommendations:

1. The effect of dynamic soil properties should not be ignored in the seismic free field response analysis.
2. The nonlinear behaviour of the soil integrated with the pore water pressure generation (nonlinear analysis) must be incorporated in the time history analysis for structural analysis, if the chosen sites of interest are prone to liquefaction.

7.6 SUMMARY

Stability of pile foundations in seismic active regions depends on the mutual interactions (both inertial and kinematic) of underlying soil and pile due to the incoming waves. The kinematic response of two pile configurations has been studied in detail for different seismic events with increasing intensity of PBRA. Dynamic BNWF model has been utilised for the study and validation of the adopted model has been performed against the centrifuge results of single pile foundation reported by Boulanger et al. (1999). The nonlinear GRA results presented in the previous chapter have been made use of in terms of free field soil displacements. Results are presented independently for the single pile and the 2×2 pile group, in terms of displacement and bending moments along the depth of the pile. A comparison is drawn for the seismic performance of single and 2×2 pile group in liquefiable soils. It has been concluded that pile group yields relatively lesser response compared to the single pile in liquefiable soils.

CHAPTER VIII. CONCLUDING REMARKS

8.0 SUMMARY OF THE THESIS

The dynamic soil behaviour is being characterised by strain dependent dynamic properties and liquefaction potential parameters. Since the soils of different regions differ in their properties, determination of soil specific properties for different regions and associated response is essential for effective dynamic analysis. Therefore, the main objective of present research is to establish the region-specific dynamic soil properties sampled from two active seismic regions of India (north and northeastern locations). Six typical soils (four sand and two clay samples) have been considered for the study. The dynamic testing programme (a series of four independent testing techniques) has been adopted such that a comprehensive dynamic characterisation of chosen soils over a wide range of strains is achieved. The results obtained were presented in terms of simplified empirical relationships with region-specific best-fit parameters. Application of the established dynamic soil properties has been demonstrated through the equivalent linear and nonlinear effective stress seismic ground response studies. Results obtained from the ground response studies were further utilised in seismic analysis of pile foundations based on Winkler spring approach. Interesting observations and corresponding conclusions drawn from the current study are presented in this chapter along with the limitations and extendable future scope.

8.1 MAJOR CONCLUSIONS/CONTRIBUTIONS

Major conclusions and contributions from the current study are presented below.

Dynamic characterisation through experimental program

- The obtained dynamic soil properties from the element tests are consistent with the literature suggested trends, however, G/G_{max} of the tested sands plot higher while damping ratio values are overestimated in the literature curves.

- Empirical relationships for the evaluation of strain-dependent dynamic properties have been established for the tested soils, based on the experimental results. Design G/G_{max} and D curves have been developed at practical range of mean effective confining pressures for direct application in the typical soils.
- The BP sand in its loose state experienced liquefaction in the first few cycles of undrained cyclic shearing, confirming to the fact that the river bed soils in northeastern Indian region are prone to sudden pore pressures and significant strain accumulation in case of mild to intense seismic events (CSR≥0.15). Empirical formulations for pore water pressure model have been presented for BP sand at three different effective confining pressures.
- The G/G_{max} and D ratio curves of PC and RS are not affected by the effective confining pressure, meaning that same curves may be utilised for such soils at any depth. Stiffer G/G_{max} and softer damping ratio was obtained for RS specimens than the PC specimens, despite having similar gradation properties.

Seismic ground response studies

- On adopting the literature suggested G/G_{max} and D curves in seismic ground response analysis, significant underestimation of seismic demands (30-40% in terms of PGA and spectral accelerations) has been observed compared to the experimentally obtained data of regional specific soils. This observation infers that mere utilisation of standard curves in seismic design may often lead to unreliable results.
- Nonlinear effective stress seismic response studies showed consistent results in comparison to the laboratory tests results. The chosen sites in northeastern India experienced high amplification (close to 2.0) for low to moderate seismic events (0.05g and 0.138g), and attenuation beyond due to the high viscous damping resulted from high shear strains.
- The surficial loose sand layers of northeastern India exhibited liquefaction up to a depth of 15m from the surface for high intensity (PBRA≥0.10g) motions.
- Despite the same depth of liquefaction by increased intensity of ground motions, the magnitude of shear strains are enhanced for high intensity motions.

Seismic analysis of pile foundations

- Pile foundations exhibited excessive lateral deformations in cases of liquefiable soils due to the additional lateral deformations caused by the liquefied soils.
- The response of piles abruptly changes at the vicinity of liquefiable and non-liquefiable zones: increased displacements and sharp bending moment contrast is observed. This has been attributed to the sharp stiffness contrast existing at the interfaces of liquefiable and non-liquefiable soils, leading to infinite bending strains in the piles.
- The adopted 2×2 pile group showed a relatively better seismic performance (reduced lateral displacements and bending moments) compared to the single pile of similar geometry, in case of liquefiable soils. The absence of pile-soil-pile mutual interaction in liquefied soils is the prime reason for this effect.

8.2 LIMITATIONS OF THE STUDY

The outcome presented in the thesis can be applied judiciously considering the limitations below mentioned.

- The relative density values mentioned in all the element tests are based on initial bulk density and the consolidated densities are not taken in to account.
- Seismic ground response analyses presented in the current study are based on 1D analysis and dimensional effects (2D and 3D) of seismic wave propagation are not considered.
- Since, the laboratory element tests were performed on reconstituted specimens, adoption of test results in GRA studies should be considered only as a demonstration purpose and may not purely represent the actual scenario.
- Conclusions drawn from the seismic analysis of pile supported structures are based on discrete Winkler spring approach and kinematic interactions. The continuity of soil deposit and inertial interactions are not considered.

8.3 FUTURE RESEARCH SCOPE

Any research is infinite and always poses scope for further research. Following are some of the identified extendable research ideas from this thesis.

- Dynamic tests on various other soils from other locations of India can be attempted on undisturbed specimens, with varying parameters of investigation. A generalized shear modulus reduction and damping model may be developed using the results.
- Comprehensive dynamic testing program can be planned on fully saturated specimens (both at low strain and high strain range) to understand the effects of saturation on the dynamic soil properties over wide strain range.
- A series of element tests (CTX or DSS) in undrained conditions can be performed on cohesionless and cohesive soils of the regions with varying indices, to develop a generalized pore water pressure model.
- Since the present experimentation was performed on disturbed specimens, for more accurate estimation of the dynamic response of the insitu soils, laboratory testing of high quality undisturbed soil samples is recommended.
- Continuum analysis with advanced nonlinear models incorporating PWP (such as *Finn* model in FLAC and *UBC* model in PLAXIS) can be performed by using established strain dependent dynamic properties for Indian soils, to concrete the conclusions of this research.
- Inertial interactions may also be considered in the seismic analysis of pile foundations, provided the availability of liquefiable *t-z* (axial load transfer) and *Q-z* (end resistance) curves.
- Partial liquefaction behaviour of soils can be investigated and simplified empirical models can be developed for use in deep foundation applications.

REFERENCES

1. Abdoun T, Dobry R. (2002). Evaluation of pile foundation response to lateral spreading. *Soil Dyn Earthq Eng*, 22:1051–1058.
2. Abdoun T, Dobry R, O'Rourke TD, Goh SH. (2003). Pile response to lateral spreads: Centrifuge Modeling. *J Geotech Geoenvironmental Eng*, 129:869–878.
3. Adhikari S, Bhattacharya S. (2011). Vibrations of wind-turbines considering soil-structure interaction. *Wind and Structures*, 14 (2): 85-112.
4. Anastasopoulos I, Gazetas G, Drosos V, Georgarakos T, Kourkoulis R. (2008). Design of bridges against large tectonic deformation. *Earthq Eng Eng Vib*, 7(4):345–368.
5. Andrus R, Stokoe KH. (2000). Liquefaction resistance of soils from shearwave velocity. *J Geotech Geoenvironmental Eng*, ASCE 126(11):1015–1025.
6. API (2014). *Recommended practice for planning, designing and constructing fixed offshore platforms — working Sstress design*. American Petroleum Institute, *API* 2A-WSD (RP 2A-WSD) 22nd Edition, Washington.
7. Arulnathan R, Boulanger RW, Riemer M. (1998). Analysis of bender element tests. *Geotech Test J*, 21(2):120–131.
8. Ashour M, Ardalan H. (2012). *p–y* curve and lateral response of piles in fully liquefied sands. *Canadian Geotechnical Journal*, 49(6):633-650.
9. Ashour M, Norris G. (2003). Lateral loaded pile response in liquefiable soil. *J Geotech Geoenvironmental Eng*, 129(5):404–414.
10. ASTM D2487 (2017). *Standard Practice for classification of soils for engineering purposes (Unified Soil Classification System)*. American Society for Testing and Materials Stand Guid, D5521-05:1–5.
11. ASTM D3999 (2013). *Standard test methods for the determination of the modulus and damping properties of soils using the cyclic triaxial apparatus*. American Society for Testing Materials Stand Guid, 91:1–16.
12. ASTM D4015 (2014). *Standard test methods for modulus and damping of soils by resonant-column*. American Society for Testing and Materials Stand Guid, 1–22.
13. ASTM D422-63 (2007). *Standard test method for particle-size analysis of soils*. American Society for Testing and Materials Stand Guid, West Conshohocken, PA 63:1–8.
14. ASTM D6913 (2017). *Standard test methods for particle-size distribution (gradation) of soils using sieve analysis*. American Society for Testing and Materials Stand Guid, West Conshohocken, PA
15. Bai L. (2011). Preloading effects on dynamic sand behaviour by resonant column tests. *PhD Thesis*, Technischen Universität Berlin, Germany.
16. Balreddy MS, Dinesh SV, Sitharam TG. (2016). Influence of sand and low plasticity clay mixtures on the liquefaction and postliquefaction behavior. *Japanese Geotechnical Society Special Publication*, 2(21):806-810.
17. Basu D, Boga M, Dey A. (2019). A time-domain nonlinear effective-stress non-Masing approach of ground response analysis of Guwahati city, India. *Earthq Eng Eng Vib*, 18(1):61–75.
18. Bhattacharya S. (2003). Pile instability during earthquake. *PhD Thesis*, University of Cambridge, UK
19. Bhattacharya S, Madabhushi SPG, Bolton MD. (2004). An alternative mechanism of pile failure in liquefiable deposits during earthquakes. *Géotechnique*, 54(3):203–213.

20. Bhattacharya S, Tokimatsu K, Goda K, Sarkar R, Shadlou M, Rouholamin M. (2014). Collapse of Showa Bridge during 1964 Niigata earthquake: A quantitative reappraisal on the failure mechanisms. *Soil Dyn Earthq Eng*, 65:55–71.
21. Blaney GW, O'Neill MW. (1986). Measured lateral response of mass on single pile in clay. *J Geotech Eng*, 112:443–457.
22. Boominathan A, Dodagoudar GR, Suganthi A, Uma Maheswari R. (2008). Seismic hazard assessment of Chennai city considering local site effects. *J Earth Syst Sci*, 117(2):853–863.
23. Boore DM. (1983). Stochastic simulation of high-frequency ground motions based on seismological models of the radiated spectra. *Bull Seismol Soc Am*, 73(6A):1865–1894
24. Boulanger BRW, Curras CJ, Kutter BL, Wilson DW, Abghari A. (1999). Seismic soil-pile-structure interaction experiments and analyses. *J Geotech Geoenvironmental Eng*, 125(9):750–759.
25. Brandenberg SJ. (2005). Behaviour of pile foundations in liquefied and laterally spreading ground. *PhD Thesis*, Unversity of California Davis, US
26. Bray JD, Stewart JP, Baturay MB, Durgunoglu T, Onalp A, Sancio RB, Ural D, Ansal A, Bardet JB, Barka A, Boulanger R, Cetin O, Erten D. (2000). Damage patterns and foundation performance in Adapazari. *Earthquake Spectra*, 16(S1):163-189.
27. Brown BDA, Morrison C, Reese LC. (1988). Lateral load behaviour of pile group in sand. *J Geotech Eng*, 114:1261–1276.
28. BS EN 1997-1. (2004). *Geotechnical design Part 1: General rules*. British Standards, UK.
29. Byrne P. (1991). A cyclic shear-volume coupling and pore-pressure model for sand. In: *Second International Conference on Recent Advances in Geotechnical Earthquake Engineering and Soil Dynamics*. St. Louis, Missouri, 47–55
30. Carlton BD. (2014). An improved description of the seismic response of sites with high plasticity soils, organic clays, and deep soft soil deposits. *PhD Thesis*, University of California, Berkeley
31. Chattaraj R, Sengupta A. (2016). Liquefaction potential and strain dependent dynamic properties of Kasai River sand. *Soil Dyn Earthq Eng*, 90:467–475.
32. Chatterjee K, Choudhury D. (2016). Influences of local soil conditions for ground response in kolkata city during earthquakes. *Proc Natl Acad Sci India Sect A Phys Sci*, 88(4):515-528.
33. Chatterjee K, Choudhury D, Dilli Rao V, Poulos HG. (2019). Seismic response of single piles in liquefiable soil considering P-delta effect. *Bull Earthq Eng*, 17(6):2935-2961.
34. Chehat A, Hussien MN, Abdelazize M, Chekired M. (2018). Stiffness-and damping-strain curves of sensitive Champlain clays through experimental and analytical approaches. *Can Geotech J*, 56(3):364-377.
35. Chiaradonna A, Tropeano G, d'Onofrio A, Silvestri F. (2018). Development of a simplified model for pore water pressure build-up induced by cyclic loading. *Bull Earthq Eng*, 16(9):3627-3652.
36. Choobbasti AJ, Zahmatkesh A. (2016). Computation of degradation factors of p-y curves in liquefi able soils for analysis of piles using three-dimensional finite-element model. *Soil Dyn Earthq Eng*, 89:61–74.
37. Choudhury D, Phanikanth VS, Mhaske SY, Phule RR, Chatterjee K. (2015). Seismic liquefaction hazard and site response for design of piles in Mumbai City. *Indian Geotech J*, 45(1):62–78.
38. Chung R, Yokel F, Drnevich V. (1984). Evaluation of dynamic properties of sands by resonant column testing. *Geotech Test J*, 7(2):60-69.
39. Clayton CRI, Priest JA, Bui M, Zervos A, Kim SG. (2009). The Stokoe resonant column apparatus: effects of stiffness, mass and specimen fixity. *Geotechnique*, *59*(5), 429-437.
40. COSMOS https://strongmotioncenter.org/vdc/scripts/default.plx. Accessed 28 Apr 2017
41. CSI (Computers and Structures, Inc.) (2011). CSI analysis reference manual for SAP2000, ETABS, SAFE, and CSiBridge.

42. Cubrinovski M, Bradley B. (2008). Assessment of seismic performance of soil–structure systems. In: *Proceedings of the 18th New Zealand Geotechnical Society 2008 Symposium, Auckland*, New Zealand, 111–127.
43. Darendeli M. (2001). Development of a new family of normalized modulus reduction and material damping. *PhD Thesis*, University of Texas
44. Dash S, Rouholamin M, Lombardi D, Bhattacharya S. (2017). A practical method for construction of *p-y* curves for liquefiable soils. *Soil Dyn Earthq Eng*, 97:478–481.
45. Dash SR, Bhattacharya S, Blakeborough A. (2010). Bending – buckling interaction as a failure mechanism of piles in liquefiable soils. *Soil Dyn Earthq Eng*, 30(1-2):32–39.
46. Dash SR, Govindaraju L, Bhattacharya S. (2009). A case study of damages of the Kandla Port and Customs Office tower supported on a mat-pile foundation in liquefied soils under the 2001 Bhuj earthquake. *Soil Dyn Earthq Eng*, 29(2):333–346.
47. Dash HK, Sitharam TG. (2011). Undrained monotonic response of sand–silt mixtures: effect of nonplastic fines. *Geomechanics and Geoengineering: An International Journal*, 6(1):47-58.
48. Desai SS, Choudhury D (2015) Site-specific seismic ground response study for nuclear power plants and ports in Mumbai. *Nat Hazards Rev*, 16(4):04015002.
49. DNV-OS-J101 (2013). *Design of offshore wind turbine structures*, DET NORSKE VERITAS, Oslo, Norway, www.dnv.com
50. Dobry R, Pierce W, Dyvik R, Thomas GE, Ladd RS. (1985). *Pore pressure model for cyclic straining of sand*. Civil Engineering Department, Rensselaer Polytechnic Institute, Troy
51. Drnevich VP, Hall JR., Richart Jr F. (1967). Effects of amplitude of vibration on the response of soft clay deposits. In: *Int Symp Geotech Eng of Soft Soils*. 51–87
52. Drnevich VP, Hardin BO, Shippy DJ. (1978). Modulus and damping of soils by the resonant column method. Dyn Geotech Testing, *Am Soc Test Mater Spec Tech Publ* 654:91–125
53. Dutta TT, Saride S, Jallu M. (2017). Effect of saturation on dynamic properties of compacted clay in a resonant column test. *Geomechanics and Geoengineering*: *An International Journal*, *12*(3), 181-190.
54. Ec L, Sh Y, Rahardjo H. (2005). Measuring shear wave velocity using bender elements. *Geotech Test J*, 28(5):488–498
55. El Mohtar CS, Bobet A, Drnevich VP, Jonston CT, Santagata MC. (2014). Pore pressure generation in sand with bentonite: from small strains to liquefaction. *Géotechnique*, 64(2):108–117.
56. El Mohtar CS, Drnevich VP, Santagata M, Bobet A. (2013). Combined resonant column and cyclic triaxial tests for measuring undrained shear modulus reduction of sand with plastic fines. *Geotech Test J*, 36(4):1–9.
57. EN 1998-1. (2004). Eurocode 8: Design of structures for earthquake resistance - Part 5: Foundations, retaining structures and geotechnical aspects
58. Esteva L. (1988). The Mexico Earthquake of September 19, 1985-consequences, lessons, and impact on research and practise. *Earthq Spectra*, 4(3):413–426
59. Experto Geotechnical Consultants and Research Private Limited (2015). Geotechnical report for proposed cosmetic factory plant at Pachoria, Dadara, North Guwahati, Guwahati, Kamrup, Assam. *Feasibility Report*, GMDA/RTP/95/Geotech 4/18, Guwahati, India.
60. Finn WDL, Bhatia SK. (1982). Prediction of seismic pore water pressures. In: *10th International conference in soil mechanics and foundations*. Stockholm, 201–206
61. Finn WDL, Fujita N. (2002). Piles in liquefiable soils: seismic analysis and design issues. *Soil Dyn Earthq Eng*, 22(9-12):731–742
62. Garala T, Madabhushi SPG. (2018). Seismic behaviour of soft clay and its influence on the response of friction pile foundations. *Bull Earthq Eng*, 17(4):1919-1939.

63. Gazetas G, Dobry R. (1984). Horizontal response of piles in layered soils. *J Geotech Eng*, 110(1):20–40.
64. GDSLab Manual (2014). RCA GDS Resonant Column (GDSRCA). 1–6
65. Gerolymos N, Gazetas G. (2006). Winkler model for lateral response of rigid caisson foundations in linear soil. *Soil Dyn Earthq Eng*, 26(5):347–361.
66. Ghasemi-fare O, Pak A. (2016). Numerical investigation of the effects of geometric and seismic parameters on liquefaction-induced lateral spreading. *Soil Dyn Earthq Eng* 89:233–247.
67. Govindaraju L. (2005). Liquefaction and dynamic properties of sandy soils. *PhD Thesis*, IISc Bangalore
68. Govindaraju L, Bhattacharya S. (2012). Site-specific earthquake response study for hazard assessment in Kolkata city, India. *Natural hazards*, *61*(3), 943-965.
69. Haldar S, Babu GLS. (2010). Failure mechanisms of pile foundations in liquefiable soil : Parametric Study. *Int J Geomec*, 10(2):74–84
70. Hamada M, O'Rourke TD. (1992). *Case studies of liquefaction and lifeline performance during past earthquakes*, Technical Report NCEER-92-0001, National Center for Earthquake Engineering Research, Buffalo, New York.
71. Hanks TC, McGuire RK. (1981). The character of high-frequency strong ground motion. B*ull Seismol Soc Am*, 71(6):2071–2095
72. Hanumantharao C, Ramana GV. (2008). Dynamic soil properties for microzonation of Delhi, India. *J Earth Syst Sci*, 117(2):719–730
73. Hardin BO. (1970). S*uggested methods of test for shear modulus and damping of soils by the resonant column*. Special procedures for testing soil and rock for engineering purposes, ASTM, Philadelphia, 516-529.
74. Hardin BO. (1978). The nature of stress-strain behaviour of soils. In: *Earthquake Engineering and Soil Dynamics*. Pasadena, CA, ASCE, 3–90
75. Hardin BO, Black WL. (1968). Vibration modulus of normally consolidated clay. *J of Soil Mech Found Div*, 98(6), 603-624.
76. Hardin BO, Drnevich VP. (1972). Shear modulus and damping in soils: Measurement and parameter effects. *J Soil Mech Found Div*, 98(SM6):603–624
77. Hardin B, Music, J. (1965). Apparatus for vibration of soil specimens during the triaxial test. In *Instruments and Apparatus for Soil and Rock Mechanics*. ASTM International.
78. Hardin BO, Richart FE. (1963). Elastic wave velocities in Granular soils. *J Soil Mech Found Div*, 89:33–65
79. Hashash YM, Park D. (2001). Non-linear one-dimensional seismic ground motion propagation in the Mississippi embayment. *Engineering Geology*, *62*(1-3), 185-206.
80. Hashash YMA, Musgrouve MI, Harmon JA, Okan I, Groholski DR, Phillips CA, Park D. (2016). DEEPSOIL 6.1, *User Manual*
81. Head K. (1992). *Manual of soil laboratory testing*, Volume 3. *Wiley & Sons*, New York
82. Heshmati AA, Shahnazari H, Sarbaz H. (2015). The cyclic threshold shear strains in very dense clean sand. *Eur J Environ Civ Eng*, 19(7):884–899.
83. Hetenyi M. (1946). *Beams on elastic foundation*. University of Michigan, Ann Arbor
84. Hoyos LR, Suescún EA, Puppala AJ. (2011). Small strain stiffness of unsaturated soils using a suction-controlled resonant column device with bender elements. In: *J. Han and D.E. Alzamora, eds. Advances in Geotechnical Engineering*, GSP 211, Geo-Institute of ASCE, *Proceedings of Geo-Frontiers*, Dallas, TX, 4313–4322.
85. Hsu C-C, Vucetic M. (2004). Volumetric threshold shear strain for cyclic settlement. *J Geotech Geoenvironmental Eng*, 130(1):58–70.
86. Hsu C-C, Vucetic M. (2006). Threshold shear strain for cyclic pore-water pressure in cohesive

soils. *J Geotech Geoenvironmental Eng,* 132(10):1325–1335.
87. Hwang HHM, Lee CS. (1992). Parametric study of site response analysis. *Soil Dyn Earthq Eng,* 10(6):282–290
88. Hyde AF, Higuchi T, Yasuhara K. (2006). Liquefaction, cyclic mobility, and failure of silt. *J Geotech Geoenvironmental Eng*, *132*(6), 716-735.
89. Idriss IM, Boulanger RW. (2006). Semi-empirical procedures for evaluating liquefaction potential during earthquakes. *Soil Dyn Earthq Eng,* 26(2-4):115–130.
90. Iida K. (1938.) The velocity of elastic waves in sand. *Bull Earthq Res Inst,* 16:131–145
91. Imai T, Tonouchi K. (1982). Correlation of N-value with S-wave velocity and shear modulus. In: *Proceedings of the 2nd European symposium on penetration testing*. Amsterdam, pp 57–72
92. IS:1893 (Part 1). (2016). *Criteria for earthquake resistant design of structures*. Bureau of Indian Standards, New Delhi, India
93. IS:2911 (part1/Section 2) (2010). *Design and construction of pile foundations* - code of practice. Bureau Indian Standards, New Delhi, India
94. Ishibashi I, Zhang X. (1993). Unified dynamic shear moduli and damping ratios of sand and clay. *Soils Found,* 33(1):182–191.
95. Ishihara, K. (1996). *Soil behaviour in earthquake geotechnics,* Oxford Science Publication UK.
96. Ishihara K, Li S. (1972). Liquefaction of saturated sand in triaxial torsion shear test. *Soils Found,* 12(2):19–39
97. Ishihara T. (1993). Liquefaction and flow failure during earthquakes. *Geotechnique* 43(3):351–415
98. Ivsic T. (2006). A model for presentation of seismic pore water pressures. *Soil Dyn Earthq Eng,* 26(2-4):191–199
99. Iwasaki T, Tatsuoka F. (1977). Effects of grain size and grading on dynamic shear moduli of sands. *Soils Found,* 17(3):19–35.
100. Iwasaki T, Tatsuoka F, Takagi Y. (1978). Shear moduli of sand under cyclic torsional shear loading. *Soils Found,* 18(1):39–56.
101. Jafari MK, Shafiee A, Razmkhah A. (2002). Dynamic properties of fine grained soils in south of Tehran. *J Seismol Earthq Eng,* 4(1):25–35
102. Jakka RS, Datta M, Ramana G V. (2010). Liquefaction behaviour of loose and compacted pond ash. *Soil Dyn Earthq Eng,* 30(7):580–590.
103. JRA (Japan Road Association). (2002). *Seismic design specifications of highway bridges.* Maruzen, Tokyo, Japan.
104. Kavvadas M. (1993). Kinematic seismic response and bending of free-head piles in layered soil. *Geotechnique,* 43(2):207–222
105. Kawamura S, Nishizawa T, Wada T. (1985). *Damage to piles due to liquefaction found by excavation twenty years after earthquake*. Nikkei Architecture, Tokyo, Japan, 27:130-134 (in Japanese)
106. Kayal JR, Arefiev SS, Barua S, Hazarika D, Gogoi N, Kumar A, Chowdhury SN, Kalita S. (2006). Shillong plateau earthquakes in northeast India region: Complex tectonic model. *Curr Sci,* 91(1):109–114
107. Kayal JR, Arefiev SS, Baruah S, Hazarika D, Gogoi N, Gautam JL, Baruah S, Dorbath C, Tatevossian R. (2012). Large and great earthquakes in the Shillong plateau-Assam valley area of Northeast India Region: Pop-up and transverse tectonics. *Tectonophysics* 532186–192.
108. Khattri KN. (1999). Probabilities of occurrence of great earthquakes in the Himalaya. *Proc Indian Acad Sci Earth Planet Sci,* 108(2):87–92
109. Kiku H, Yoshida N. (2000). Dynamic deformation property tests at large strains. In 12th *World Conf Earthq Eng,* New Zealand, 1–7

110. Kirar B, Maheshwari BK. (2017). Dynamic Properties of soils at large strains in Roorkee region using field and laboratory tests. *Indian Geotech J*, 48(1):125–141.
111. Kirar B, Maheswari B. (2013). Effects of silt content on dynamic properties of Solani sand. In: *Seventh International Conference on Case Histories in Geotechnical Engineering*, pp 1–7
112. Knappett JA, Madabhushi SP. (2008). Liquefaction-Induced Settlement of Pile Groups in Liquefiable and Laterally Spreading Soils. *J Geotech Geoenvironmental Eng*, 134(11):1609–1618.
113. Kokusho T. (1980). Cyclic triaxial test of dynamic soil properties for wide strain range. *Soils Found*, 20(2):45–59
114. Kondner R, Zelasko J. (1963). A hyperbolic stress-strain formulation for sands. In: *Proceedings of the 2nd Pan American Conference on Soil Mechanics and Foundations Engineering*, 282–324
115. Kramer SL. (1996). *Geotechnical Earthquake Engineering*, 1st edn. Prentice-Hall, New Jersey
116. Krishna AM, Bhattacharya S, Choudhury D. (2014). Seismic requalification of geotechnical structures. *Indian Geotechnical J*, 44(2):113–118.
117. Kumar A, Harinarayan NH, Baro O. (2017). Nonlinear soil response to ground motions during different earthquakes in Nepal, to arrive at surface response spectra. *Nat Hazards*, 87(1):13–33.
118. Kumar A, Choudhury D, Katzenbach R. (2016). Effect of earthquake on combined pile – raft foundation. *International Journal of Geomechanics*, 16(5):04016013.
119. Kumar SS. (2018). Evaluation of dynamic response of soils subjected to regular and irregular excitations using cyclic triaxial tests. *PhD Thesis*, Indian Institute of Technology Guwahati, India
120. Kumar SS, Krishna AM. (2013). Seismic ground response analysis of some typical sites of Guwahati City. *Int J Geotech Earthq Eng*, *4*(1):83-101.
121. Kumar SS, Krishna AM, Dey A. (2018a). Importance of site-specific dynamic soil properties for seismic ground response studies, *Int J Geotech Earthq Eng*, 9(1):78–98.
122. Kumar SS, Krishna AM, Dey A. (2017). Evaluation of dynamic properties of sandy soil at high cyclic strains. *Soil Dyn Earthq Eng*, 99:157–167.
123. Kumar SS, Krishna AM, Dey A. (2018b.) Dynamic properties and liquefaction behaviour of cohesive soil in northeast India under staged cyclic loading. *J Rock Mech Geotech Eng*, 10(5):958-967.
124. Kumar SS, Dey A, Krishna AM (2015) Dynamic response of river bed sands using cyclic triaxial tests. In: *Proceedings of 5th Indian Young Geotechnical Engineers Conference (5IYGEC)*: extended abstracts. Shweta Publications, pp.174-176.
125. Kumar SS, Murali Krishna A, Dey A. (2014). Parameters influencing dynamic soil properties: a review treatise. *Int J Innov Res Sci*, 3:47–60
126. Kuriyabashi E, Iwasaki T, Tatsuoka F. (1975). Effects of stress-strain conditions on dynamic properties of sands. In: *Japanese Society of Soil Civil Engineers*, 242, 105–114
127. Kyle B, Mark MR, Nathan DE, Daily WD. (1998). Shear modulus and damping relationships for gravels. *J Geotech Geoenvironmental Eng*, 124(5):396–405
128. Lanzo G, Vucetic M, Doroudian M. (1997). Reduction of shear modulus at small strains in simple shear. *J Geotech Geoenvironmental Eng*, 123(11):1035–1042.
129. Lawrence FV. (1963). Propagation velocity of ultrasonic waves through sand. *MIT Research Report*, R63-8.
130. Lin ML, Huang TH, You JC. (1996). The effects of frequency on damping properties of sand. *Soil Dyn Earthq Eng*, 15(4):269–278.
131. Lombardi D, Bhattacharya S. (2016). Evaluation of seismic performance of pile-supported models in liquefiable soils. *Earthq Eng Struct Dyn*, 45(6):1019–1038.
132. Lombardi D, Bhattacharya S. (2014). Modal analysis of pile-supported structures during seismic liquefaction, *Earthq Eng Struct Dyn*, 43(1):119–138.
133. Lombardi D, Bhattacharya S, Hyodo M, Kaneko T. (2014). Undrained behaviour of two silica

sands and practical implications for modelling SSI in liquefiable soils. *Soil Dyn Earthq Eng*, 66:293–304.
134. Lombardi D, Dash SR, Bhattacharya S, Ibraim E, Wood DM, Taylor CA. (2017). Construction of simplified design py curves for liquefied soils. *Géotechnique*, *67*(3), 216-227.
135. Lv YR, Ng CWW, Lam SY, Liu HL, Ma LJ. (2017). Geometric effects on piles in consolidating ground: centrifuge and numerical modeling. *J Geotech Geoenvironmental Eng*, 143(9):04017040.
136. Madabhushi G, Knappett J, Haigh S. (2010). *Design of pile foundations in liquefiable soils*. Imperial College Press.
137. Maheshwari BK, Kirar B. (2017). Dynamic properties of soils at low strains in Roorkee region using resonant column tests. *Int J Geotech Eng*, 1–12.
138. Martin G, Finn W, Seed H. (1975). Fundamentals of liquefaction under cyclic loading. *J Geotech Engg*, 101:423–438
139. Matasovic N, Vucetic M. (1995). Generalized cyclic-degradation-pore- pressure generation model for clays. *J Geotech Eng*, 121(1):33–42
140. Matasovic N, Vucetic M. (1994). Cyclic characterisation of liquefiable sands. *J Geotech Geoenvironmental Eng*, 119(11):1805–1822
141. Matlock H, Reese LC. (1961). Foundation analysis of offshore pile supported structures. In: *5th Int. Conf. on Soil Mechanics and Foundation Engineering*, Paris, 91–97
142. Menq F-Y. (2003). Dynamic properties of sandy and gravelly soils. *PhD Thesis*, University of Texas, Austin
143. Mercado V, El-sekelly W, Abdoun T, Pájaro C. (2018). A study on the effect of material nonlinearity on the generation of frequency harmonics in the response of excited soil deposits. *Soil Dyn Earthq Eng*, 115:787–798.
144. Mohanty P, Dutta SC, Bhattacharya S. (2017). Proposed mechanism for mid-span failure of pile supported river bridges during seismic liquefaction. *Soil Dyn Earthq Eng*, 102:41–45.
145. Mondal G, Prashant A, Jain SK. (2012). Simplified seismic analysis of soil-well-pier system for bridges. *Soil Dyn Earthq Eng*, 32(1):42–55.
146. Monkul MM, Gültekin C, Gülver M, Akin O, Eseller-Bayat E. (2015). Estimation of liquefaction potential from dry and saturated sandy soils under drained constant volume cyclic simple shear loading. *Soil Dyn Earthq Eng*, 75:27–36.
147. Mortezaie A, Vucetic M. (2016). Threshold shear strains for cyclic degradation and cyclic pore water pressure generation in two clays. *J Geotech Eng*, 142(5):1–14.
148. Mylonakis G. (2001). Simplified model for seismic pile bending at soil layer interfaces. *Soils Found*, 41(4):47–58
149. Mylonakis G, Gazetas G. (2000). Seismic soil-structure interaction: beneficial or detrimental? *J Earthq Eng*, 4(3):277–301.
150. Mylonakis G, Syngros C, Gazetas G, Tazoh T. (2006). The role of soil in the collapse of 18 piers of Hanshin expressway in the Kobe earthquake. *Earthq Eng Struct Dyn*, 35(5):547–575.
151. Nath SK, Raj A, Thingbaijam KKS, Kumar A. (2009). Ground motion synthesis and seismic scenario in Guwahati City—a stochastic approach. *Seismological Research Letters*, 80(2):33–242.
152. Nikitas G, Vimalan NJ, Bhattacharya S. (2016). An innovative cyclic loading device to study long term performance of offshore wind turbines. *Soil Dyn Earthq Eng*, 82:154–160.
153. Nikitas G. (2015). Experimental proof of concept of a low-cost liquefaction mitigation technique for residential buildings. *MSc Thesis*, University of Bristol, UK
154. Nikolaou S, Mylonakis G, Gazetas G, Tazoh T. (2001). Kinematic pile bending during earthquakes : analysis and field measurements. *Geotechnique*, 51(5):425–440
155. Nogami BT, Otani J, Konagai K, Chen H. (1992). Nonlinear soil - pile interaction model for dynamic lateral motion. *Journal of Geotechnical Engineering*, 118(1):89–106

156. Novak M. (1974). Dynamic stiffness and damping of piles. *Can. Geotech. J.* 11(4):574–598
157. Novak M (1991) Piles under dynamic loads. In: *Proc Second Int Conf Recent Adv Geotech Earthq Eng Soil Dyn*, 2433–2456
158. Pagliaroli A, Aprile V, Chamlagain D, Lanzo G, Poovaodom N. (2018). Assessment of site effects in the Kathmandu valley, Nepal, during the 2015 Mw 7.8 Gorkha earthquake sequence using 1D and 2D numerical modelling. *Eng Geol*, 239:50–62.
159. Park CB, Miller RD, Xia J. (1999). Multichannel analysis of surface waves. *Geophysics*, 64(3):800–808.
160. Park D, Hashash YMA. (2008). Rate-dependent soil behaviour in seismic site response analysis. *Can Geotech J*, 45(4):454–469.
161. Park D, Kishida T. (2018). Shear modulus reduction and damping ratio curves for earth core materials of dams. *Can Geotech J*, 56(1):14-22
162. Peacock W, Seed HB. (1968). Sand liquefaction under cyclic loading simple shear conditions. *J Soil Mech Found Div*, 94:689–708
163. Phillips C, Hashash YMA. (2009). Damping formulation for nonlinear 1D site response analyses. *Soil Dyn Earthq Eng*, 29(7):1143–1158.
164. PHRI (1997). *Handbook on liquefaction remediation of reclaimed land*. Balkema
165. Poulos HG, Davis EH. (1980). *Pile foundation analysis and design*. New York, NY, USA: Wiley
166. Prakash S, Sharma HD. (1990). *Pile foundations in engineering practice*. John Wiley & Sons.
167. Puri N, Jain A. (2014). Preliminary investigation for screening of liquefiable areas in Haryana state, India. *ISET J. Earthq. Technol*, *51*(1-4), 19-34.
168. Raghu Kanth STG, Sreelatha S, Dash SK. (2008). Ground motion estimation at Guwahati city for an Mw 8.1 earthquake in the Shillong plateau. *Tectonophysics*, 448(1-4):98–114.
169. Ramirez J, Barrero AR, Chen L, Dashti S. (2018). Site response in a layered liquefiable deposit : evaluation of different numerical tools and methodologies with centrifuge experimental results. *J Geotech Geoenvironmental Eng*, 144(10):1–22.
170. Randolph MF. (1981). The response of flexible piles to lateral loading. *Géotechnique*, 31(2):247–259.
171. Ranjan R. (2005). *Seismis response analysis of Dehradun City, India*. International Institute for Geo-Information Science and Earth Observations-Enschede, Netherlands
172. Hanumantharao C, Ramana GV. (2009). Site specific ground response analyses at Delhi, India. *Electron J Geotech Eng*, 14-25.
173. Rollins KM, Lane JD, Gerber TM. (2005). Measured and computed lateral response of a pile group in sand. *J Geotech Geoenvironmental Eng*, *131*(1), 103-114.
174. Rouholamin M. (2016). An experimental investigation of transient dynamics of pile-supported structures in liquefiable soils, *PhD Thesis*, University of Surrey.
175. Rouholamin M, Bhattacharya S, Orense RP. (2017). Effect of initial relative density on the post-liquefaction behaviour of sand. *Soil Dyn Earthq Eng*, 97:25–36.
176. Saeedi M, Dehestani M, Shooshpasha I, Ghasemi G, Saeedi B. (2018). Numerical analysis of pile-soil system under seismic liquefaction. *Eng Fail Anal*, 94:96–108.
177. Saran S. (1999). *Soil dynamics and machine foundations*. Galgotia Publication, New Delhi, India
178. Sarkar R, Bhattacharya S, Maheshwari BK (2014) Seismic requalification of pile foundations in liquefiable soils. *Indian Geotechnical J*, 44(2):183–195.
179. Saxena SK, Reddy KR. (1989). Dynamic moduli and damping ratios for Monterey No.0 sand by resonant column tests. *Soils Found*, 29(2):37–51.
180. Seed HB, Idriss IM. (1970). *Soil moduli and damping factors for dynamic response analyses*. Report EERC 70-10, Earthquake Engineering Research Center; University of California, Berkeley.
181. Seed HB, Idriss IM. (1971). Simplified procedure for evaluating soil liquefaction potential. *J Soil*

Mech Found Div, 97:1249–73
182. Seed HB, Lee KL. (1966). Liquefaction of saturated sands during cyclic loading. *J Soil Mech Found* Div, 92:105–134
183. Seed HB, Martin PP, Lysmer J. (1975). *The generation and dissipation of pore water pressures during soil liquefaction*. Berkeley, CA
184. Seed HB, Peacock WH. (1971). Test procedures for measuring soil liquefaction characteristics. *J of Soil Mech and Found Div*, 97(8):1099-1119.
185. Seed HB, Wong RT, Idriss I, Tokimatsu K. (1986). Moduli and damping factors for dynamic analyses of cohesionless soils. *J Geotech Engg*, 112(11):1016–1032
186. Sezen H. (2000). *Structural engineering reconnaissance of the August 17, 1999 Earthquake: Kocaeli (Izmit), Turkey* (No. 9) Pacific Earthquake Engineering Research Center
187. Seed HB, Romo MP, Sun JI, Jaime A, Lysmer J. (1988). The Mexico earthquake of September 19, 1985—Relationships between soil conditions and earthquake ground motions. *Earthquake spectra*, *4*(4):687-729.
188. Shadlou M, Bhattacharya S. (2014). Dynamic stiffness of pile in a layered elastic continuum. *Geotechnique*, 64(4):303–319.
189. Shanker K, Basudhar PK, Patra NR. (2007). Buckling of piles under liquefied soil conditions. *Geotech Geol Eng*, 25(3):303–313.
190. Shirley DJ. (1978). An improved shear wave transducer. *J Accoustical Soc Am*, 63(5):163–1645.
191. Shirley DJ, Hampton LD, Shirley DJ, Hampton LD. (1978). Shear-wave measurements in laboratory sediments. *J Accoustical Soc Am*, 63(2):607–613.
192. Simonelli AL, Di Sarno L, Durante MG, Sica S, Bhattacharya S, Dietz MS, Dihoru L, Taylor CA, Cairo R, Chidichimo A, Dente G, Modaressi A, Todo Bom LA, Kaynia AM, Anoyatis G, Mylonakis G. (2014). Experimental assessment of seismic pile-soil interaction. In *Seismic Evaluation and Rehabilitation of Structures*, pp. 455-475. Springer, Cham.
193. Sitharam T., Govindaraju L, Srinivasa Murthy B. (2004). Evaluation of liquefaction potential and dynamic properties of silty sand using cyclic triaxial testing. *Geotech Test J*, 27(5):423-429.
194. Sitharam TG, Dash H K, Jakka RS. (2013). Postliquefaction undrained shear behavior of sand-silt mixtures at constant void ratio. *Int J of Geomechanics*, 13(4):421-429.
195. Souto A, Hartikainen J, Ozudogru K. (1994). Measurement of dynamic parameters of road pavement materials by the bender element and resonant column tests. *Geotechnique*, 44(3):519–526
196. SPAN Consultants Private Limited (2005). Consultancy services for feasibility study and DPR for construction of bridge across Brahmaputra River including approaches near Guwahati, NH-31, Assam (Package C-III/12), Detailed Project Report, Vol X - Drawings, Part - II, National Highway Authority of India (NHAI), Ministry of Road Transport and Highways, Government of India, New Delhi.
197. Sridharan A, Nagaraj HB. (2004). Coefficient of consolidation and its correlation with index properties of remolded soils. *Geotechnical Testing Journal*, 27(5):469-474.
198. Stokoe KH, Hwang SK, Darendeli M, Lee NJ. (1995). *Correlation study of nonlinear dynamic soils properties*. Final Report to Westinghouse Savannah River Company. Aiken, S.C.
199. Stokoe KH, Woods RD. (1972). In situ shear wave velocity by cross-hole method. *J Soil Mech Found Div*, 98(SM5):443–460.
200. Subramaniam P, Banerjee S. (2016). Torsional shear and resonant column tests on cement treated marine clay. *Indian Geotechnical J*, 46(2):183-191.
201. Tatsuoka F, Iwasaki T, Takagi Y. (1978). Hysteretic damping of sands under cyclic loading and its relation to shear modulus. *Soils and Found*, 18(2):25–39.
202. Tatsuoka F, Iwasaki T, Yoshida S, Fukushima S, Sudo, H. (1979). Shear modulus and damping by

drained tests on clean sand specimens reconstituted by various methods. *Soils and Found, 19*(1): 39-54.
203. Tokimatsu K, Hosaka Y. (1986). Effects of sample disturbance on dynamic properties of sand. *Soils and Found, 26*(1): 53-64.
204. Tombari A, El MH, Dezi F. (2017). Impact of ground motion duration and soil non-linearity on the seismic performance of single piles. *Soil Dyn Earthq Eng* 100:72–87.
205. Torabi H, Rayhani MT. (2017). Analysis of sensitive clays : case study — Leda clay in Ottawa Canada. *Bull Earthq Eng*, 15:123–147.
206. Troncoso J. (1990). Failure risks of abandoned tailings dams. In: I*nternational Symposium on Safety and Rehabilitation of Tailings Dams, International Commission on Large Dams*. Paris, 82–89
207. Vaid YP, Thomas J. (1995). Liquefaction and postliquefaction behavior of sand. *Journal of Geotechnical Engineering*, 121(2):163-173.
208. Vardanega PJ, Bolton M. (2013). Stiffness of clays and silts : normalizing shear modulus and shear strain. *J Geotech Geoenvironmental Eng*, 139(9):1575–1589.
209. Viggiani G, Atkinson JH. (1995). Interpretation of bender element tests. *Geotechnique*, 8(32):149–154
210. Vucetic M. (1995). Cyclic threshold shear strains in soils. *J Geotech Geoenvironmental Eng*, 120(12):2208–2228
211. Vucetic M, Dobry R. (1991). Effect of soil plasticity on cyclic response. *J Geotech Geoenvironmental Eng*, 117(1):89–107
212. Vucetic M, Dobry R. (1988). Cyclic triaxial strain-controlled testing of liquefiable sands. *Adv triaxial Test soil rock*, 475–485.
213. Vucetic M, Lanzo G, Doroudian M. (1998). Damping at small strains in cyclic simple shear test. *J Geotech Geoenvironmental Eng, 124*(7):585-594.
214. Wang S, Kutter BL, Chacko J, Wilson DW, Boulanger RW, Abghari A. (1998). Nonlinear seismic soil-pile structure interaction. *Earthq Spectra*, 14(2):377–396
215. Weaver TJ, Ashford SA, Rollins KM. (2005). Response of 0.6 m sast-in-steel-shell pile in Liquefied Soil under Lateral Loading. *J Geotech Geoenvironmental Eng*, 131(1):94–102
216. Wilson BDW, Boulanger RW, Kutter BL. (2000). Observed seismic lateral resistance of liquefying sand. *J Geotech Geoenvironmental Eng*, 126(10):898–906
217. Winkler E. (1867). *Theory of elasticity and strength*. Dominicus Prague, Czechoslovakia
218. Xenaki VC, Athanasopoulos GA. (2003). Liquefaction resistance of sand-silt mixtures: An experimental investigation of the effect of fines. *Soil Dyn Earthq Eng*, 23(3):183–194.
219. Yashinsky M, Oviedo R, Ashford S, Fargier-Gabaldon L, Hube M. (2010). *Performance of highway and railway structures during the February 27, 2010 Maule Chile earthquake*. EERI/PEER. FHWA Bridge Team Report.
220. Yee E, Stewart JP, Tokimatsu K. (2013). Elastic and large-strain nonlinear seismic site response from analysis of vertical array recordings. *J Geotech Geoenvironmental Eng*, 139(10):1789–1801.
221. Yoshida, N. (2015). *Seismic ground response analysis*. Dordrecht: Springer.
222. Yoshida N (2014). Comparison of seismic ground response analyses under large earthquakes. *Indian Geotechnical Journal*, 44(2):119–131.
223. Yoshida N, Tazoh T, Wakamatsu K, Yasuda S, Towhata I, Nakazawa H, Kiku H. (2007). Causes of Showa Bridge collapse in the 1964 Niigata earthquake based on eyewitness testimony. *Soils and Found*, 47(6):1075-1087.
224. Youd TL, Idriss IM. (2001). Liquefaction resistance of soils: summary report from the 1996 NCEER and 1998 NCEER/NSF workshops on evaluation of liquefaction resistance of soils. *Journal of geotechnical and geoenvironmental engineering*, 127(4):297-313.

225. Zhang J, Andrus RD, Juang CH. (2005). Normalized shear modulus and material damping ratio relationships. *J Geotech Geoenvironmental Eng*, 131(4):453–464.

भारतीय प्रौद्योगिकी संस्थान गुवाहाटी
Indian Institute of Technology Guwahati

PUBLICATIONS

Journal Papers:

1. **Dammala PK**, Kumar SS, Krishna AM, Bhattacharya S (2019) Dynamic soil properties and liquefaction potential of northeast Indian soil for nonlinear effective stress analysis. *Bull Earthq Eng*, 17(6): 2899-2933.
2. **Dammala PK**, Jalbi S, Bhattacharya S, Krishna AM, Bouzid DJ (2018) Impedance functions for double D shaped caisson foundations. *International Journal of Testing and Evaluation*, ASTM 47(3):1900-1919.
3. **Dammala PK**, Krishna AM, Bhattacharya S, Nikitas G, Rouholamin M. (2017). Dynamic soil properties for seismic ground response studies in Northeastern India. *Soil Dynamics and Earthquake Engineering*, 100:357-370
4. **Dammala PK,** Bhattacharya S, Krishna AM, Kumar SS, Dasgupta K. (2017). Scenario based seismic re-qualification of caisson supported major bridges–A case study of Saraighat Bridge. *Soil Dynamics and Earthquake Engineering*, 100:270-275.

Journal Papers (outside Ph.D. Work)

5. Rele R, **Dammala PK,** Bhattacharya S, Balmukund R (2019) Seismic Behaviour of Rocking Bridge Pier supported by Novel Elastomeric Pads on Pile Foundation. *Soil Dynamics and Earthquake Engineering*, 124, 98-120.
6. Bali Reddy, S., **Dammala PK**, & Murali Krishna, A. (2015). Evaluation of the optimum mixing ratio of a sand-tire chips mixture for geoengineering applications. *Journal of Materials in Civil Engineering*, *28*(2), 06015007.

Book Chapters:

1. **Dammala, P. K.,** Jalbi, S., Bhattacharya, S., Adapa, M. K. (2018, July). Simplified methodology for stiffness estimation of double D shaped caisson foundations. In *Civil Infrastructures Confronting Severe Weathers and Climate Changes Conference* (pp. 49-62). Springer, Cham.
2. **Dammala, P. K.,** Krishna, A. M. (2019). Dynamic characterisation of soils using various methods for seismic site response studies. In *Frontiers in Geotechnical Engineering* (pp. 273-301). Springer, Singapore.

3. **Dammala, P. K.,** Krishna, A. M. (2019). Kinematic response of pile foundations in liquefiable soils, In: *Proc. of International Conf on Earthquake Geotechnical Engg 2019* (pp. 1944-1951), Rome, Italy.

Conferences:

1. **Dammala PK**, Krishna AM, (2018) Seismic requalification of a pile supported structure – Pseudo static approach, Proc. of *Indian Geotechnical Conference 2018*, Bangalore
2. **Dammala PK**, Rouholamin M, Nikitas G, Bhattacharya S, Krishna AM (2018) Lateral behaviour of pile foundations during partial liquefaction, In: *Proc. of IFCEE 2018*, Florida, GSP 294.
3. **Dammala PK**, Rouholamin M, Nikitas G, Bhattacharya S, Krishna AM, (2017) Bending response of pile foundations during partial liquefaction. In: *Proceedings of Indian Geotechnical Conference 2017*, IIT Guwahati, India
4. **Dammala PK**, Krihsna AM, Bhattacharya S, Aingaran S (2016) Cyclic reponse of cohesionless soil using cyclic simple shear testing. In: *6th International Conference on Recent Advances in Geotechnical Earthquake Engineering. ICRAGEE*, New Delhi, India
5. **Dammala PK**, Krishna AM, Bhattacharya S, A (2015) Cyclic threshold shear strains in cohesionless soils based on stiffness degradation. In: *Proceedings of Indian Geotechnical Conference 2015*, CoE Pune, India
6. **Dammala PK**, Krishna AM (2014) Geotechnical concerns in seismic analysis of structures for earthquake disaster mitigation, In: *One day national seminar on role of geotechnology in disaster mitigation*, IIT Bhubaneswar, India